Improved Design Method for Cambered Stepped Hulls with High Deadrise

Raymond J. Bay

Thesis submitted to the Faculty of the
Virginia Polytechnic Institute and State University
in partial fulfillment of the requirements for the degree of

Master of Science
in
Ocean Engineering

Stefano Brizzolara, Chair
Alan J. Brown
Eric G. Paterson

April 29, 2019
Blacksburg, Virginia

Keywords: CFD, Planing Surface, Cambered Step Hull

Improved Design Method for Cambered Stepped Hulls with High Deadrise

Raymond J. Bay

(ABSTRACT)

Eugene Clement created a design method for swept-back cambered step hulls with deadrise. The cambered step is designed to carry 90% of the planing vessels weight with the remaining 10% being support by a stern mounted hydrofoil. The method requires multiple design iterations in order to achieve an optimal design. Clement stated that the method was not suitable for cambered planing surfaces with high deadrise angles greater than 15 degrees. The goal of this thesis is to create a design procedure for swept-back cambered planing surfaces with high deadrise angles that does not require multiple iterations to obtain an optimal design. Computational fluid dynamics (CFD) program STAR CCM+ is used to generate a database for performance characteristics for a wide range of designs varying deadrise angle, load requirements, trim angle, and different camber values. The simulations are first validated with experimental data for two different cambered steps designed by Stefano Brizzolara and tested in the tow tank at the United States Naval Academy. A series of validation studies utilizing fixed and overset meshes led to a final simulation set up with an overset mesh that allowed for accurate prediction of drag, trim moment, wetted keel length, and the wake profile aft of the cambered planing surface. The database is fitted such that the final equations for optimal design values such as camber, trim angle, drag (shear and pressure), wetted keel length, wetted surface area, and trim moment are in terms of deadrise angle and lift. The optimized design equations are validated with CFD simulation.

Improved Design Method for Cambered Stepped Hulls with High Deadrise

Raymond J. Bay

(GENERAL AUDIENCE ABSTRACT)

Eugene Clement developed a new design method to improve the performance of ultra-fast planing crafts. A planing craft uses the force generated from the flow of water over the bottom to lift the vessel without the use of the static buoyancy force that classic boat designs rely on. Clement wanted to improve the performance of the planing vessel by reducing the total drag force caused by the flow of water on the bottom of the vessel. ClementâĂŹs design method involves reducing the wetted surface area which reduces drag. Reducing the wetted surface area would normally cause the lifting force on the vessel to reduce, but with the addition of curvature in the smaller wetted surface area, the lifting force would remain the same. ClementâĂŹs new design method requires multiple iterations to obtain an optimal design. The method limits the angle of the vessels bottom relative to horizontal to under 15 degree. The goal of this thesis is to create a new design method for planing vessels with bottoms that have an incline of 15 degrees or more relative to horizontal. The design method is created using Computational Fluid Dynamics (CFD) solver to model the planing surface moving through water. The CFD solver is validated with experimental test performed at the United States Naval Academy. The improved design method uses equations that can predict the forces and other design characteristics based on the desired vessel weight and seakeeping requirements.

Acknowledgments

This work has been possible thanks to the support of the US Navy Office of Naval Research grant N00014-17-1-2344.

Contents

List of Figures

List of Tables

Chapter 1

Introduction

1.1 Background

Traditional ships are characterized by the Froude number defined by the vessels length using Equation 1.1 where the vessels velocity is defined by V, the gravitational constant g, and the length of the hull at the waterline L_{WL}. This non-dimensional number is used for determining the wave resistance of the vessel. Typical Froude number range for displacement ships where the hydrostatic force is dominant over the hydrodynamic forces is any value less than 0.4. Froude number range for semi-displacement hulls is 0.4-0.5 to 1.0-1.2 where at operating speed the vessel is not mainly supported by the hydrostatic force. Froude numbers greater than 1.0-1.2 denote planing vessels where the hydrodynamic forces are responsible for lifting the boat.

$$Fn_L = \frac{V}{\sqrt{L_{WL}g}} \tag{1.1}$$

Froude number as defined in Equation 1.1 is not as practical for planing vessels due to the changing waterline length. Instead a Froude number equation based on displacement weight is more practical for planing hulls. This Froude number is call a volumetric Froude number and is defined in Equation 1.2. The planing regime is noted as having a volumetric Froude number greater than 3.0. The work presented in this paper is conducting in the planing regime where the volumetric Froude number is greater than 3.0.

$$Fn_\nabla = \frac{V}{\sqrt{g\nabla^{1/3}}} \tag{1.2}$$

1.2 Planing Hull Theory

The basics of planing can be understood with the simple rectangular flat plate example in Figure 1.1. The maximum pressure for the flat plate is located at the intersection of the stagnation line and the surface of the flat plate. The water forward of the intersection builds up and travels up the surface and becomes spray which is noted by the spray root label in Figure 1.1.

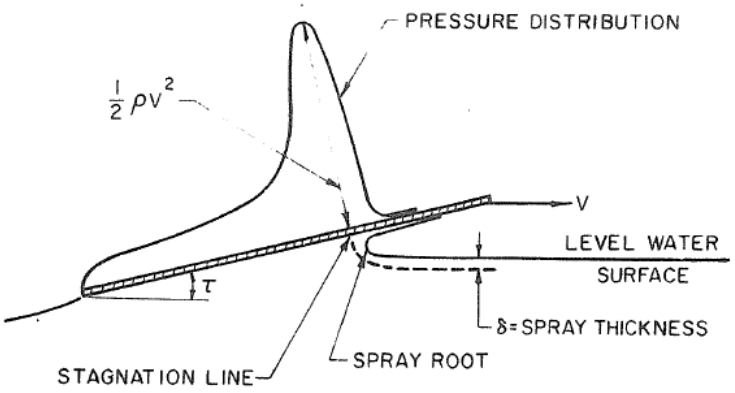

Figure 1.1: Pressure Distribution on Flat Planing Surface [9]

Flat planing surface are not a desired design for any sea conditions other than calm water due to the hard impact of waves slamming on a flat bottom. The addition of deadrise angle β shown in Figure 1.2 reduces the harshness of the slamming in waves. The addition of deadrise angle sweeps the spray root and stagnation line aft on the bottom of the hull. As mentioned for the flat plate case, the location of maximum pressure occurs along the stagnation line represented by the line from point O to point C in Figure 1.2. The spray root line is represented by line from point O to point B.

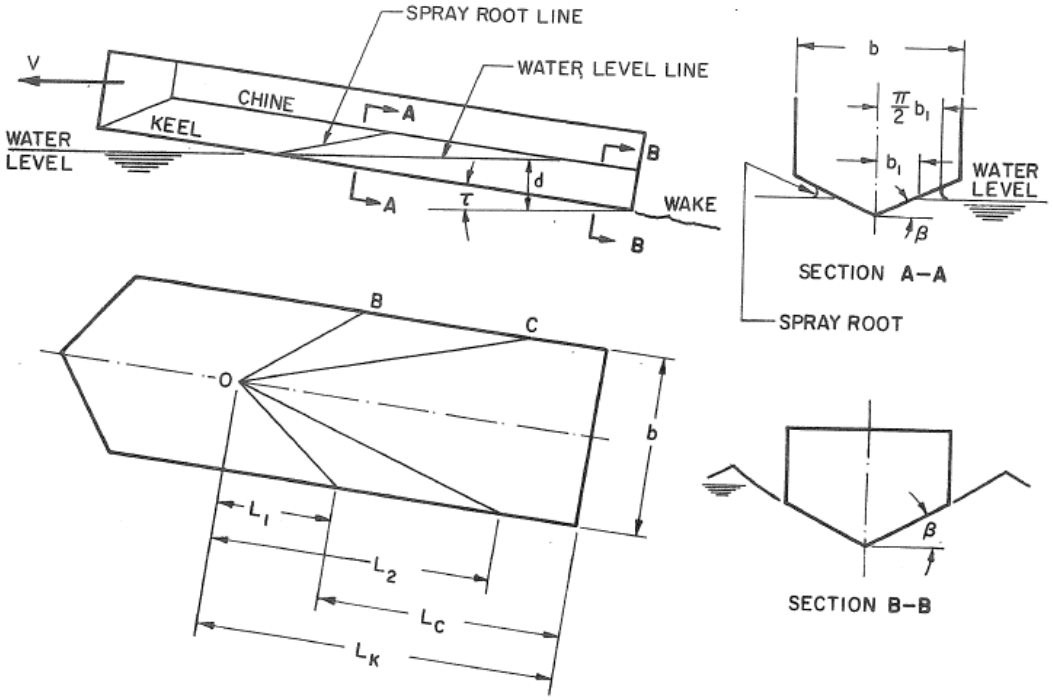

Figure 1.2: Waterlines on Planing Surface with Deadrise [9]

1.3 Clement's Dynaplane Concept

The planing hull design can be modified with the addition of steps in the planing surface to reduce the wetted surface area and therefor reducing the friction drag. Eugene Clement [4] used the Johnson three term equation to produce a more efficient step in terms of lift-to-drag ratio. Johnson defined Equation 1.9 (Johnson three term equation) to determine the camber shape to be applied to a plate which proved to increase lift-to-drag ratio compared to a flat plate. Clement combine the idea that high aspect ratio lifting surfaces and hulls with steps improve lift-to-drag ratio in reference [3]. Designing the cambered step with sweep, as shown in Figure 1.3, reduces the wetted surface area and therefor the drag as well [3]. Clement designed a complete cambered step hull with a hydrofoil shown in Figure 1.3. The cambered step is represented by the larger shaded region near the middle of the boat. The cambered step is designed to carry 90% of the weight. The remaining 10% is to be carried on a hydrofoil represented by the small shaded region at the stern of the planing hull. Clement's design process for the cambered section is presented in Section 1.3.1.

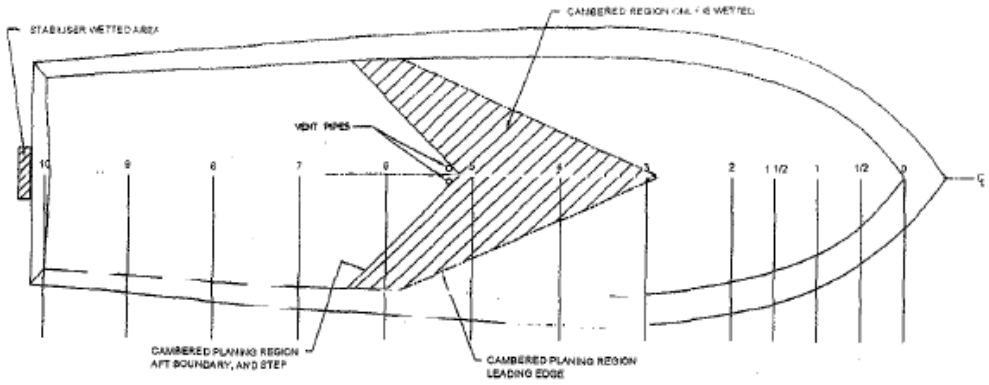

Figure 1.3: Cambered Step Planing Hull [4]

1.3.1 Clement's Cambered Step Design Procedure

The dynaplane hull design procedure is based on emprical data and approximate correlations. The procedure for designing the cambered step portion of the dynaplane hull is presented in the following seventeen steps.

1. Clement's method starts by determine the lift coefficient for the cambered step responsible for lifting 90% of the vessels weight using Equation 1.3.

$$C_{Lb_\beta} = \frac{0.9W}{\frac{1}{2}\rho V^2 b^2} \tag{1.3}$$

2. Determine deadrise angle β based on sea-keeping requirements. Deadrise angle selected should be greaer than 5 degrees and less than 15 degrees.

3. Select chord to beam length ratios for the centerline and chine location. Clement favored a centerline chord to beam length ratio l_r/b of 0.8 and a chine chord to beam length ratio l_t/b of 0.2. This ratio was preferred because it equates to an aspect ratio of 2. Johnson utilized an aspect ratio of 2 for determining the three term camber curvature equation.

4. Calculate aspect ratio using Equation 1.4

$$AR = \frac{b}{\frac{l_r + l_t}{2}} \tag{1.4}$$

5. Determine trim angle τ from Figure 1.4 with the selected deadrise angle β.

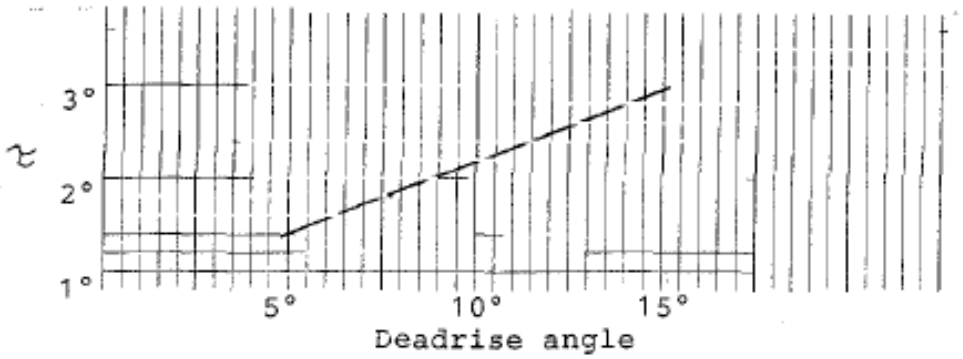

Figure 1.4: Deadrise Angle versus Trim Angle for Cambered Planing Surface [4]

6. Determine the horizontal angle between spray root line and centerline using Equation 1.5 from Savitsky method for pristmatic planing hulls which is plotted in Figure 1.5. Clement stated that an additional 5 degrees should be added for a cambered planing surfaces.

$$\gamma = \tan^{-1}\left[\frac{\pi \tan\tau}{2\tan\beta}\right] \tag{1.5}$$

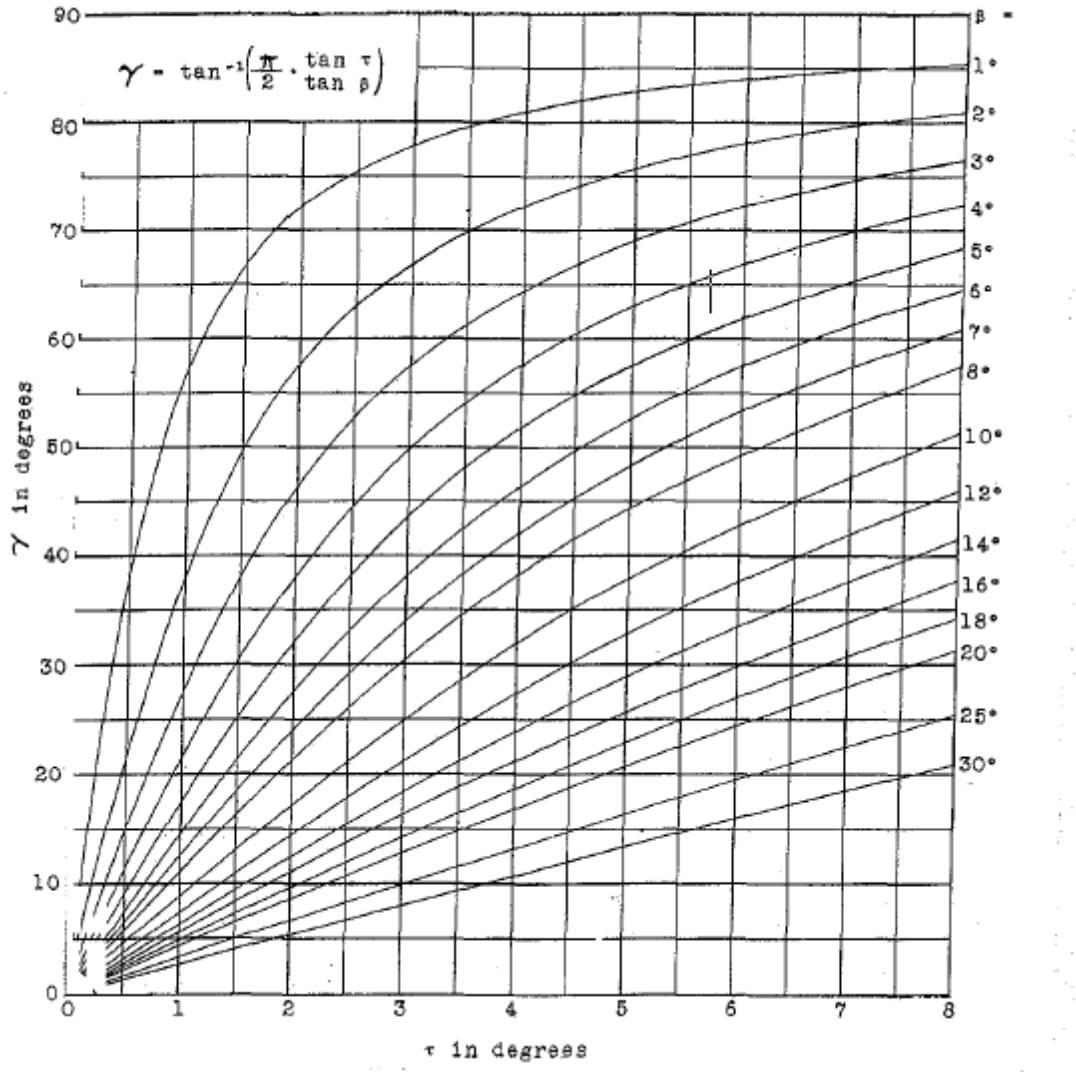

Figure 1.5: Spray Root Line to Centerline Angle from Plan View γ Versus Trim Angle τ with Varying Deadrise Angle β for Prismatic Planing Surface [4]

7. Determine the sweep angle of the 50% chord line of the cambered planing surface using Equation 1.6, or referencing the plot in Figure 1.6.

$$\phi = \tan^{-1}\left[\frac{1 - \tan\gamma\left(\frac{l_r}{b} - \frac{l_t}{b}\right)}{\tan\gamma}\right] \tag{1.6}$$

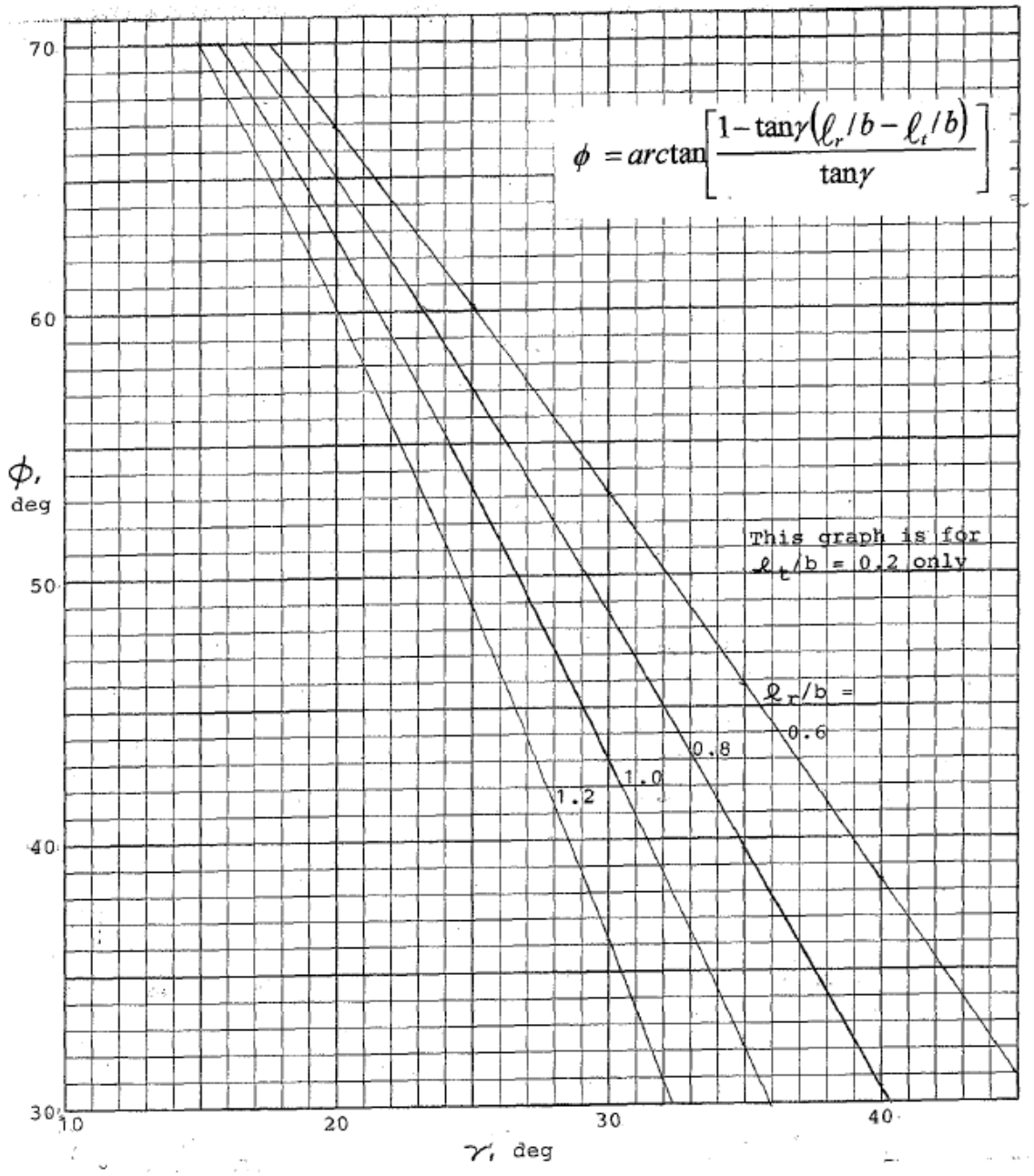

Figure 1.6: Sweep Angle of 50% Chord ϕ Versus Spray Root Line to Centerline Angle γ for $l_t/b = 0.2$ [4]

8. Determined the sweep angle of the step using Equation 1.7, or referencing Figure 1.7

$$\theta = \tan^{-1}\left[2\tan\phi - \frac{1}{\tan\gamma}\right] \tag{1.7}$$

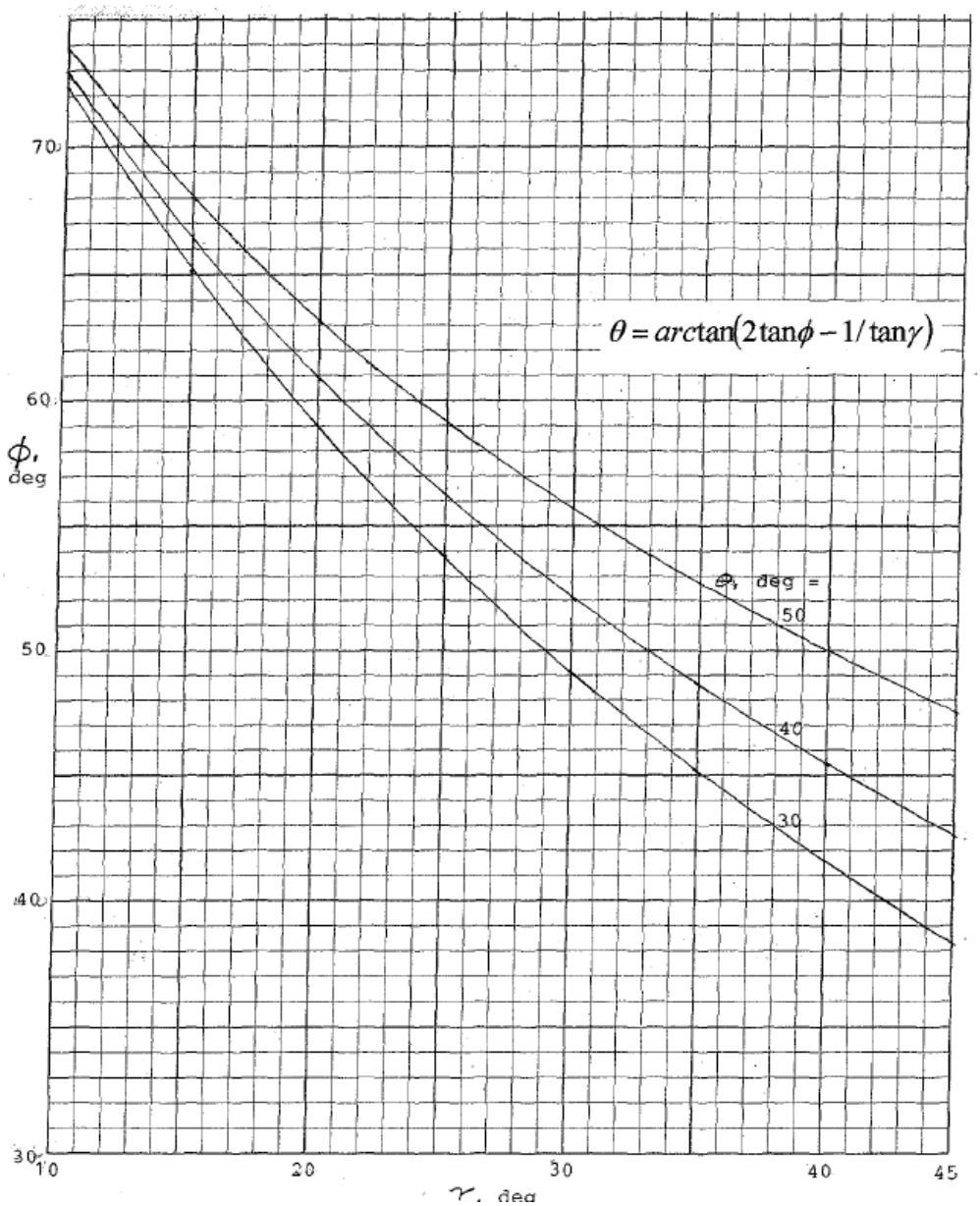

Figure 1.7: Step Sweep Angle θ Versus Spray Root Line to Centerline Angle γ [4]

9. Determine the lift coefficient for the flat plate using Equation 1.8, or the plot in Figure 1.8 and calculate $(C_{Lb_\beta}/C_{Lb,0})_D L$. DL Stands for Davidson Laboratory.

$$C_{Lb_\beta} = C_{Lb_0} - 0.0065\beta C_{Lb_0}^{0.6} \tag{1.8}$$

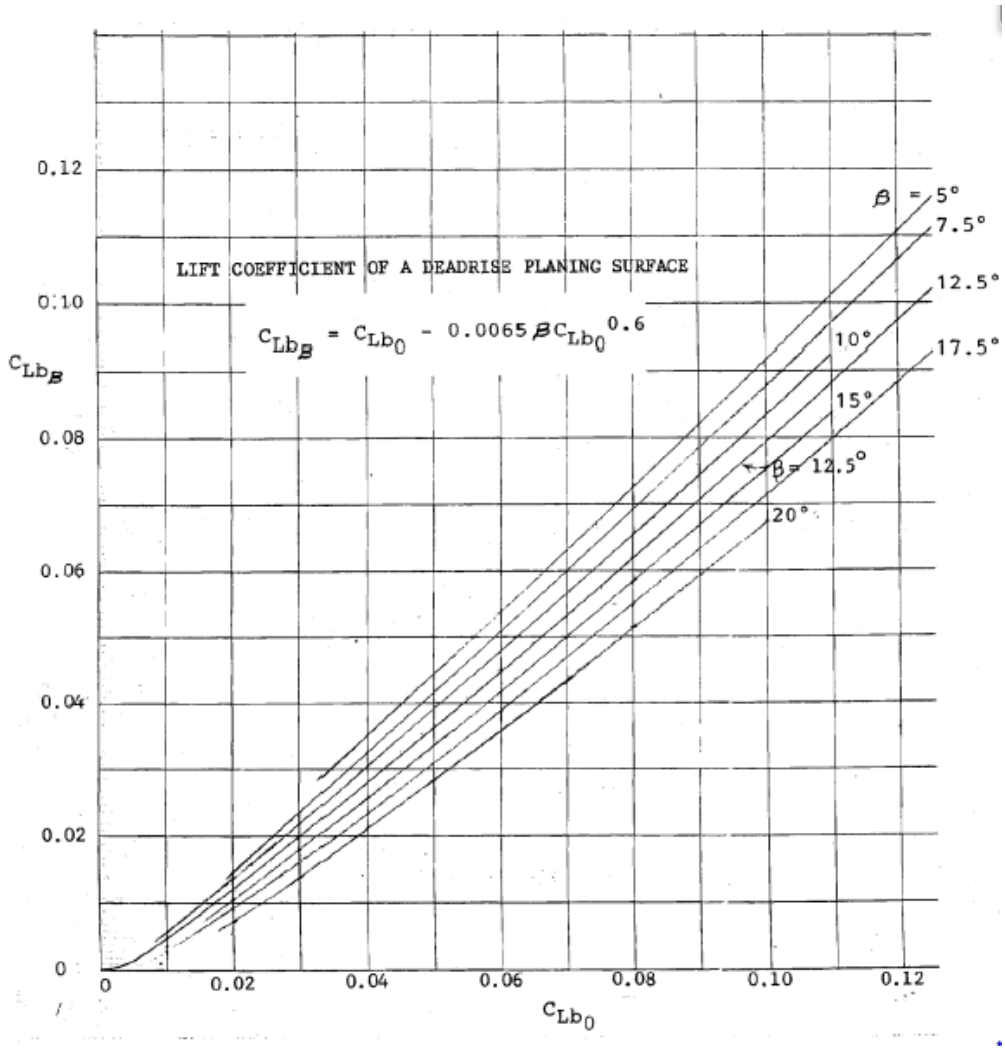

Figure 1.8: Lift Coefficient with Deadrise versus Lift Coefficient without Deadrise for Prismatic (Uncambered) Planing Surfaces [4]

10. Determine $(C_{Lb_\beta}/C_{Lb,0})_{Exp}/(C_{Lb_\beta}/C_{Lb,0})_{DL}$ from Figure 1.9

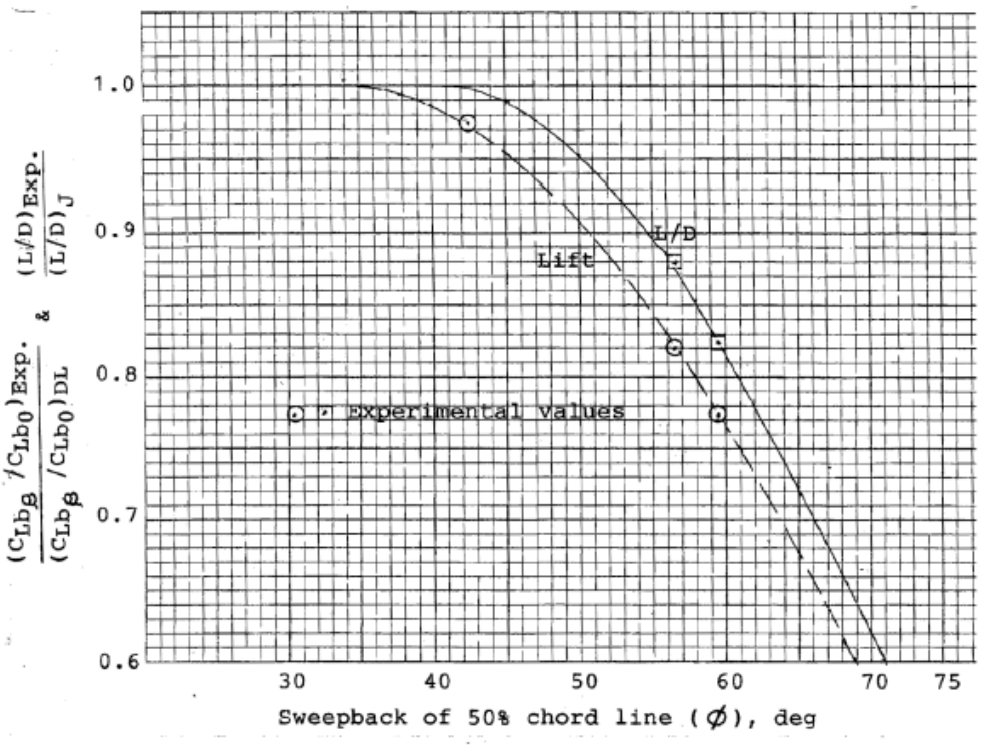

Figure 1.9: Cambered Planing Surfaces - Corrections for Sweep back Angle to Lift and L/D [4]

11. Determine $(C_{Lb_\beta}/C_{Lb,0})_{Exp}$ by multiplying the value from step 9 by the value from step 10.

12. Determine C_{Lb_o} by dividing C_{Lb_β} by the value from step 11.

13. Determine $(L/D)_J$ using Figure 1.10.

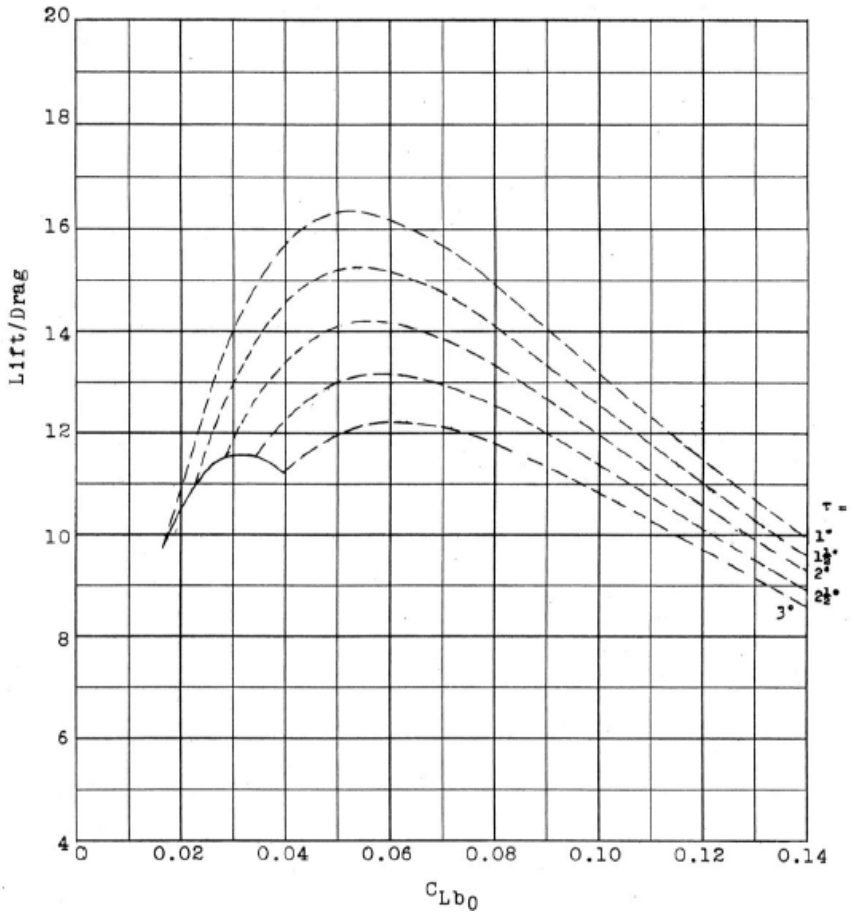

Figure 1.10: Lift/Drag versus C_{Lb_0} for Rectangular Planing Surfaces Having the Johnson Three-Term Section and Zero Deadrise, Re = 107, Aspect Ratio = 2.0. [4]

14. Determine $(LD)_{Exp}/(LD)_J$ from Figure 1.9

15. Determine $(LD)_Exp$ by multiplying the value from step 13 by the value from step 14.

16. Multiply the value from step 15 by 0.925 to determine the the lift-to-drag ratio for the planing vessel including the rear hydrofoil.

17. Determine the two-dimensional lift coefficient using the plot in Figure 1.11

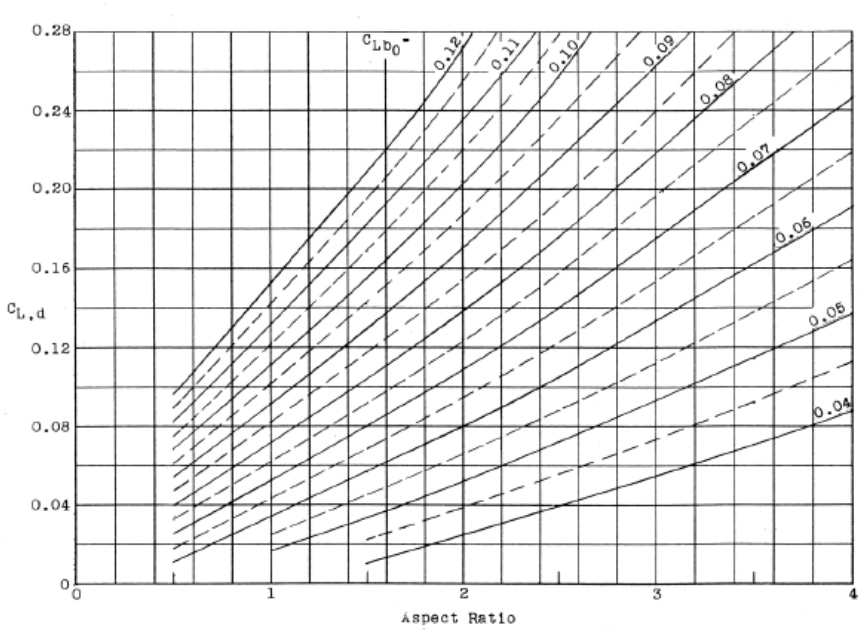

Figure 1.11: $C_{L,d}$ versus Aspect Ratio for Rectangular Planing Surfaces Having the Johnson Three-Term Section and Zero Deadrise, $\tau = 2.5$ deg [4]

Using two-dimensional lift coefficient and the chord lengths at the centerline and chine, plot the camber curvature curves using Equation 1.9. Then use the angles determine above to locate the curves and created a surface between the two curves in a computer aided program of choice. Figure 1.12 shows the angles determined above from a plan view for an arbitrary cambered step.

$$\frac{Y}{C_{L,d}} = \left(-20X^{3/2} + 80X^2 - 64X^{5/2}\right)\left(\frac{1}{7.5\pi}\right) \tag{1.9}$$

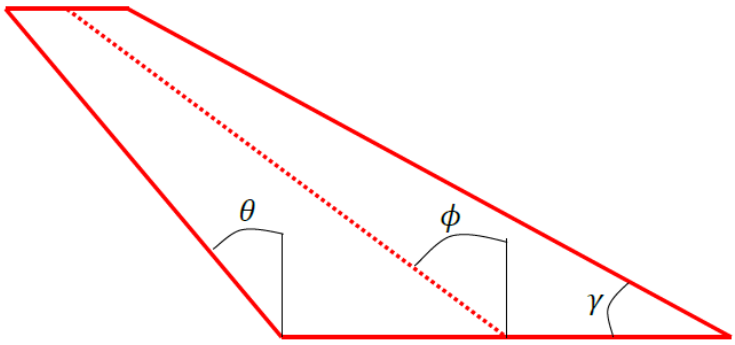

Figure 1.12: Camber Step Surface Angles

1.4 Motivation

Eugene Clement stated that cambered step hulls were limited to deadrise angles under 15 degrees without giving a reason. Stefano Brizzolara challenged this idea performing a proof of concept study. Brizzolara showed a 31% decrease in total resistance over displacement as shown in Figure 1.13. Further information regarding Brizzolara's study of high deadrise ($\beta \geq 15$) cambered step hulls can be found in reference [2].

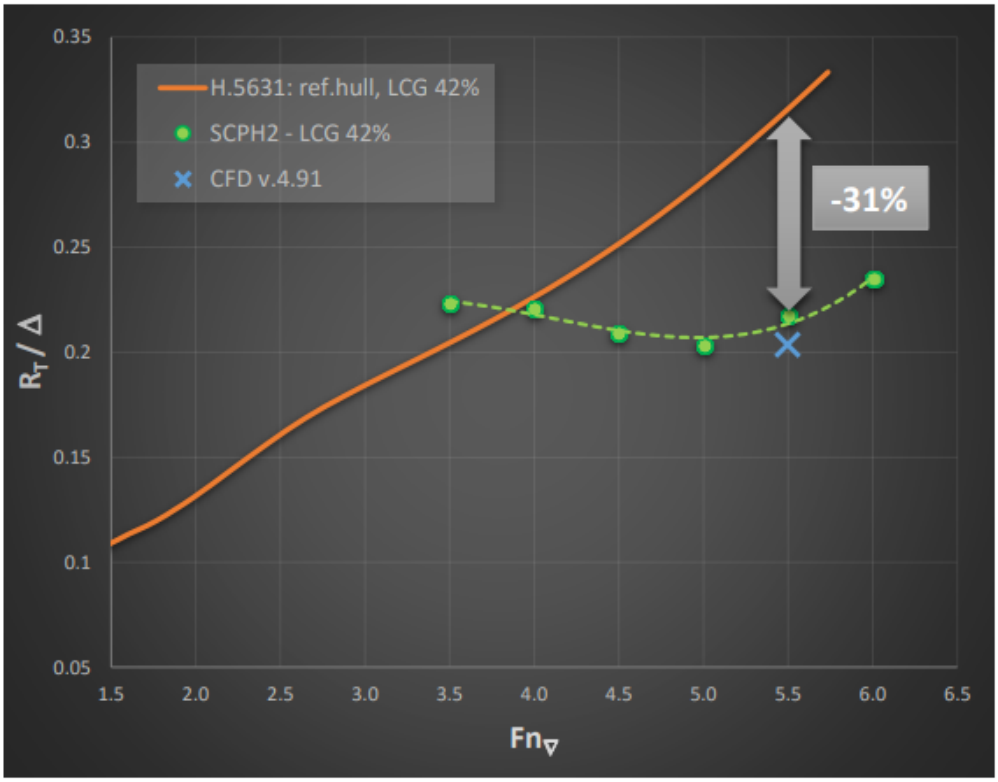

Figure 1.13: Comparison of model scale total resistance over displacement for the SCPH2 (step-A) and the original model 5631, same displacement (36.34lbs), same LCG=42%. CFD predicted Resistance is also included at design speed. [2]

In this thesis, two cambered step surfaces designed by Brizzolara were used to validate simulations with experimental data from the United States Naval Academy. Following the validation study is a proof of concept on an improved cambered step surface design procedure for vessels with high deadrise. Previous method from Clement requires multiple iterations to achieve an optimized design. The method presented in Chapter 3 will take a desired deadrise and load requirement and use a set of equations determined from a database to predict the optimized design and its performance values.

Chapter 2

CFD Validation

Creating a design procedure for cambered step planing surfaces with the use of computational fluid dynamics (CFD) requires the CFD simulation to be validated with experimental data. The CFD validation is performed using Star CCM+ with two models with different camber characteristics described in Section 2.1. The CFD simulations are validated with the experimental results in Section 2.2 from the United States Naval Academy Hydromechanics Laboratory (USNA) which will be used in Chapter 3 for creating a design method for an optimal cambered stepped planing surface.

2.1 Geometry

Two cambered step planing surface geometries designed by S. Brizzolara are considered for validation. The two cambered steps have the same two-dimensional design lift coefficient $C_{L,d}$ of 0.236. Step-A has a constant camber distribution across the beam of the planing surface resulting in a constant two dimensional design lift coefficient of 0.236. Step-B has a parabolic camber distribution with the max camber at a quarter beam distance away from the keel. The two dimensional design lift coefficient at max camber is 0.2916. The lift coefficient at the keel and chine are 0.1416. This results in an average lift coefficient over the beam of the planing surface of 0.236. The camber distribution for Step-A and Step-B is shown in Figure 2.1. The two dimensional design lift coefficient is used in the Johnson three-term camber curve equation (Equation 1.9) to determined the shape of the cambered section.

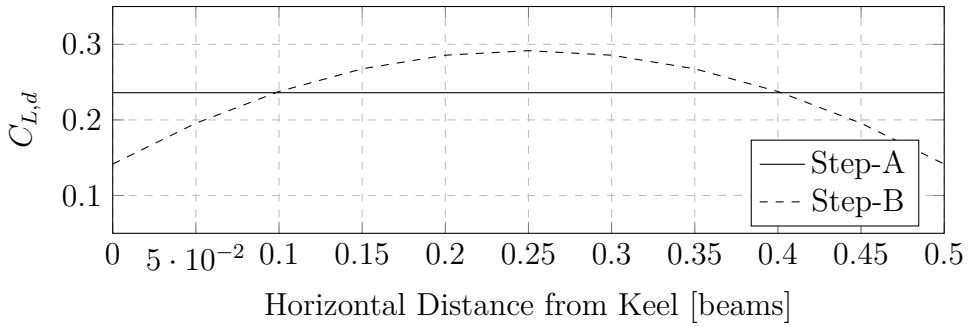

Figure 2.1: Step-A and Step-B Camber Distribution [1]

The difference in planing surface shape is shown in the profile view in Figure 2.2. Step-A has a draft of 0.384 inches below the horizontal keel line. Step-B has a draft of 0.055 inches below the horizontal keel line. Step-A and Step-B have a high deadrise angle of 21.75 degrees.

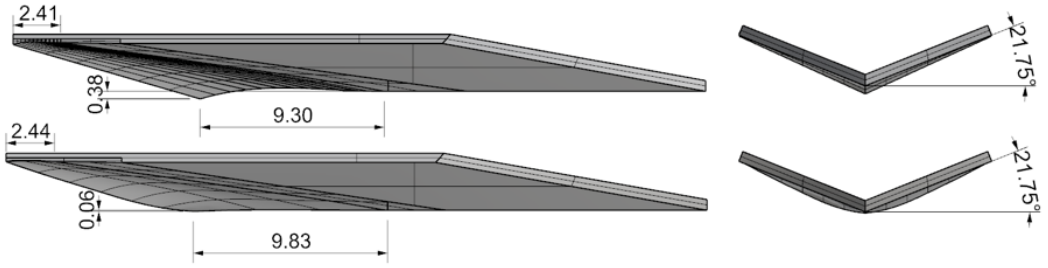

Figure 2.2: Step A and B CAD Profile

2.2 Experimental Test

The experimental test were performed at the USNA Hydromechanics Laboratory by Dr. M. Morabito, an Assistant Professor and W. Beaver, Staff Naval Architect of the USNA. The experimental test were conducted with plexiglas models with the cambered sections printed by a three-dimensional printer by the Kevin T. Crofton Department of Aerospace and Ocean Engineering machine shop. Dr. Morabito made two modification: changing the square bow in Figure 2.3 to a sharp bow as shown in Figure 2.4 and making the cambered sections interchangeable by fitting threaded attachments to the cambered steps so that the sections could be screwed on and off from the topside instead of having to attach and re-attach the entire model from the towing post.

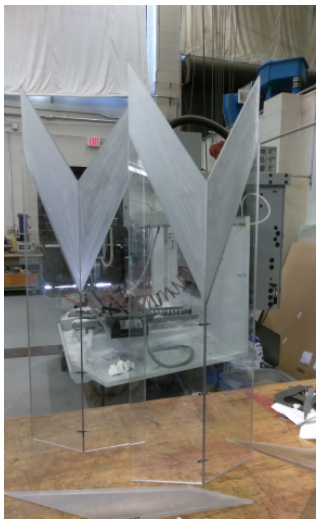

Figure 2.3: Plexiglas Models without 3D printed Cambered Sections Attached

2.2.1 Test Configuration

The experimental test was configured to measure drag, trim moment, wetted keel length, wetted chine length, draft, and wake profile at two locations of interest at a running speed of 9 m/s for all test runs. The overall experiment setup can be seen in Figure 2.4. For further information regarding the experimental test configuration than provided, refer to the test memorandum by Morabito, M. and Beaver, W. [7].

The model is connected to a pivot point that is attached to a strain gauge that measures the drag force that is attached to the tow post that is free to heave. The running draft of the model is determined by zeroing the step by lowering the model so that it is just touching the the calm water level and measuring the heave from the calm water level during the run. The trim angle of the model is fixed by a horizontal bar that extends out from above the pivot point, but below the strain gauge that measures drag. At the end of the horizontal bar is another strain gauge that measure the vertical force at the bow to determine the trim moment. This setup can be seen in Figures 2.5 and 2.6.

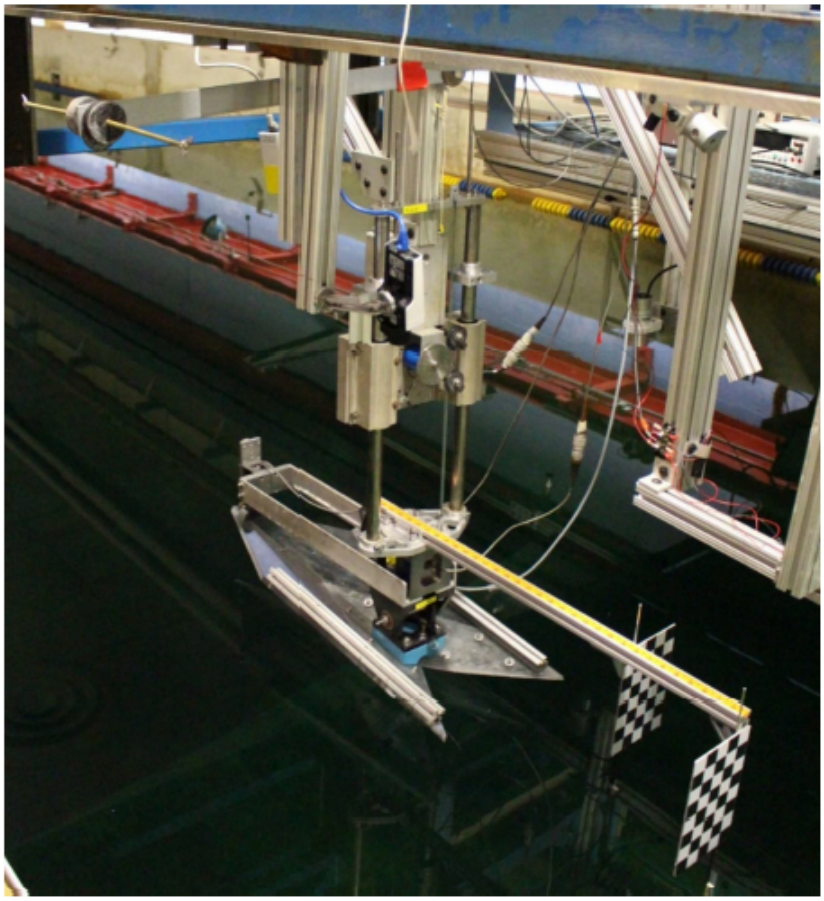

Figure 2.4: Experimental Test Configuration [7]

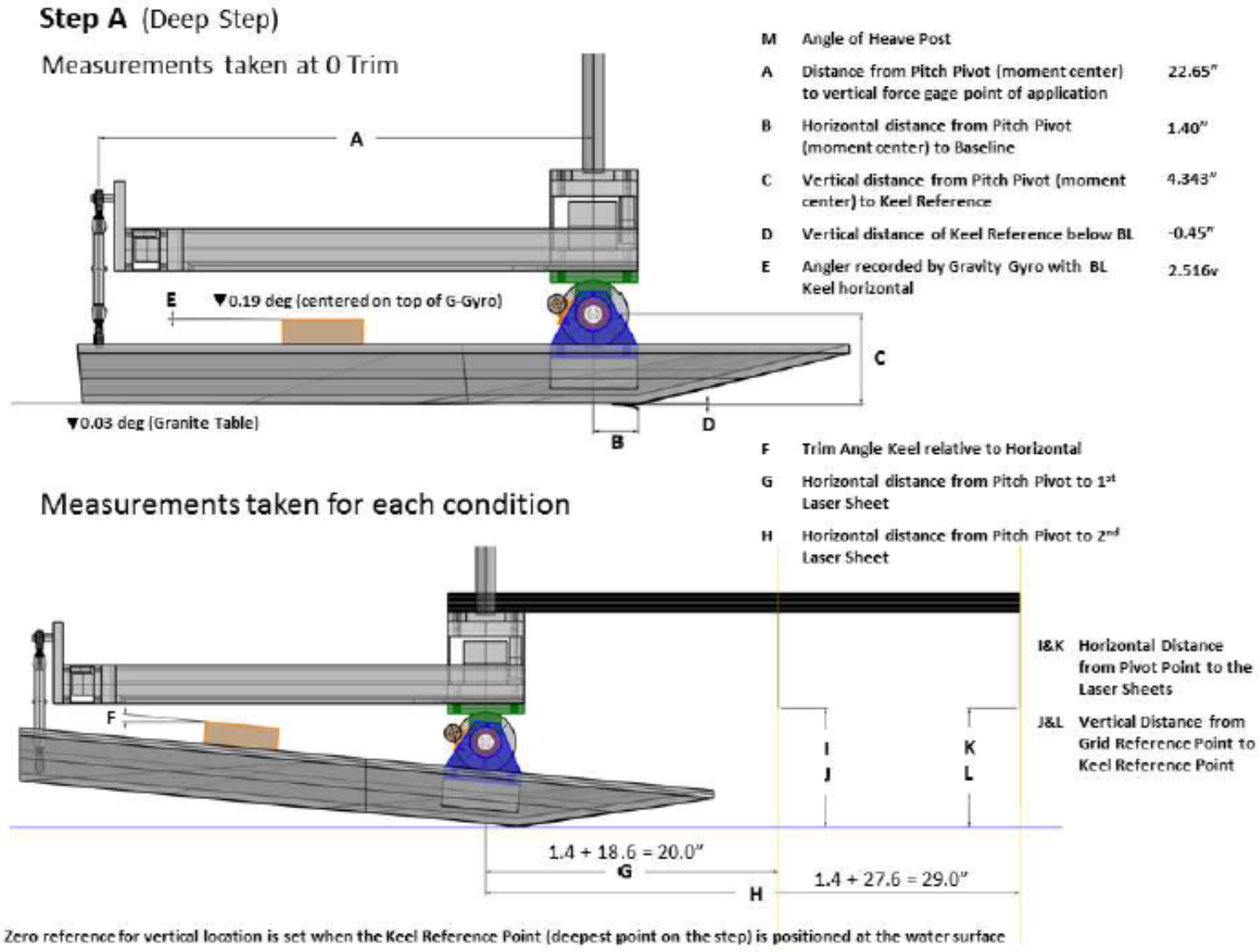

Figure 2.5: Step-A Experiment Configuration [7]

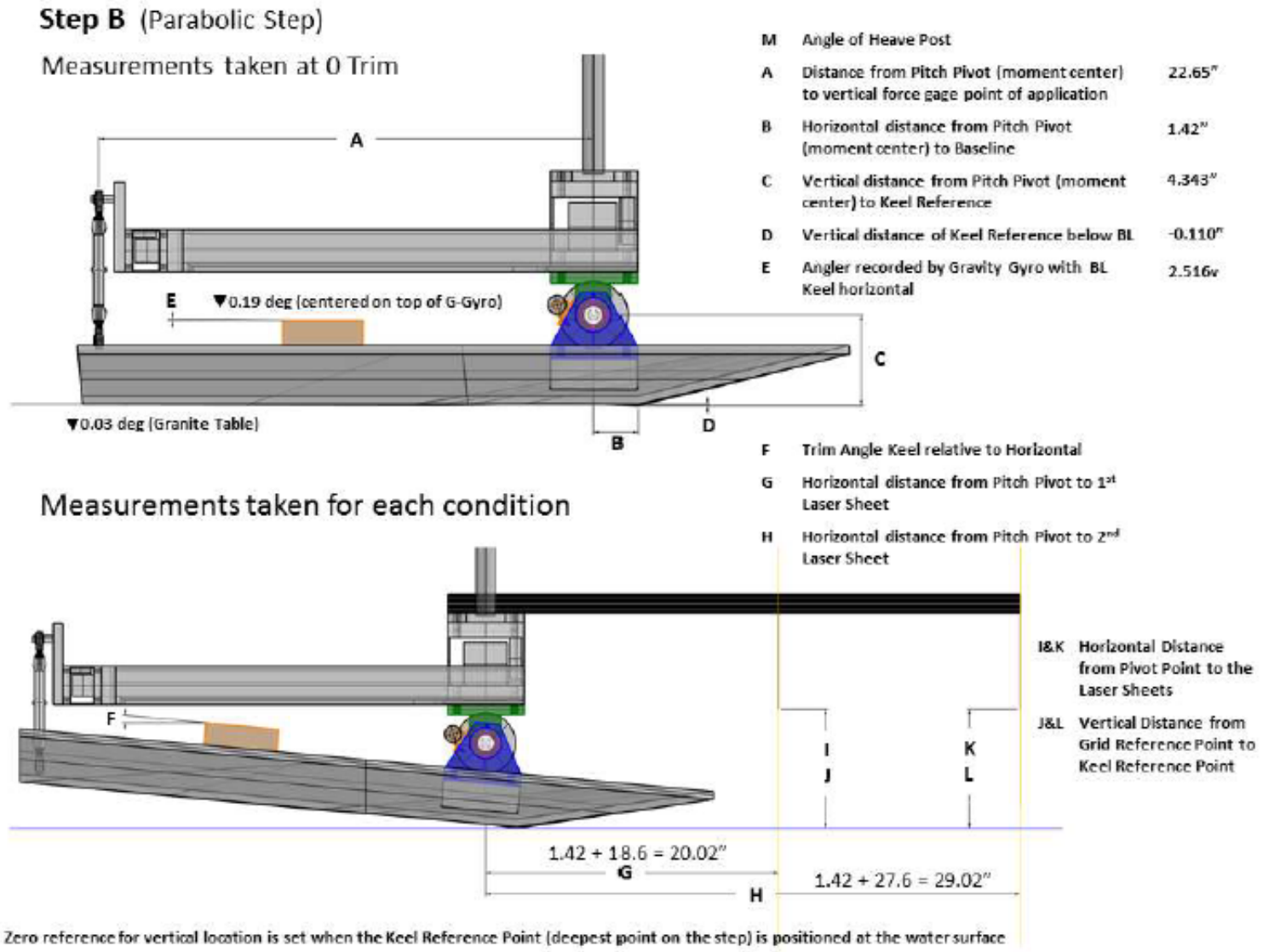

Figure 2.6: Step-B Experiment Configuration [7]

The wetted keel and chine lengths and wake profiles are measured with the camera and laser configuration in Figure 2.7. The camera facing down over the model was used to determine the wetted keel and chine lengths. The lengths were measured using pre-marked measurements on the plexiglas. The prismatic plexiglas and the cambered section are transparent for determining the wetted keel length and chine. The second camera behind the model is used for measuring the wake profile highlighted by a green and red laser located at the positions marked in Figure 2.5 and 2.6. The black and white checker board in Figure 2.4 were used as a reference point for determining the wake profile. The green laser is the forward laser position and is located at the mid section of the after body for the planing vessel in Figure 1.3. The further aft red laser is located at the hydrofoil location of planing vessel in Figure 1.3.

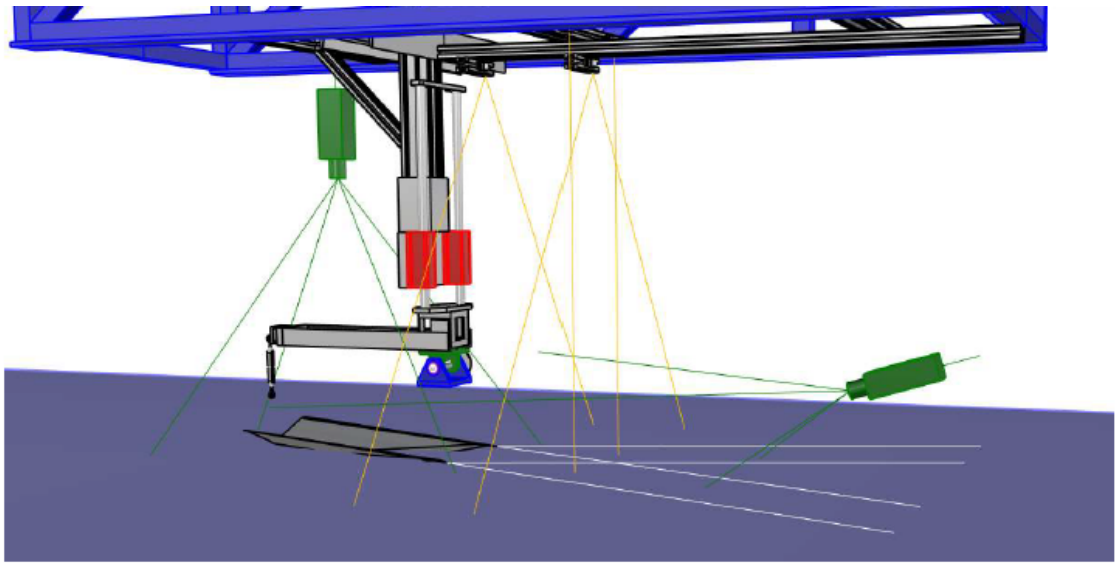

Figure 2.7: Experimental Test Laser and Camera Positioning [7]

2.3 CFD Fixed Position Planing Conditions

The validation study is initially performed utilizing fixed position simulations. Fixed in space simulations placed the planing surface at the trim angle and vertical placement relative to the calm water level. Initially the experimental draft values from Appendix A.1 were used to vertically place the planing surface, but due to inaccuracies found in the draft values the experimental wetted keel length was used to vertically position the planing surface. Using the wetted keel length to vertically position assumes zero build up of water in front of the intersection of the keel and the calm water level.

2.3.1 Fixed Position CFD Setup

The fixed position CFD simulations used a Volume of Fluid (VOF) model with either a k-epsilon or k-omega turbulence model with a time step of 2e-4 seconds. The VOF model tracks the free surface between the two fluids (water and air). The k-epsilon model is a realizable k-epsilon two-layer model that uses two transport equations. The transported variables k and ϵ are the turbulence kinetic energy and rate of dissipation of turbulence energy, respectfully. The realizable k-epsilon two-layer model has the ability to apply an all y^+ wall treatment. The k-omega model used a shear-stress transport (SST) k-omega turbulence model with the Gamma ReTheta transition model. This model combines the k-epsilon turbulence model for far-field with the k-omega for near the wall. The Gamma ReTheta model requires a free stream edge to be defined for the transition model thickness Reynolds number. The free stream edge is defined as being 10 mm thick which means the boundary layer is thinner than 10 mm.

The simulation utilizes the surface remesher, trimmed cell mesher, and prism layer mesher. The surface remesher remeshes the surface of the imported planing cambered surface to produce a quality surface mesh for the simulation. The trimmed cell mesher primarily produces hexahedral shaped cells. The prism layer mesher generates prismatic shaped cells on the wall for modelling the boundary layer flow.

The simulation mesh consist of a background mesh with two free surface mesh refinements. The background mesh is shown in Figure 2.8 and represents the simulation environment. The velocity inlet noted in Figure 2.8 is prescibed an inlet speed of 9.0 m/s and a volume fraction controlled by the VOF model. The pressure outlet noted in Figure 2.8 is governed by the hydrostatic pressure of the water and the VOF model. The remaining background mesh boundaries are defined as a symmetry plane. The free surface mesh refinements are boxed in Figure 2.9. The free surface mesh refinements generates a fier mesh to improve predictions of the water flow around the surface and in the wake aft of the planing surface where the vessel in question will have a dry after body and a surface piercing hydrofoil.

The background mesh has a total length of 3.9 meters between velocity inlet and pressure outlet with a width between the symmetry wall and side wall of 1.5 meters. The larger of the two free surface refinements in Figure 2.9 has a relative X and Y direction size refinement of 0.04 meters and 0.02 meters in the relative Z direction. The larger mesh refinement has a total length of 3.1 meters, a width of 1.5 meters from the symmetry wall, and a height of 0.2 meters. The smaller and further refined free surface refinement has a relative X and Y direction size refinement of 0.004 meters and 0.002 meters in the relative Z direction. The small free surface mesh refinement has a length of 1.4 meters, a width of 0.26 meters from the symmetry plane, and a height of 0.1 meters. The planing surface bottom consisting of the forebody, cambered section, and transom have a prism layer consisting of three layers with a total thickness of 0.002 meters and a stretching ratio of 1.2. The stretching ratio value defines the thickness of each prism cell layer relative to the previous layer. The planing surface refinement has a target cell size of 0.004 with a minimum cell size of 0.002 meters.

The mesh is also given a surface growth rate ratio 1.1 which limits the size of the the connecting mesh edges.

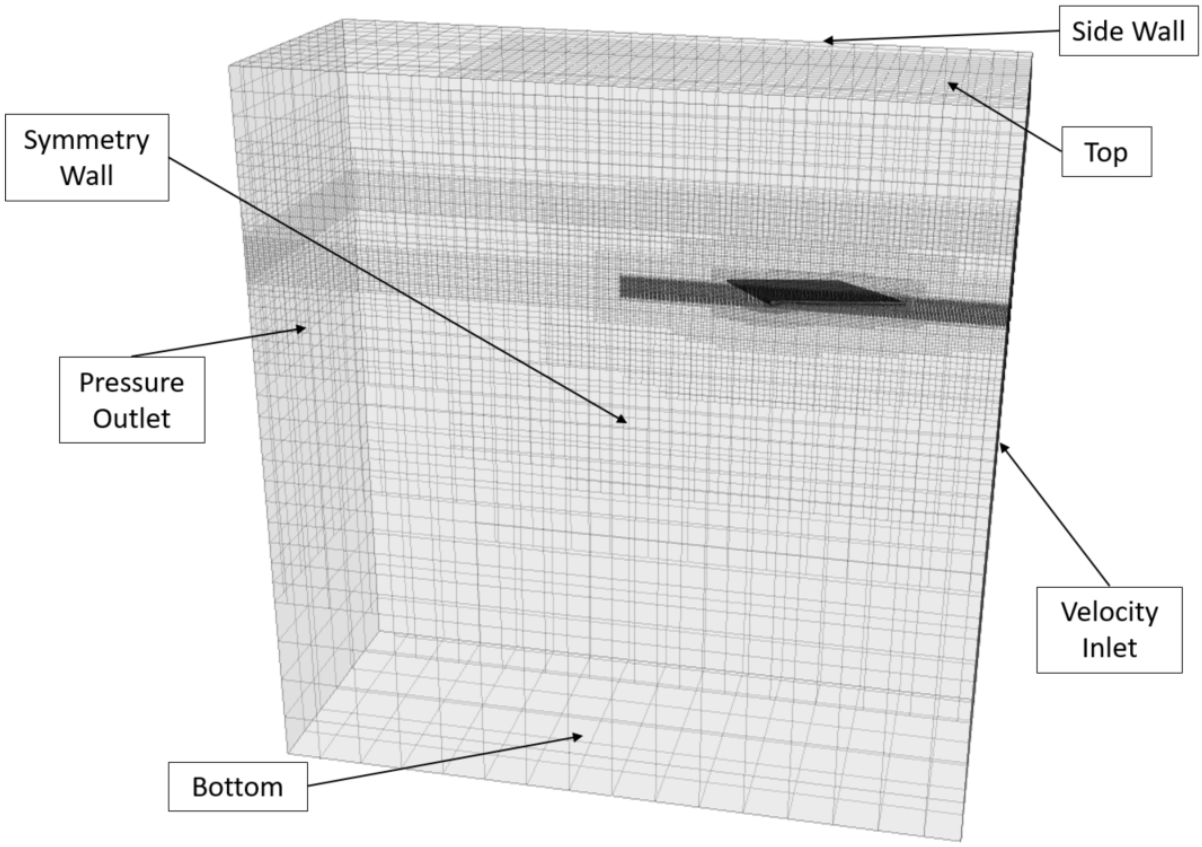

Figure 2.8: CFD Fixed Position Simulation Environment Setup

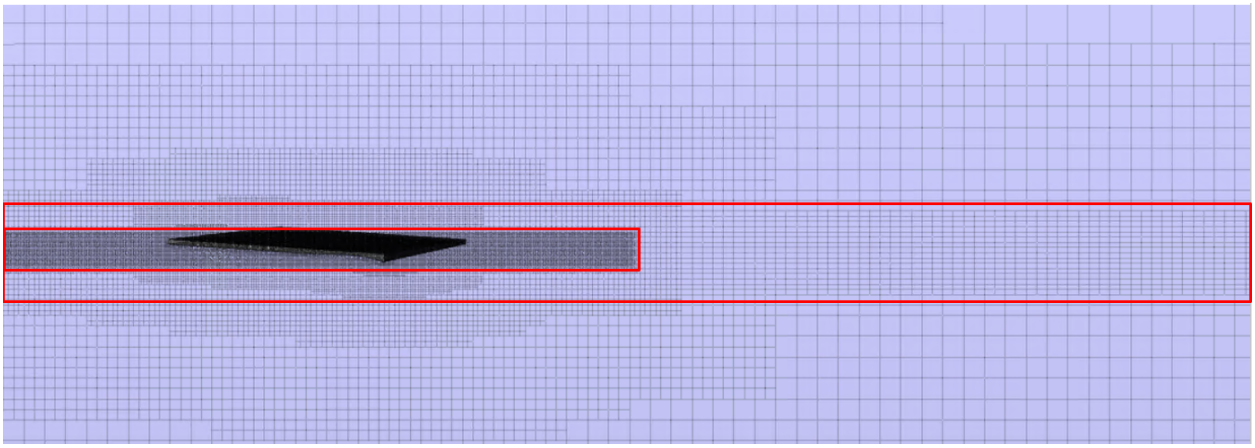

Figure 2.9: CFD Fixed Position Mesh with Large and Small Free Surface Refinement Mesh Boxed in Red

2.3.2 Fixed Position Mesh Uncertainty

The calculation of the mesh uncertainty is performed using the recommended procedures and guidelines from the International Towing Tank Conference (ITTC) in reference [8]. The mesh uncertainty study is performed using the minimum of three meshes with an average cubic cell count ratio 1.7. The mesh setup and number of cells for each refinement is presented in Tables 2.1–2.3. The mesh scene for each grid refinement is shown in Figures 2.10-2.12. The mesh scenes have a transverse plane to show difference in mesh refinements.

Table 2.1: Fixed Position Large Free Surface Mesh Refinements

Refinement #	# Cell (M)	r_{avg}	Relative Cell Size X [m]	Y [m]	Z [m]
1	0.567	–	0.07	0.07	0.035
2	2.517	1.64	0.04	0.04	0.02
3	15.457	1.83	0.03	0.03	0.015

Table 2.2: Fixed Position Small Free Surface Mesh Refinements

Refinement #	# Cell (M)	r_{avg}	Relative Cell Size X [m]	Y [m]	Z [m]
1	0.567	–	0.007	0.007	0.0035
2	2.517	1.64	0.004	0.004	0.002
3	15.457	1.83	0.003	0.003	0.0015

Table 2.3: Fixed Position Planing Surface Mesh Refinements

Refinement #	# Cell (M)	r_{avg}	Target Surface Size X [m]	Minimum Surface Size Y [m]	Prism Layer Thickness Z [m]
1	0.567	–	0.007	0.0035	0.0035
2	2.517	1.64	0.004	0.002	0.002
3	15.457	1.83	0.003	0.0015	0.0015

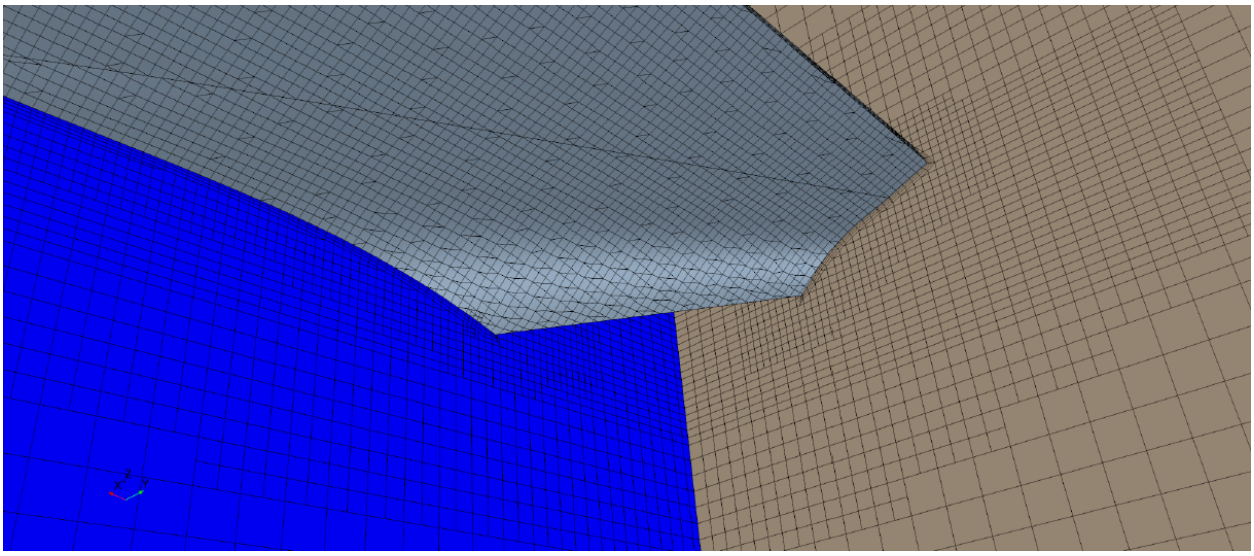

Figure 2.10: Run 16 – Fixed Position Mesh Refinement 1

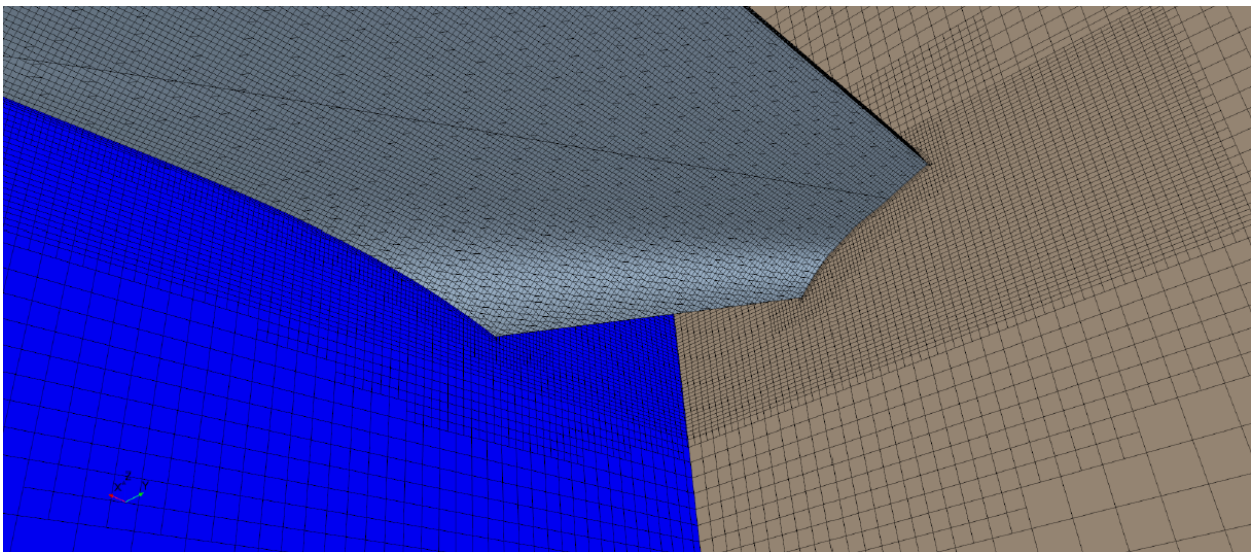

Figure 2.11: Run 16 – Fixed Position Mesh Refinement 2

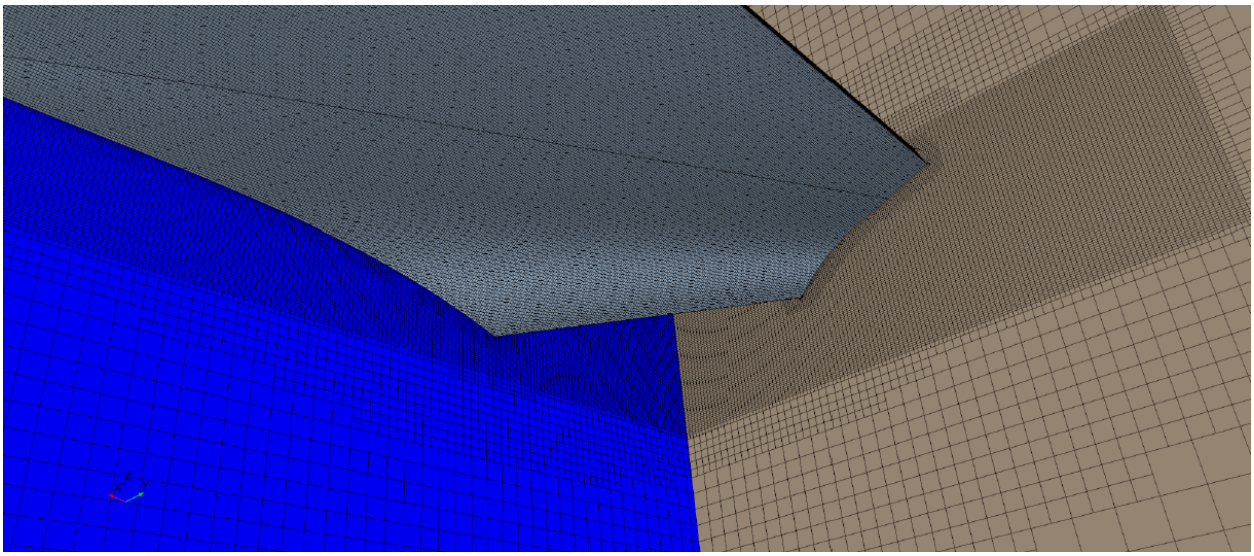

Figure 2.12: Run 16 – Fixed Position Mesh Refinement 3

The lift and drag values for the three mesh refinements discussed are reported in Table 2.4. Performing the calculations for mesh uncertainty following the ITTC procedure, the lift results are monotonically converging. The lift results have an uncertainty of 0.13 pounds. However, the drag is not showing divergence. Further mesh refinement would be necessary to obtain convergence for the drag. Further mesh refinement was not performed for the fixed position cases due to lack of agreement for lift values between EFD and CFD presented in Section 2.3.3.

Refinement #	Lift [lbf]	Drag [lbf]
1	40.057	7.013
2	40.582	7.032
3	40.782	7.139

Table 2.4: Fixed Position Run 16 – Lift and Drag Values with Varying Mesh Refinements

2.3.3 Fixed Position Results

CFD simulations results obtained with the second mesh refinement are compared with the experimental results for validation. During the experiment the weight of the model was applied, the trim was fixed, the model towed at constant speed of 9 m/s, and was free to heave. At steady state the model reaches the dynamic draft that achieves the equilibrium between the hydrodynamic forces and the weight.

Lift-to-Drag Ratios

The lift-to-drag plots for fixed position simulations are shown in Figures 2.13–2.18. The full results for fixed position simulations are located in Appendix Section A.2.1. The CFD results for step-A with the fixed position simulation showed a poor correlation with the experimental results with the exception to run 16. Run 16 is step-A at a nominal trim of 4 degrees with a experimental weight of 40 pounds. The CFD lift and drag results have a less than 3% difference with the experimental results. The CFD and experimental results for run 16 are shown in Figure 2.14. Step-B showed a stronger overall correlation with the experimental results, but were still considered weak.

The initial fixed position results lead to trying the SST k-omega turbulence model. The results from the difference turbulence model produce similar lift values with an increase in drag force. Due to the small change in results by changing the turbulence model, sensitivity studies were conducted on the planing surfaces position in the simulation and potential surface roughness. The sensitivity studies, presented in Section 2.3.4, explore the experimental uncertainty in the trim angle and wetted keel length that effect the fixed position of the model in the fixed positions simulation. The sensitivity studies still showed no appreciable improvement on the CFD results.

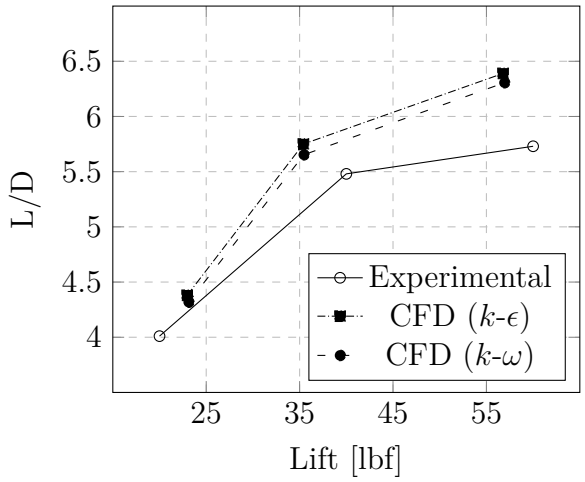

Figure 2.13: Step-A Lift-to-Drag (Fixed Position Nominal Trim of 3°)

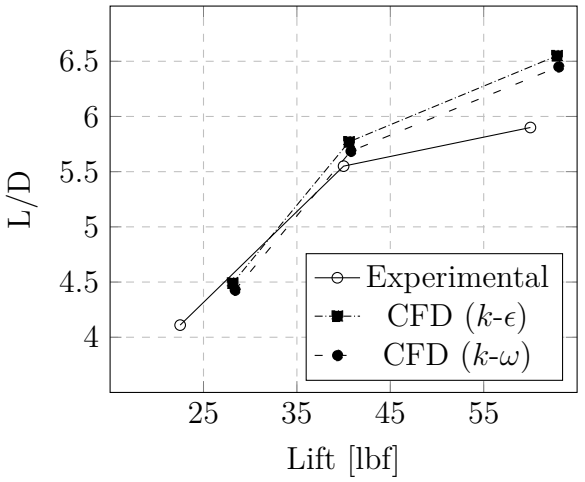

Figure 2.14: Step-A Lift-to-Drag (Fixed Position Nominal Trim of 4°)

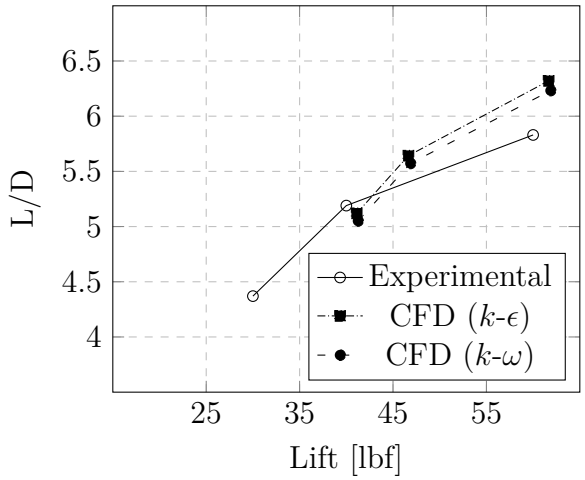

Figure 2.15: Step-A Lift-to-Drag (Fixed Position Nominal Trim of 5°)

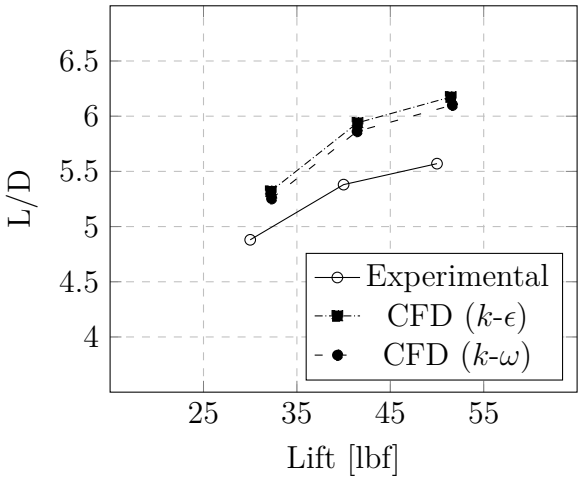

Figure 2.16: Step-B Lift-to-Drag (Fixed Position Nominal Trim of 3°)

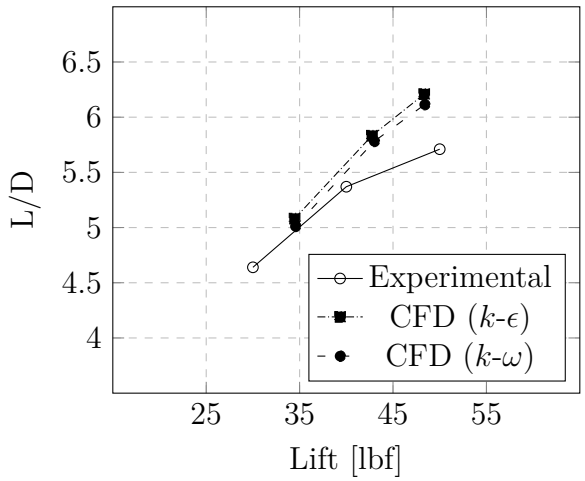

Figure 2.17: Step-B Lift-to-Drag (Fixed Position Nominal Trim of 4°)

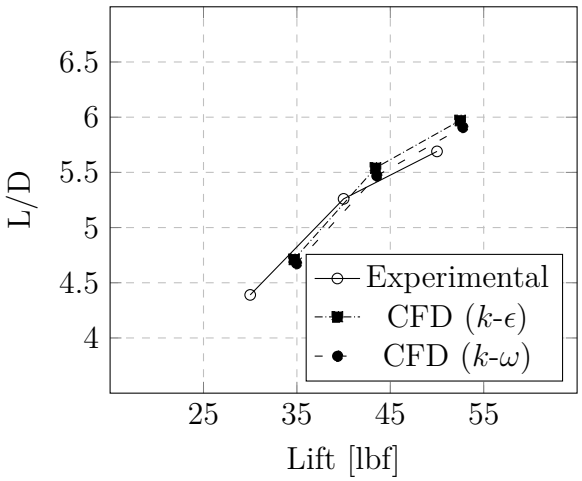

Figure 2.18: Step-B Lift-to-Drag (Fixed Position Nominal Trim of 5°)

Wake Profile Comparison

For the design of a stepped planing hull, great interest is given to the prediction of the free surface shape in the wake of the stepped planing surface. Dr. Morabito, a professor at the USNA, developed a technique, based on computer vision reconstruction of the 3D shape of the wake measured on transverse planes (transverse cuts) at two different longitudinal distance from the step (see lasers sheets in Figure 2.19a. The wake profile results showed a strong correlation between the experiment and fixed position simulations for both step designs at all nominal trim angles and loads. The wake profile comparison for run 26 with fixed conditions is shown in Figure 2.20. The green and red dots represent the CFD data and

the black dots represent the experimental data. The corresponding image of the experimental run with the green and red laser locations are shown in Figure 2.19a which can be compared to Figure 2.19b. Simulation for run 26 have an error for lift and drag of 12% and 16%, respectively, but still have a strong wake profile comparison. The decision to proceed to free heave simulations came due to the validation of the wake profiles for fixed simulations despite no validation of the hydrodynamic forces. These results are discussed in Section 2.4.

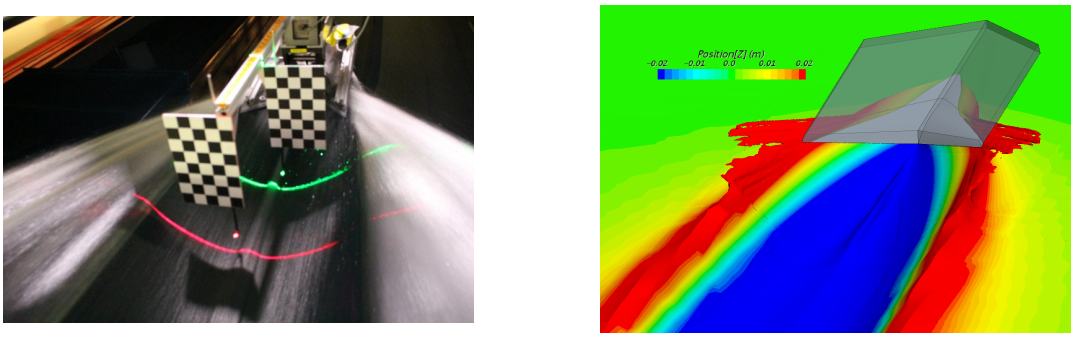

(a) EFD

(b) CFD

Figure 2.19: Laser Wake Profile (Run 26)

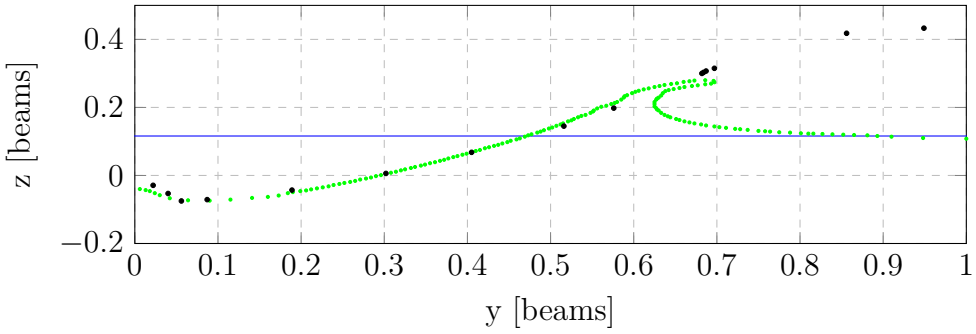

(a) Green Laser

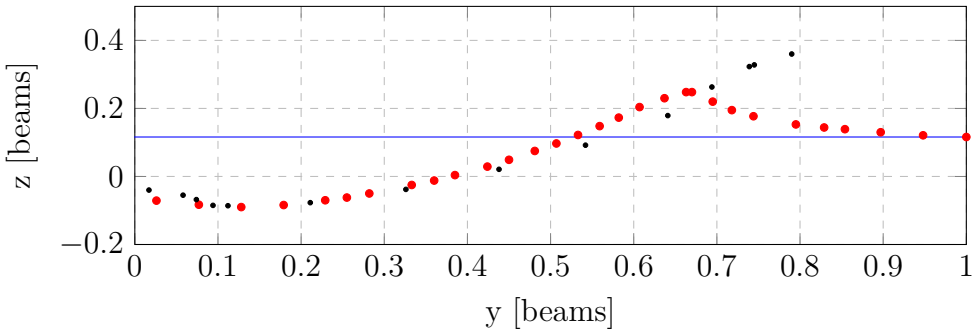

(b) Red Laser

Figure 2.20: Fixed Position Wake Profile Comparison (Run 26)

Pressure and Friction Coefficients

Important to note the difference in pressure distribution on the planing surface for step-A and step-B. Step-A location of maximum pressure is located on the keel as shown in Figure 2.21. Step-B maximum pressure occurs in two locations instead of one like Step-A as shown in Figure 2.22. The two regions having maximum camber correlate quite well with the region of maximum pressure for both step-A and step-B. This difference in maximum pressure location for step-A and step-B is consistent for all loads and trim angles.

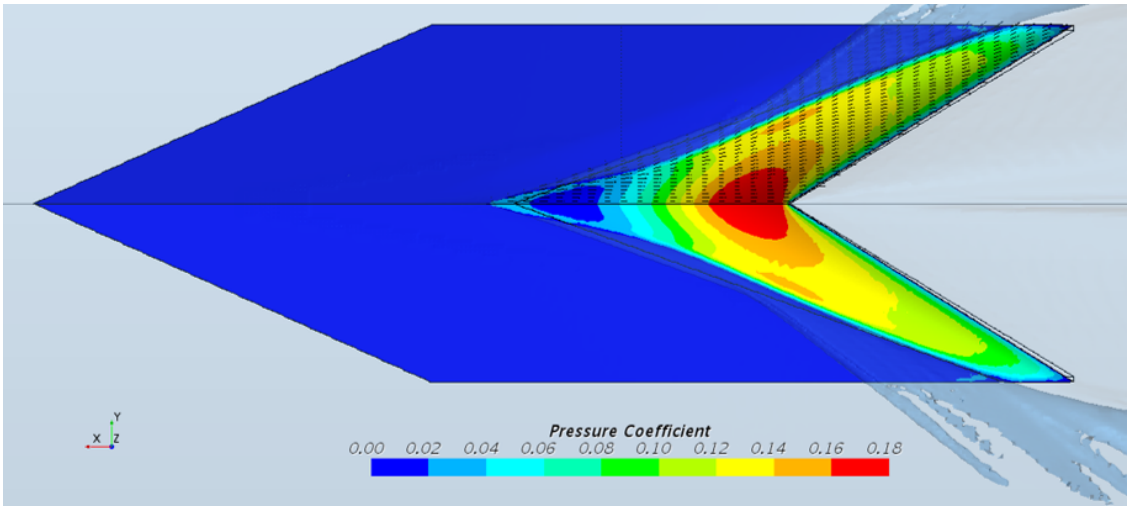

Figure 2.21: Fixed Position Step-A at $\tau = 4°$ and $L = 40lbs$ (Run 16 – Coefficient of Pressure Distribution

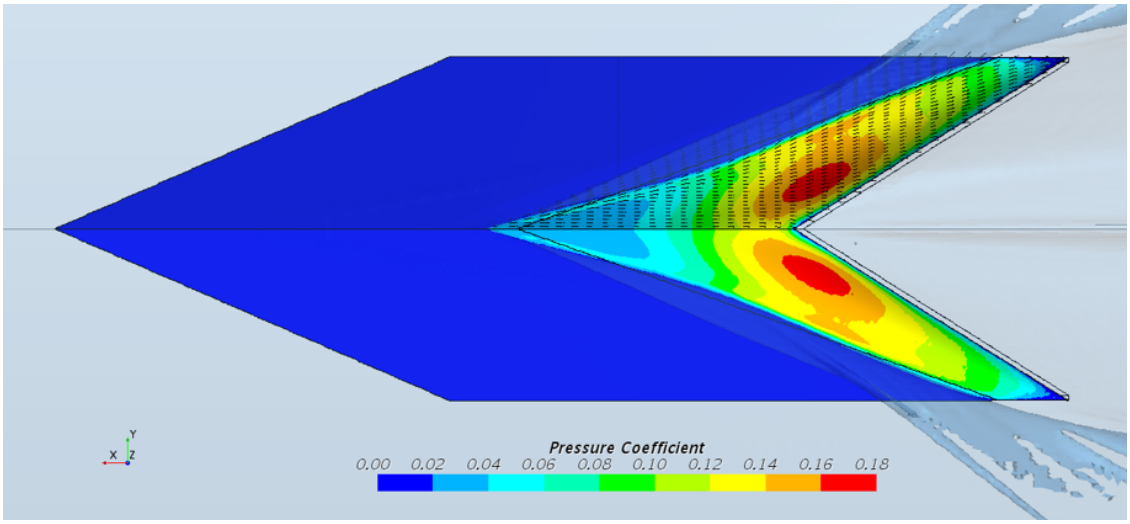

Figure 2.22: Fixed Position Step-B at $\tau = 4°$ and $L = 40lbs$ (Run 31 – Coefficient of Pressure Distribution

2.3.4 Fixed Position Sensitivity Studies

Fixed Position Uncertainty in Trim Study

The test memorandum from the USNA Hydromechanics Laboratory [7] stated that the model was not completely fixed and required a inclinometer to get an accurate trim angle. The inclinometer has an uncertainty of 0.1 degrees. To test the sensitivity to trim angle readings, runs 10, 16, and 26 were tested at trim angles plus and minus 0.1 degrees from the reported trim angle value. The results of this study and their comparison to the experimental results are presented in Tables 2.5–2.7. The results of this study showed small variations in the predicted lift and drag values and it was determined that the uncertainty in trim angle was not the cause of the differences between experimental and CFD results.

Table 2.5: Fixed Position Run 10 - Trim ±0.1° Data

	Trim [°]	Lift [lbf]	%E(L)	Drag [lbf]	%E(D)	L/D
CFD	3.85	26.95	20%	6.10	11%	4.42
	3.95	28.12	25%	6.27	15%	4.49
	4.05	29.39	31%	6.44	18%	4.56
EFD	3.95	22.5	-	5.47	-	4.11

Table 2.6: Fixed Position Run 16 - Trim ±0.1° Data

	Trim [°]	Lift [lbf]	%E(L)	Drag [lbf]	%E(D)	L/D
CFD	3.76	38.72	-3.2%	6.85	-4.8%	5.65
	3.86	40.58	1.5%	7.03	-2.3%	5.77
	3.96	42.49	6.2%	7.26	0.9%	5.85
EFD	3.86	40	-	7.20	-	5.55

Table 2.7: Fixed Position Run 26 - Trim ±0.1° Data

	Trim [°]	Lift [lbf]	%E(L)	Drag [lbf]	%E(D)	L/D
CFD	2.62	33.16	-17%	5.95	-18%	5.57
	2.72	35.40	-12%	6.16	-16%	5.75
	2.82	37.69	-5.8%	6.39	-12%	5.90
EFD	2.72	40	-	7.30	-	5.48

Fixed Position Uncertainty in Wetted Keel Length Study

The experimental wetted keel length is used to vertically position the planing surface due to the inaccuracies associated with experimental draft values. The wetted keel lengths are determined by pre-measured markings on the plexiglas. To test the sensitivity to potential uncertainty in the measured wetted keel length, the planing surfaces were vertically placed assuming a plus, or minus, 5% of the experimental wetted keel length. This sensitivity study was conducted for the same runs from the trim sensitivity study, runs 10, 16, and 26. The results of this sensitivity study are presented in Tables 2.8–2.10. The results showed no appreciable changes in the predicted lift and drag values.

Table 2.8: Fixed Position Run 10 - Wetted Keel Length ±5% Data

	L_k [in]	Lift [lbf]	%E(L)	Drag [lbf]	%E(D)	L/D
CFD	4.75	27.27	21%	6.20	13%	4.40
	5	28.12	25%	6.27	15%	4.49
	5.25	28.88	28%	6.33	16%	4.56
EFD	5	22.5	-	5.47	-	4.11

Table 2.9: Fixed Position Run 16 - Wetted Keel Length ±5% Data

	L_k [in]	Lift [lbf]	%E(L)	Drag [lbf]	%E(D)	L/D
CFD	9.5	38.21	-4.5%	6.88	-4.4%	5.55
	10	40.58	1.5%	7.03	-2.3%	5.77
	10.5	42.83	7.1%	7.24	0.5%	5.92
EFD	10	40	-	7.20	-	5.55

Table 2.10: Fixed Position Run 26 - Wetted Keel Length ±5% Data

	L_k [in]	Lift [lbf]	%E(L)	Drag [lbf]	%E(D)	L/D
CFD	14.25	33.20	-17%	5.95	-19%	5.58
	15	35.40	-12%	6.16	-16%	5.75
	15.75	37.59	-6.0%	6.38	-13%	5.90
EFD	15	40	-	7.30	-	5.48

Fixed Position Roughness Study

The simulations presented have assumed a smooth wall treatment for the planing surface. The production of the cambered planing surface required the surface to be sanded to smooth the surface of imperfections from printing. To test possible roughness scenarios, nine additional fixed position simulations were ran for different roughness heights.

The roughness study tested roughness heights 50, 100, and 150 microns. The addition of roughness has a small effect on the predicted lift, but large effect on the predicted drag. A roughness height of 50 microns produced the strongest correlation with the experimental results as shown in Figure 2.23. The predicted drag error is reduced to under 3% for runs 41 and 42 with a roughness height of 50 microns as shown in Table 2.11. The addition of roughness has a negative effect on the prediction of the drag with no change to the inaccurate lift prediction for run 40.

Table 2.11: Fixed Position Roughness Study Data

Run #	Trim [°]	L_k [in]	r [μm]	Lift [lbf]	%E(L)	Drag [lbf]	%E(D)	L/D
40	3.09	12.7	EFD	30	-	6.15	-	4.88
			0	32.20	7.3%	6.05	-1.6%	5.32
			50	32.10	7.0%	6.60	7.2%	4.87
			100	32.03	6.8%	6.84	11%	4.68
			150	32.00	6.7%	6.91	12%	4.63
41	3.01	16	EFD	40	-	7.44	-	5.38
			0	41.49	3.7%	6.98	-6.1%	5.94
			50	41.20	3.0%	7.63	2.5%	5.40
			100	41.01	2.5%	7.95	6.9%	5.16
			150	40.98	2.5%	8.02	7.8%	5.11
42	3.01	20	EFD	50	-	8.98	-	5.57
			0	51.47	2.9%	8.34	-7.2%	6.17
			50	50.92	1.8%	9.22	2.6%	5.53
			100	50.56	1.1%	9.68	7.8%	5.23
			150	50.57	1.1%	9.76	8.6%	5.18

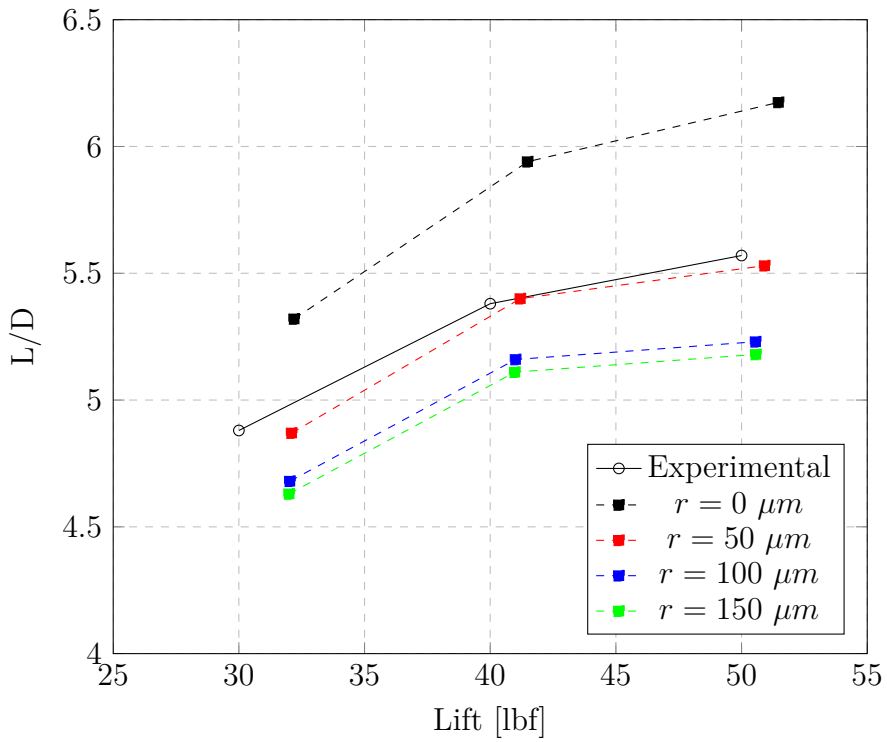

Figure 2.23: Step-B Lift-to-Drag Roughness Study (Fixed Position Nominal Trim of 3°)

The friction and pressure coefficient plots for run 41 at various roughness levels are shown in Figures 2.24–2.27. The drag values for the planing surface with roughness height of 100 and 150 microns did not vary a large amount in Table 2.11 and that same trend can be seen in Figures 2.26 and 2.27. Varying the roughness heights from smooth to 150 microns showed no effect on the coefficient of pressure.

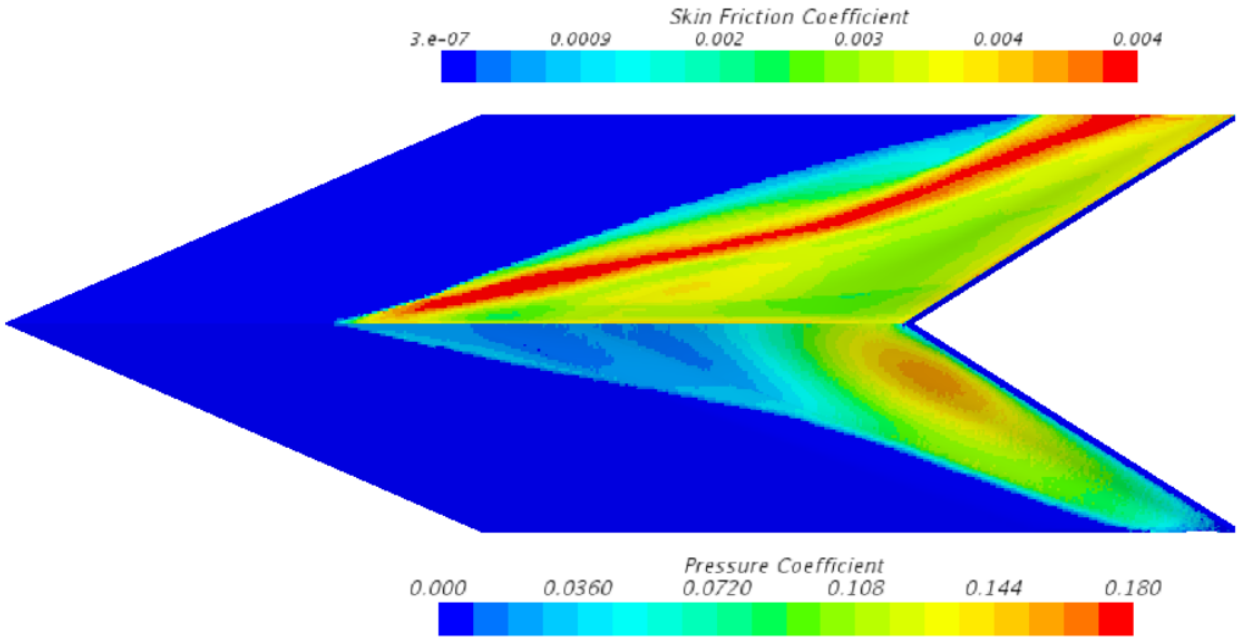

Figure 2.24: Smooth Surface Run 41 – Friction and Pressure Coefficient Plots

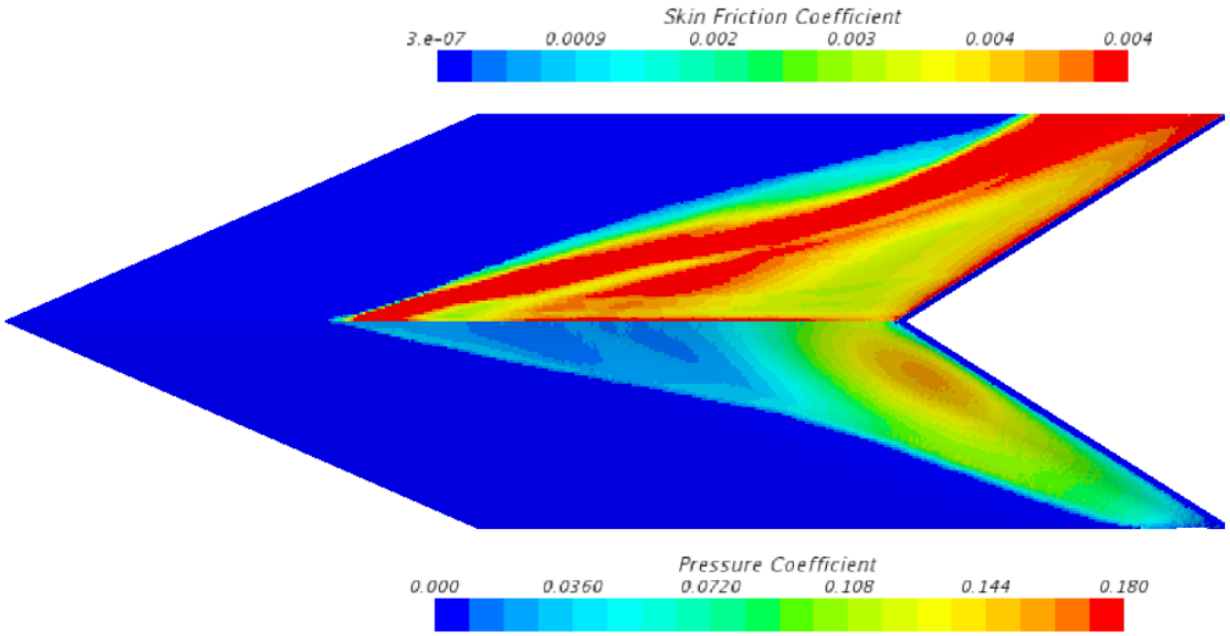

Figure 2.25: Surface Roughness Height of 50μm Run 41 – Friction and Pressure Coefficient Plots

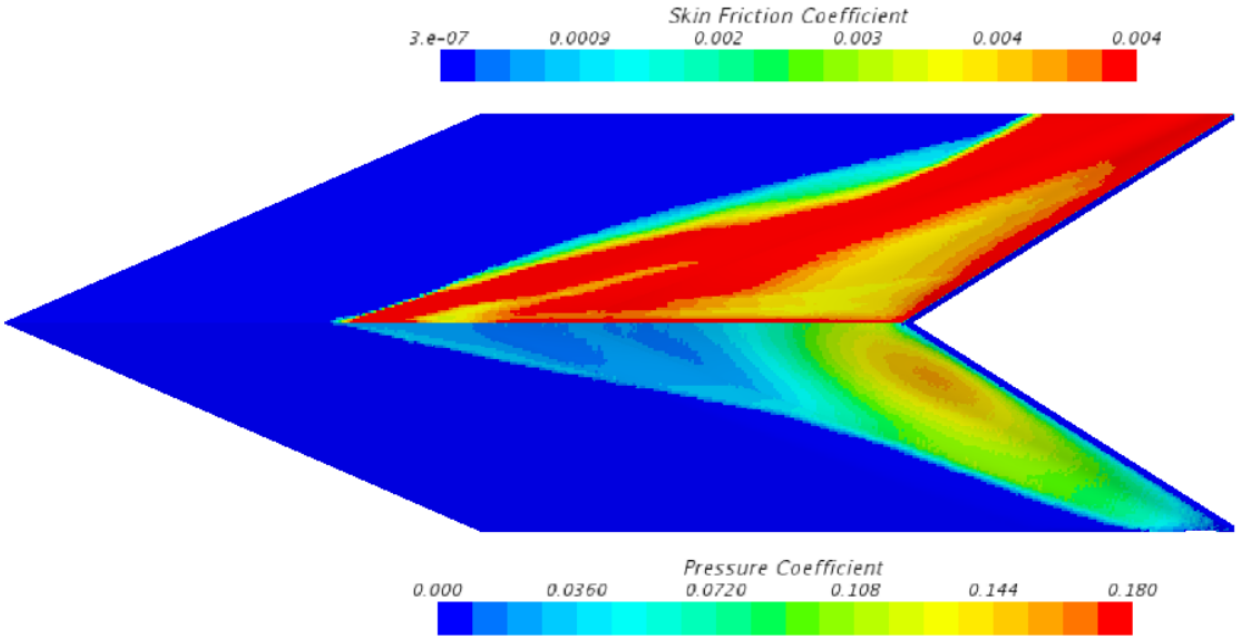

Figure 2.26: Surface Roughness Height of 100μm Run 41 – Friction and Pressure Coefficient Plots

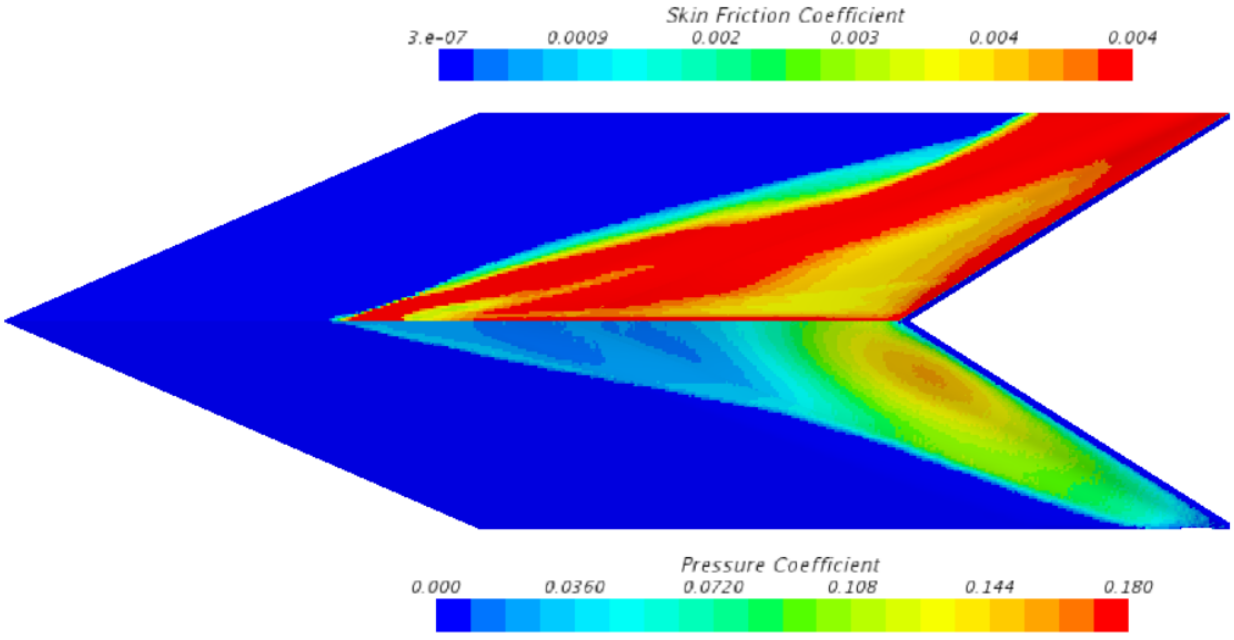

Figure 2.27: Surface Roughness Height of 150μm Run 41 – Friction and Pressure Coefficient Plots

2.4 CFD Free Heave Planing Conditions

The validation of the simulation in Star CCM+ switches from fixed position to free heave simulations. The wetted keel length and trim angle are initially used to position the planing surface as performed in the fixed position simulations. The model is now allowed to heave freely as was the case for the experimental results. In addition to drag forces, the trim moment, wetted keel lengths, drafts, and wake profiles will be analyzed in detail.

2.4.1 Free Heave CFD Setup

The free heave simulations are setup very similar to the fixed position simulations with the same meshers and free surface refinements applied. With the addition of the overset mesh, a reflection issue from the pressure outlet was occuring which led to the lengthening of the background mesh from 3.9 meters to 9.9 meters. The smaller and more refined free surface refinement is larger in all directions. The finer free surface is wider to increase accuracy of the spray away from the hull increasing from 0.26 meters to 1.25 meters from the symmetry plane. The refinement is lengthen from 1.4 meters to 1.8 meters to have a fine mesh at the location of the hydrofoil. The final change to the free surface refinement is the vertical distance is increased from 0.1 meter to 0.44 meters to allow for the overset mesh to freely move up and down without the overset mesh moving outside the mesh refinement region.

The overset mesh is marked by the smallest of the three red boxes in Figure 2.30 and is highligthed in Figure 2.29 with a total length of 1.0 meter, a width of 0.18 from symmetry plane, and a height of 0.15 meters. The overset mesh is set to have the same mesh as the finer free surface mesh discussed in Section 2.3.1. The overset mesh encloses the planing surface and is set to heave with the planing surface while the background and the two free surface refinement meshes remains stationary. The boundary cells of the overset mesh are called donor cells and the background cells that are overlapping the donor cells are called acceptor cells. Background cells inside the overset mesh and not considered an acceptor cell become inactive. The transition from background cells to acceptor and donor cells to overset cells can be seen in Figures 2.31–2.33 as a darker patch of cells resembling a box. Important to create a large enough free surface refinement so that the overset mesh does not heave near or below the boundary of the refinement. During the validation studies, a difference in the convergence of the results was seen with respect to the fixed attitude case.

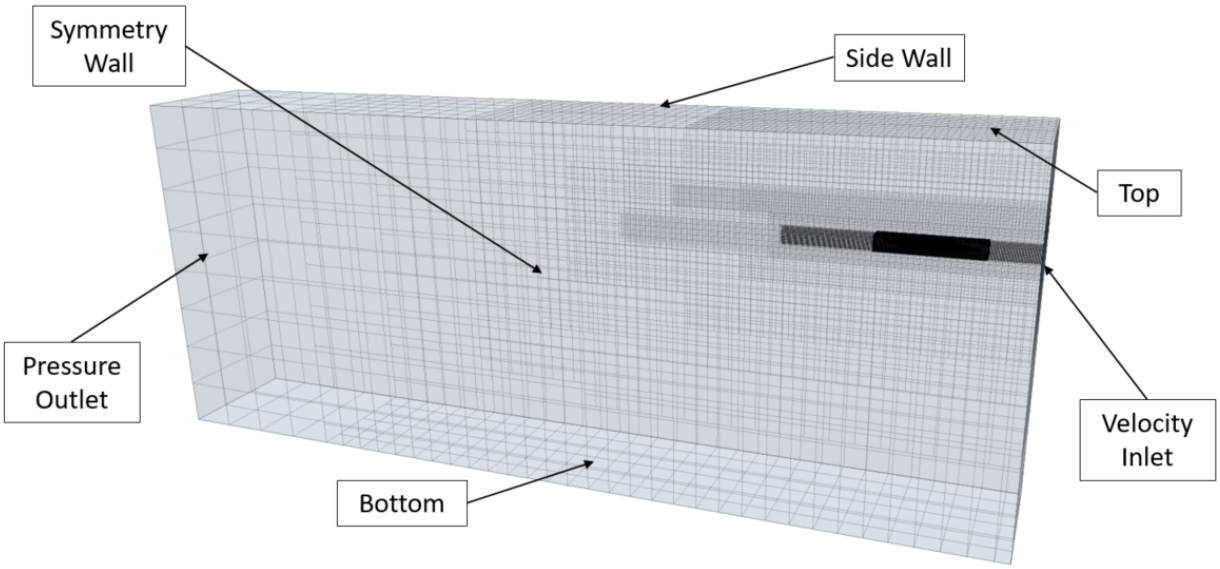

Figure 2.28: CFD Free Heave Simulation Enviroment Setup

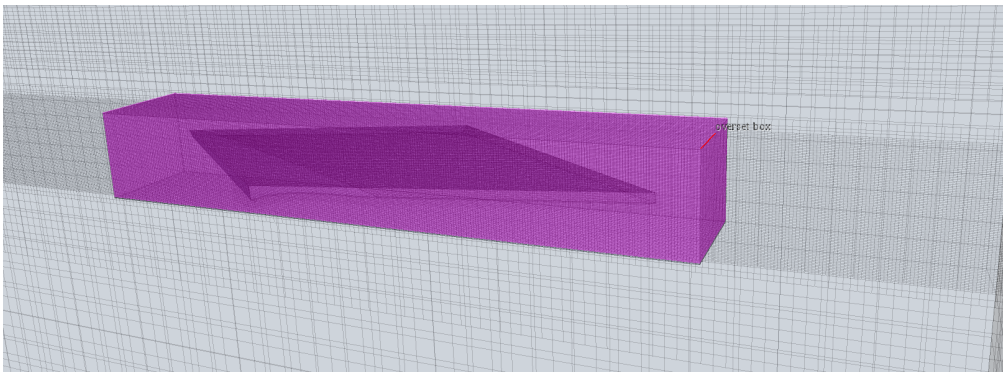

Figure 2.29: CFD Free Heave Simulation Overset Mesh

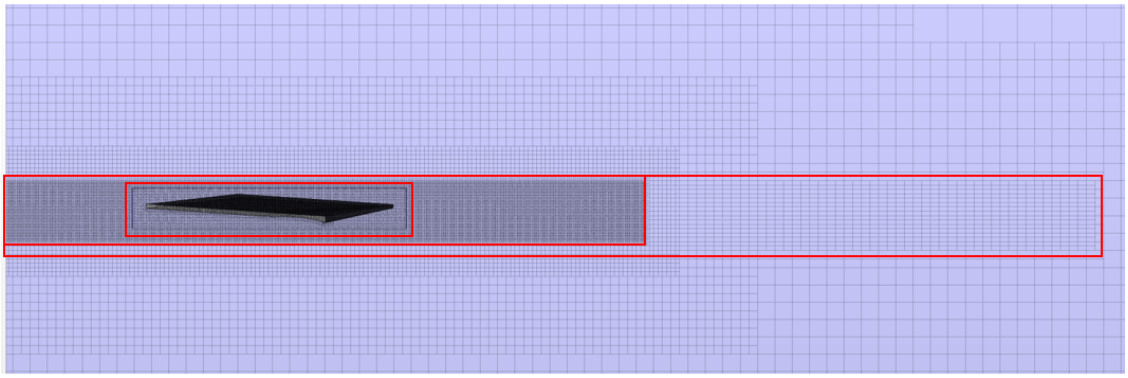

Figure 2.30: CFD Free Heave Mesh

2.4.2 Free Heave Mesh Uncertainty

The calculation of the mesh uncertainty is performed the same as mention in Section 2.3.2. The mesh uncertainty study is again performed using the minimum of three meshes with an average cubic cell count ratio of 1.1. The mesh setup and number of cells for each refinement is presented in Tables 2.12–2.14. The mesh scene for each grid refinement is shown in Figures 2.31-2.33. The mesh scenes have a transverse plane to show difference in mesh refinements.

Table 2.12: Free Heave Large Free Surface Mesh Refinements

Refinement #	# Cell (M)	r_{avg}	Relative Cell Size X [m]	Y [m]	Z [m]
1	5.758	–	0.0448	0.048	0.0224
2	8.055	1.12	0.04	0.04	0.02
3	11.481	1.12	0.0355	0.0355	0.0177

Table 2.13: Free Heave Small Free Surface Mesh Refinements

Refinement #	# Cell (M)	r_{avg}	Relative Cell Size X [m]	Y [m]	Z [m]
1	5.758	–	0.00448	0.00448	0.00224
2	8.055	1.12	0.004	0.004	0.002
3	11.481	1.12	0.00355	0.00355	0.00177

Table 2.14: Free Heave Planing Surface Mesh Refinements

Refinement #	# Cell (M)	r_{avg}	Target Surface Size X [m]	Minimum Surface Size Y [m]	Prism Layer Thickness Z [m]
1	5.758	–	0.00448	0.00224	0.00224
2	8.055	1.12	0.004	0.002	0.002
3	11.481	1.12	0.00355	0.00177	0.00177

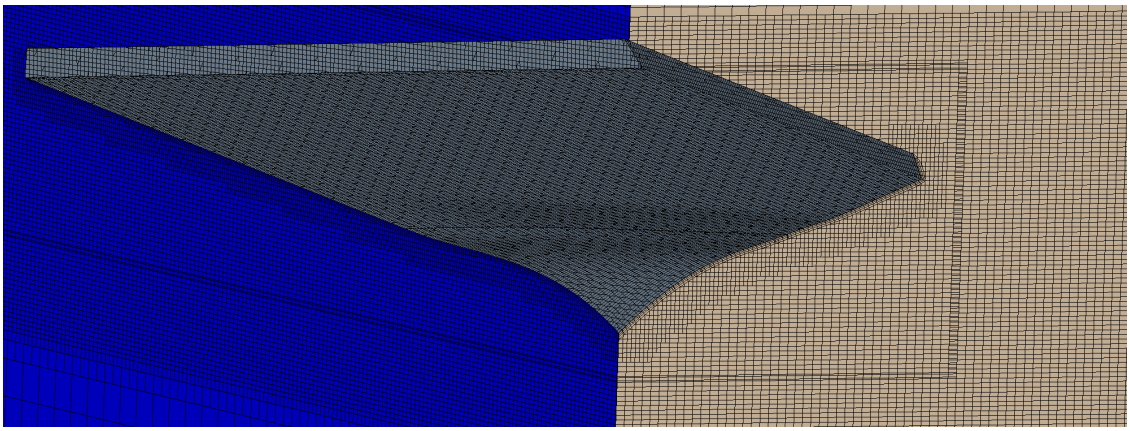

Figure 2.31: Run 16 – Free Heave Mesh Refinement 1

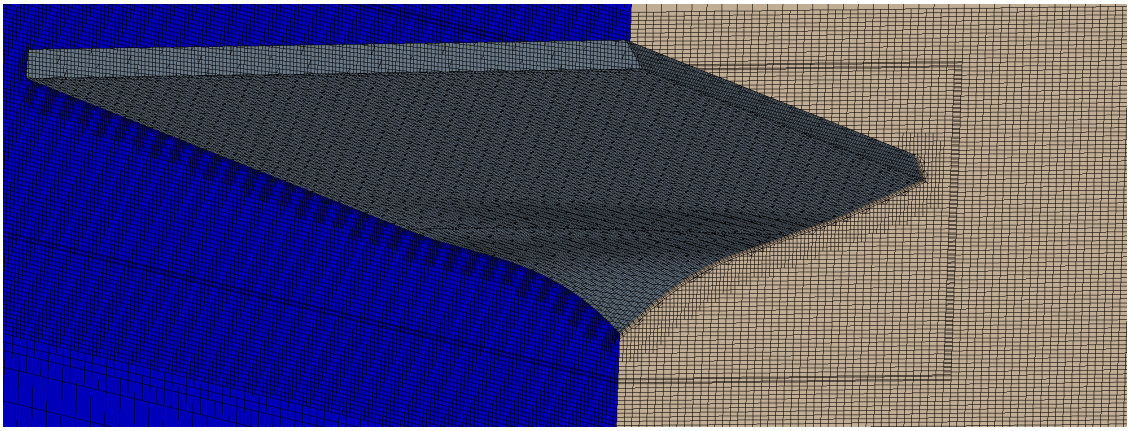

Figure 2.32: Run 16 – Free Heave Mesh Refinement 2

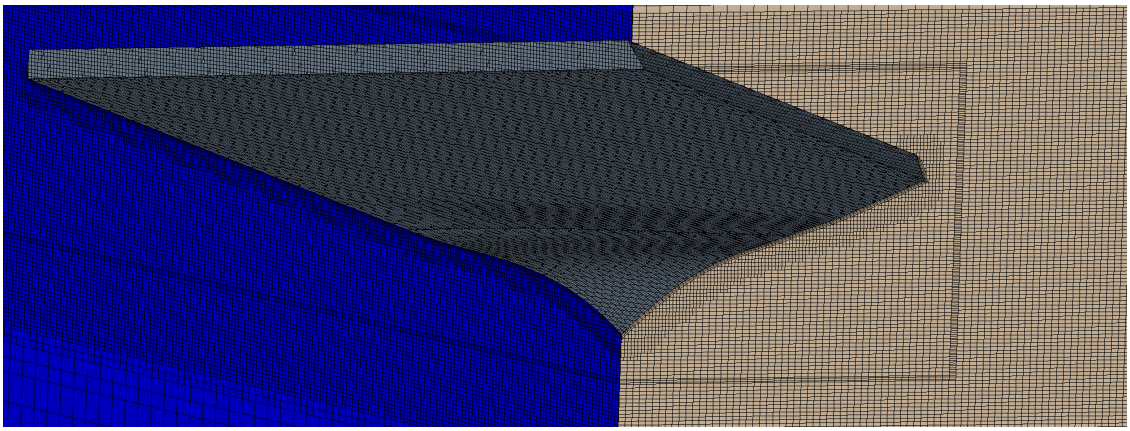

Figure 2.33: Run 16 – Free Heave Mesh Refinement 3

The drag and trim moment values for the three mesh refinements discussed for free heave are reported in Table 2.15. The convergence ratio for drag force and trim moment are less than zero giving an oscillatory convergence. Performing the mesh uncertainty study with more than three refinements, or increasing the average r value, would help give a monotonic convergence ratio. The uncertainty is calculated using the ITTC oscillatory convergence uncertainty equation resulting in an uncertainty of 0.0169 pounds and 0.418 pounds-inch for drag force and trim moment, respectively.

Refinement #	Drag [lbf]	Trim Moment [lbf-in]
1	6.998	-102.096
2	6.964	-101.773
3	6.968	-102.610

Table 2.15: Free Heave Run 16 – Drag and Trim Moment Values with Varying Mesh Refinements

2.4.3 Free Heave Results

The free heave results compare lift-to-drag, trim moment, wake profile, and wetted keel length. A table copy of the CFD results can be found in Appendix Section A.2.2 where the corresponding run numbers are listed. Sensitivity Studies utilizes the pressure and friction coefficient plots in Appendix Section A.3. Important note regarding the experimental data: run 48 has a reported trim angle that is not consistent with the data grouping trim angle given and is not predictable by CFD. Run 48 is the 60 pound case for step-B at a nominal trim angle of 3 degrees. The reported trim angle is 3.8 degrees which was used for CFD predictions.

Lift to Drag Ratios

The lift-to drag ratios for both step-A and step-B under predicted the drag for high load cases with a gradual increase in error with increase in load. Exception to this trend is step-A at a nominal trim of 5 degrees. The predicted drag values produced a drag error of less than 5% for low loads with an increase to 5%-10% at high load cases. In the fixed position simulations step-B shows a stronger agreement with the experimental data compared to step-A and this trend continues with the free heave simulations as shown in Figures 2.34-2.39.

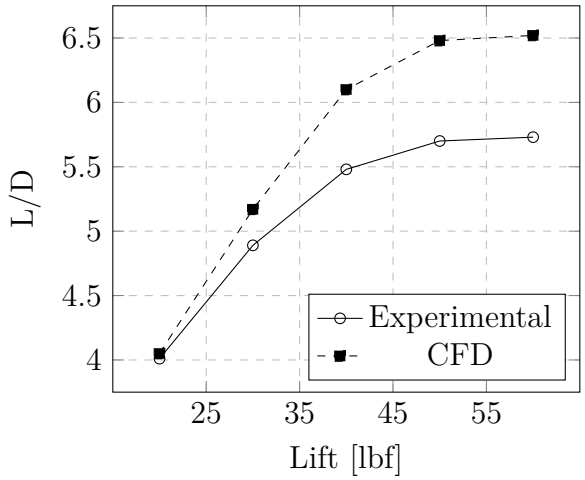

Figure 2.34: Step-A Lift-to-Drag (Free Heave Nominal Trim of 3°)

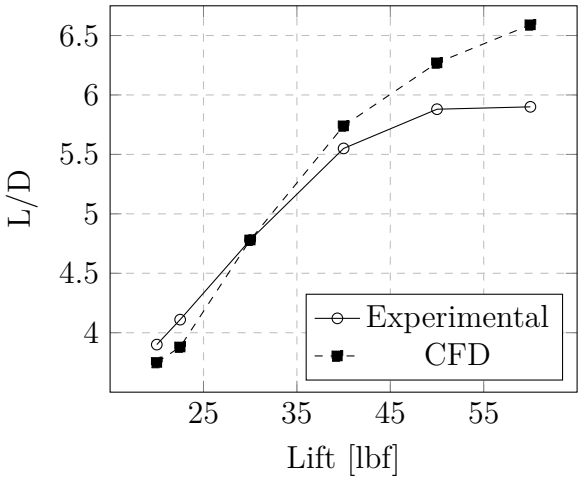

Figure 2.35: Step-A Lift-to-Drag (Free Heave Nominal Trim of 4°)

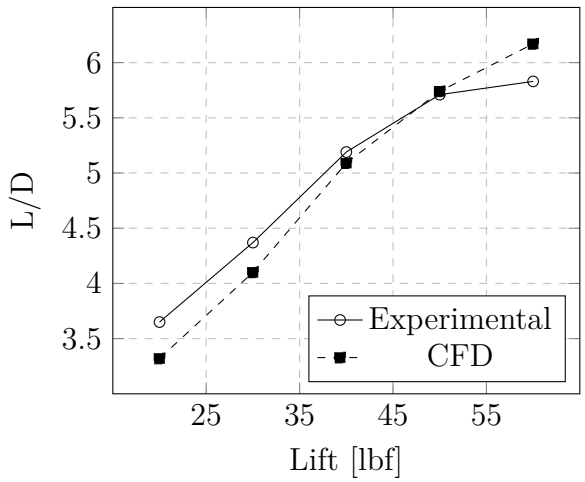

Figure 2.36: Step-A Lift-to-Drag (Free Heave Nominal Trim of 5°)

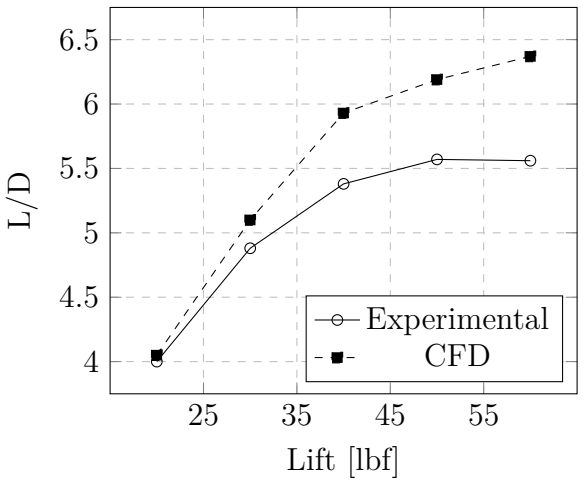

Figure 2.37: Step-B Lift-to-Drag (Free Heave Nominal Trim of 3°)

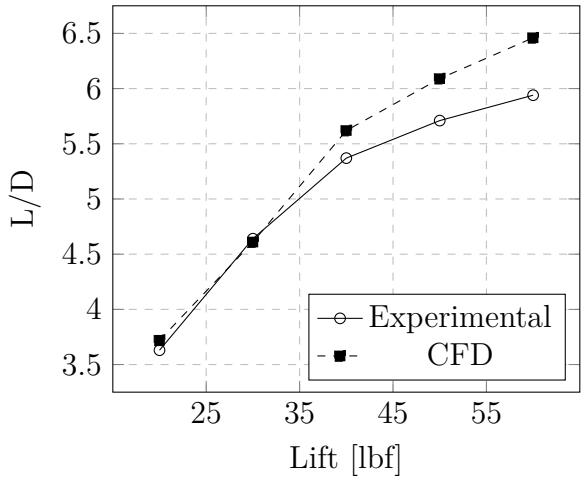

Figure 2.38: Step-B Lift-to-Drag (Free Heave Nominal Trim of 4°)

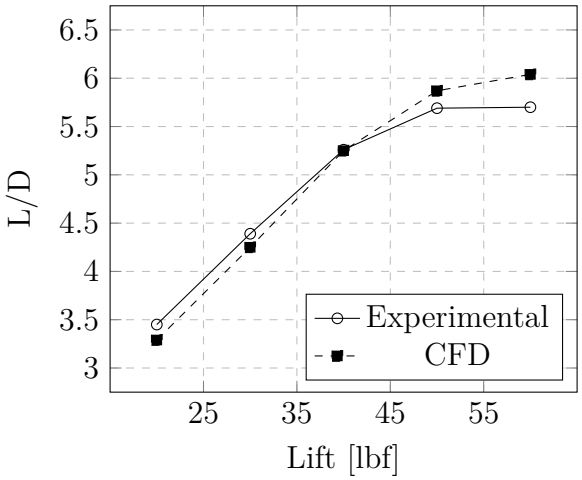

Figure 2.39: Step-B Lift-to-Drag (Free Heave Nominal Trim of 5°)

Moment Versus Lift

As seen for the lift-to-drag ratios, the accuracy of the predictions decreased with increasing loads with the exception to step-A at 5 degrees. The trim moment is under predicted as well for both step-A and step-B. For low loads, the predicted error ranged from 5% to 10%. For higher loads the predicted error is greater than 10%.

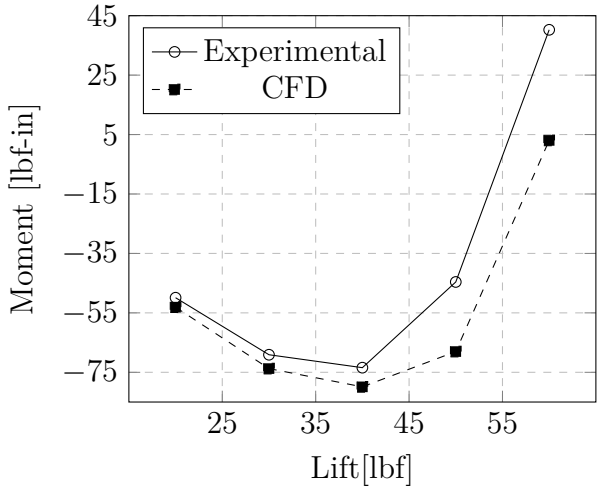

Figure 2.40: Step-A Trim Moment (Free Heave Nominal Trim of 3°)

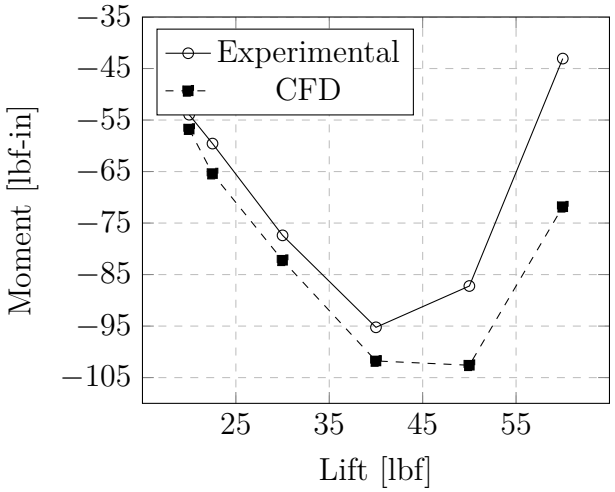

Figure 2.41: Step-A Trim Moment (Free Heave Nominal Trim of 4°)

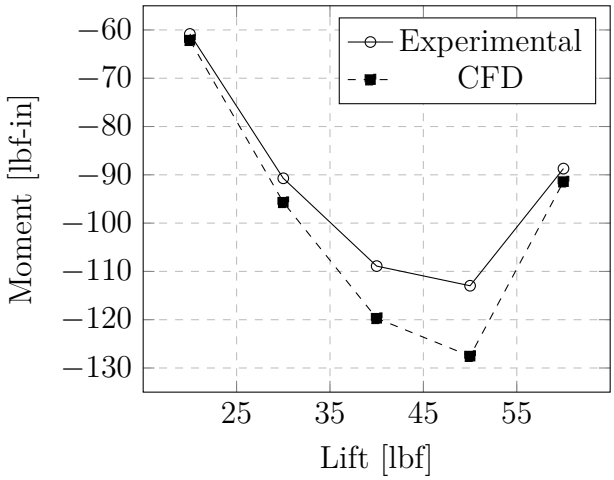

Figure 2.42: Step-A Trim Moment (Free Heave Nominal Trim of 5°)

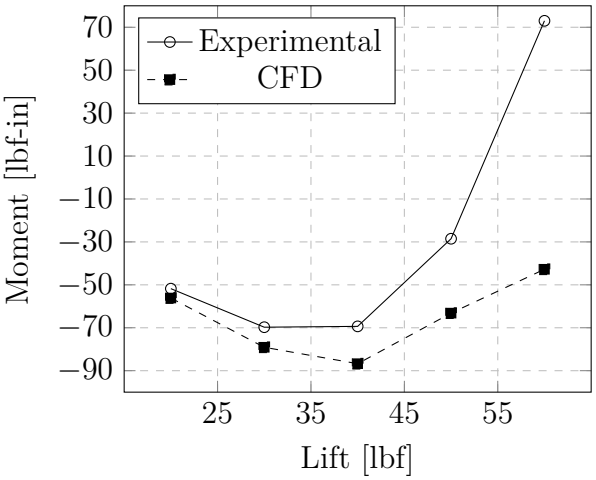

Figure 2.43: Step-B Trim Moment (Free Heave Nominal Trim of 3°)

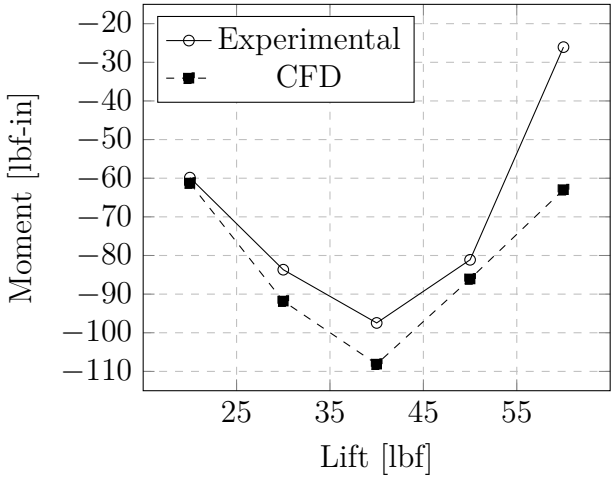

Figure 2.44: Step-B Trim Moment (Free Heave Nominal Trim of 4°)

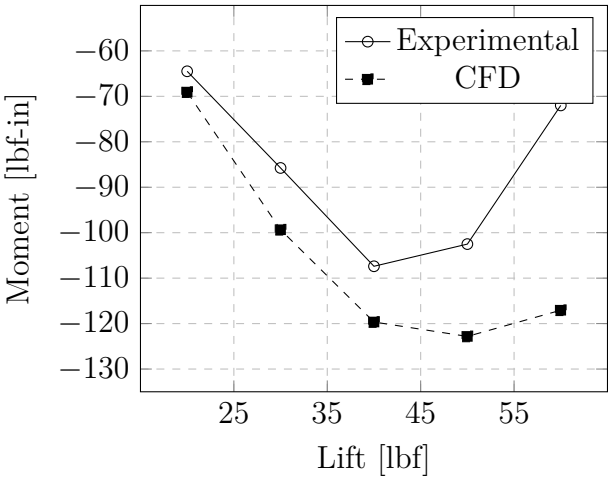

Figure 2.45: Step-B Trim Moment (Free Heave Nominal Trim of 5°)

Wake Profile Comparison

Experimental wake profiles are measured by green and red lasers and are represented by black dots in the wake profile plots. The CFD measured wake profiles are measured at the same locations and are represented by green and red dots to match the experimental laser colors. Consistent with the fixed position wake profile predictions, free heave also predicted the wake profile correct at both the red and green laser locations. In addition to predicting the wake within the beam of the planing surface, the increased size of the free surface refinement allowed for an improved predictions of the spray from the wake as shown in Figure 2.47. Wake profile comparison for all the runs can be found in Appendix Section A.4.

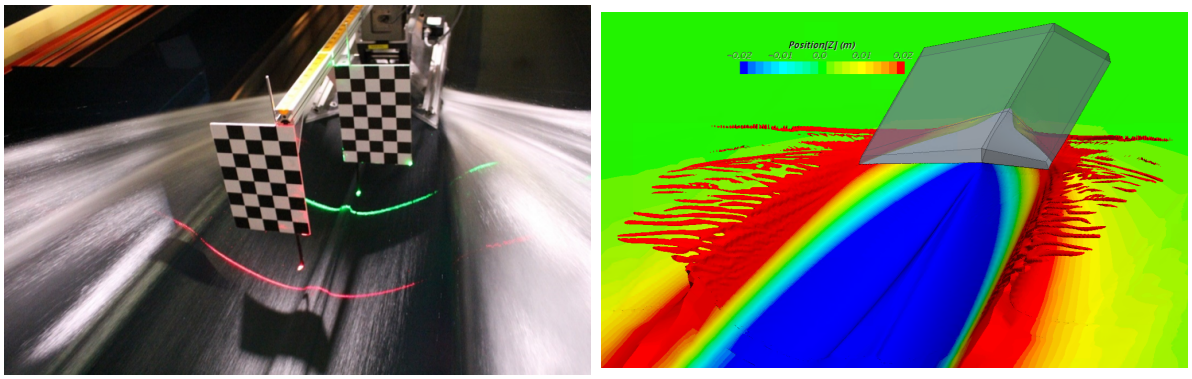

Figure 2.46: Laser Wake Profile (Run 16)

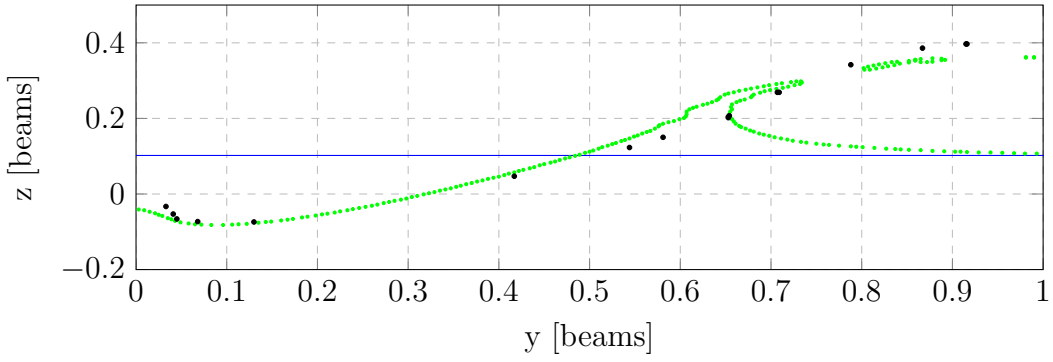

(a) Green Laser

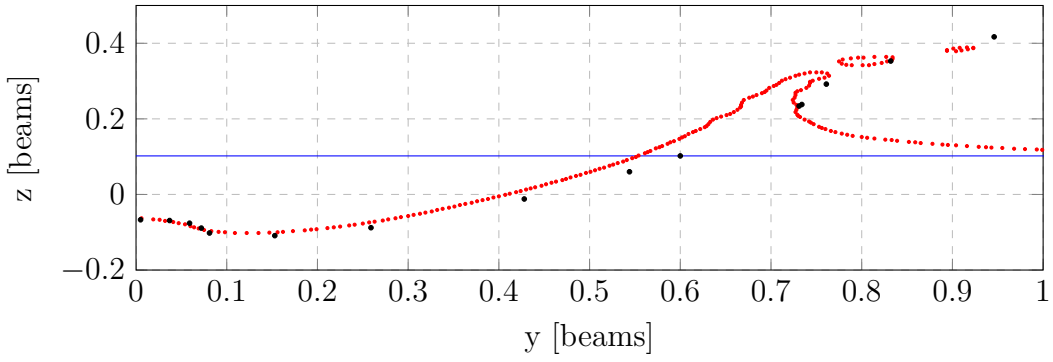

(b) Red Laser

Figure 2.47: Wake Profile Comparison (Run 16)

Wetted Keel Length

Inconsistent with the trends for trim moment and lift-to-drag ratio, the predictions for wetted keel length were accurate with a few small variations for certain experiment runs. The questionable run number 48 is obviously wrong looking at Figure 2.51 at 60 pounds. The more accurate predictions for wetted keel length puts into question the sensitivity of measured forces on the model during experiment and if the small size of the model tested comes with its on uncertainties.

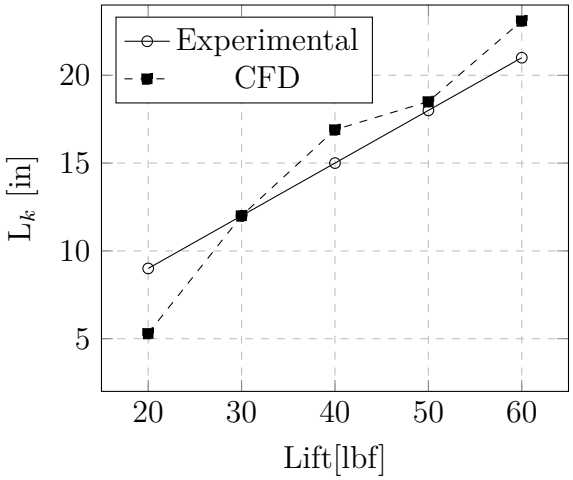

Figure 2.48: Step-A Wetted Keel Length (Free Heave Nominal Trim of 3°)

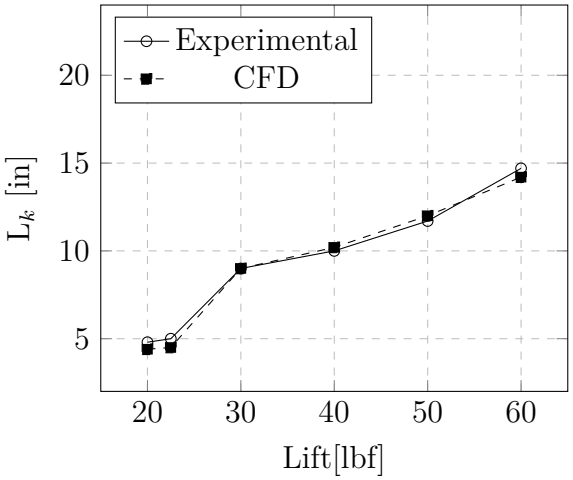

Figure 2.49: Step-A Wetted Keel Length (Free Heave Nominal Trim of 4°)

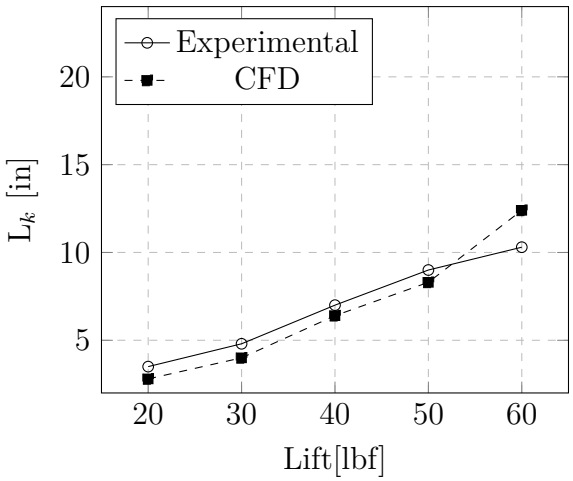

Figure 2.50: Step-A Wetted Keel Length (Free Heave Nominal Trim of 5°)

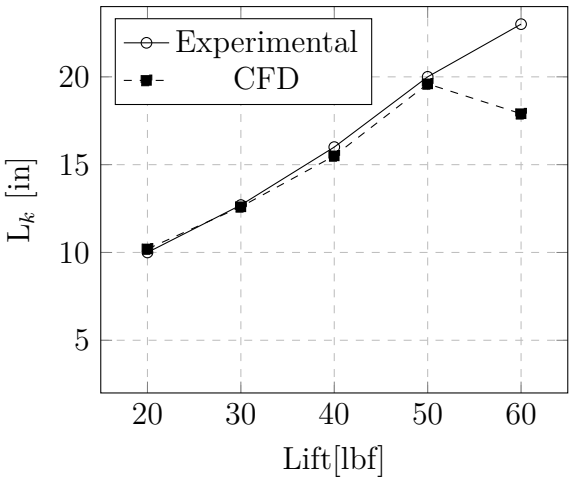

Figure 2.51: Step-B Wetted Keel Length (Free Heave Nominal Trim of 3°)

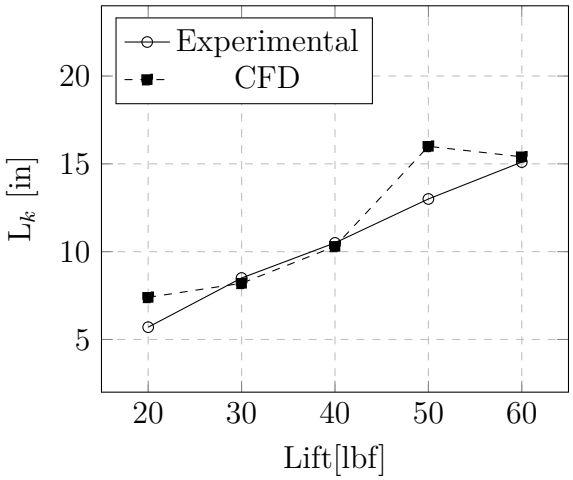

Figure 2.52: Step-B Wetted Keel Length (Free Heave Nominal Trim of 4°)

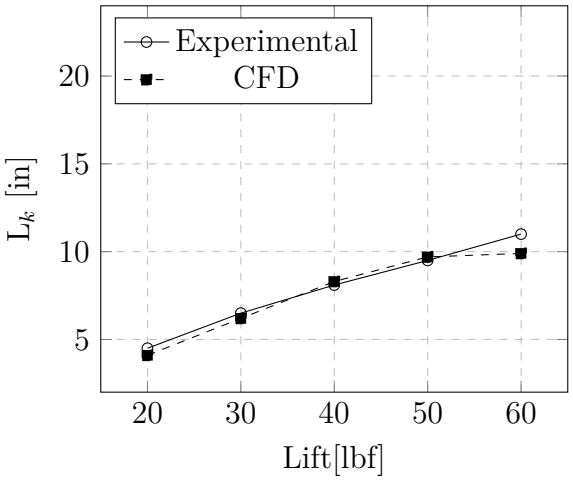

Figure 2.53: Step-B Wetted Keel Length (Free Heave Nominal Trim of 5°)

2.4.4 Free Heave Sensitivity Studies

The CFD simulation has a strong agreement with the wake profile data for all the experimental test runs. The simulations struggle to show a strong agreement for the drag and trim moment for certain cases. In attempt to strengthen the validation of the CFD simulations with the experimental results, further investigations were performed. These investigations looked into different turbulence models and wall functions, setting a courant number, testing uncertainty in experimental trim values, and a roughness study.

Free Heave K-Omega Versus K-Epsilon Turbulence Model

The k-omega turbulence model was tested using the SST variation described in Section 2.3.1. The results of this test are presented in Table 2.16. The difference between turbulence models is small and showed no appreciable difference on the CFD predictions. The friction and pressure coefficients for the k-epsilon and k-omega turbulence models showed no noticeable changes.

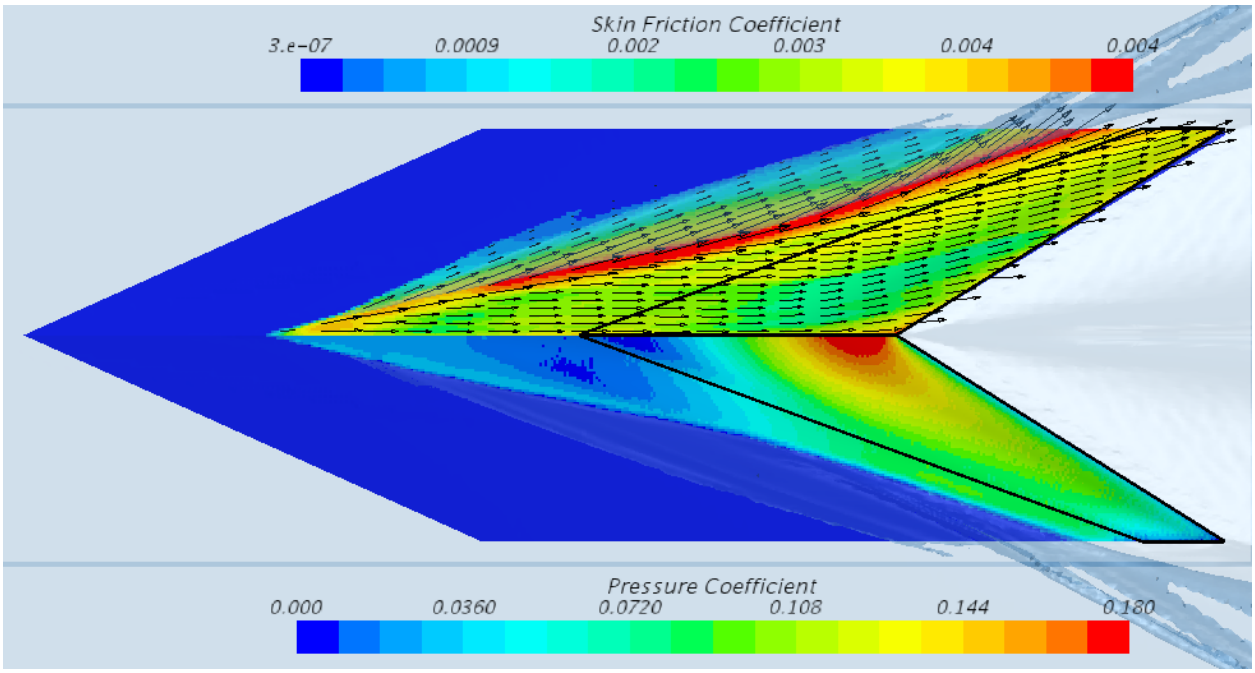

(a) k-ϵ

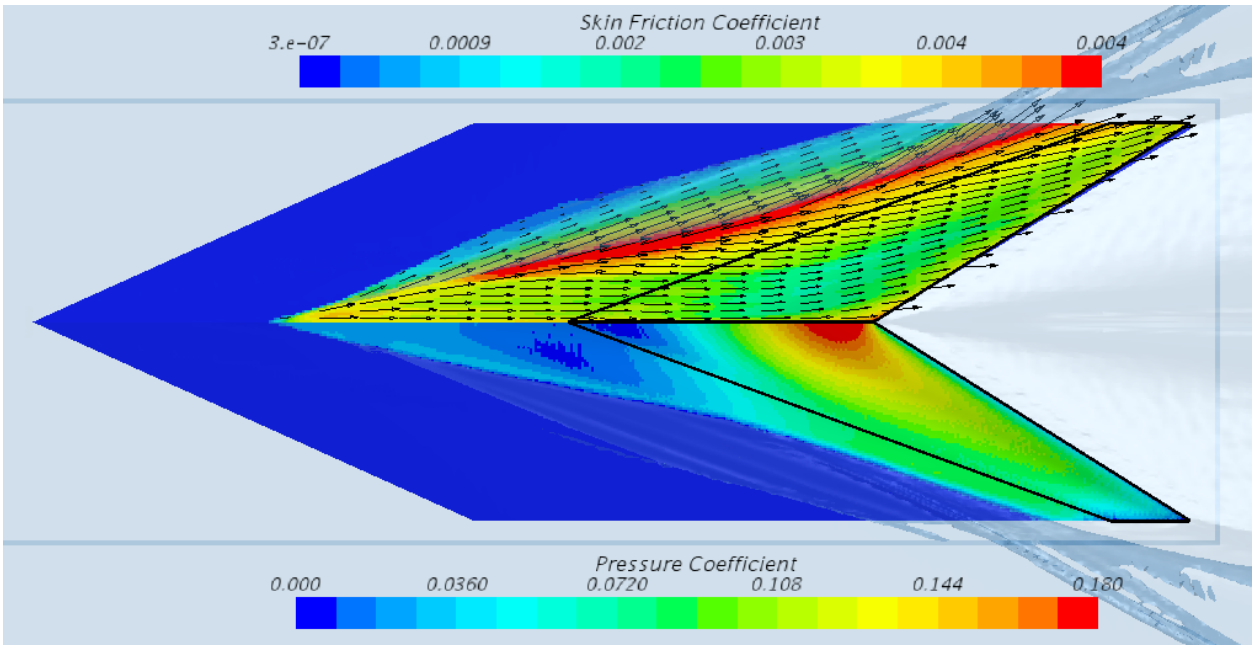

(b) k-ω

Figure 2.54: Free Heave Run 27 - k-ϵ Versus k-ω Turbulence Models Effect on Friction and Pressure Coefficient

Table 2.16: Free Heave Run 27 - Turbulence Model Study Data

Turbulence Model	D_S [lbf]	D_P [lbf]	Drag	%E(D) [lbf-in]	L/D	M_y [in]	%E(M) [in]	L_{cp} [in]	L_k	Draft
k-ϵ	3.00	4.72	7.71	-12%	6.48	-68.02	52%	-1.36	18.5	1.31
k-ω	3.05	4.69	7.74	-12%	6.46	-67.76	52%	-1.36	18.4	1.31
EFD	-	-	8.77	-	5.70	-44.60	-	-0.88	18	1.39

Free Heave $Y^+ \leq 1$

Professor Frederick Stern of the University of Iowa has been performing a validation using the same experimental results. Stern sets his simulations to have a y^+ less than, or equal to one. This led to setting up a simulation with y^+ less than, or equal to one. The y^+ plot on the planing surface for both wall treatments is shown in Figure 2.55. The difference in the results is noticeable, but did not improve the CFD predictions relative to the all y^+ treatment. The results of this study are reported in Table 2.17. The difference in skin friction is noticeable in the friction and pressure coefficient plots shown in Figure 2.56

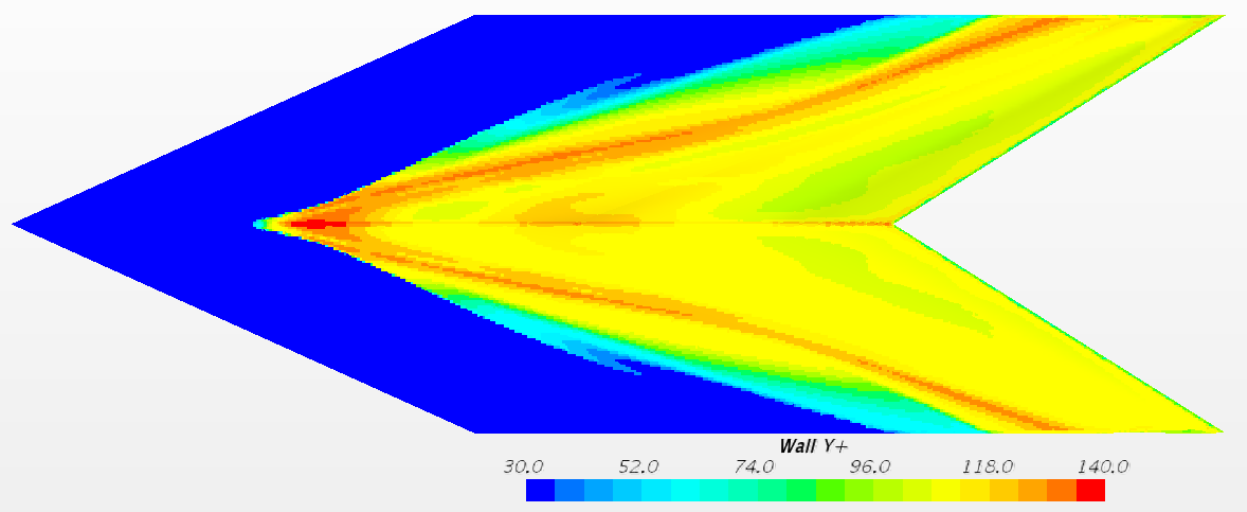

(a) All y^+ Treatment

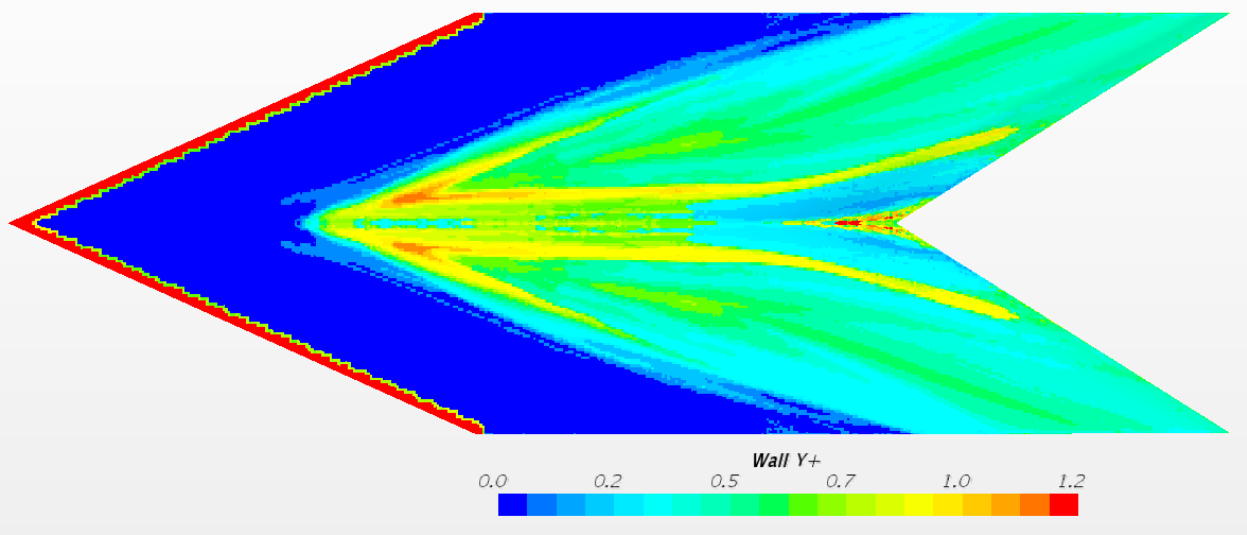

(b) $Y^+ < 1$

Figure 2.55: Free Heave Run 27 - y^+ Plots for All y^+ and $y^+ < 1$ Treatments

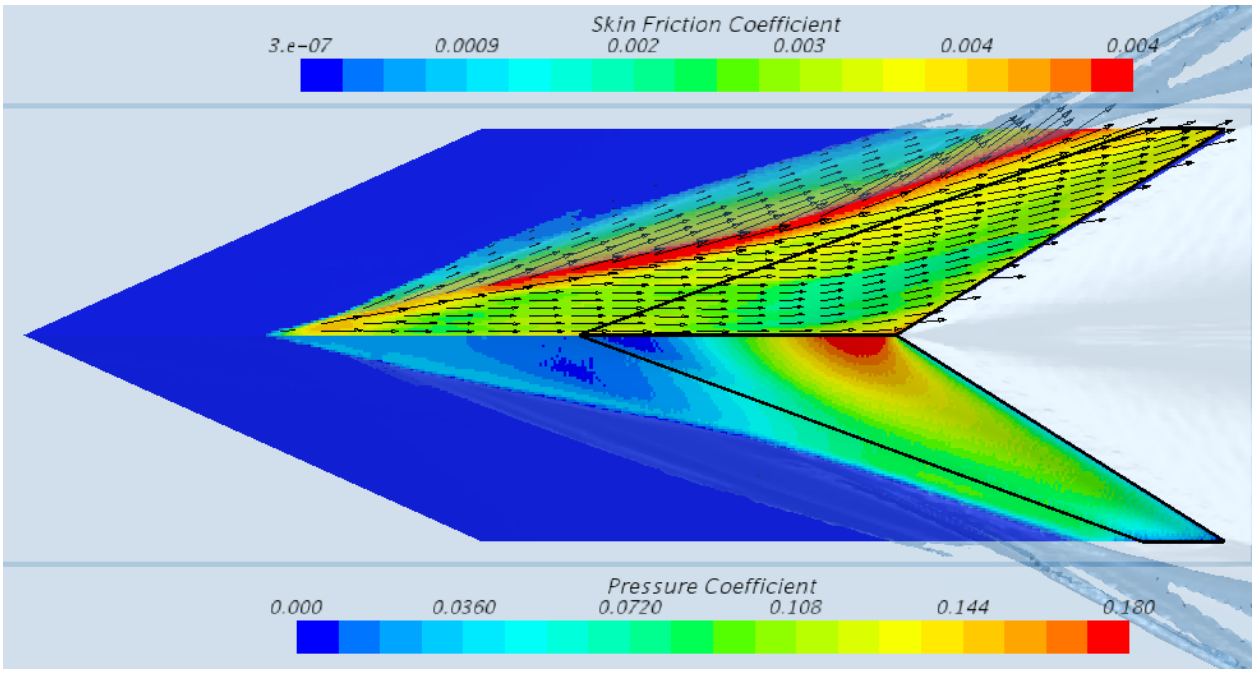

(a) All y^+ Treatment

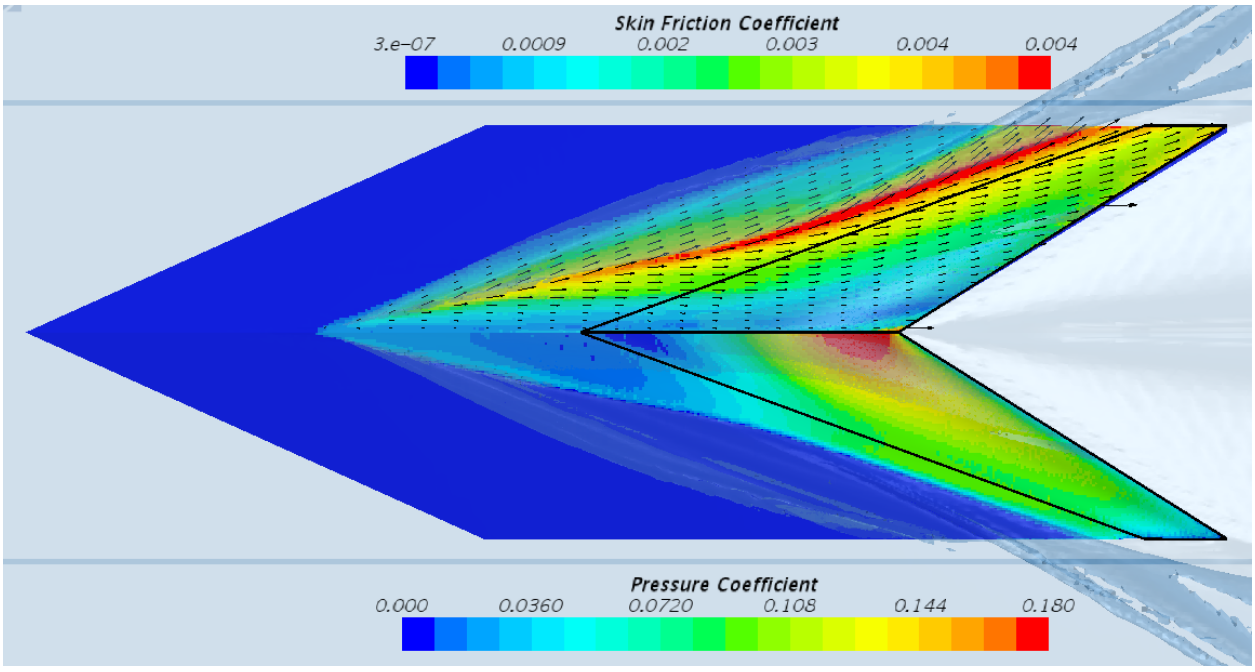

(b) $Y^+ < 1$

Figure 2.56: Free Heave Run 27 - Different Wall Treatment Effect on Friction and Pressure Coefficient

Table 2.17: Free Heave Run 27 - Y^+ Study Data

Y^+	D_S [lbf]	D_P [lbf]	Drag [lbf]	%E(D)	L/D	M_y [lbf-in]	%E(M)	L_{cp} [in]	L_k [in]	Draft [in]
EFD	-	-	8.77	-	5.70	-44.60	-	-0.88	18	1.39
all	3.00	4.72	7.71	-12%	6.48	-68.02	52%	-1.36	18.5	1.31
< 1	2.17	4.93	7.10	-19%	7.04	-80.58	81%	-1.61	16.9	1.25

Free Heave Uncertainty in Trim

The experimental data from the USNA Hydromechanics Laboratory stated that there was an uncertainty of 0.1 degrees for the trim angle for the planing surface. To further investigate a possible reason for the CFD disagreement with the experiment, simulations were setup and ran to study the possible effect the uncertainty had on the experimental data. The results of this study are reported in Table 2.18. The results showed no significant impact on the CFD predictions.

Table 2.18: Free Heave Run 16 – Trim $\pm 0.1°$ Data

Trim [°]	Drag [lbf]	%E(D)	L/D	M_y [lbf-in]	%E(M)	L_{cp} [in]	L_k [in]	L_c [in]	Draft [in]
3.76	6.92	-3.9%	5.78	-100.6	5.6%	-2.52	10.5	-7.6	1.035
3.86	6.96	-3.3%	5.74	-101.8	6.9%	-2.54	10.2	-7.8	1.036
3.96	7.04	-2.2%	5.68	-104.5	9.7%	-2.61	9.5	-7.7	1.038

Free Heave Roughness Study

A roughness study was performed for the fixed position mesh for roughness height of 50, 100, and 150 microns. The fixed position roughness study showed that a roughness height of 50 microns show the strongest correlation with the experimental data. For the free heave roughness study, a roughness height of 50 microns is prescribed as a result of the data from the fixed position roughness study. Runs 24 and 27 were prescribed the roughness height. The results of this study are reported in Table 2.19. The pressure coefficient for both runs showed no difference in pressure distribution between smooth and rough planing surfaces. The friction coefficient for both runs show visible difference in pressure distribution between smooth and rough planing surfaces. The pressure and friction coefficient plots for runs 24 and 27 are shown in Figures 2.57 and 2.58, respectively.

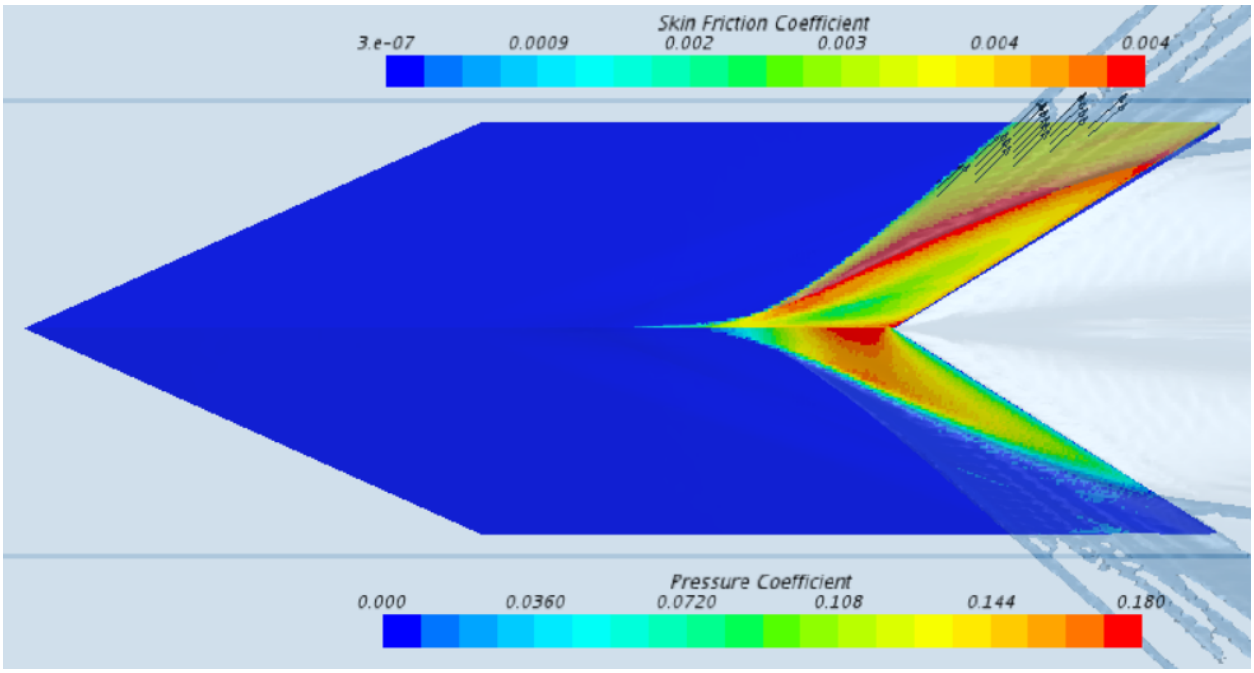

(a) Smooth Surface

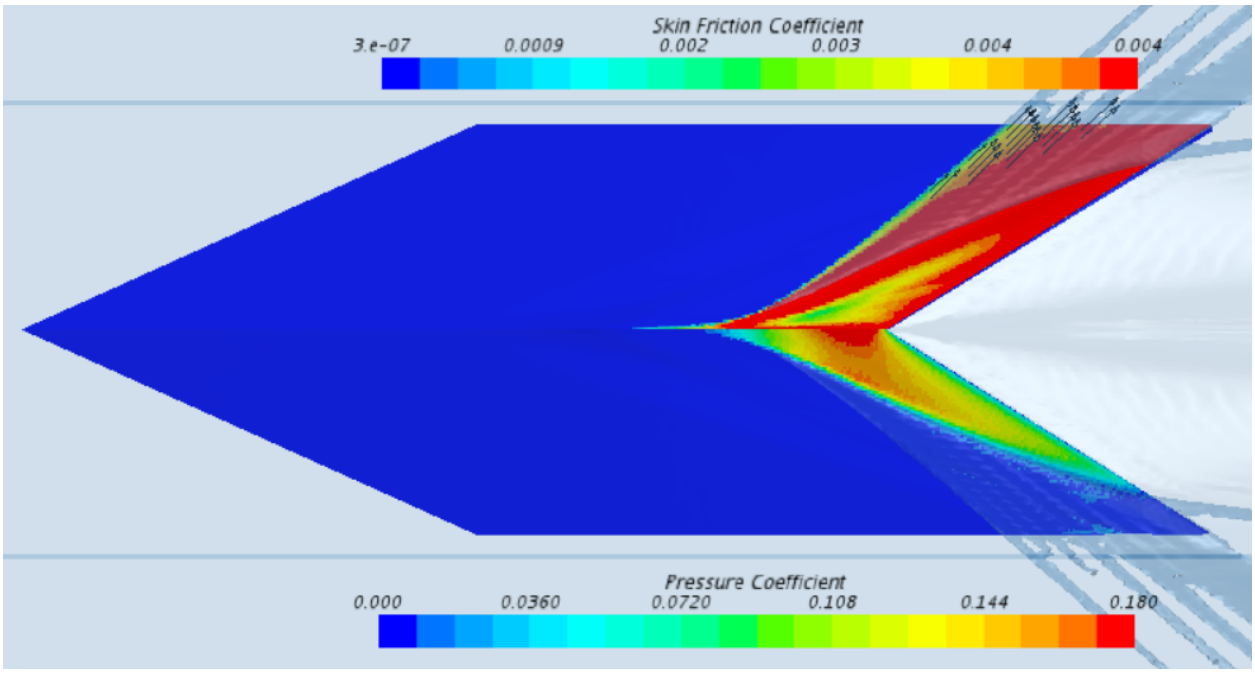

(b) Roughness Height of 50 μm

Figure 2.57: Free Heave Run 24 – Different Roughness Study on Friction and Pressure Coefficient

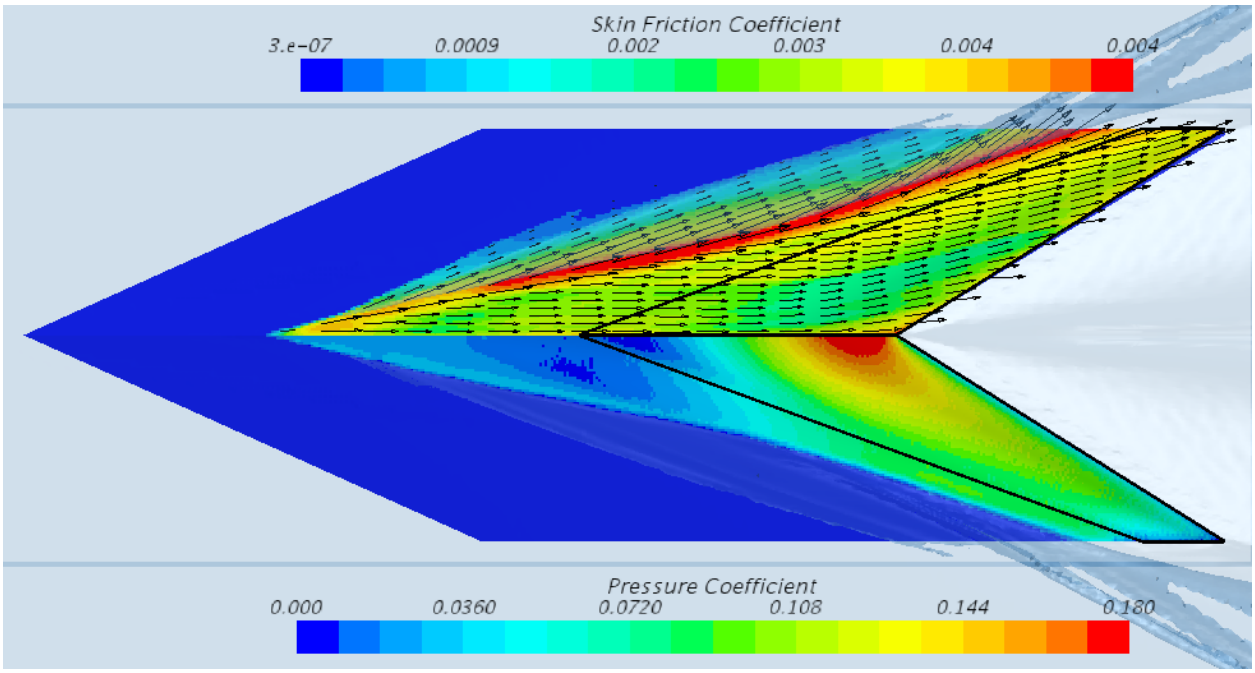

(a) Smooth Surface

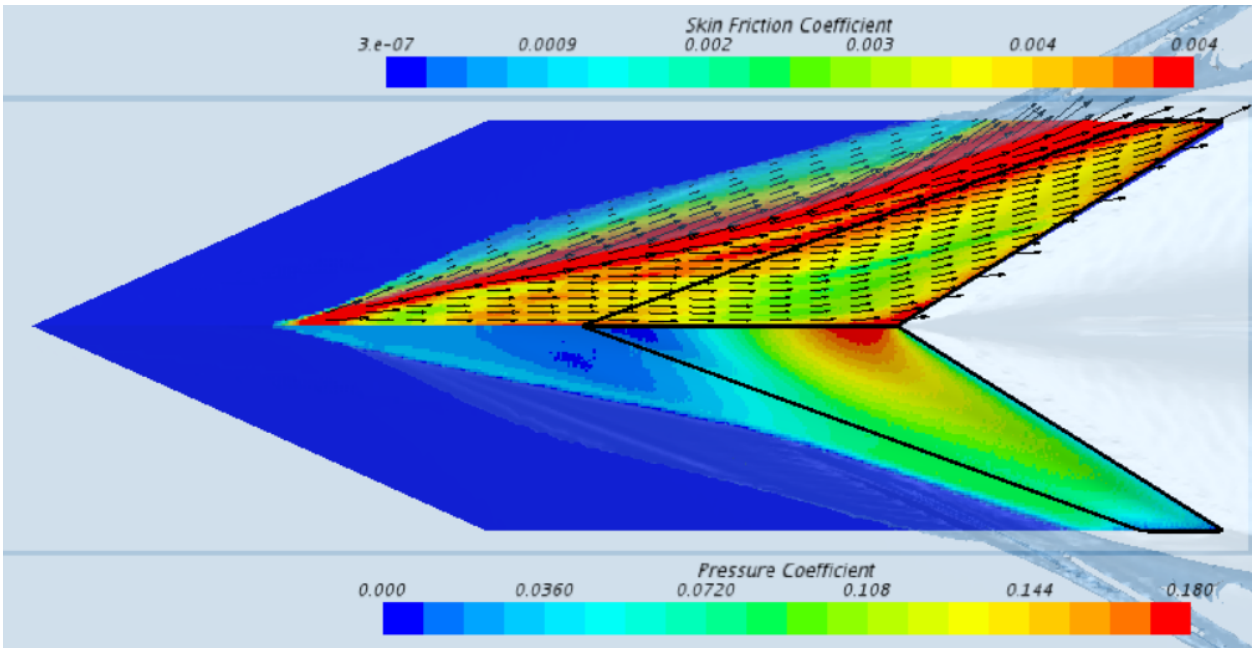

(b) Roughness Height of 50 μm

Figure 2.58: Free Heave Run 27 – Different Roughness Study on Friction and Pressure Coefficient

Table 2.19: Free Heave Roughness Study Data

Run #	r [μm]	D_S [lbf]	D_P [lbf]	Drag [lbf]	%E(D)	L/D	M_y [lbf-in]	%E(M)	L_{cp} [in]	L_k [in]	Draft [in]
24	EFD	-	-	4.98	-	4.01	-49.90	-	-2.42	9	0.93
	0	1.25	3.69	4.94	-0.8%	4.05	-53.08	6.4%	-2.65	5.3	0.792
	50	1.66	3.66	5.32	6.8%	3.76	-54.24	8.7%	-2.71	5.4	0.791
27	EFD	-	-	8.77	-	5.70	-44.60	-	-0.88	18	1.39
	0	3.00	4.72	7.71	-12%	6.48	-68.02	53%	-1.36	18.5	1.313
	50	3.87	4.63	8.50	-3.2%	5.89	-66.21	49%	-1.32	18.1	1.313

Free Heave Courant Number

The final sensitivity studies courant number versus using a constant time step. Setting the courant number so that the courant number on the surface is less than one would mean that a fluid particle would only past from one cell to the next in a time step. Courant number greater than one means that a fluid particle is travelling over more than one cell in a given time step. The courant number plots for a courant number less than one versus the time step of 2e-4 seconds is shown Figure 2.59. Figure 2.60 shows that prescribing a courant number of less than one has no difference on the pressure and skin friction coefficients. This is consistent with the data in Table 2.20 that shows no significant change in CFD predictions.

Table 2.20: Free Heave Run 27 – Courant Number Study Data

	D_S [lbf]	D_P [lbf]	Drag [lbf]	%E(D)	L/D	M_y [lbf-in]	%E(M)	L_{cp} [in]	L_k [in]	Draft [in]
EFD	-	-	8.77	-	5.70	-44.60	-	-0.88	18	1.39
$\Delta t = 2(10^4)$s	3.00	4.72	7.71	-12%	6.48	-68.02	53%	-1.36	18.5	1.313
CFL<1	3.08	4.70	7.78	-11%	6.43	-68.62	54%	-1.37	18.2	1.313

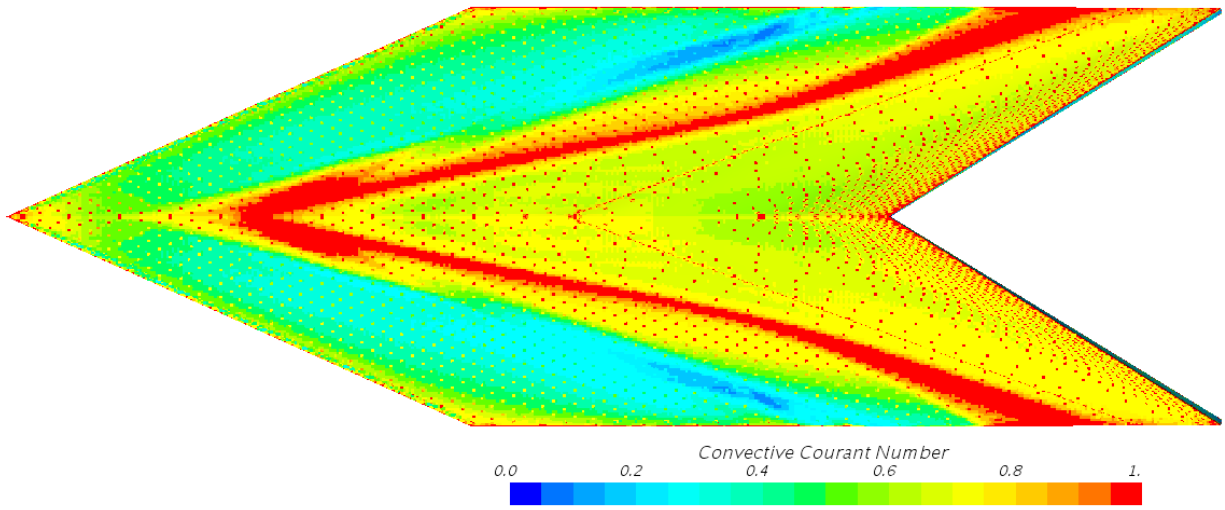

(a) Time Step = 2e-4s (k-ϵ)

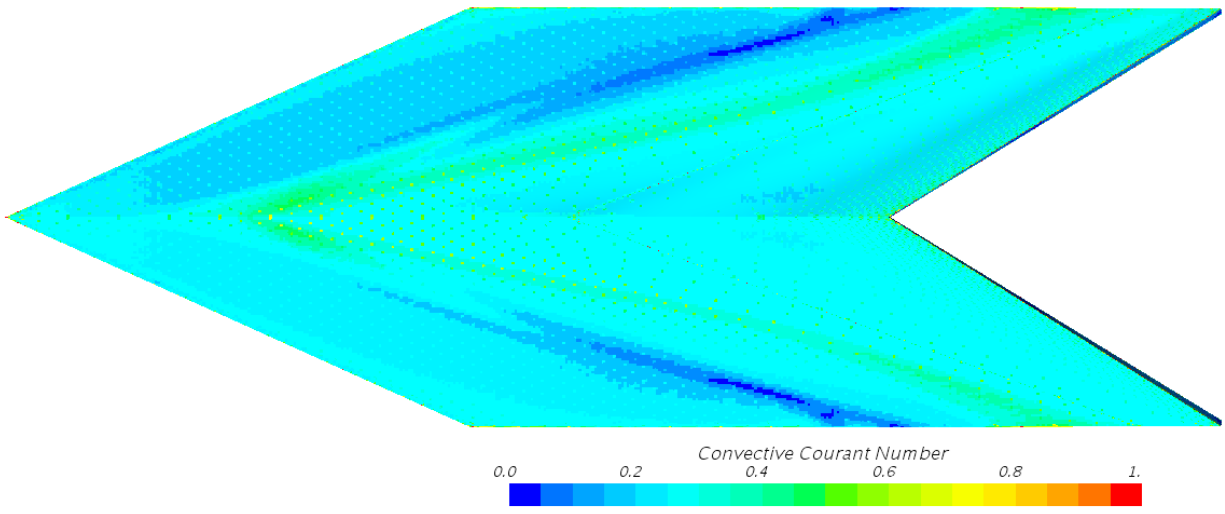

(b) CFL< 1 (k-ω)

Figure 2.59: Free Heave Run 27 – Courant Number Study

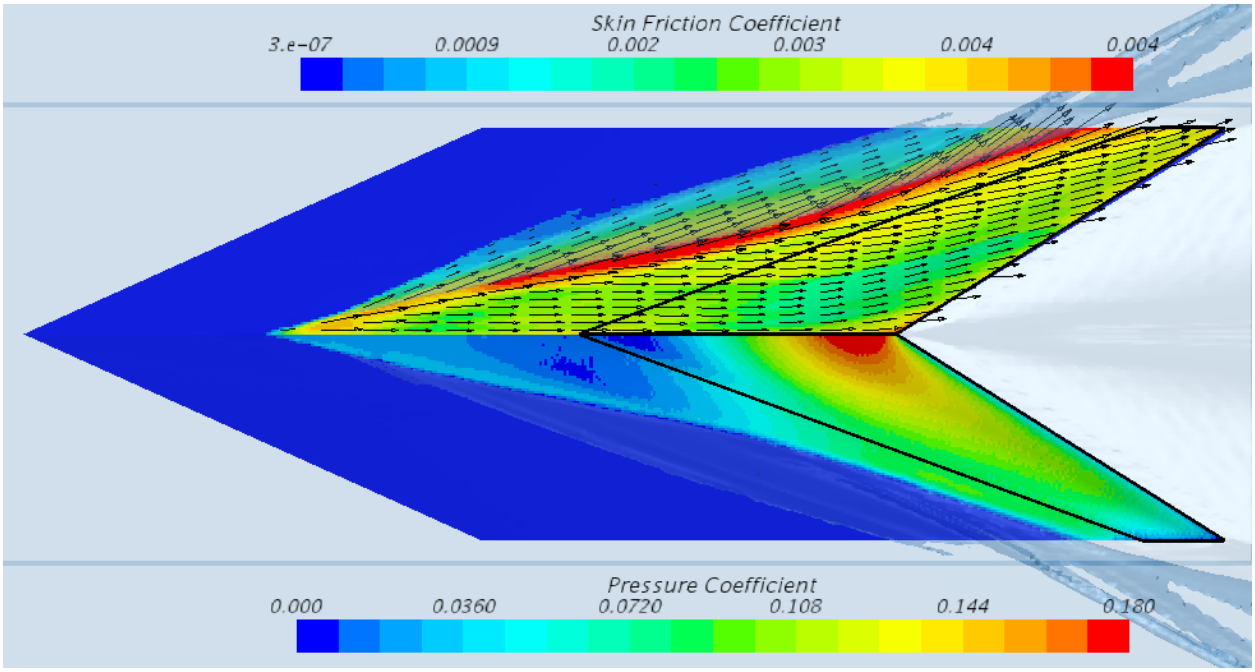

(a) Time Step = 2e-4s (k-ϵ)

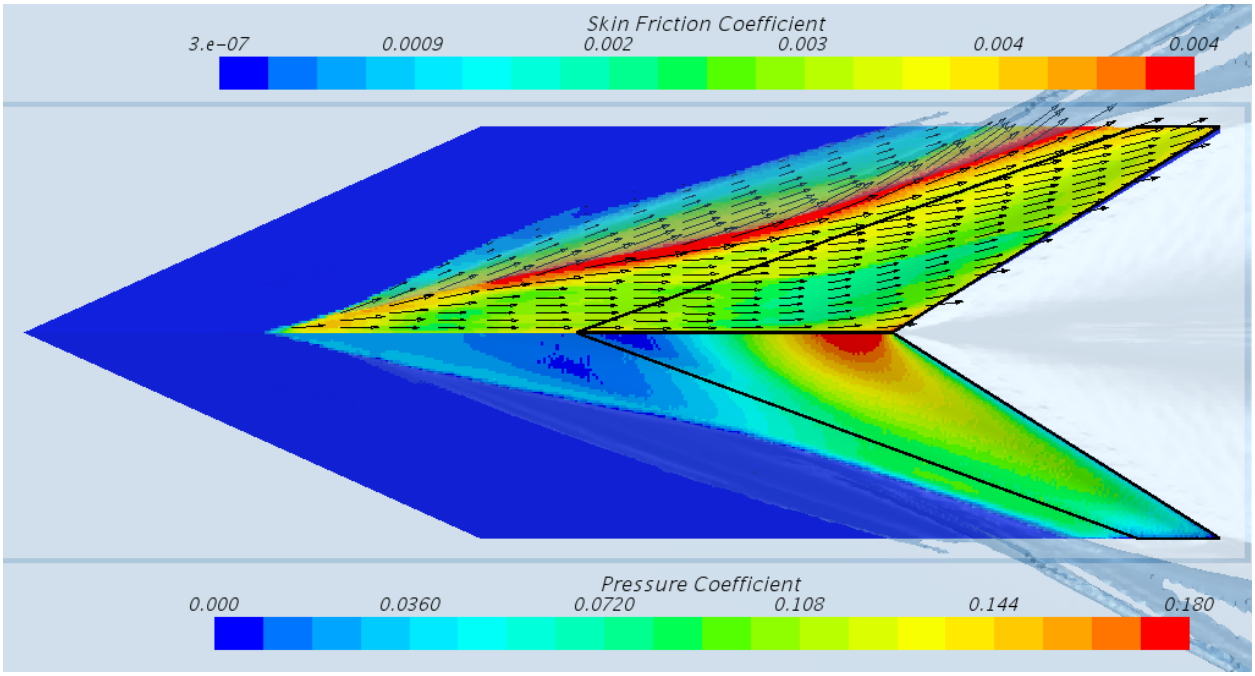

(b) CFL$<$ 1 (k-ω)

Figure 2.60: Free Heave Run 27 – Courant Number Effect on Friction and Pressure Coefficient

Chapter 3

Improved Cambered Step Design Procedure

The design process for a cambered step planing surface required the use of Clement's method. The method requires several iteration to obtain an optimal performance (lift-to-drag ratio) as discussed in Section 1.4. The purpose of this improved design method is to develop a database that can be used to create equations based on a desired load and high deadrise angle for strong sea-keeping characteristics that produces an optimal performance without multiple iterations.

3.1 Camber Planing Surface Generator Code

The design of the cambered step planing surfaces utilizes the equations from the Clement's method in Section 1.3.1. A MatLab script was written to produce text files with the coordinates for the cambered section at the centerline and chine for the purpose of importing to the desired computer aided design (CAD) program. The code accounts for beam, deadrise, trim, and camber when assigning coordinates. This code is presented in Appendix B.1

The MatLab script inputs are two-dimensional design lift coefficient, deadrise angle, trim angle, and beam. From the inputs, a chine and centerline chord length is determined. The chord lengths are equal to 80% and 20% of the beam length for the centerline and chine, respectively. The chord length equations are set to produce a camber surface with an aspect ratio (Equation 1.4) equal to 2. Adjusting the percent values allows for a varying aspect ratio. Then the horizontal angle between the spray root line and centerline, γ, is solved for using Equation 1.5. The script adds 5 degrees to the calculated angle which is consistent with Clement's theory, in Section 1.3.1, that the cambered section adds an additional 5 degrees to the spray root angle. The script then solves for the angle of sweep of the 50% chord line (Equations 1.6) and the sweptback angle of the step (Equation 1.7). The code then calculates the shape of the Johnson three-term cambered curve shape (Equation 1.9) and then locates the coordinates for the cambered curve at the chine according to beam, deadrise, and the horizontal angle between the spray root line and centerline. The coordinates are then imported into CAD as shown in Figure 3.1. The forward most part of the centerline cambered section is located at the origin (0,0,0) and the cambered section at the chine would be placed

according to beam, deadrise, trim and camber. Important to note that the cambered planing surface is not rotated to the design trim angle despite being placed according to trim. Trim also effects the spray root angle γ. After importing the points, connect the points to make two curves and extend a forebody in front of the cambered curve lines and place a deck surface for a desired model thickness. For this study, decks were located half an inch above the bottom of the planing surface. A finished product after rotating the body to the design trim is shown in Figure 3.2.

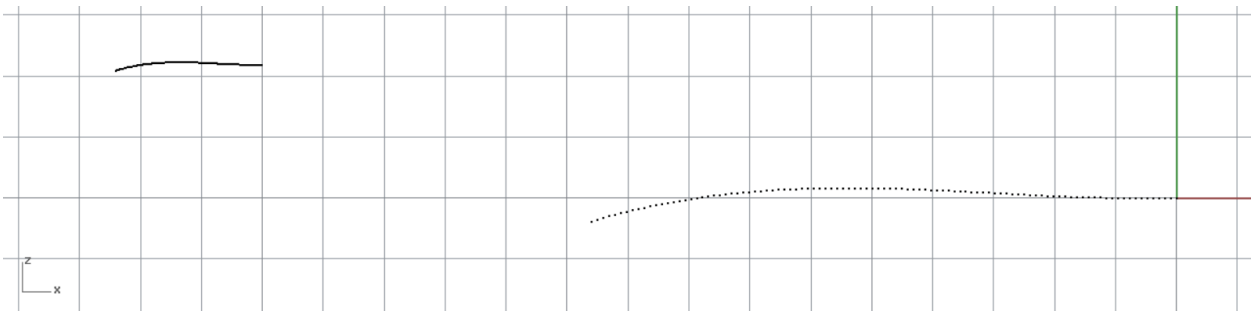

Figure 3.1: Points from Cambered Planing Surface Generator Code (Profile View)

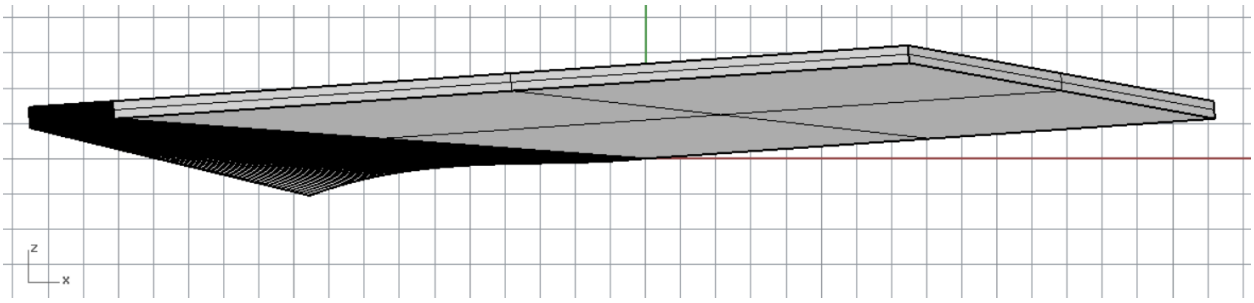

Figure 3.2: Finished CAD Model for Cambered Step Planing Surface (Profile View)

3.2 Design Space

Design constraints were set to limit the scope of the investigation on an improved design method from the Clement's method for cambered step surfaces with high deadrise. The maximum wetted keel length, aspect ratio, trim angle range, and beam were set to be consistent with the model used for validation of the simulation. Additional constraints such as deadrise angle and camber were broaden to expand on the designs used for validation. The design space for the database that will be fitted in Section 3.3.1 is:

- Speed of the planing surface is limited to 9 m/s ($Fn_{\nabla} \geq 3.16$).

- Aspect ratio of the cambered section is equal to two ($AR = 2$).
- The beam of the model is to be set at 12 inches ($b = 12$ in).
- High deadrise angle range of 15 to 25 degrees ($15° \leq \beta \leq 25°$).
- Maximum wetted keel length of 25.84 inches ($L_{k,max} = 25.84$ in).
- Planing surface support a minimum weight of 20 pounds ($W_{min} = 20$ lbf).
- Dynamic trim angle range of 3 to 5 degrees ($3° \leq \tau \leq 5°$).
- Constant Two-dimensional design lift coefficient range of 0.136 to 0.336 across the beam ($0.136 \leq C_{L,d} \leq 0.336$).

From the design space, twenty-seven designs were simulated at varying loads starting at 20 pounds and varied in 20 pound step sizes until maximum performance (lift-to-drag ratio) is obtained, or the maximum wetted keel length is reached. Load step sizes were smaller when nearing the maximum wetted keel length. The twenty-seven designs varied in deadrise, two-dimensional design lift coefficient, and trim angle. The designs tested deadrise angles 15, 20, and 25 degrees, two-dimensional design lift coefficients of 0.136, 0.236, and 0.336, and for 3, 4, and 5 degrees of trim angle. The designs tested for the database are as followed.

- Design 1: $C_{L,d} = 0.136$, $\beta = 15°$, $\tau = 3°$
- Design 2: $C_{L,d} = 0.136$, $\beta = 15°$, $\tau = 4°$
- Design 3: $C_{L,d} = 0.136$, $\beta = 15°$, $\tau = 5°$
- Design 4: $C_{L,d} = 0.236$, $\beta = 15°$, $\tau = 3°$
- Design 5: $C_{L,d} = 0.236$, $\beta = 15°$, $\tau = 4°$
- Design 6: $C_{L,d} = 0.236$, $\beta = 15°$, $\tau = 5°$
- Design 7: $C_{L,d} = 0.336$, $\beta = 15°$, $\tau = 3°$
- Design 8: $C_{L,d} = 0.336$, $\beta = 15°$, $\tau = 4°$
- Design 9: $C_{L,d} = 0.336$, $\beta = 15°$, $\tau = 5°$
- Design 10: $C_{L,d} = 0.136$, $\beta = 20°$, $\tau = 3°$
- Design 11: $C_{L,d} = 0.136$, $\beta = 20°$, $\tau = 4°$
- Design 12: $C_{L,d} = 0.136$, $\beta = 20°$, $\tau = 5°$
- Design 13: $C_{L,d} = 0.236$, $\beta = 20°$, $\tau = 3°$
- Design 14: $C_{L,d} = 0.236$, $\beta = 20°$, $\tau = 4°$
- Design 15: $C_{L,d} = 0.236$, $\beta = 20°$, $\tau = 5°$
- Design 16: $C_{L,d} = 0.336$, $\beta = 20°$, $\tau = 3°$
- Design 17: $C_{L,d} = 0.336$, $\beta = 20°$, $\tau = 4°$
- Design 18: $C_{L,d} = 0.336$, $\beta = 20°$, $\tau = 5°$
- Design 19: $C_{L,d} = 0.136$, $\beta = 25°$, $\tau = 3°$
- Design 20: $C_{L,d} = 0.136$, $\beta = 25°$, $\tau = 4°$
- Design 21: $C_{L,d} = 0.136$, $\beta = 25°$, $\tau = 5°$
- Design 22: $C_{L,d} = 0.236$, $\beta = 25°$, $\tau = 3°$
- Design 23: $C_{L,d} = 0.236$, $\beta = 25°$, $\tau = 4°$
- Design 24: $C_{L,d} = 0.236$, $\beta = 25°$, $\tau = 5°$
- Design 25: $C_{L,d} = 0.336$, $\beta = 25°$, $\tau = 3°$
- Design 26: $C_{L,d} = 0.336$, $\beta = 25°$, $\tau = 4°$
- Design 27: $C_{L,d} = 0.336$, $\beta = 25°$, $\tau = 5°$

3.3 Database Results

The designs were tested at varying loads until the maximum lift-to-drag ratio was found, or maximum wetted keel length achieved. Figures 3.3-3.8 show the overall trends for designs varying in deadrise. These plots were used for determining the load range to be considered. In Section 3.3.1, the process of curve fitting the data to determine optimal designs will start by producing three-dimensional plots of the data in Figures 3.3-3.8. Data was collected for shear, pressure, and total drag, trim moment, draft, wetted keel length, and wetted surface area. The trim moment was measure around the most forward point of the cambered step (located at the origin in both the CAD and simulation file). The full results of the database for the designs presented in Section 3.2 can be found in Appendix Section B.2.

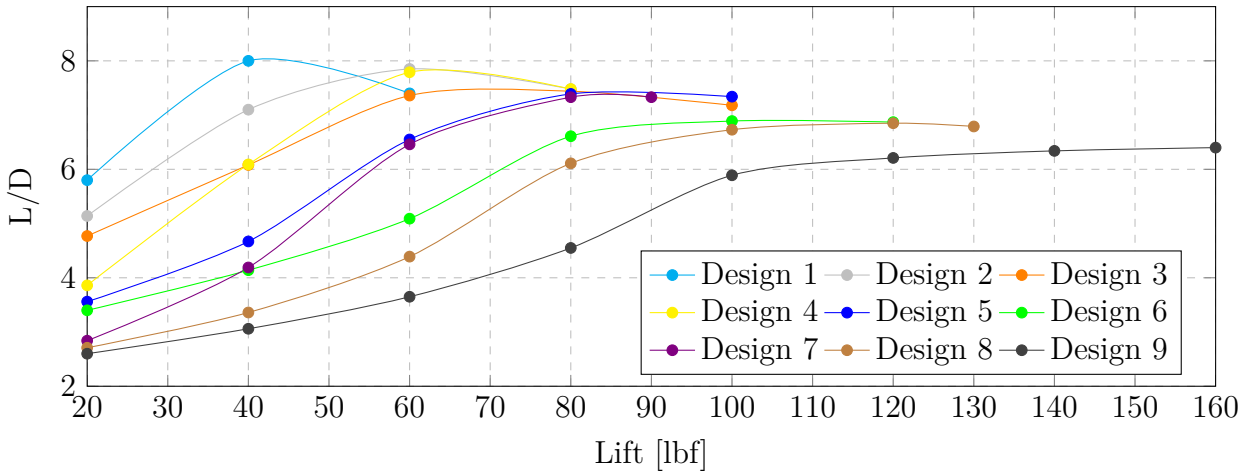

Figure 3.3: L/D Versus Lift at $\beta = 15°$ for Varying 2D Lift Coefficient

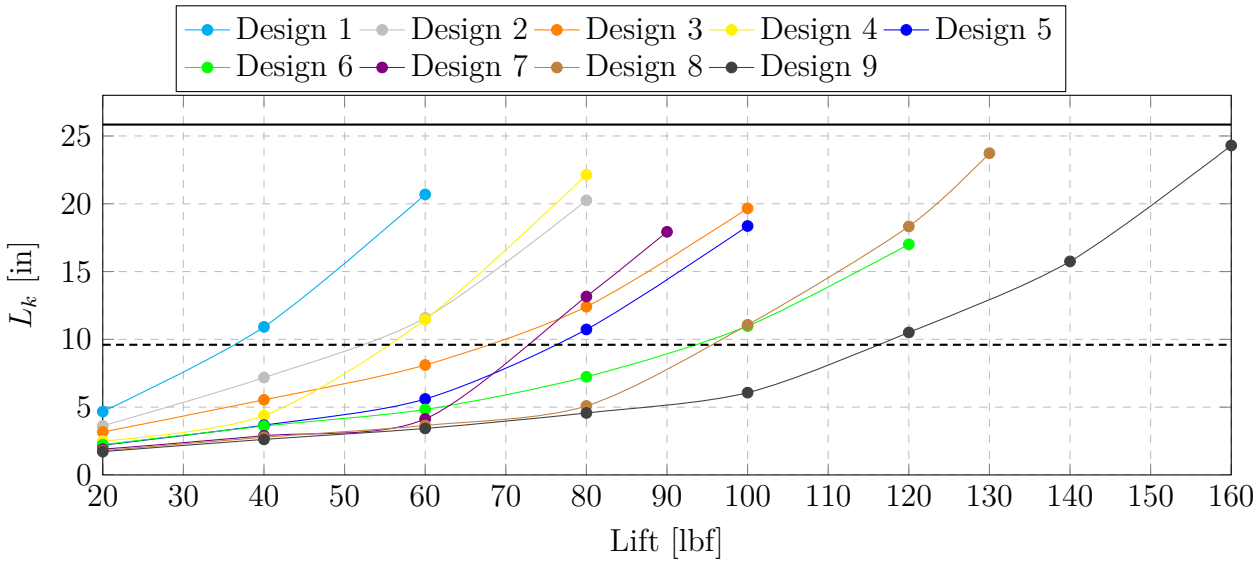

Figure 3.4: Wetted Keel Length Versus Lift at $\beta = 15°$ for Varying 2D Lift Coefficient

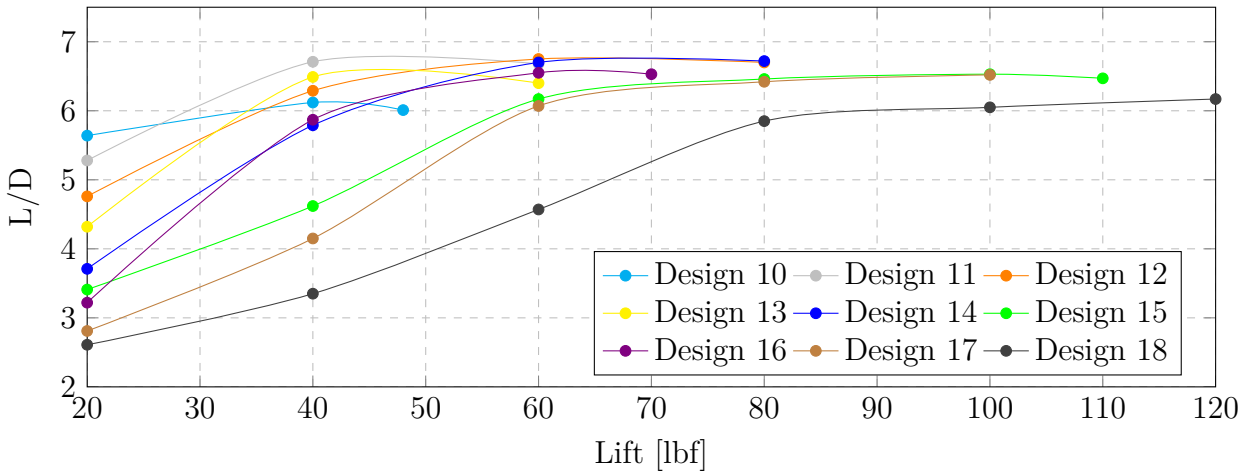

Figure 3.5: L/D Versus Lift at $\beta = 20°$ for Varying Two-Dimensional Lift Coefficient

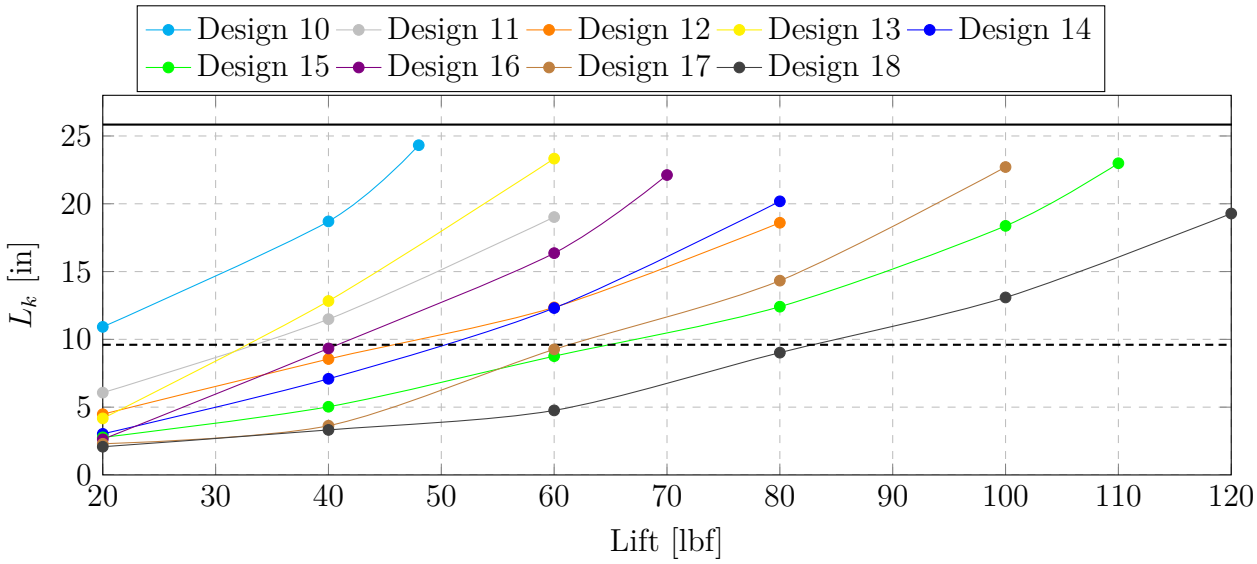

Figure 3.6: Wetted Keel Length Versus Lift at $\beta = 20°$ for Varying 2D Lift Coefficient

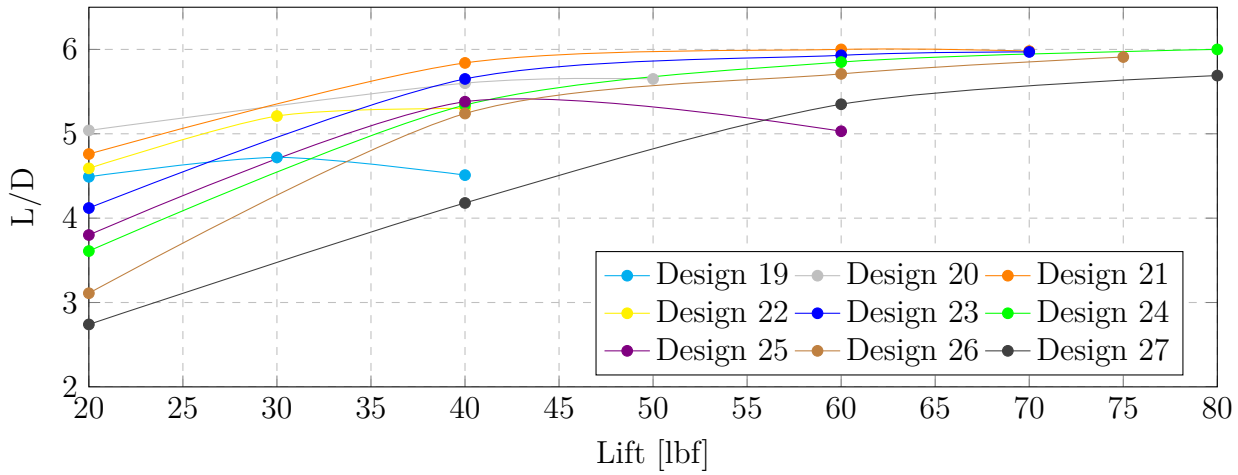

Figure 3.7: L/D Versus Lift at $\beta = 25°$ for Varying Two-Dimensional Lift Coefficient

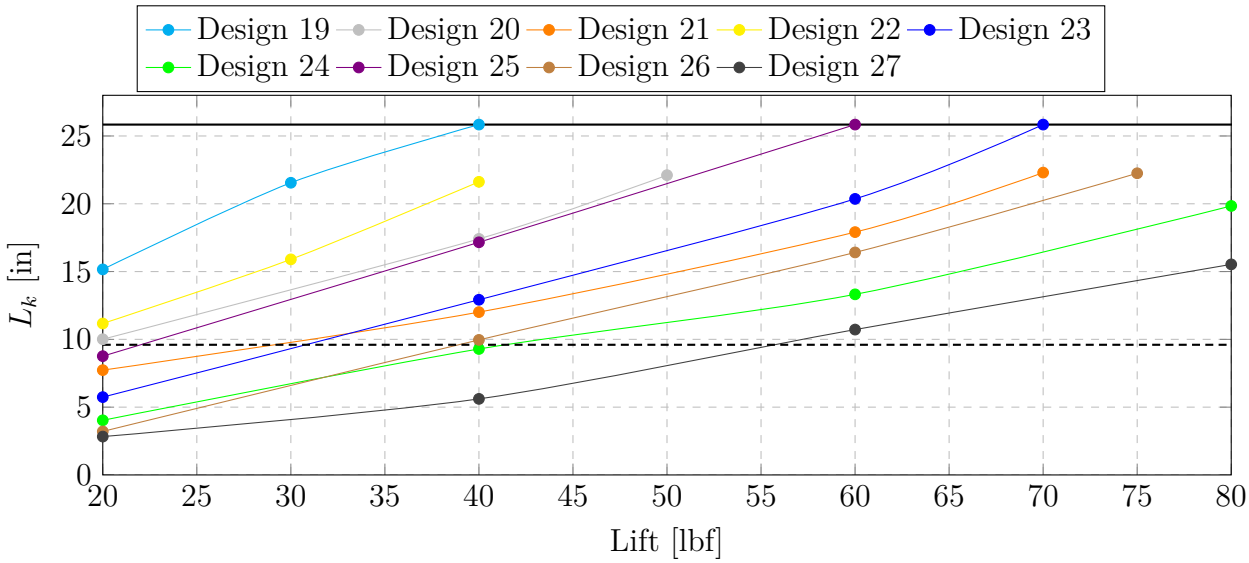

Figure 3.8: Wetted Keel Length Versus Lift at $\beta = 25°$ for Varying Two-Dimensional Lift Coefficient

3.3.1 Database Surface Fit

To improve upon the Clement's method, the data needs to be fitted in such a way that produces equations based on the desired sea-keeping (deadrise) and load (lift) requirements. In this section, the process for determining an optimum design will be presented. Further discussion regarding this process and its validity will be discussed further in this section and will be tested against two additional CFD simulations at a design not previously tested in Section 3.4.

The code utilizes a double *for* loop that loops through different lift and dead rise values. For this project, lift was varied from 20 to 100 pounds in increments of 2 pounds and the deadrise was was from 15 to 25 degrees in increments of 1 degree. The first step involves plotting and fitting surface equations to the lift-to-drag ratios for the varying trim and lift values at the two-dimensional lift coefficients and deadrises from the database in Appendix Section 3.3. The surfaces for the varying deadrise and two-dimensional lift coefficient can be seen in Figure 3.9.

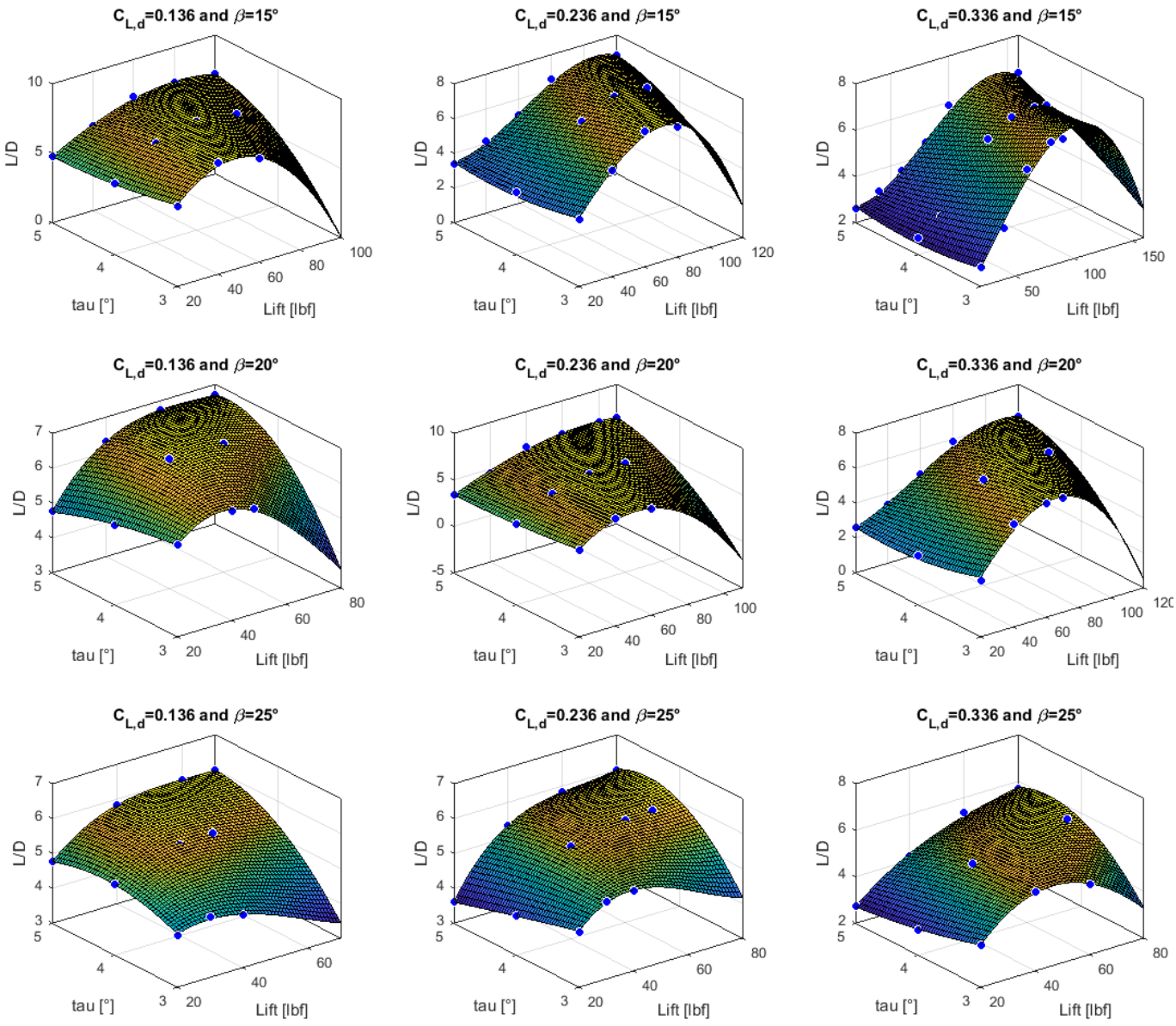

Figure 3.9: Lift-to-Drag Surfaces for Varying Deadrise and 2D Lift Coefficient

Using the surface fit equations generated, lift-to-drag ratios were determine for the lift value determine by the *for* loop with varying trim angle. From this array of points for lift-to-drag ratios and trim angle for each two-dimensional lift coefficient and deadrise from the database, a surface was fitted for lift-to-drag ratios based on trim angle and two-dimensional lift coefficient for the three deadrise angles from the database at the lift for the given *for* loop. There are now three equations for lift-to-drag ratios at 15, 20, and 25 degrees of deadrise that depend on two-dimensional lift coefficients. For the three equation, the maximum lift-

to-drag ratio is found and the corresponding two-dimensional lift coefficient and trim angle are noted. With this data, a curve equation can be fitted for maximum lift-to-drag ratio, trim angle, and two-dimensional lift coefficient for varying deadrise angles for the lift value in the *for* loop. The deadrise angle for the specific loop is then plugged into these equations and a design lift-to-drag ratio, trim angle, and two-dimensional lift coefficient are saved in their corresponding matrix of optimal designs based on deadrise angles and lift values. This matrix has been plotted in Figure 3.10 and fitted resulting in the optimal lift-to-drag ratio equation (Equation 3.1) based on lift and deadrise. This equation has a strong correlation to the matrix with a coefficient of determination value (R^2) of 0.9955 and root meat square error (RMSE) value of 0.0435.

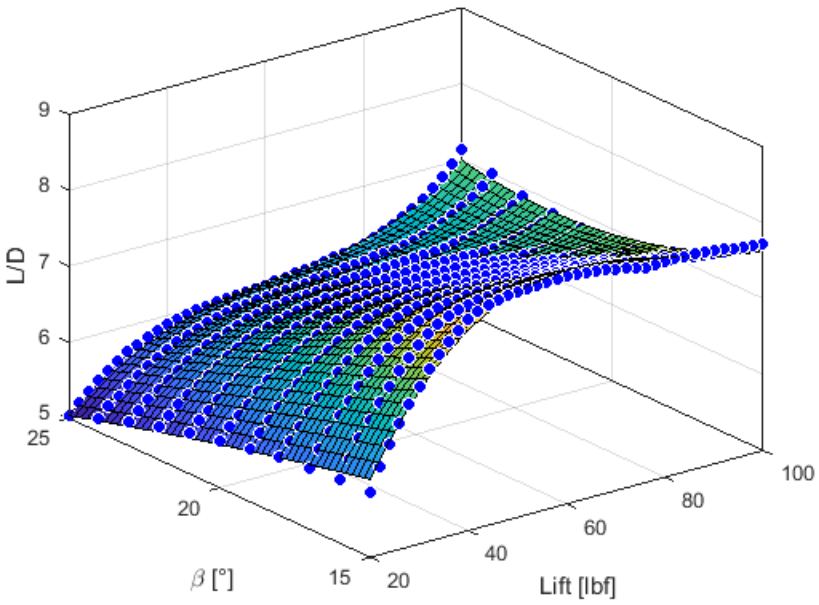

Figure 3.10: Lift-to-Drag Values for Optimal Designs

$$\begin{aligned}(L/D)_{opt} = \; & -0.04446 + 0.4221L + 0.2699\beta - 0.003922L^2 - 0.01675L\beta \\ & - 0.005788\beta^2 + 1.135(10^{-5})L^3 + 7.324(10^{-5})L^2\beta + 0.0002101L\beta^2\end{aligned} \tag{3.1}$$

The matrix for two-dimensional lift coefficient is plotted and fitted in Figure 3.11. The fitted equation for the optimal two-dimensional lift coefficient (Equation 3.2) does not have as strong a correlation as the optimal lift-to-drag ratio. The optimal two-dimensional lift coefficient equation has a coefficient of determination value (R^2) of 0.9093 and root meat square error (RMSE) value of 0.0141. The bad fit can be contributed to the range of two-dimensional lift coefficient values tested. Testing values outside the design space stated in

Section 3.2 would have improved the fitment because it is seen from looking at the trend that optimal designs at lower lift and deadrise values would have a two-dimensional lift coefficient value below 0.136 (design space lower limit).

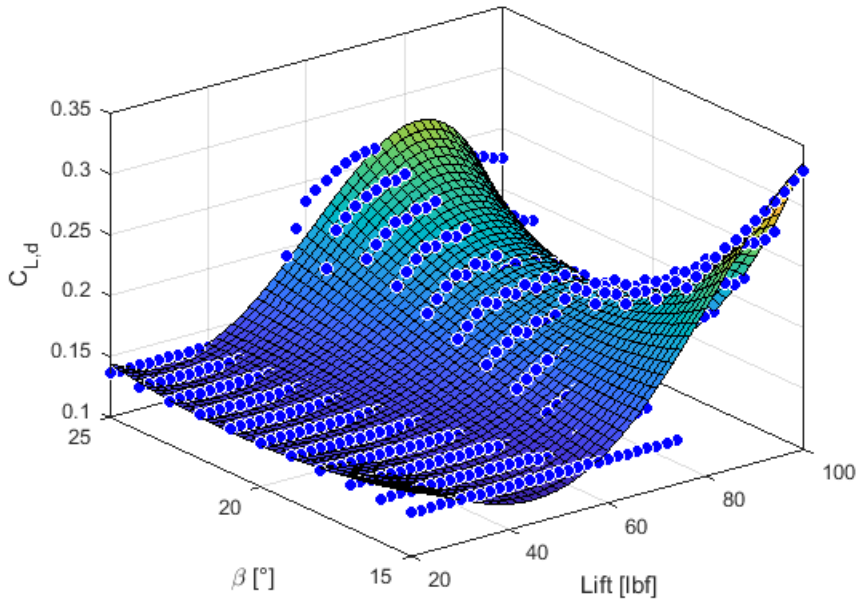

Figure 3.11: Two-Dimensional Lift Coefficient Values for Optimal Designs

$$\begin{aligned}(C_{L,d})_{opt} = {} & 1.032 - 0.03372L - 0.1013\beta - 8.422(10^{-5})L^2 + 0.004745L\beta \\ & + 0.002725\beta^2 + 8.117(10^{-6})L^3 - 4.059(10^{-5})L^2\beta - 0.0001402L\beta^2 \\ & - 1.912(10^{-17})\beta^3 - 2.401(10^{-8})L^4 - 1.923(10^{-7})L^3\beta + 1.653(10^{-6})L^2\beta^2 \\ & + 2.179(10^{-19})L\beta^3\end{aligned} \tag{3.2}$$

The limitations of the two-dimensional lift coefficient range tested effected the trim angle fitment as well. This can be seen in the plotting and fitment of the optimal trim angle matrix in Figure 3.12. Equation 3.3 for optimal trim angle has a coefficient of determination value (R^2) of 0.9042 and root meat square error (RMSE) value of 0.1842 degrees.

$$\begin{aligned}(\tau)_{opt} = {} & 8.605 - 0.06464L - 1.044\beta - 0.002664L^2 + 0.02551L\beta + 0.03293\beta^2 \\ & + 8.362(10^{-6})L^3 + 4.465(10^{-5})L^2\beta - 0.000778L\beta^2 + 1.671(10^{-16})\beta^3\end{aligned} \tag{3.3}$$

The remaining data to be fitted is the pressure and shear drag, wetted keel length, draft, and wetted surface area. This requires the same process as fitting the optimal lift-to-drag

ratio, but instead of finding the location of maximum performance at a given deadrise and lift, the optimal trim and two dimensional lift coefficient is use to determine the optimal design values for pressure and shear drag, wetted keel length, draft, and wetted surface area.

The optimal design pressure drag matrix and the surface fit are shown in Figure 3.13. Equation 3.4 for optimal design pressure drag has a coefficient of determination value (R^2) of 0.9976 and root meat square error (RMSE) value of 0.1269 pounds.

$$\begin{aligned}(D_P)_{opt} = {} & 0.8315 - 0.5293L + 1.316\beta + 0.003848L^2 + 0.04161L\beta - 0.1162\beta^2 \\ & - 1.123(10^{-5})L^3 - 9.202(10^{-5})L^2\beta - 0.0007417L\beta^2 + 0.002516\beta^3\end{aligned} \tag{3.4}$$

The optimal design shear drag matrix and the surface fit are shown in Figure 3.14. Equation 3.5 for optimal design shear drag has a coefficient of determination value (R^2) of 0.9843 and root meat square error (RMSE) value of 0.1464 pounds.

$$\begin{aligned}(D_S)_{opt} = {} & -14.15 + 0.5615L + 0.9727\beta - 0.003303L^2 - 0.03975L\beta + 0.0008077\beta^2 \\ & + 1.417(10^{-5})L^3 + 6.488(10^{-5})L^2\beta + 0.0008481L\beta^2 - 0.0006414\beta^3\end{aligned} \tag{3.5}$$

The optimal design trim moment matrix and the surface fit are shown in Figure 3.15. Equation 3.6 for optimal design trim moment has a coefficient of determination value (R^2) of

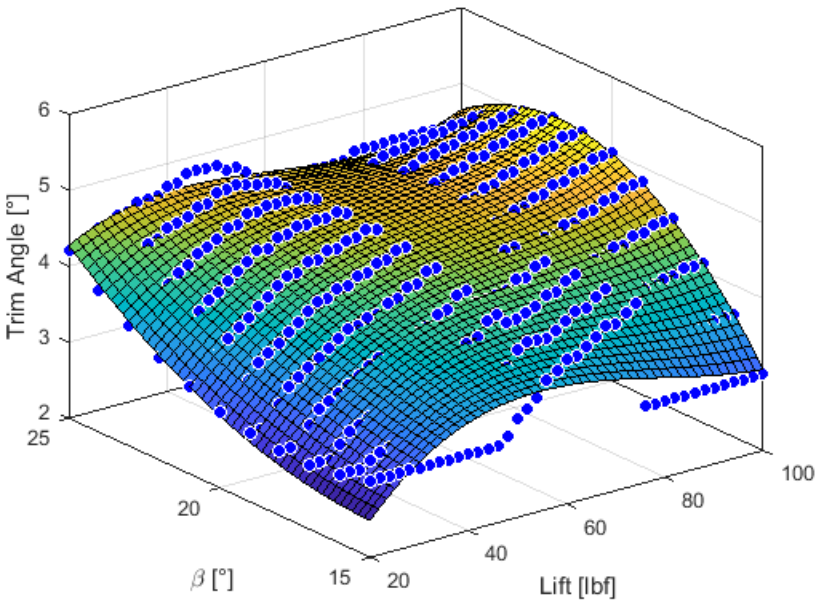

Figure 3.12: Trim Values for Optimal Designs

0.9455 and root meat square error (RMSE) value of 38.1229 pounds per inch.

$$\begin{aligned}(M_y)_{opt} = & -5.198(10^4) + 148.8L + 1.188(10^4)\beta + 10.02L^2 - 83.49L\beta - 992.8\beta^2 \\ & + 0.02275L^3 - 1.666L^2\beta + 10.53L\beta^2 + 35.74\beta^3 - 0.001071L^4 \\ & + 0.007753L^3\beta + 0.05847L^2\beta^2 - 0.4591L\beta^3 - 0.4698\beta^4 \\ & + 4.262(10^{-6})L^5 - 1.227(10^{-6})L^4\beta - 0.0001762L^3\beta^2 - 0.000613L^2\beta^3 \\ & + 0.006689L\beta^4\end{aligned} \tag{3.6}$$

The optimal design wetted keel length matrix and the surface fit are shown in Figure 3.16. Equation 3.7 for optimal design wetted keel length has a coefficient of determination value (R^2) of 0.9862 and root meat square error (RMSE) value of 0.6716 inches. It is important to not that the matrix has values larger than allowed by the model used for this study. This is considered to be outside the area of interest due to its extreme variation from the original design concept of Clement's discussed in Chapter 1.

$$\begin{aligned}(L_k)_{opt} = & -198.9 + 6.526L + 21.72\beta - 0.005074L^2 - 0.8406L\beta - 0.407\beta^2 \\ & - 0.0004884L^3 + 0.003952L^2\beta + 0.02768L\beta^2 - 0.01307\beta^3 + 2.422(10^{-6})L^4 \\ & - 6.715(10^{-7})L^3\beta - 8.924(10^{-5})L^2\beta^2 - 0.0002433L\beta^3 + 0.0003405\beta^4\end{aligned} \tag{3.7}$$

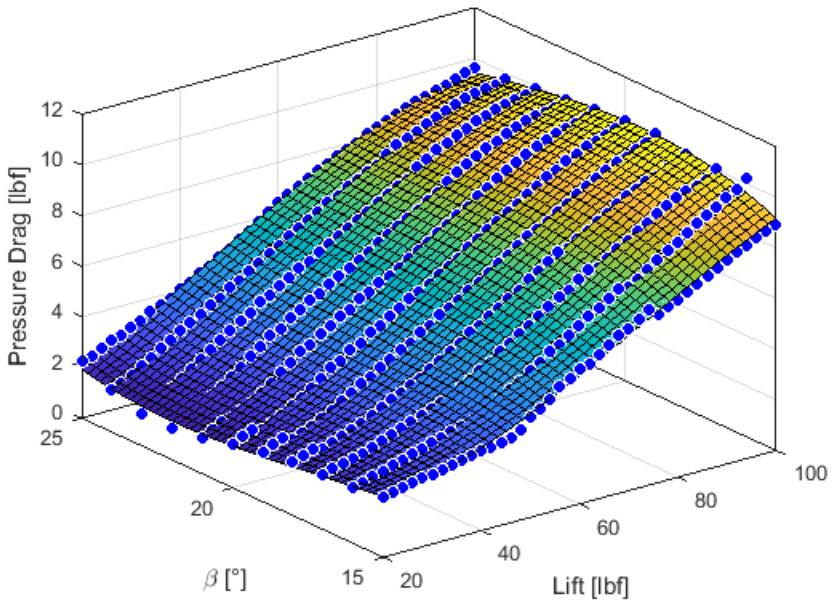

Figure 3.13: Pressure Drag Values for Optimal Designs

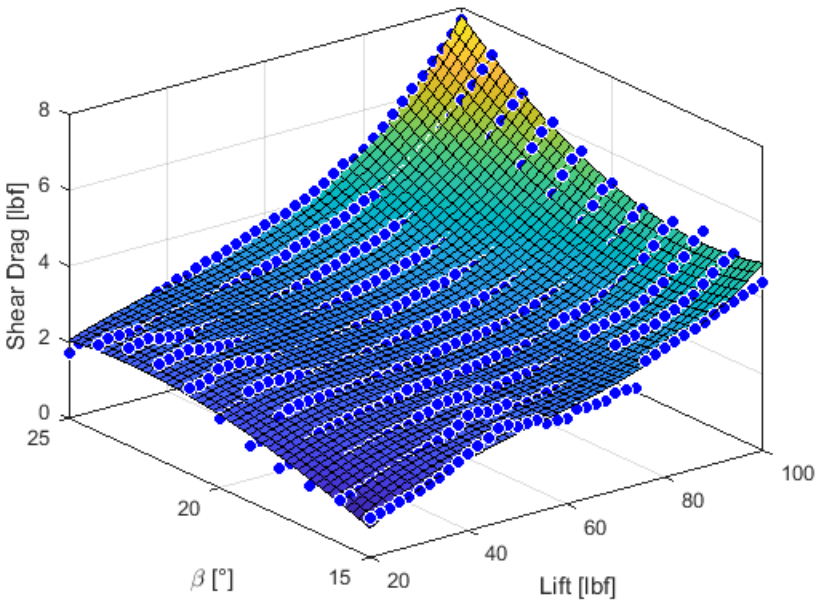

Figure 3.14: Shear Drag Values for Optimal Designs

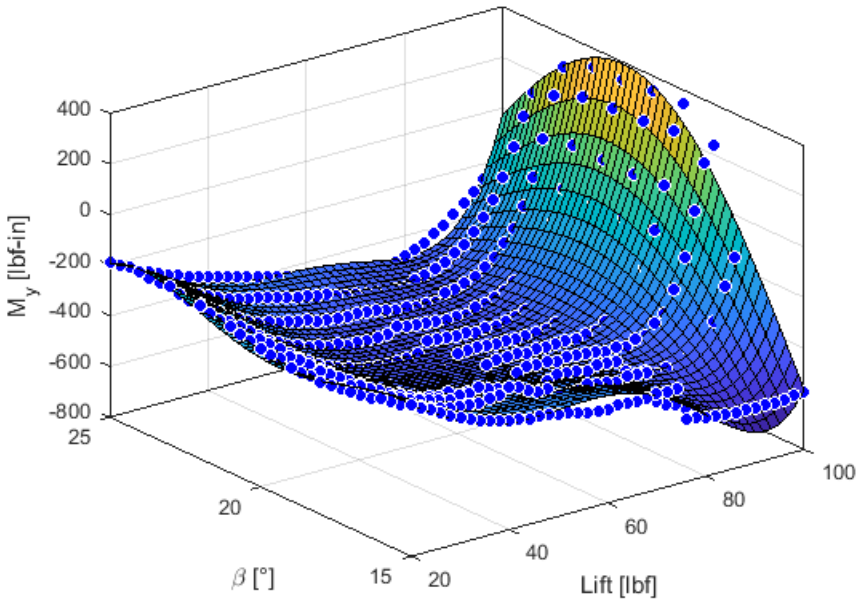

Figure 3.15: Trim Moment Values for Optimal Designs

The optimal design draft matrix and the surface fit are shown in Figure 3.17. Equation 3.8 for optimal design draft has a coefficient of determination value (R^2) of 0.9951 and root meat square error (RMSE) value of 0.0385 inches.

$$\begin{aligned}(T)_{opt} = {} & 6.749 + 0.2713L - 1.79\beta - 0.0001476L^2 - 0.03653L\beta + 0.168\beta^2 \\ & - 2.872(10^{-5})L^3 + 0.0002099L^2\beta + 0.00124L\beta^2 - 0.006224\beta^3 \\ & + 1.401(10^{-7})L^4 + 6.24(10^{-8})L^3\beta - 5.183(10^{-6})L^2\beta^2 - 1.062(10^{-5})L\beta^3 \\ & + 8.007(10^{-5})\beta^4\end{aligned} \tag{3.8}$$

The optimal design wetted surface area matrix and the surface fit are shown in Figure 3.18. Equation 3.9 for optimal design wetted surface area has a coefficient of determination value (R^2) of 0.9809 and root meat square error (RMSE) value of 10.0575 square inches.

$$\begin{aligned}(A_w)_{opt} = {} & -482 + 21.43L + 36.1\beta - 0.1925L^2 - 1.186L\beta - 0.681\beta^2 + 0.0009197L^3 \\ & + 0.003073L^2\beta + 0.0241L\beta^2 - 0.002151\beta^3\end{aligned} \tag{3.9}$$

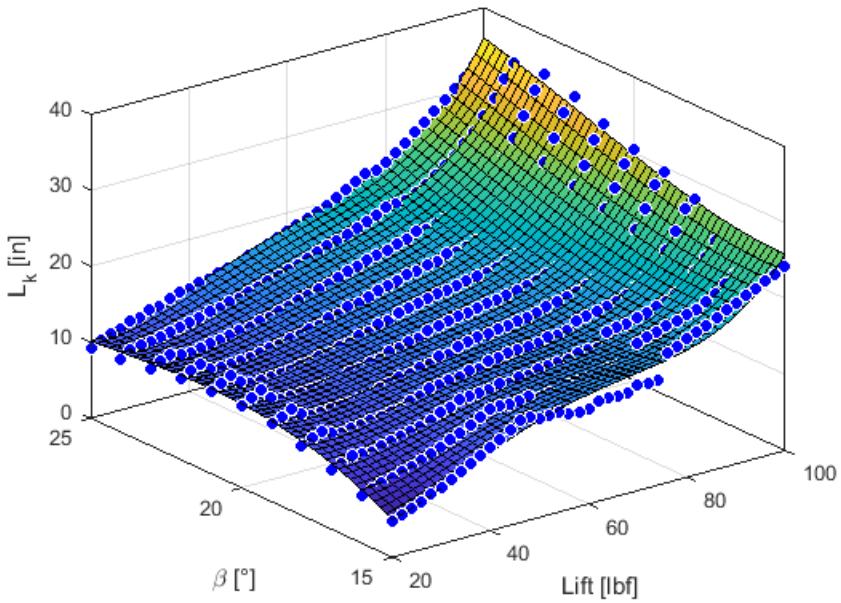

Figure 3.16: Wetted Keel Length Values for Optimal Designs

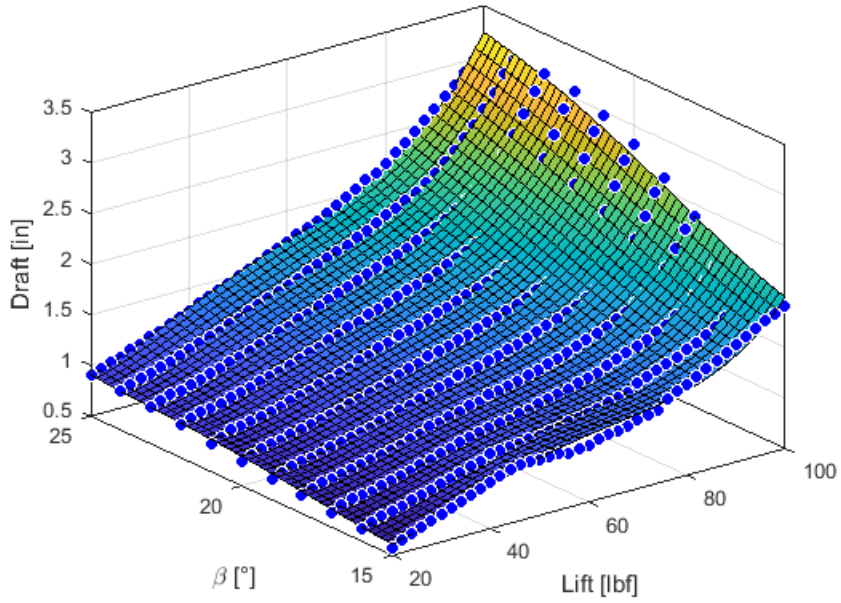

Figure 3.17: Draft Values for Optimal Designs

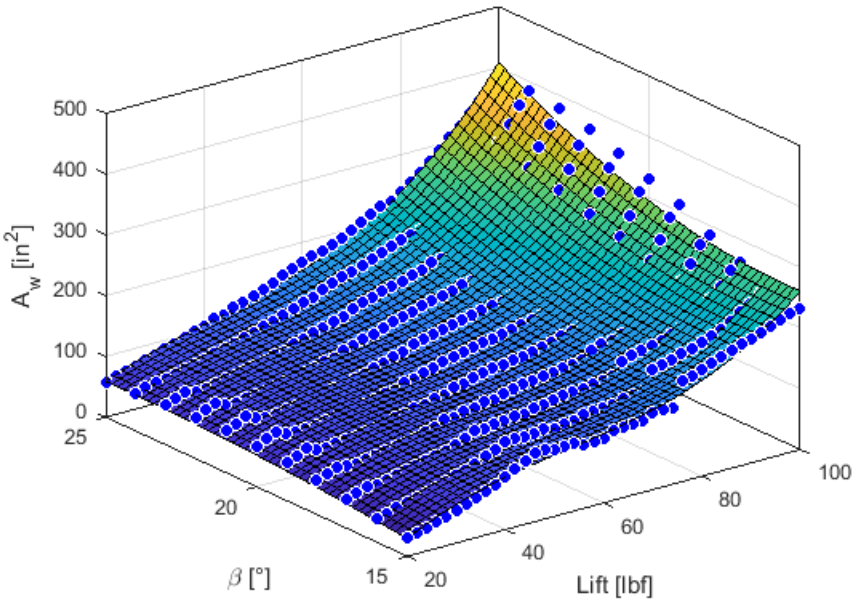

Figure 3.18: Wetter Surface Area Values for Optimal Designs

3.4 Improved Cambered Step Design Procedure Validation

Two cases were tested in the range of designs not as effected by the limitations caused by the small range of two dimensional lift coefficients and trim angle tested for the database. The first design test has a required lift of 50 pounds with a deadrise of 17.75 degrees. The second test has a required lift of 75 pounds with a higher deadrise of 22 degrees. Equations 3.2 and 3.3 are used to determined the design of the optimal design for the desired sea-keeping and load requirements. Equations 3.1 and 3.4-3.9 are used to predict the performance of the cambered planing surface. The results of the CFD simulations and the equations are presented in Tables 3.1 and 3.2. The error from the calculated values are small with two exceptions. The first exception is the trim moment for the first design test. The difference between the CFD value and the equation value is greater than 3% and is greater than the calculated by the RMSE value of 38.1229 pounds per inch for the trim moment equation. The second exception is the wetted surface area and the wetted keel length. The percent error for both are greater than 3%. The wetted surface area is within the range of error determined by the RMSE value of 10.0575 square inches. The wetted keel length is outside the range of error determined by the RMSE value of 0.6716.

	D_S		D_P		D	L/D	M_y	T	L_k	A_w
	[lbf]	[%]	[lbf]	[%]	[lbf]		[lbf-in]	[in]	[in]	[in^2]
CFD	2.34	34%	4.55	66%	6.89	7.25	-411.87	1.004	12.02	100.73
Equations	2.33	34%	4.58	67%	6.82	7.34	-452.51	1.048	12.37	100.65
Error	0.4%	-0.8%	-0.6%	-1.7%	1.1%	-1.1%	-9.9%	-4.4%	-2.9%	0.1%

Table 3.1: Design Test #1: $L = 50$ lbf, $\tau = 3.97°$, $\beta = 17.75°$, and $C_{L,d} = 0.1367$

	D_S		D_P		D	L/D	M_y	T	L_k	A_w
	[lbf]	[%]	[lbf]	[%]	[lbf]		[lbf-in]	[in]	[in]	[in^2]
CFD	3.52	30%	8.13	70%	11.65	6.44	-522.77	1.684	16.66	162.14
Equations	3.55	31%	7.91	69%	11.49	6.53	-508.31	1.716	17.42	170.15
Error	-0.7%	-2.2%	2.7%	1.3%	1.4%	-1.4%	2.8%	-1.9%	-4.6%	-4.9%

Table 3.2: Design Test #2: $L = 75$ lbf, $\tau = 4.65°$ $\beta = 22°$ $C_{L,d} = 0.2159$

Chapter 4

Conclusions

4.1 Summary

Clement's design method for swept-back cambered step hulls has two limitations: high dead-rise angles and multiple iterations. To improve and expand upon the Clement method, two cambered step hulls were designed and then tested in the tow tank at the United States Naval Academy. The two cambered surfaces utilized a constant camber (step-A) and a parabolic camber (step-B) distribution. Simulations ran using STAR CCM+ were validated with the experimental results. The results of the validation show a strong correlation for low load values with a less than 5% difference between experimental and CFD lift-to-drag ratio results. At higher loads the correlation is weaker with a 5%-10% difference between experimental and CFD for lift-to-drag ratio results. The trim moment showed a low correlation of 5%-10% difference between experimental and CFD at low load values with a steep increase in erro at high loads with the exception of step-A at a nominal trim angle of 5 degrees. Step-A at a nominal trim angle of 5 degrees showed a less than 6% difference for trim moment except at 40 and 50 pound loads. The validated simulation is able to correctly predict the wake profile and the beginning of the spray sheet for both step designs at all load conditions.

A series of sensitivity studies were performed to test experimental trim uncertainty, different turbulence models, different wall treatments, time step, and potential surface roughness. The experimental trim study did not show significant change for the simulation prediction. The utilization of a relizable k-epsilon two layer model and a SST k-omega tubulence model did not show an appreciable difference in the simulation prediction. Testing y^+ less than 1 only worsen the trim moment predictions compared to the all y^+ wall treatment. The difference between a constant time step of 2e-4 seconds and courant number controlled time step did improve the courant number, but did not have an effect on the simulations prediction. The potential roughness of the planing surface of the model used in experimental testing was explored with varying roughness heights in the CFD simulation. The lift-to-drag ratio and trim moment predictions improved for high load cases, but worsen for low load cases.

The validated simulation was used to create a database with a limited design space for a proof of concept study showing that equations can be created to determine the optimal design and performance characteristics of a swept-back cambered planing surface for a given sea-keeping and load requirements. The equations determined from the database were then validated with two design configurations not previously tested for the database. The results

of this validation showed that the equations can determine the optimizal design and its performance characteristics within 5% for mid-range values for deadrise and lift. The plots showed that for high and low lift and deadrise angles that the accuracy of the prediction will reduce due to the limited range of two-dimensional lift coefficient that determined the camber of the planing surface.

4.2 Future Work

There is always room for improvement and this study is no exception. Future points to investigate or continue investigation on our the following.

- Continue simulations validation study with new experimental results to improve upon the predictions, particularly trim moment and drag at high loads. For further experimental studies, increase the stiffness of the model to further eliminate flex in the model.
- Extend the range of the database tested. Testing a wider range of two-dimensional lift coefficient values outside the target range would improve the results on the boundaries of the design space. To advance this proof of concept to a design method with require the addition of testing different aspect ratios, beams, and speeds.
- Study the scaling effects on the drag and trim moment for a cambered step hull for future applications to full scale models.

Bibliography

[1] Bay, R., Brizzolara, S., Stern, F., Wang, Z., Morabito, M., and Beaver, B. (2019). Efd/cfd of high deadrise cambered planing surfaces.

[2] Brizzolara S., Judge C., B. W. (2016). High deadrise stepped cambered planing hulls with hydrofoils: Scph2. a proof of concept. *SNAME Transactions*, Vol 124:312–321.

[3] Clement, E. P. (1964). A lifting surface approach to planing boat design. DTMB Report 1902.

[4] Clement, E. P. (2013). How to design an efficient stepped dynaplane boat. SNAME.

[5] Faltinsen, O. M. (2005). *Hydrodynamics of High-Speed Marine Vehicles*. Cambridge University Press, Cambridge, UK.

[6] Johnson, V. E. (1961). Theoretical and experimental investigation of supercavitating hydrofoils operating near the free water surface. Technical Report 19980228449, NASA.

[7] Morabito, M. and Beaver, W. (2017). Preliminary report on experiments on high-deadrise cambered planing surfaces. Test memorandum, United States Naval Academy, Annapolis, Maryland.

[8] of 25th International Towing Tank Conference (ITTC), R. C. (2008). Uncertainty analysis in cfd verification and validation methodology and procedures.

[9] Savitsky, D. (1964). Hydrodynamic design of planing hulls.

Appendices

Appendix A

CFD Verification and Validation

A.1 Experimental Results

Table A.1: Step-A Experimental Results

Run #	Trim [°]	Lift [lbf]	Drag [lbf]	L/D	Trim Moment [lbf-in]	Moment Arm [in]	L_k [in]	L_c [in]	Draft [in]
24	3.09	20	4.98	4.01	-49.90	-2.42	9.0	STEP	0.93
25	2.99	30	6.13	4.89	-69.09	-2.26	12.0	-9.5	1.08
26	2.72	40	7.30	5.48	-73.44	-1.81	15.0	-7.0	1.16
27	3.01	50	8.77	5.70	-44.60	-0.88	18.0	-4.2	1.39
28	3.01	60	10.48	5.73	40.25	0.66	21.0	-1.5	1.56
11	3.78	20	5.13	3.90	-53.96	-2.61	4.8	STEP	0.77
10	3.95	22.5	5.47	4.11	-59.57	-2.57	5.0	STEP	0.79
14	3.79	30	6.27	4.78	-77.39	-2.52	9.0	-9.5	1.04
16	3.86	40	7.20	5.55	-95.24	-2.34	10.0	-7.5	1.12
17	4.02	50	8.50	5.88	-87.22	-1.72	11.7	-6.0	1.27
18	4.09	60	10.17	5.90	-43.07	-0.71	14.7	-4.2	1.50
19	4.95	20	5.48	3.65	-60.83	-2.93	3.5	STEP	0.75
20	4.97	30	6.87	4.37	-90.72	-2.95	4.8	-9.5	0.86
21	4.86	40	7.71	5.19	-108.90	-2.67	7.0	-9.0	1.04
22	5.04	50	8.75	5.71	-112.97	-2.23	9.0	-5.5	1.24
23	4.96	60	10.29	5.83	-88.71	-1.46	10.3	-4.0	1.33

Table A.2: Step-B Experimental Results

Run #	Trim [°]	Lift [lbf]	Drag [lbf]	L/D	Trim Moment [lbf-in]	Moment Arm [in]	L_k [in]	L_c [in]	Draft [in]
39	2.95	20	5.00	4.00	-51.78	-2.51	10.0	STEP	0.62
40	3.09	30	6.15	4.88	-69.74	-2.51	12.7	-8.5	0.79
41	3.01	40	7.44	5.38	-69.35	-1.70	16.0	-5.5	0.95
42	3.01	50	8.98	5.57	-28.53	-0.56	20.0	-4.0	1.16
48	3.80	60	10.79	5.56	73.00	1.20	23.0	1.0	1.63
29	4.07	20	5.51	3.63	-59.85	-2.88	5.7	STEP	0.51
30	4.16	30	6.46	4.64	-83.68	-2.73	8.5	-8.0	0.73
31	4.04	40	7.45	5.37	-97.46	-2.40	10.5	-6.0	0.85
32	3.79	50	8.75	5.71	-81.12	-1.60	13.0	-4.5	0.97
33	4.10	60	10.09	5.94	-26.07	-0.43	15.1	-2.5	1.19
34	5.31	20	5.80	3.45	-64.49	-3.10	4.5	STEP	0.53
35	4.86	30	6.84	4.39	-85.76	-2.79	6.5	STEP	0.66
36	4.77	40	7.61	5.26	-107.39	-2.64	8.1	-6.0	0.78
37	4.85	50	8.79	5.69	-102.51	-2.02	9.5	-5.0	0.91
38	5.35	60	10.52	5.70	-72.00	-1.18	11.0	-3.0	1.14

A.2 CFD Results

A.2.1 Fixed

Table A.3: Step-A Fixed Position Results (k-ϵ)

Run #	Trim [°]	Lift [lbf]	Lift Error	Drag [lbf]	Drag Error	L/D
24	3.09	22.961	14.8%	5.245	5.2%	4.378
25	2.99	-	-	-	-	-
26	2.72	35.400	-11.5%	6.159	-15.6%	5.748
27	3.01	-	-	-	-	-
28	3.01	58.781	-5.4%	8.886	-15.2%	6.390
11	3.78	-	-	-	-	-
10	3.95	28.120	25.0%	6.267	14.5%	4.487
14	3.79	-	-	-	-	-
16	3.86	40.582	1.5%	7.032	-2.4%	5.771
17	4.02	-	-	-	-	-
18	4.09	62.854	4.8%	9.600	-5.6%	6.547
19	4.95	-	-	-	-	-
20	4.97	41.109	37.0%	8.029	16.8%	5.120
21	4.86	46.648	16.6%	8.268	7.3%	5.642
22	5.04	-	-	-	-	-
23	4.96	61.659	2.8%	9.756	-5.2%	6.320

Table A.4: Step-A Fixed Position Results (k-ω)

Run #	Trim [°]	Lift [lbf]	Lift Error	Drag [lbf]	Drag Error	L/D
24	3.09	23.127	15.6%	5.356	7.5%	4.318
25	2.99	-	-	-	-	-
26	2.72	35.453	-11.4%	6.271	-14.1%	5.653
27	3.01	-	-	-	-	-
28	3.01	59.936	-5.1%	9.029	-13.8%	6.306
11	3.78	-	-	-	-	-
10	3.95	28.365	26.1%	6.407	17.0%	4.427
14	3.79	-	-	-	-	-
16	3.86	40.764	1.9%	7.170	-0.5%	5.685
17	4.02	-	-	-	-	-
18	4.09	63.014	5.0%	9.769	-3.9%	6.450
19	4.95	-	-	-	-	-
20	4.97	41.256	37.5%	8.168	18.9%	5.051
21	4.86	46.868	17.2%	8.412	9.2%	5.571
22	5.04	-	-	-	-	-
23	4.96	61.872	3.1%	9.929	-3.5%	6.232

Table A.5: Step-B Fixed Position Results (k-ϵ)

Run #	Trim [°]	Lift [lbf]	Lift Error	Drag [lbf]	Drag Error	L/D
39	2.95	-	-	-	-	-
40	3.09	32.196	7.3%	6.053	-1.6%	5.319
41	3.01	41.486	3.7%	6.980	-6.1%	5.944
42	3.01	51.470	2.9%	8.337	-7.2%	6.174
48	3.80	-	-	-	-	-
29	4.07	-	-	-	-	-
30	4.16	34.464	14.9%	6.784	5.0%	5.081
31	4.04	42.740	6.9%	7.328	-1.7%	5.832
32	3.79	48.344	-3.3%	7.787	-11.0%	6.209
33	4.10	-	-	-	-	-
34	5.31	-	-	-	-	-
35	4.86	34.686	15.6%	7.360	7.7%	4.712
36	4.77	43.413	8.5%	7.844	3.1%	5.535
37	4.85	52.470	4.9%	8.790	0.0%	5.969
38	5.35	-	-	-	-	-

Table A.6: Step-B Fixed Position Results (k-ω)

Run #	Trim [°]	Lift [lbf]	Lift Error	Drag [lbf]	Drag Error	L/D
39	2.95	-	-	-	-	-
40	3.09	32.271	7.6%	6.143	-0.2%	5.253
41	3.01	41.427	3.6%	7.067	-4.9%	5.862
42	3.01	51.629	3.3%	8.464	-5.8%	6.100
48	3.80	-	-	-	-	-
29	4.07	-	-	-	-	-
30	4.16	34.551	15.2%	6.895	6.7%	5.011
31	4.04	42.993	7.5%	7.437	-0.2%	5.781
32	3.79	48.393	-3.2%	7.915	-9.6%	6.114
33	4.10	-	-	-	-	-
34	5.31	-	-	-	-	-
35	4.86	34.938	16.5%	7.475	9.3%	4.674
36	4.77	43.533	8.8%	7.962	4.6%	5.468
37	4.85	52.739	5.5%	8.927	1.6%	5.908
38	5.35	-	-	-	-	-

A.2.2 Free Heave

Table A.7: Step-A CFD Free Heave Results

Run #	Trim [°]	Lift [lbf]	Drag [lbf]	%E(D)	Shear Drag %	Pressure Drag %	L/D	M_Y [lbf-in]	%E(M_Y)	L_{cp} [in]	L_k [in]	L_c [in]	Draft [in]
24	3.09	20	4.94	-0.8%	25%	75%	4.05	-53.08	6.4%	-2.65	5.3	STEP	0.792
25	2.99	30	5.80	-5.4%	29%	71%	5.17	-73.75	6.8%	-2.46	12.0	STEP	0.985
26	2.72	40	6.56	-10.1%	37%	63%	6.10	-79.89	8.8%	-2.00	16.9	-7.5	1.151
27	3.01	50	7.71	-12.1%	39%	61%	6.48	-68.02	52.5%	-1.36	18.5	-5.6	1.313
28	3.01	60	9.20	-12.2%	44%	56%	6.52	3.03	-92.5%	0.05	23.1	-2.3	1.759
11	3.78	20	5.33	4.0%	23%	77%	3.75	-56.76	5.2%	-2.84	4.4	STEP	0.867
10	3.95	22.5	5.80	5.9%	22%	78%	3.88	-65.40	9.8%	-2.91	4.5	STEP	0.791
14	3.79	30	6.28	0.1%	23%	77%	4.78	-82.22	6.2%	-2.74	9.0	-9.5	0.979
16	3.86	40	6.96	-3.3%	25%	75%	5.74	-101.77	6.9%	-2.54	10.2	-7.8	1.036
17	4.02	50	7.97	-6.3%	27%	73%	6.27	-102.60	17.6%	-2.05	12.0	-5.9	1.177
18	4.09	60	9.11	-10.4%	31%	69%	6.59	-71.73	66.8%	-1.20	12.2	-4.1	1.373
19	4.95	20	6.02	9.9%	21%	79%	3.32	-62.12	2.1%	-3.11	2.8	STEP	0.785
20	4.97	30	7.33	6.6%	19%	81%	4.10	-95.68	5.5%	-3.19	4.0	-9.6	0.805
21	4.86	40	7.86	2.0%	19%	81%	4.10	-119.70	9.9%	-2.99	6.4	-7.8	1.046
22	5.04	50	8.71	-0.4%	20%	80%	5.74	-127.54	12.9%	-2.55	8.3	-6.2	1.118
23	4.96	60	9.72	-5.5%	26%	74%	6.17	-91.41	3.0%	-1.52	12.4	-4.3	1.440

Table A.8: Step-B CFD Free Heave Results

Run #	Trim [°]	Lift [lbf]	Drag [lbf]	%E(D)	Shear Drag %	Pressure Drag %	L/D	M_Y [lbf-in]	%E(M_Y)	L_{cp} [in]	L_k [in]	L_c [in]	Draft [in]
39	2.95	20	4.49	-1.3%	27%	73%	4.05	-56.15	8.4%	-2.81	10.2	STEP	0.551
40	3.09	30	5.88	-4.5%	30%	70%	5.10	-79.09	13.4%	-2.64	12.6	-9.1	0.707
41	3.01	40	6.75	-9.2%	36%	64%	5.93	-86.74	25.1%	-2.17	15.5	-7.0	0.869
42	3.01	50	8.08	-10.1%	43%	57%	6.19	-63.18	121.5%	-1.26	19.6	-4.9	1.080
48	3.80	60	9.41	-12.7%	36%	64%	6.37	-42.75	-156.6%	-0.71	17.9	-3.2	1.162
29	4.07	20	5.37	-2.5%	23%	77%	3.72	-61.25	2.3%	-3.06	7.4	STEP	0.646
30	4.16	30	6.51	0.7%	22%	78%	4.61	-91.80	9.7%	-3.06	8.2	-8.9	0.603
31	4.04	40	7.12	-4.5%	26%	74%	5.62	-108.12	10.9%	-2.70	10.3	-7.3	0.755
32	3.79	50	8.21	-6.2%	35%	65%	6.09	-86.07	6.1%	-1.72	16.0	-5.4	1.109
33	4.10	60	9.29	-7.9%	33%	67%	6.46	-62.97	141.5%	-1.05	15.4	-3.5	1.099
34	5.31	20	6.09	4.9%	18%	82%	3.29	-69.07	7.1%	-3.45	4.1	STEP	0.393
35	4.86	30	7.05	3.2%	19%	81%	4.25	-99.35	15.8%	-3.31	6.2	-9.0	0.551
36	4.77	40	7.62	0.1%	21%	79%	5.25	-119.65	11.4%	-2.99	8.3	-7.2	0.687
37	4.85	50	8.52	-3.1%	23%	77%	5.87	-122.82	19.8%	-2.46	9.7	-5.9	0.820
38	5.35	60	9.93	-5.6%	22%	78%	6.04	-117.06	62.6%	-1.95	9.9	-4.3	0.896

A.3 Friction and Pressure Coefficient Plots

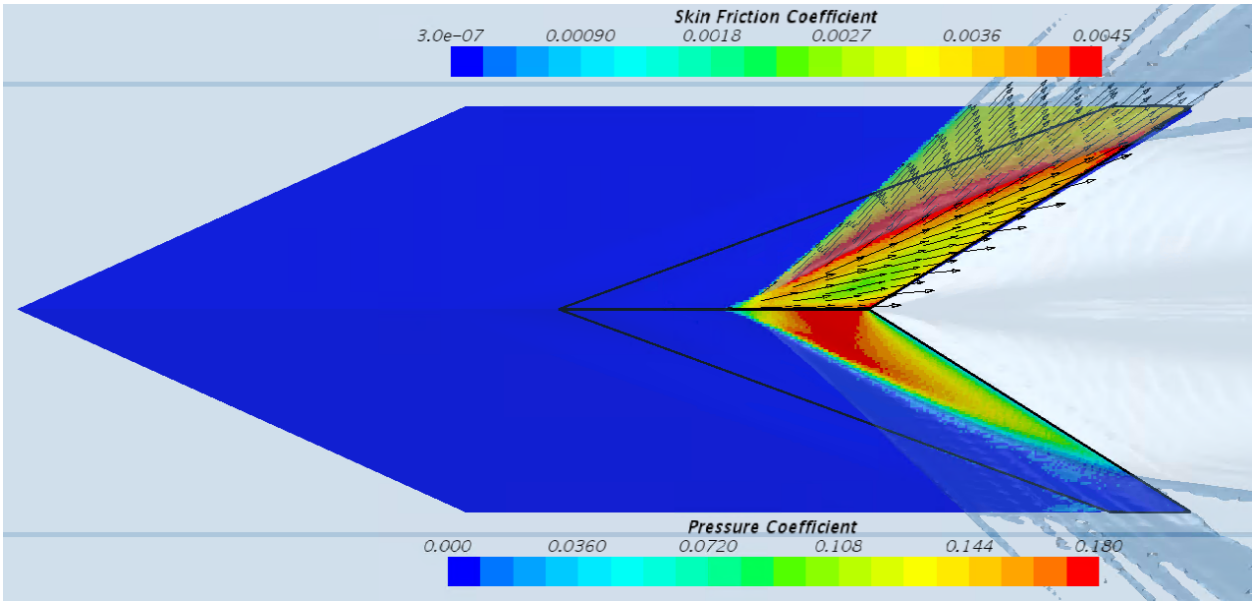

Figure A.1: Friction and Pressure Coefficient Plots (Run 11)

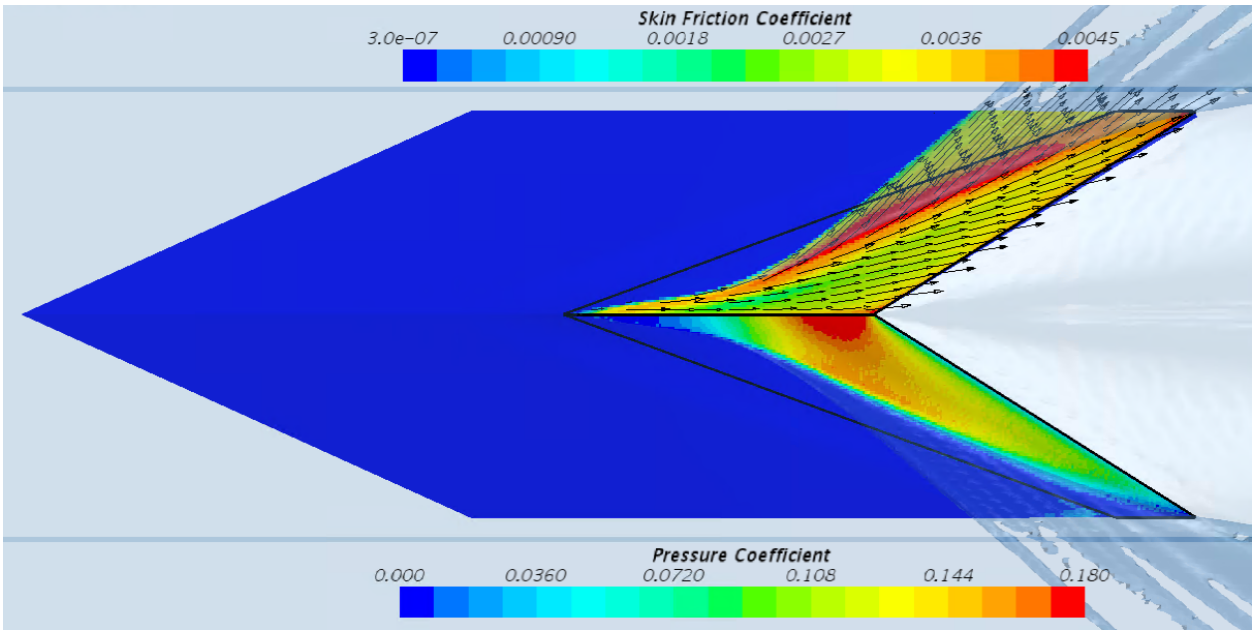

Figure A.2: Friction and Pressure Coefficient Plots (Run 14)

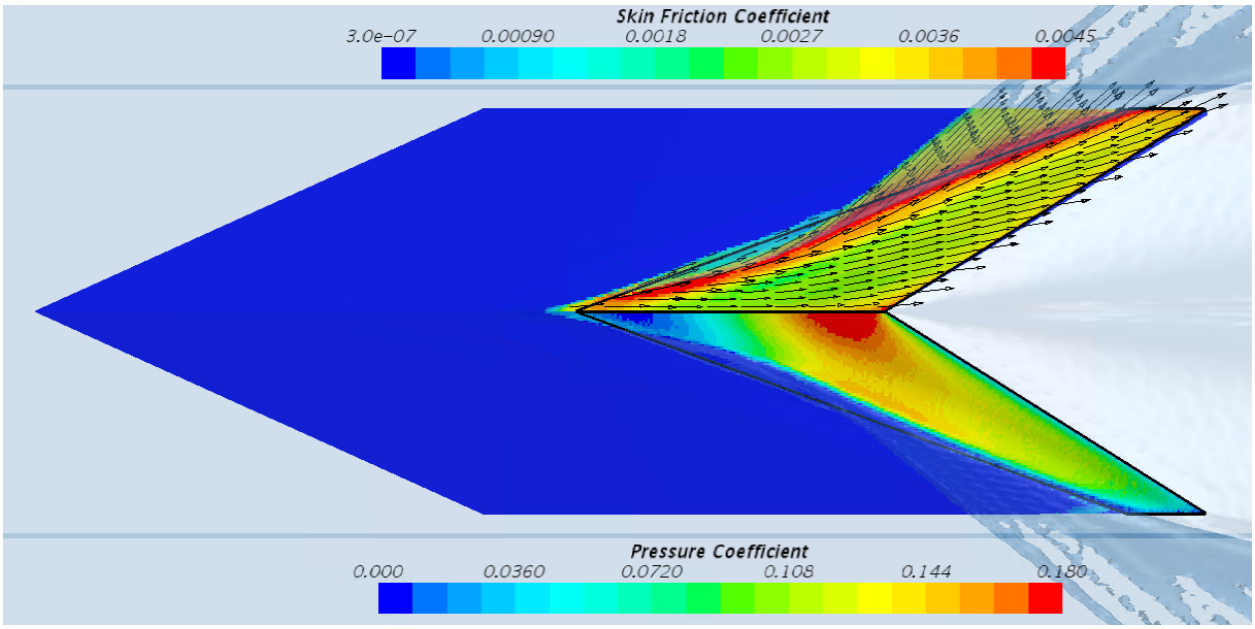

Figure A.3: Friction and Pressure Coefficient Plots (Run 16)

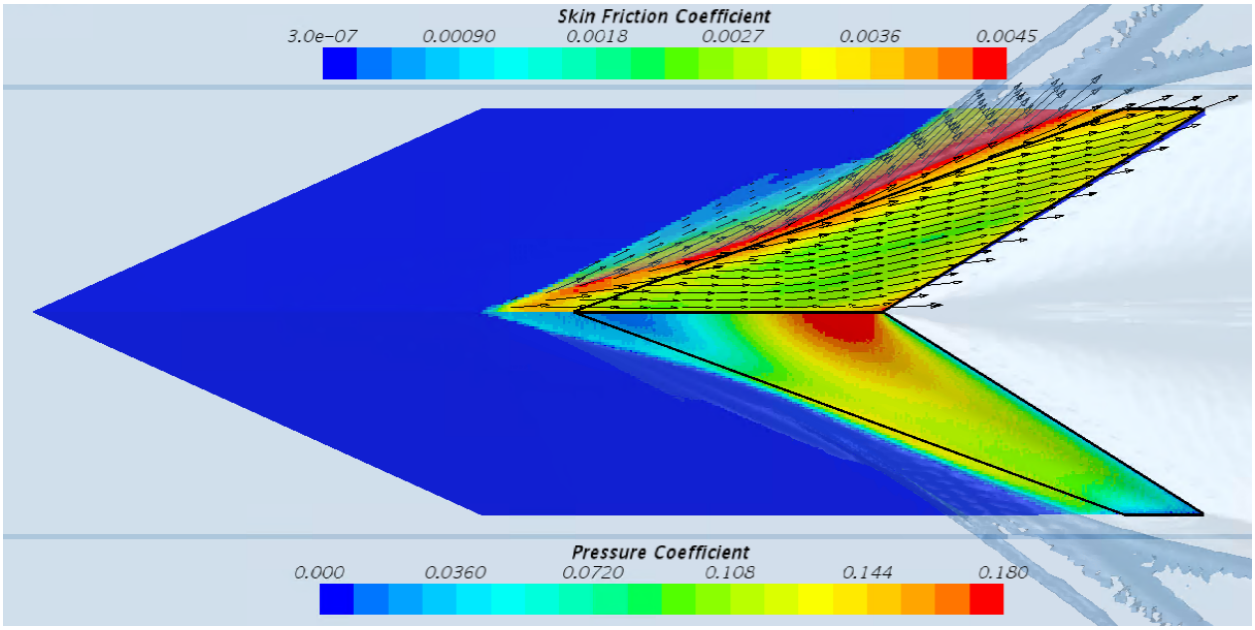

Figure A.4: Friction and Pressure Coefficient Plots (Run 17)

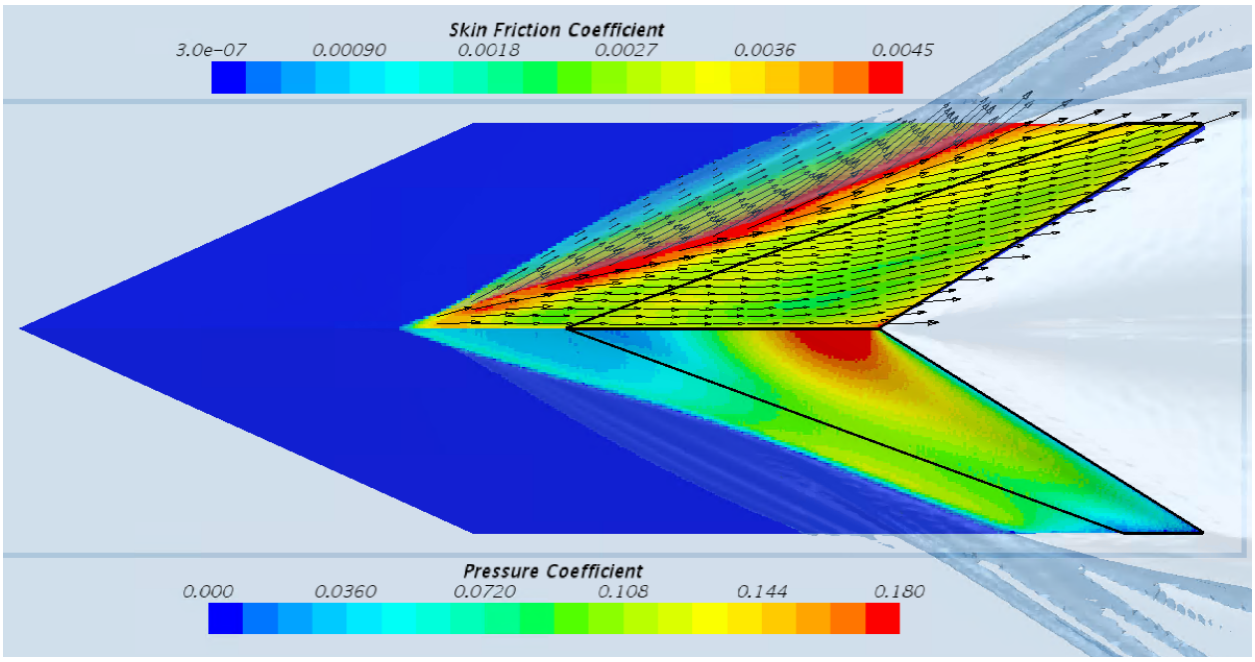

Figure A.5: Friction and Pressure Coefficient Plots (Run 18)

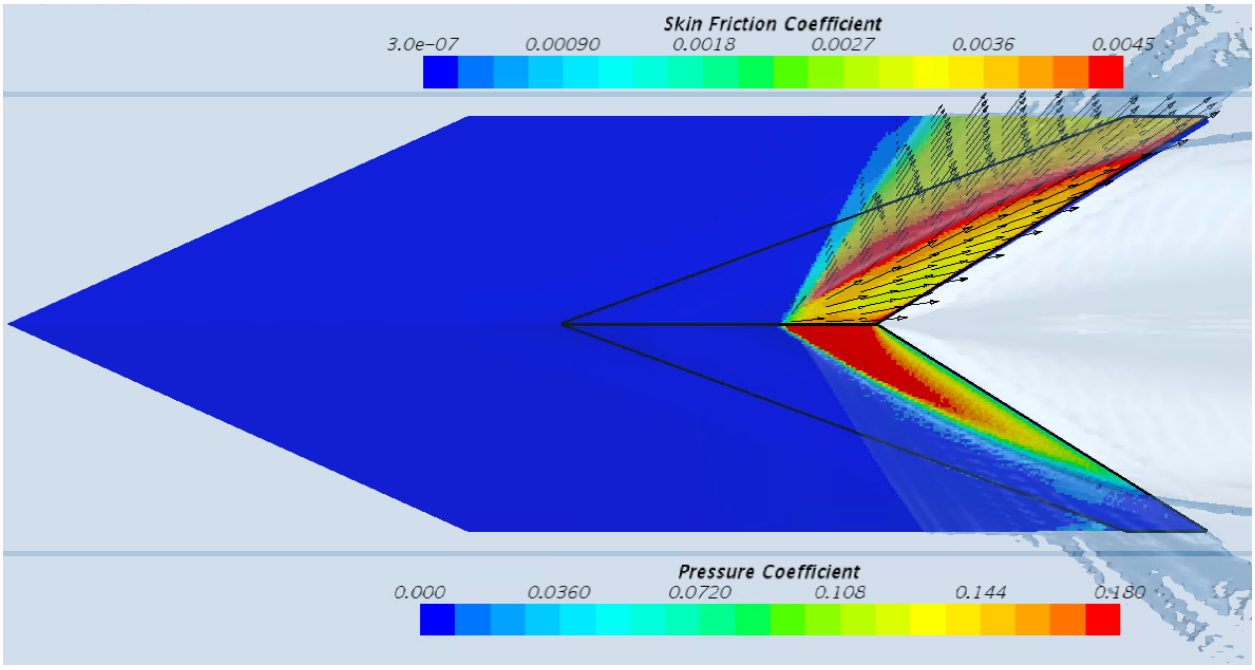

Figure A.6: Friction and Pressure Coefficient Plots (Run 19)

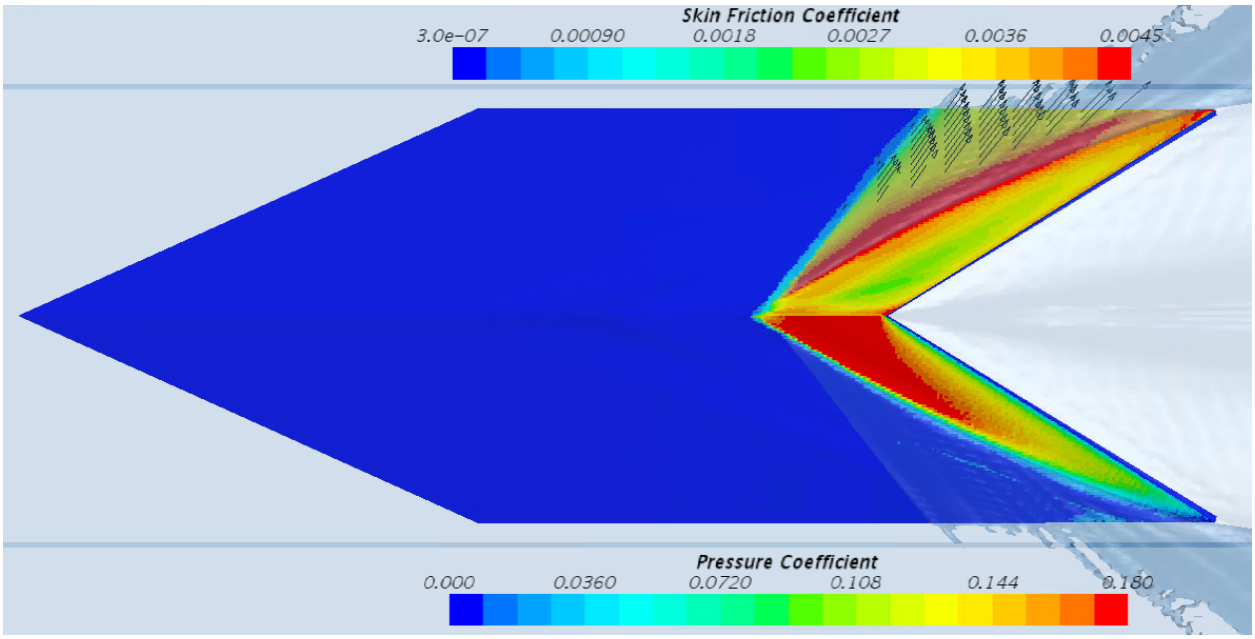

Figure A.7: Friction and Pressure Coefficient Plots (Run 20)

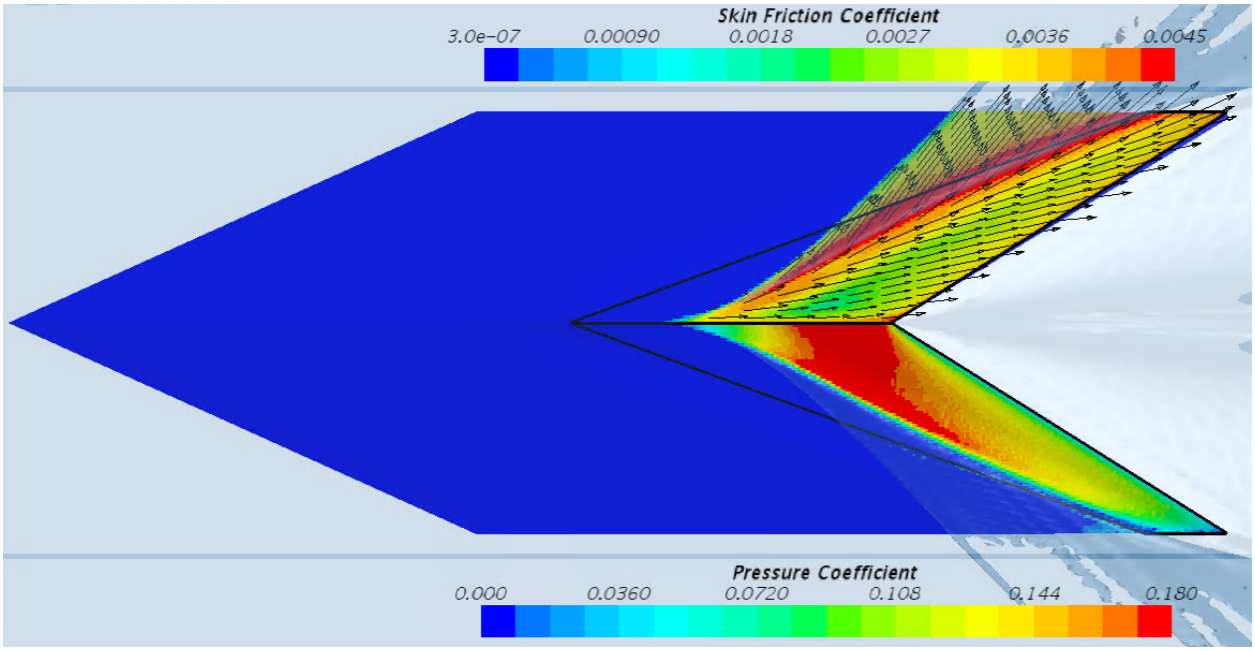

Figure A.8: Friction and Pressure Coefficient Plots (Run 21)

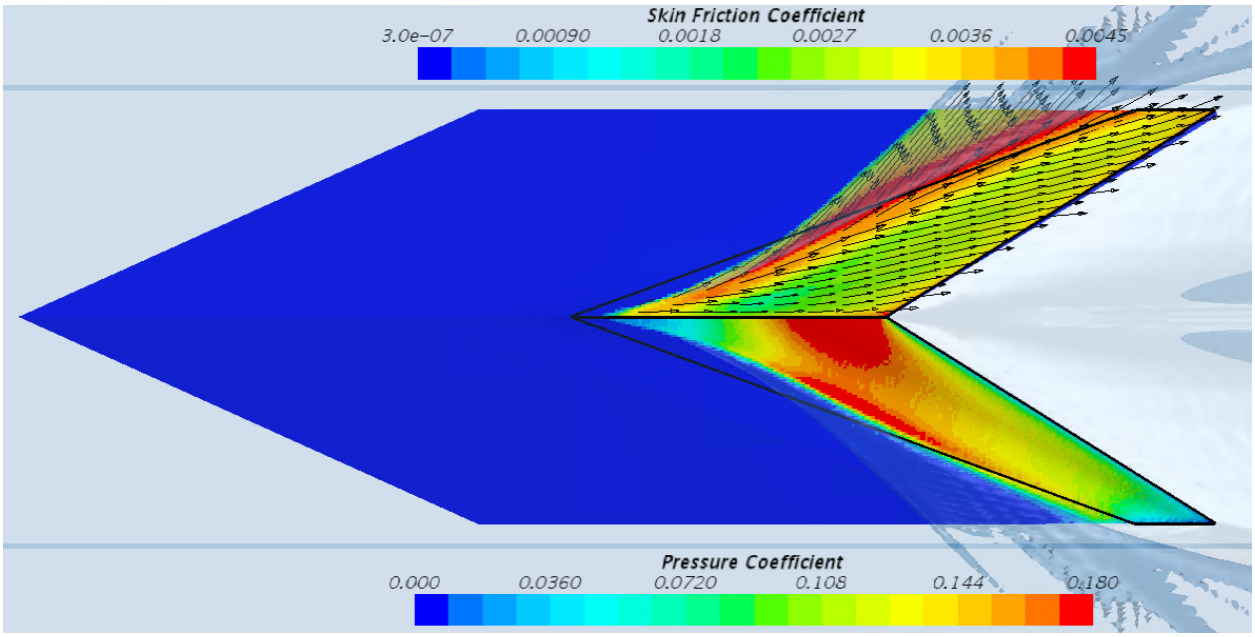

Figure A.9: Friction and Pressure Coefficient Plots (Run 22)

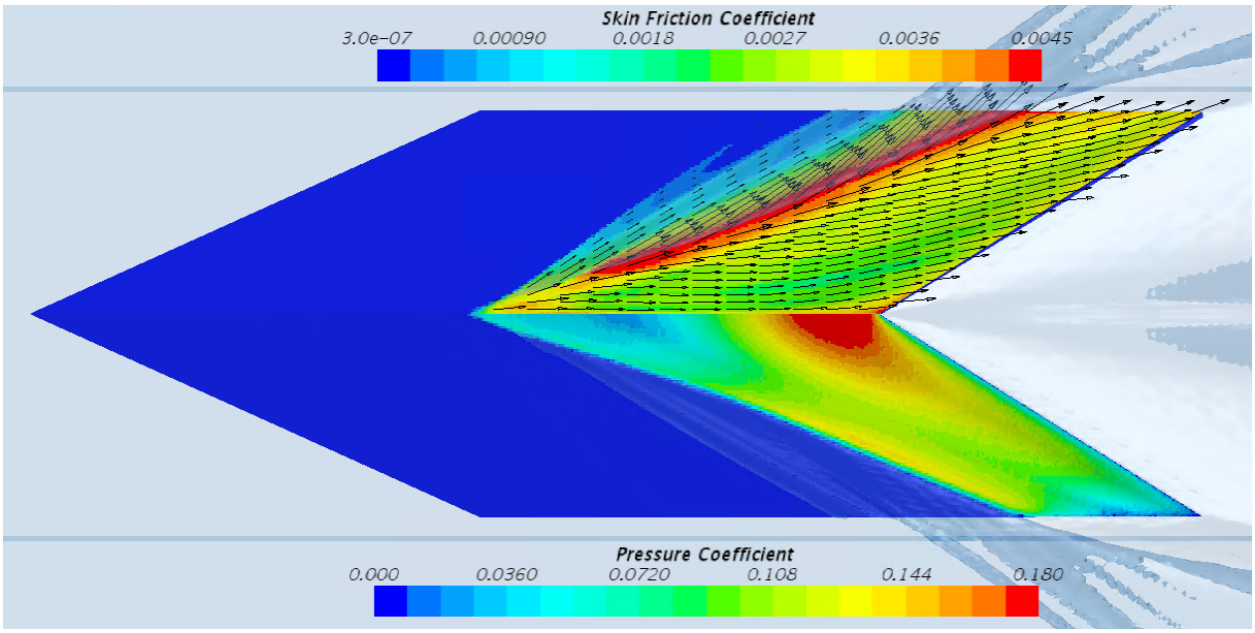

Figure A.10: Friction and Pressure Coefficient Plots (Run 23)

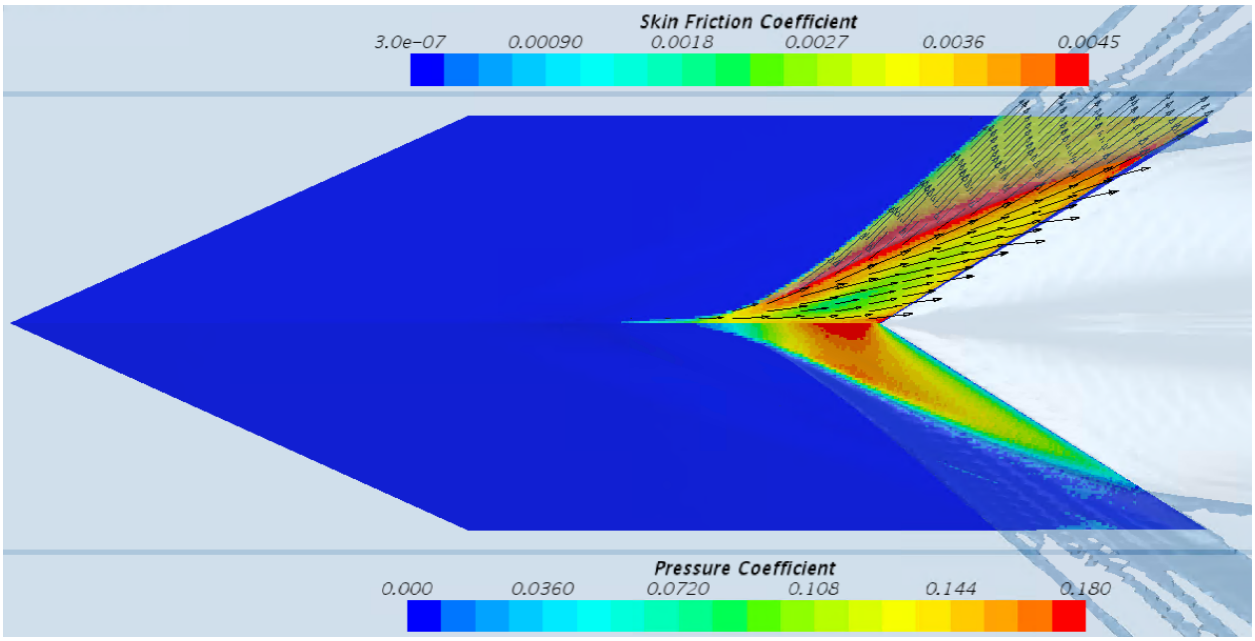

Figure A.11: Friction and Pressure Coefficient Plots (Run 24)

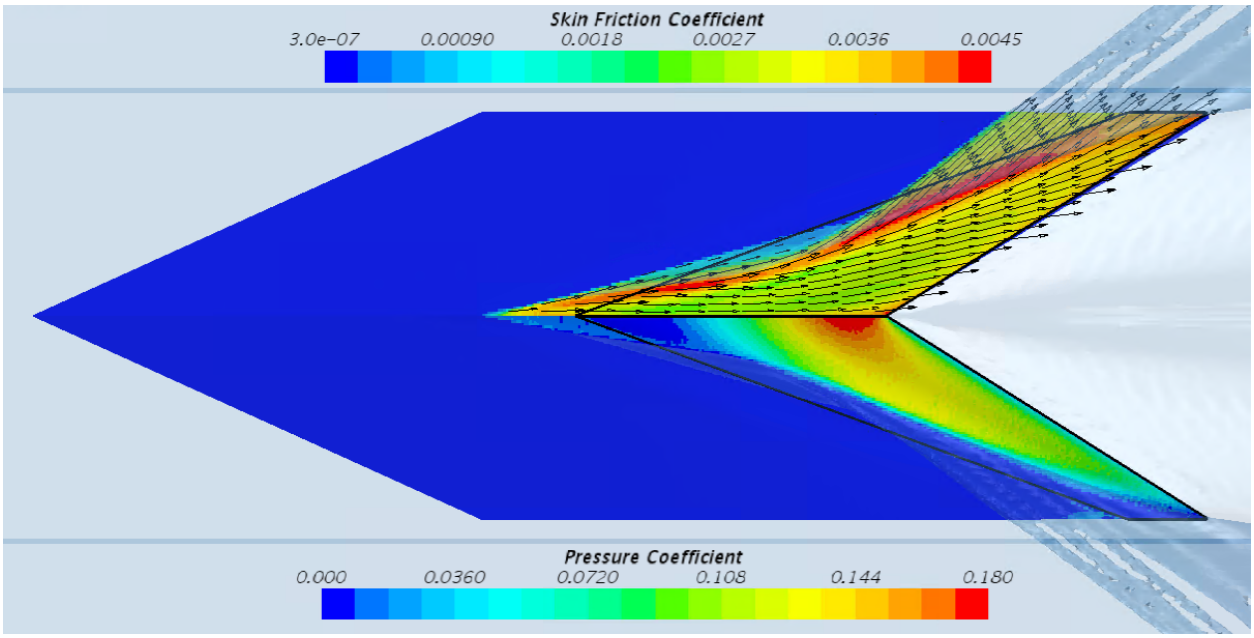

Figure A.12: Friction and Pressure Coefficient Plots (Run 25)

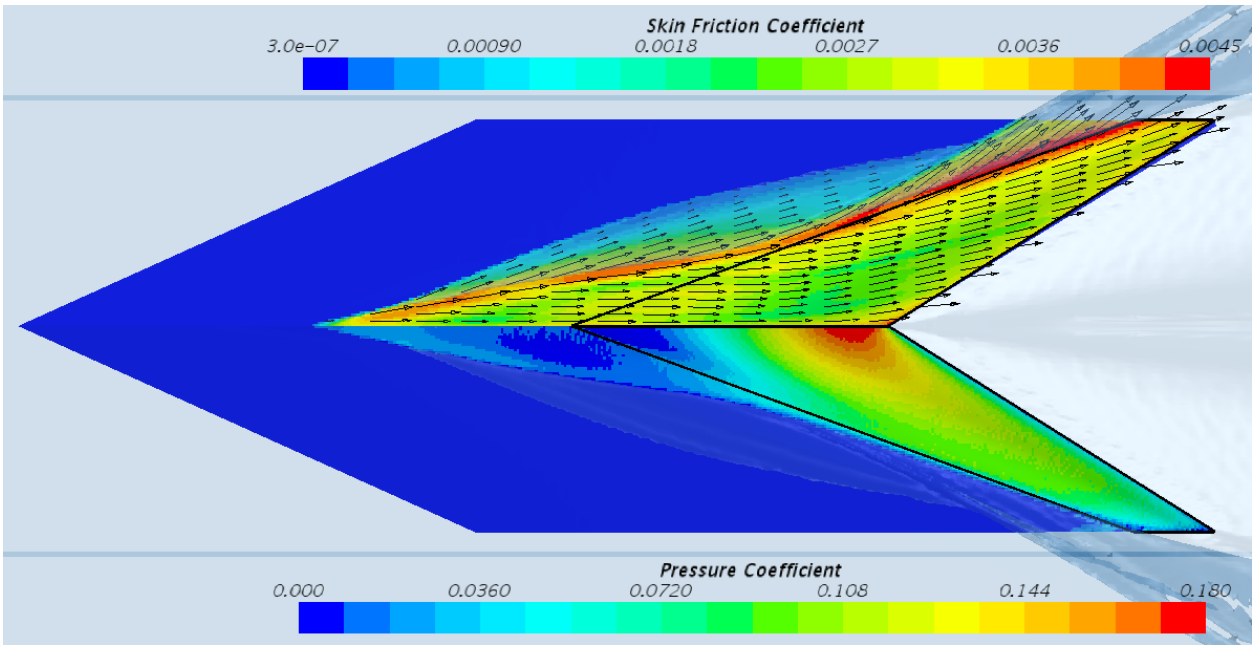

Figure A.13: Friction and Pressure Coefficient Plots (Run 26)

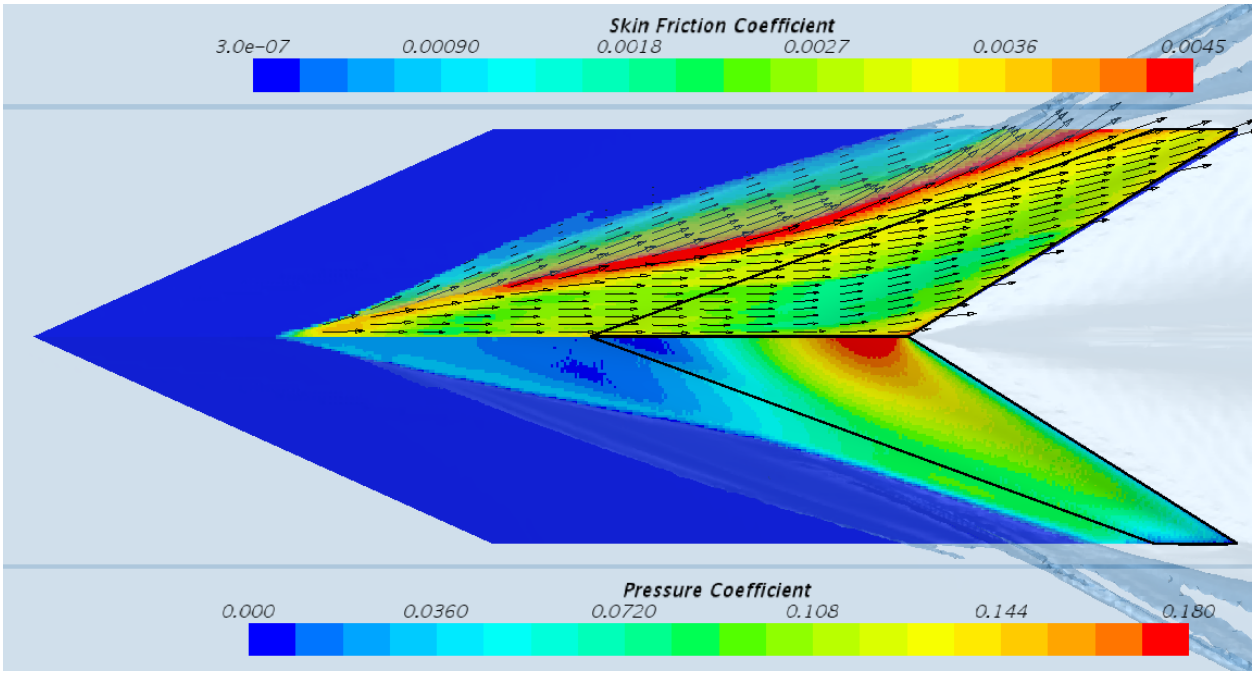

Figure A.14: Friction and Pressure Coefficient Plots (Run 27)

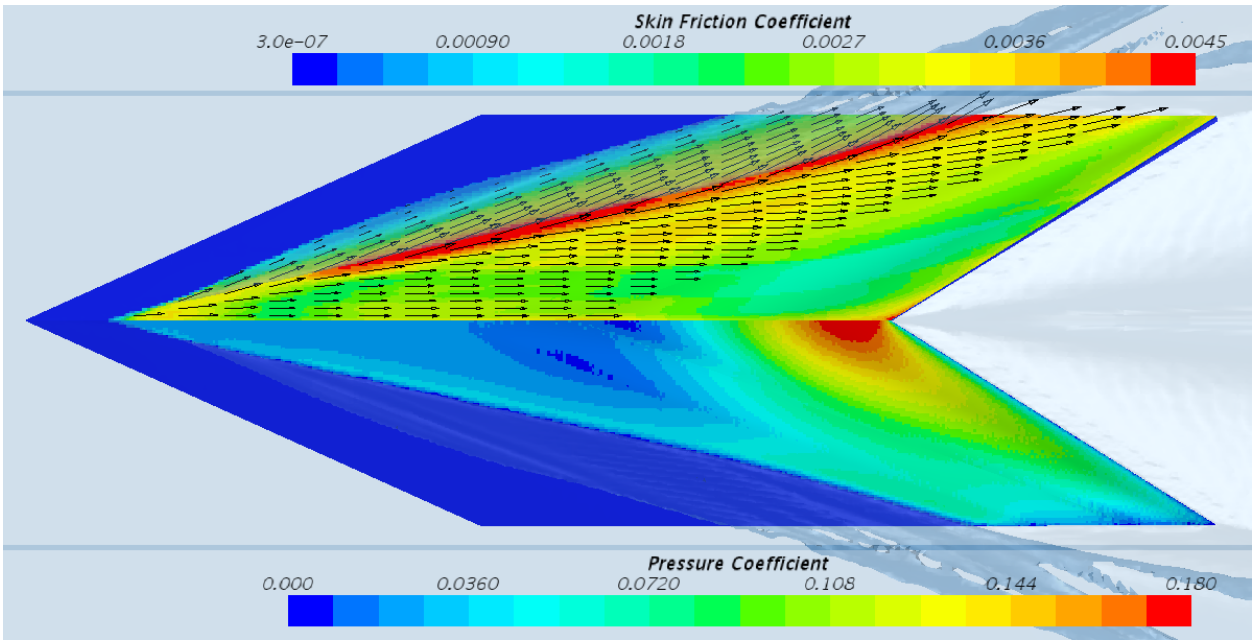

Figure A.15: Friction and Pressure Coefficient Plots (Run 28)

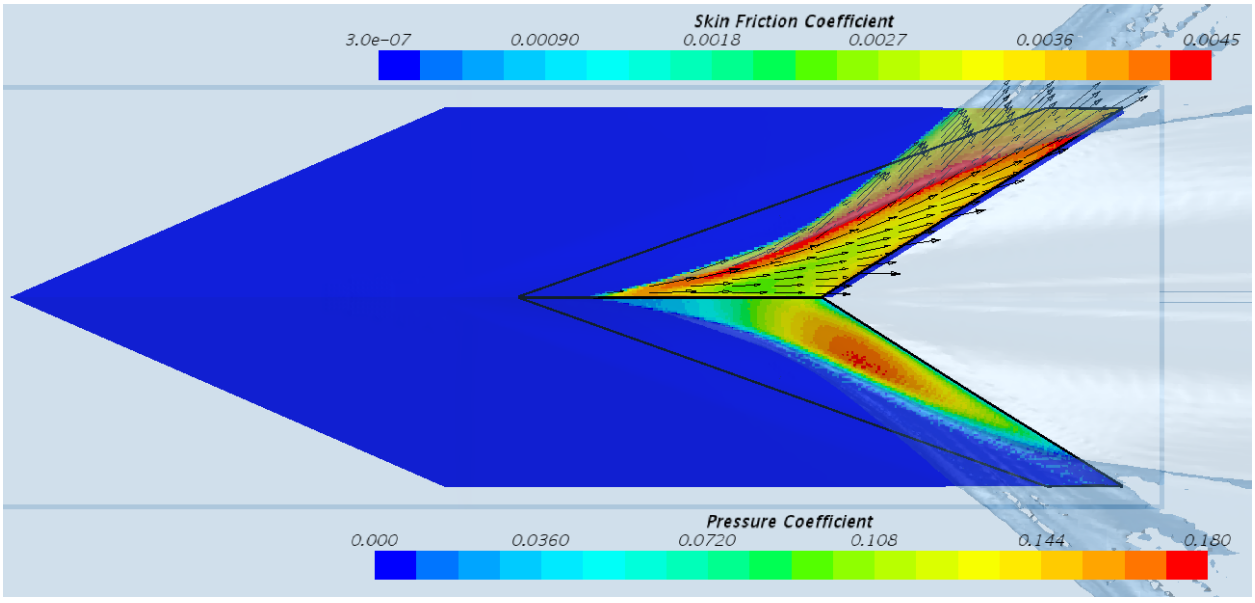

Figure A.16: Friction and Pressure Coefficient Plots (Run 29)

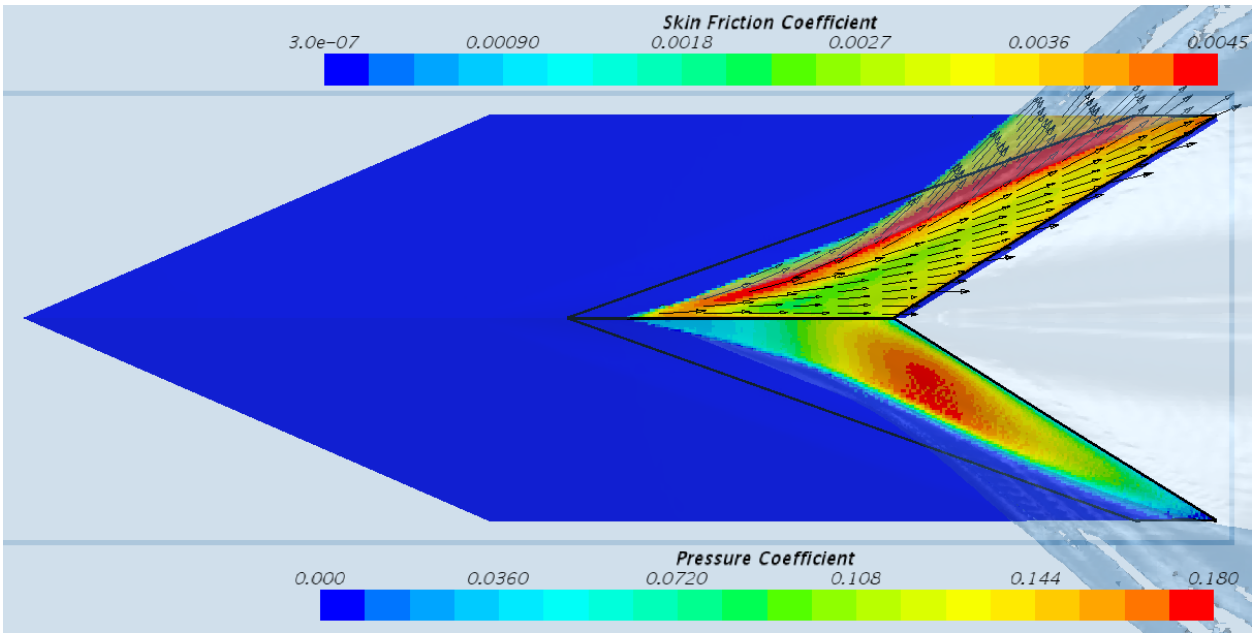

Figure A.17: Friction and Pressure Coefficient Plots (Run 30)

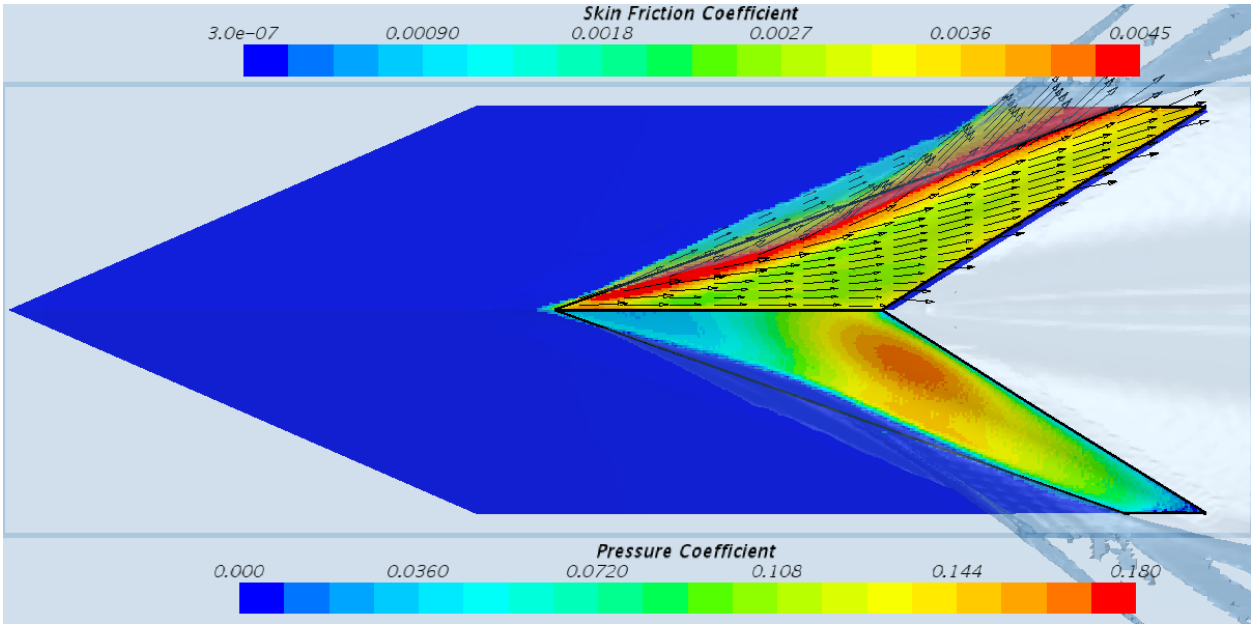

Figure A.18: Friction and Pressure Coefficient Plots (Run 31)

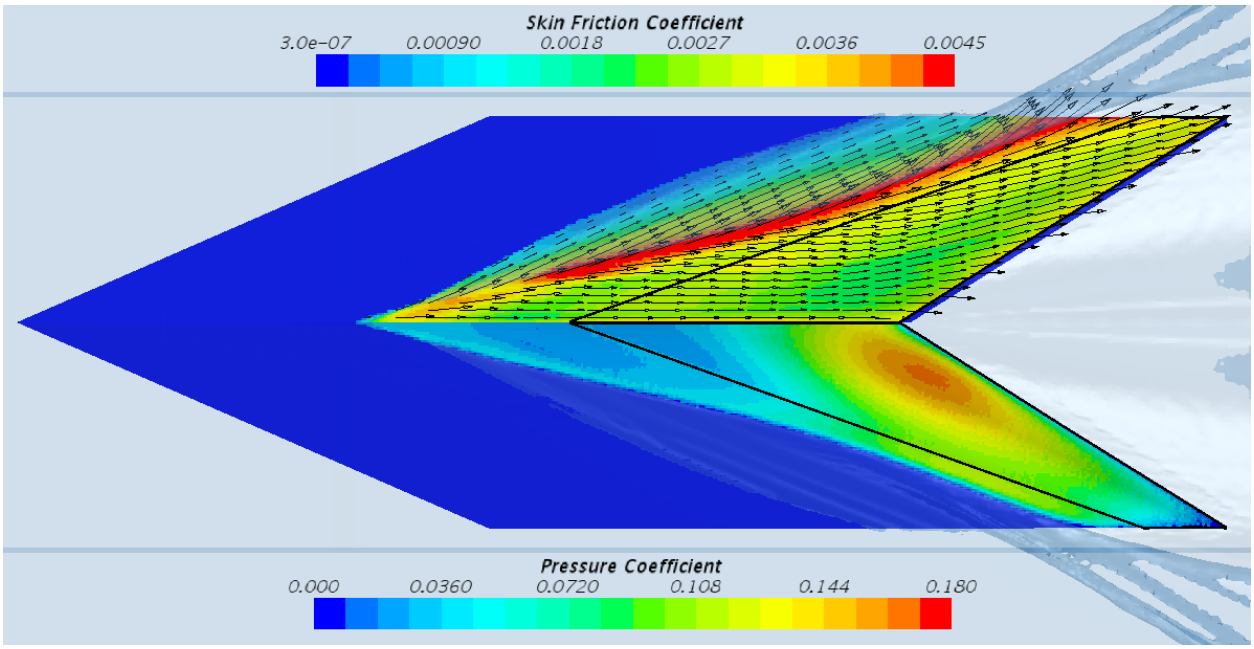

Figure A.19: Friction and Pressure Coefficient Plots (Run 32)

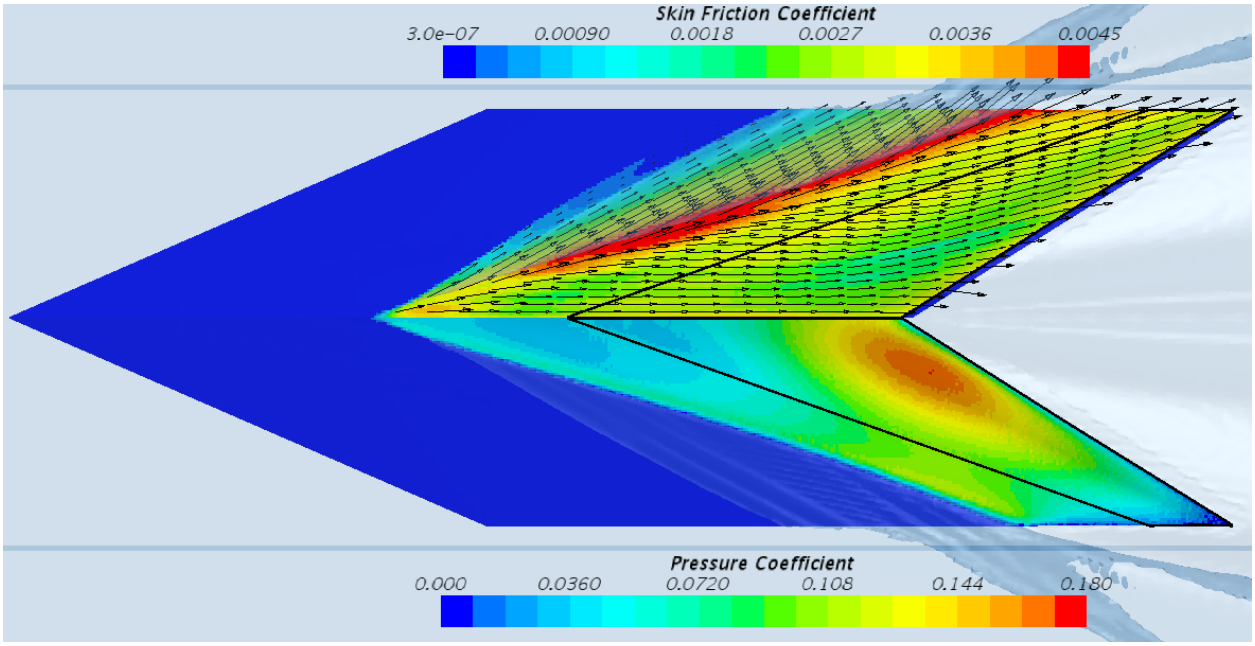

Figure A.20: Friction and Pressure Coefficient Plots (Run 33)

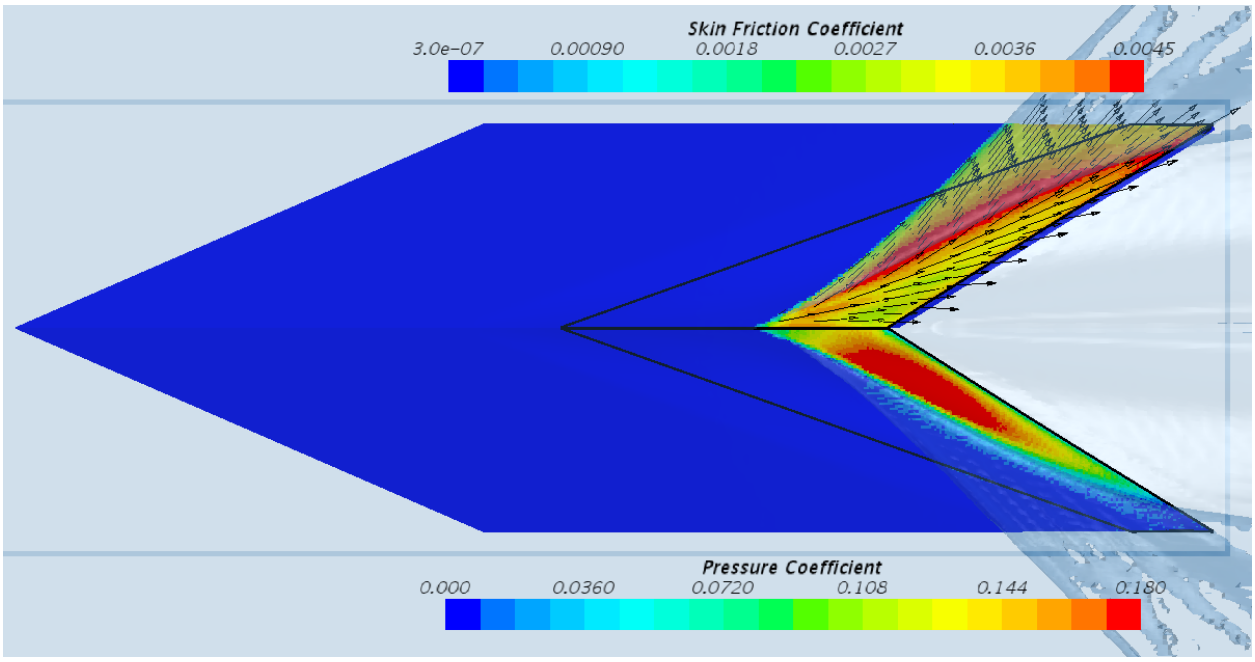

Figure A.21: Friction and Pressure Coefficient Plots (Run 34)

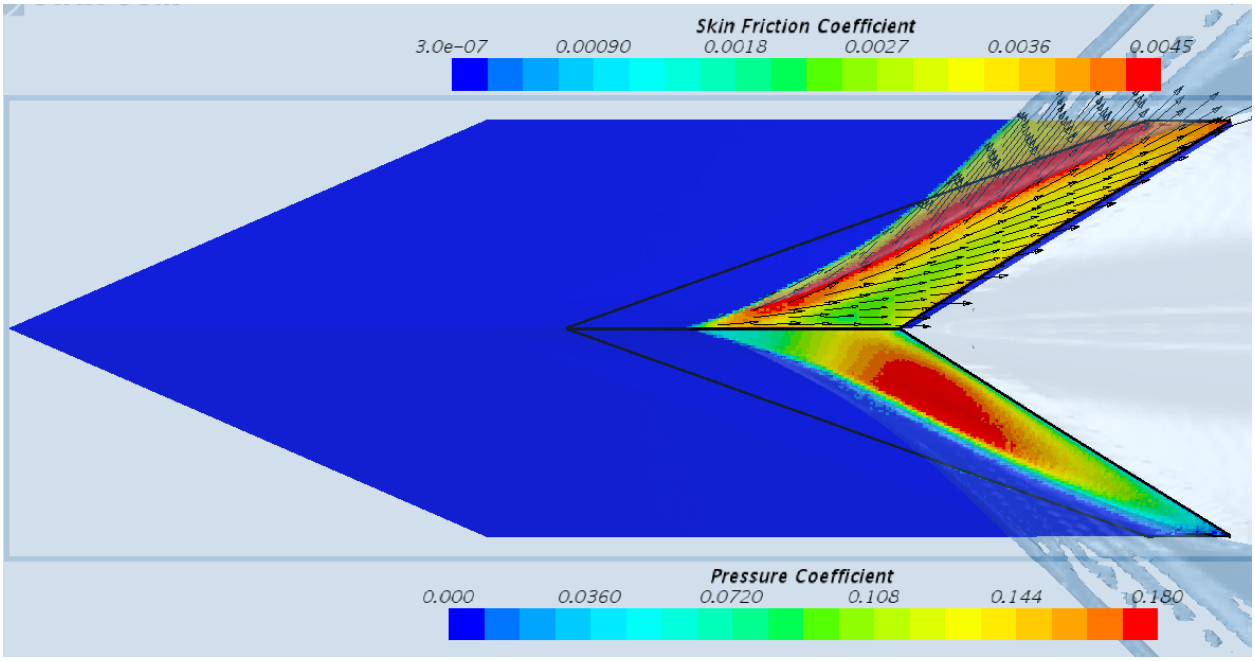

Figure A.22: Friction and Pressure Coefficient Plots (Run 35)

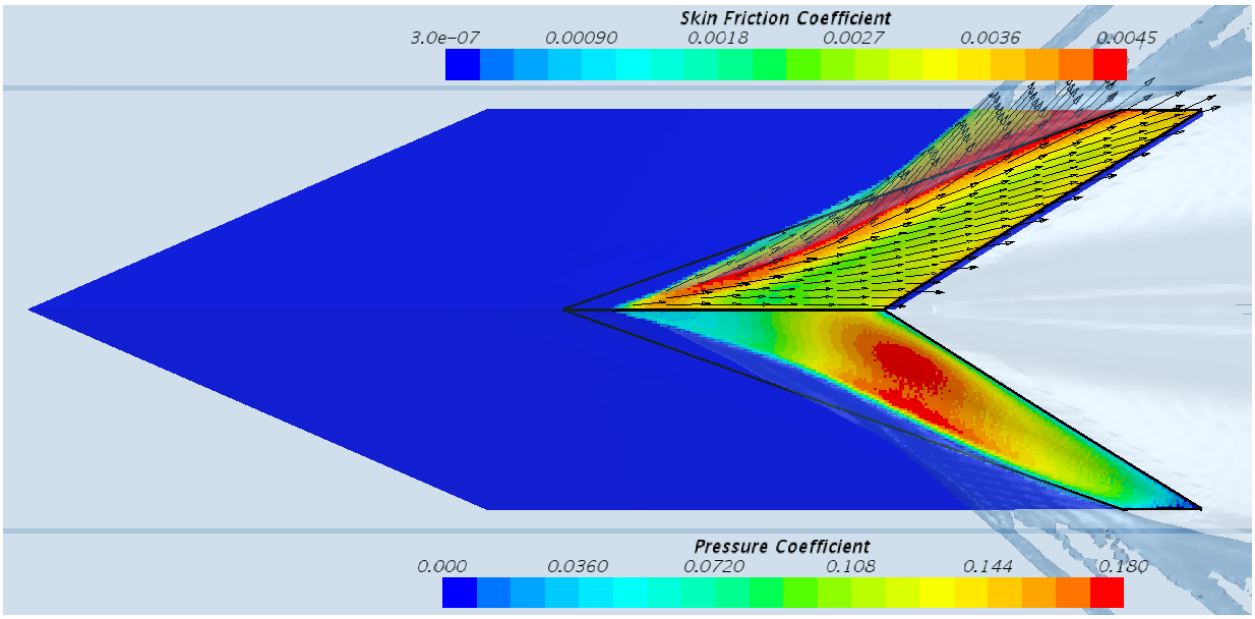

Figure A.23: Friction and Pressure Coefficient Plots (Run 36)

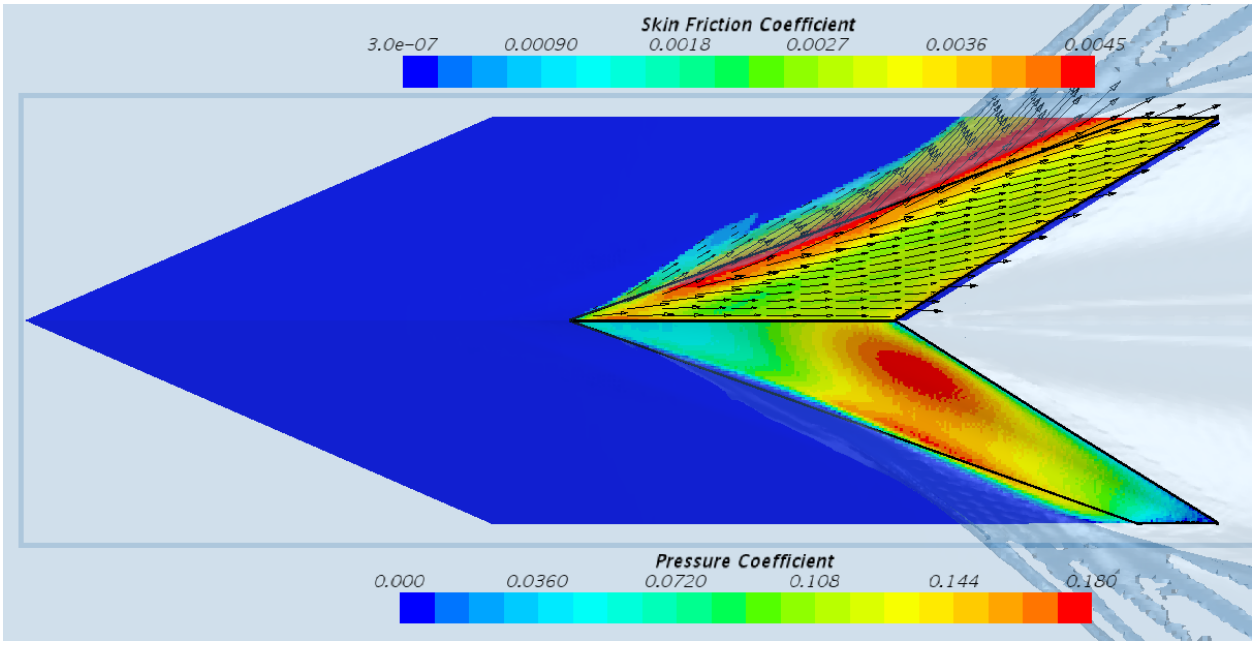

Figure A.24: Friction and Pressure Coefficient Plots (Run 37)

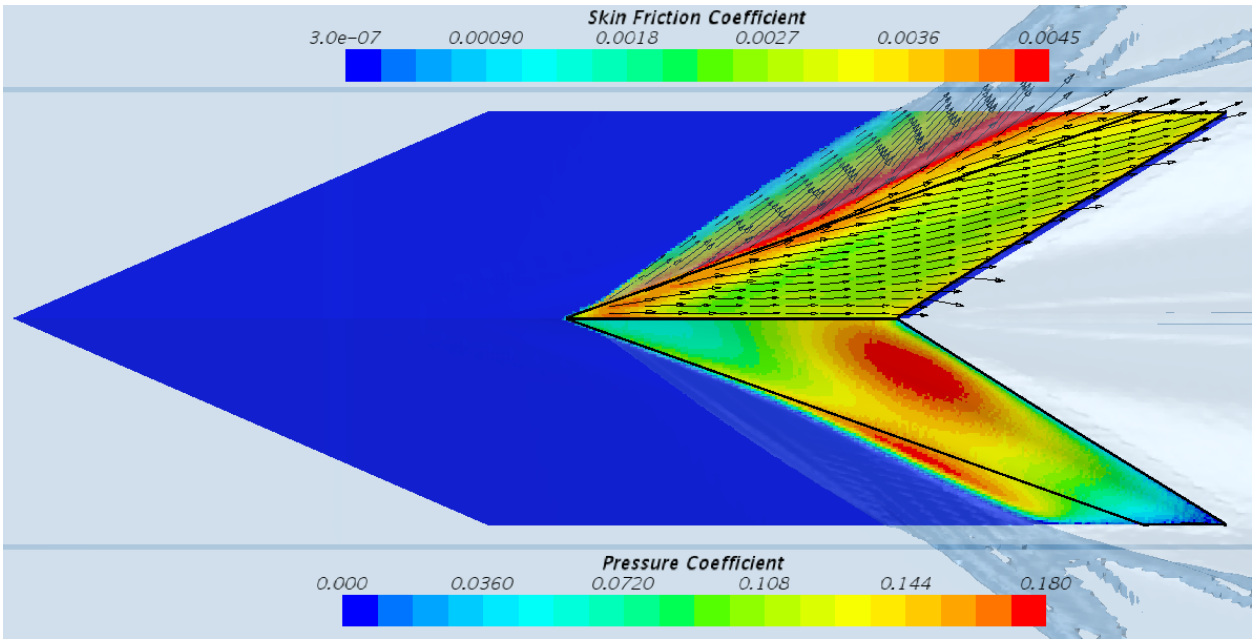

Figure A.25: Friction and Pressure Coefficient Plots (Run 38)

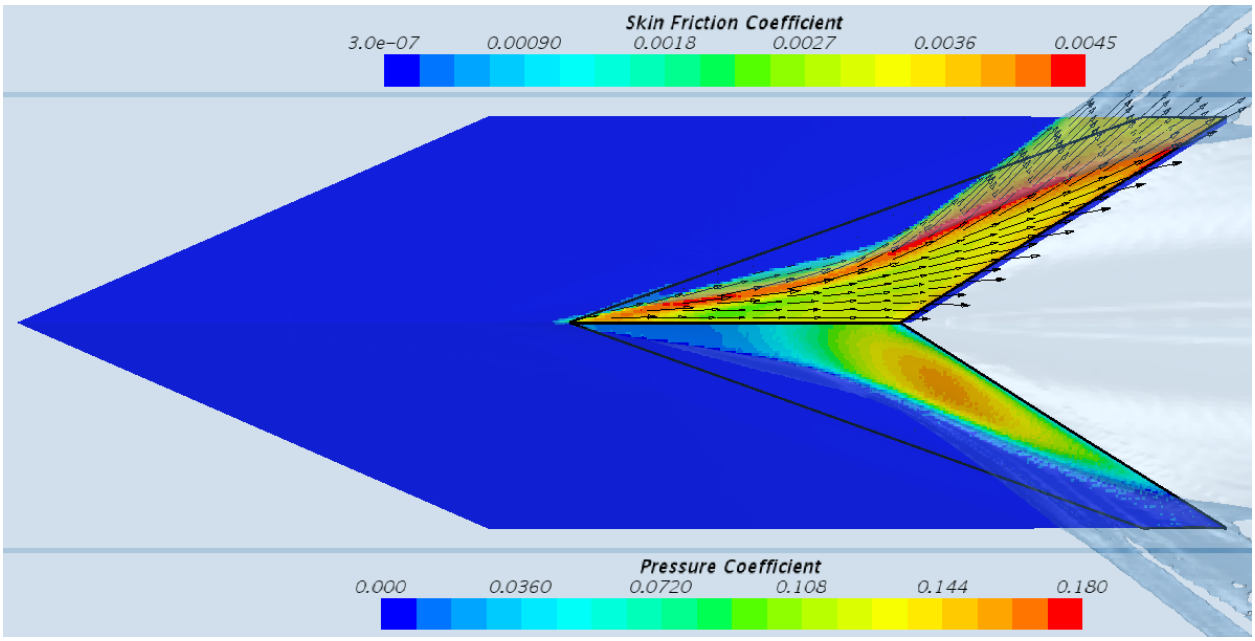

Figure A.26: Friction and Pressure Coefficient Plots (Run 39)

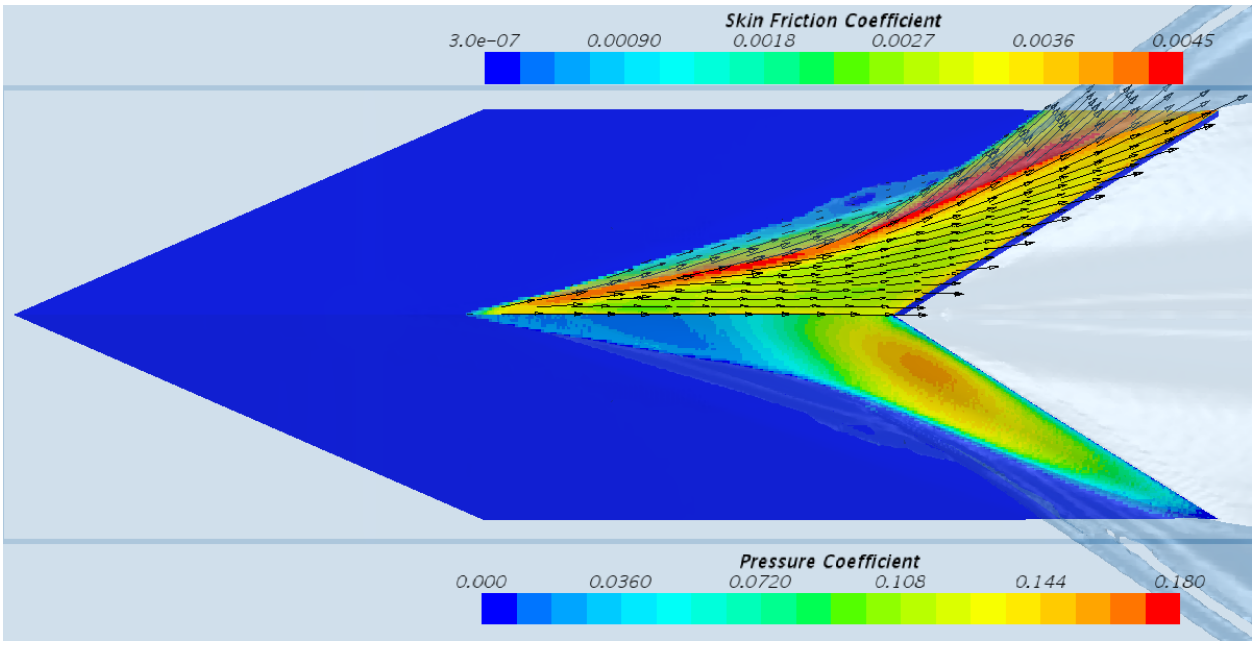

Figure A.27: Friction and Pressure Coefficient Plots (Run 40)

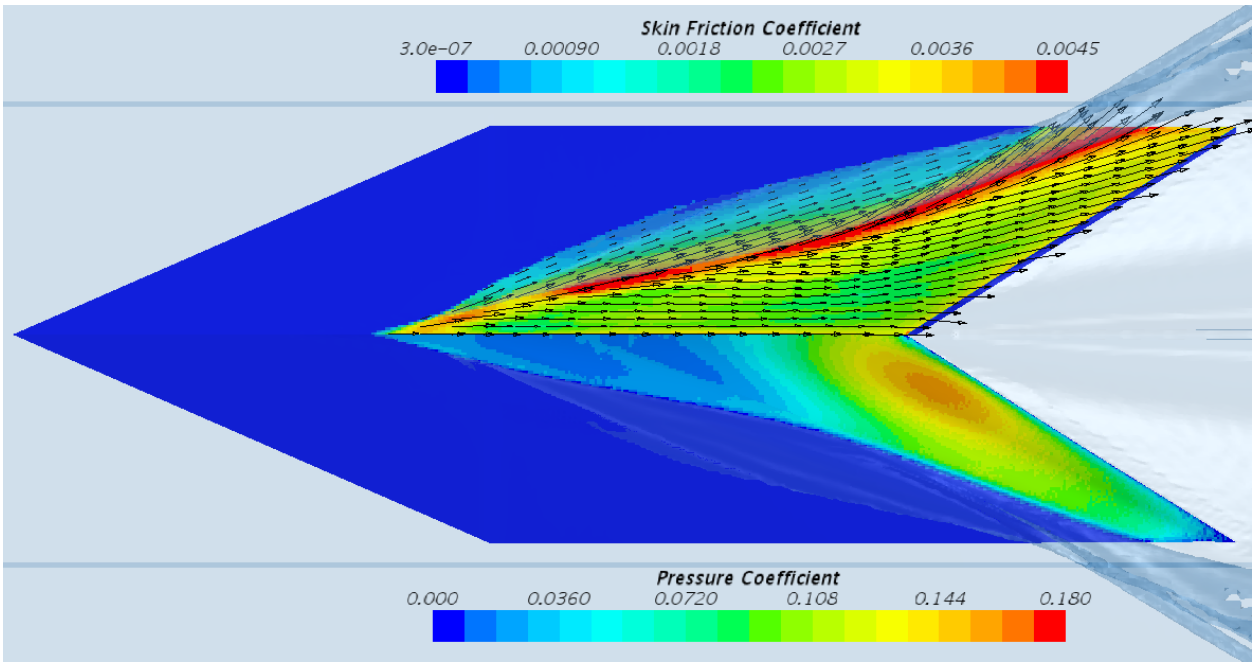

Figure A.28: Friction and Pressure Coefficient Plots (Run 41)

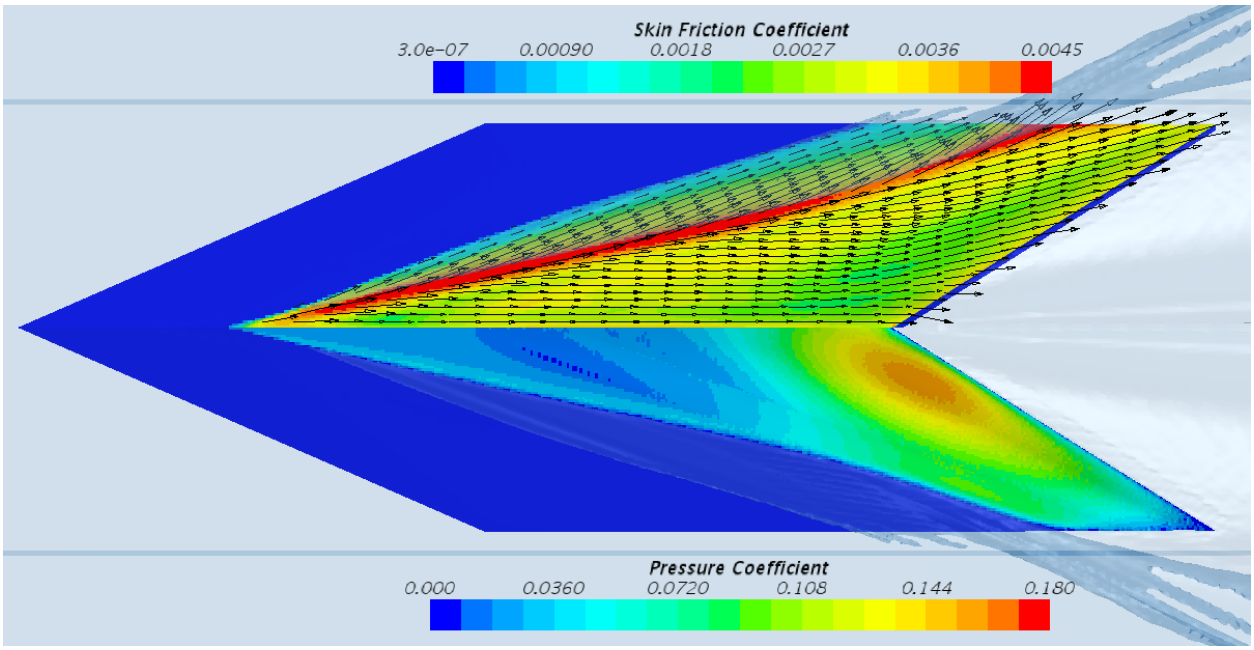

Figure A.29: Friction and Pressure Coefficient Plots (Run 42)

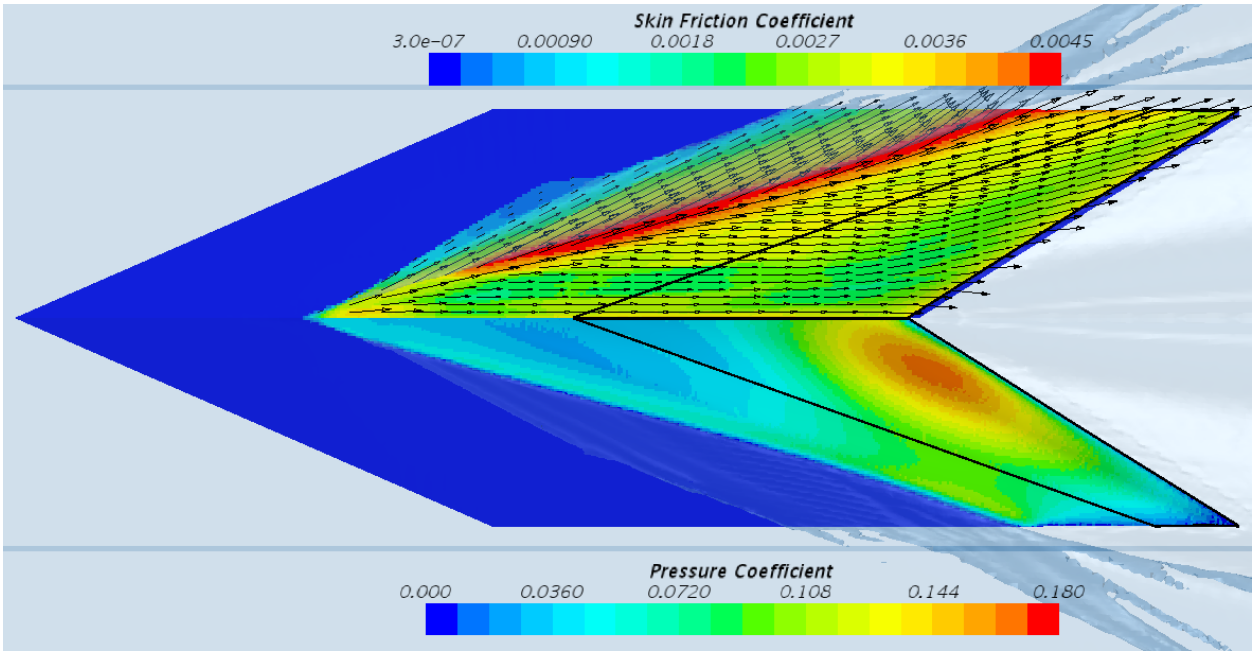

Figure A.30: Friction and Pressure Coefficient Plots (Run 48)

A.4 Wake Profile Comparison

A.4.1 Run 11 - Step A

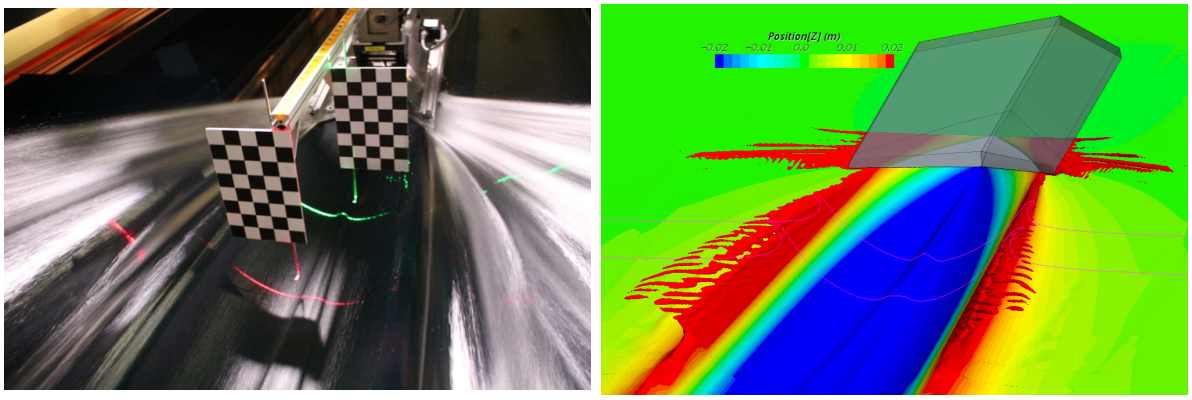

Figure A.31: Laser Wake Profile (Run 11)

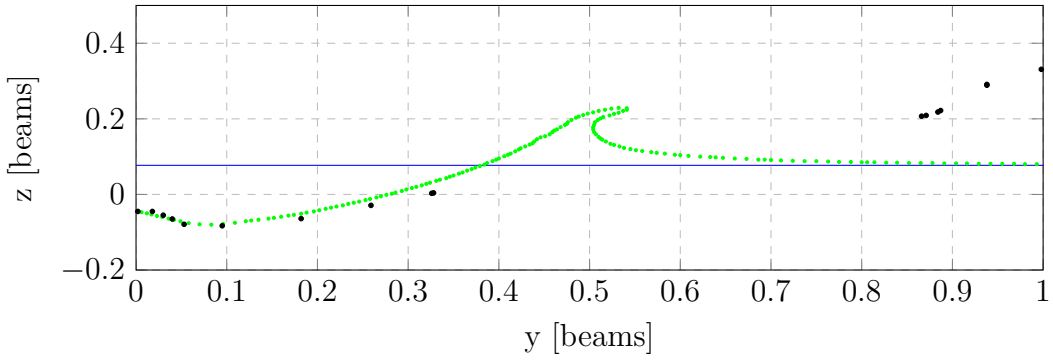

(a) Green Laser

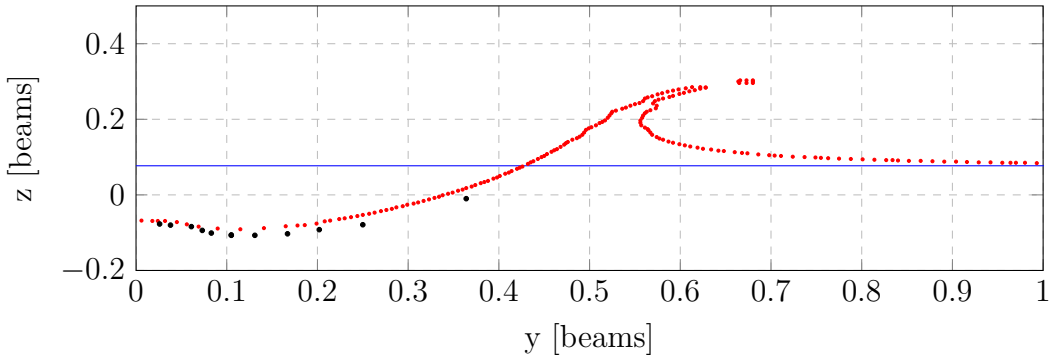

(b) Red Laser

Figure A.32: Wake Profile Comparison (Run 11)

A.4.2 Run 14 - Step A

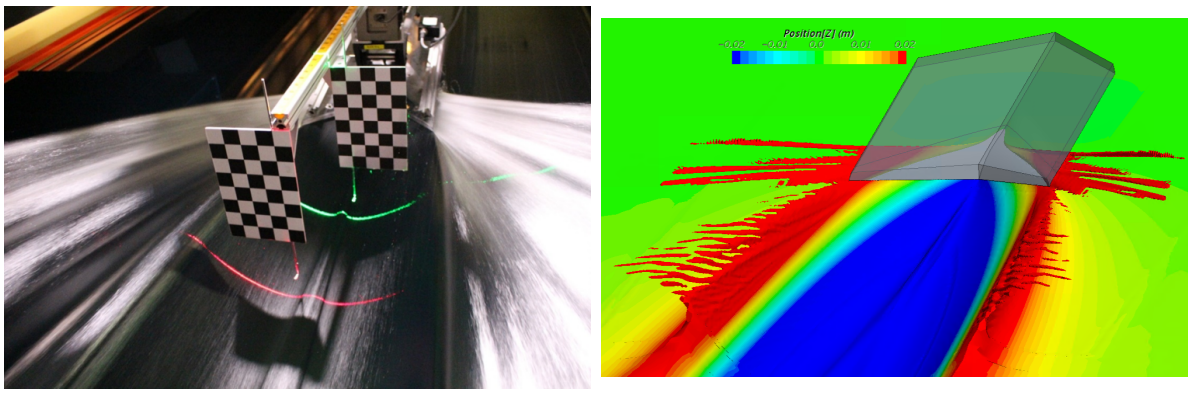

Figure A.33: Laser Wake Profile (Run 14)

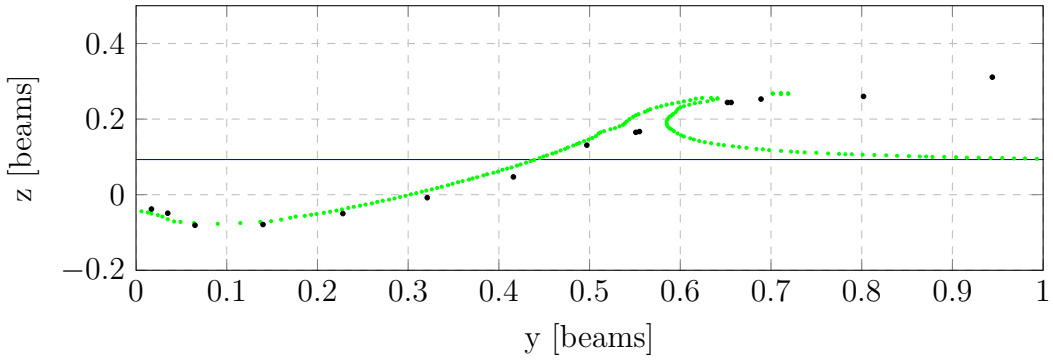

(a) Green Laser

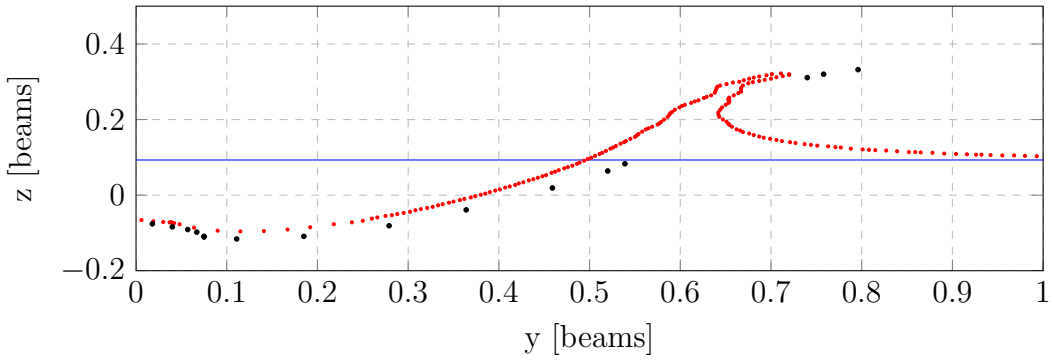

(b) Red Laser

Figure A.34: Wake Profile Comparison (Run 14)

A.4.3 Run 16 - Step A

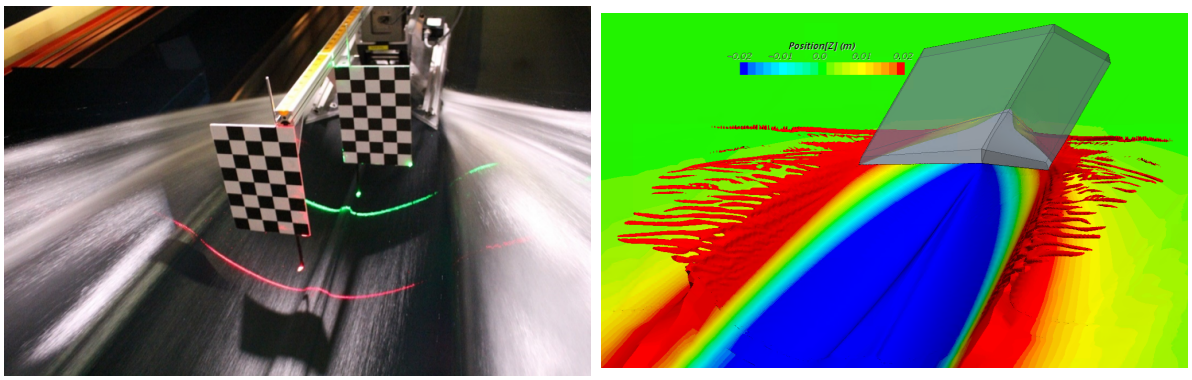

Figure A.35: Laser Wake Profile (Run 16)

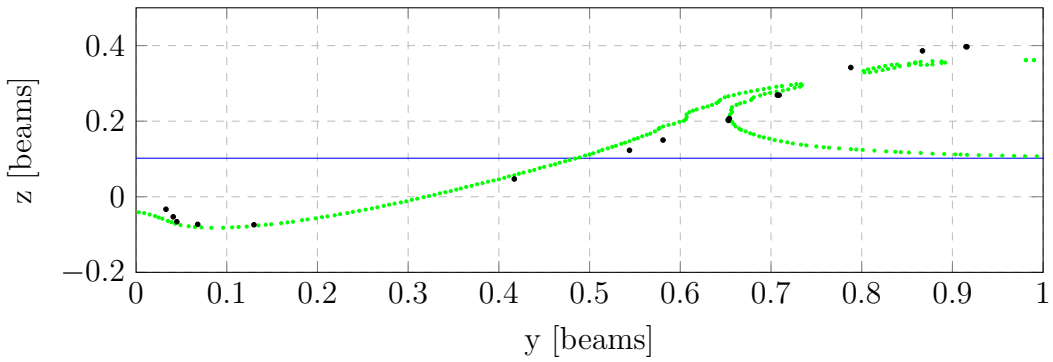

(a) Green Laser

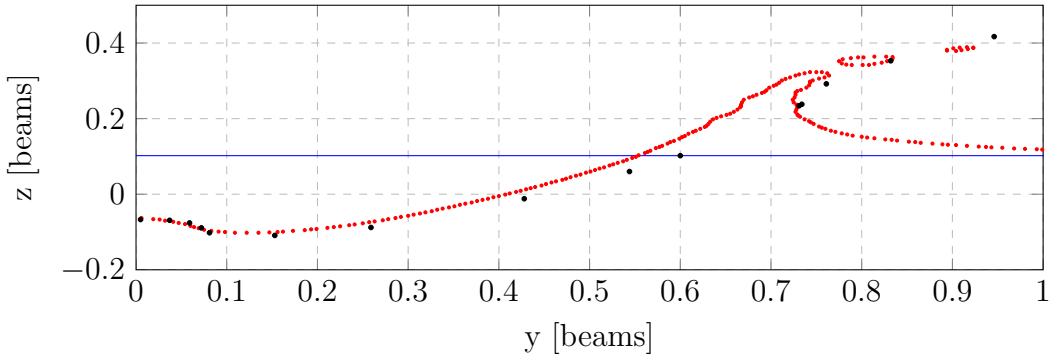

(b) Red Laser

Figure A.36: Wake Profile Comparison (Run 16)

A.4.4 Run 17 - Step A

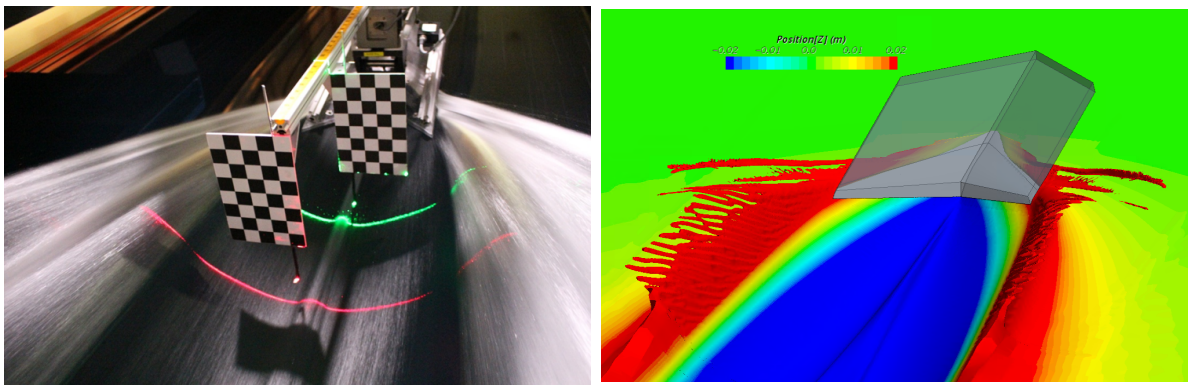

Figure A.37: Laser Wake Profile (Run 17)

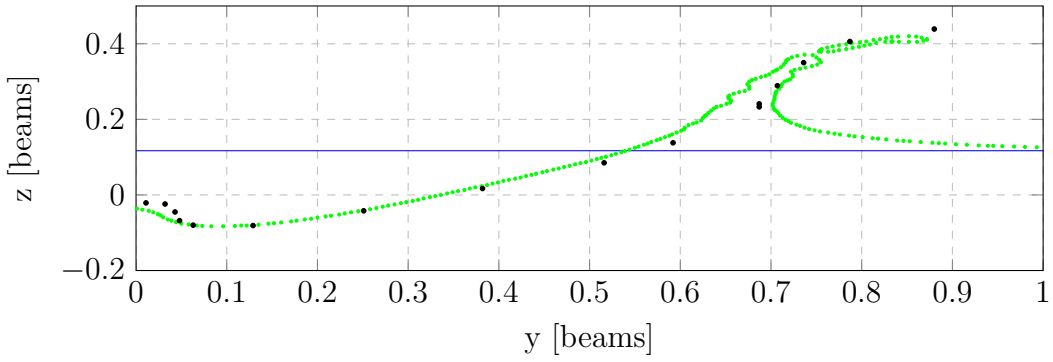

(a) Green Laser

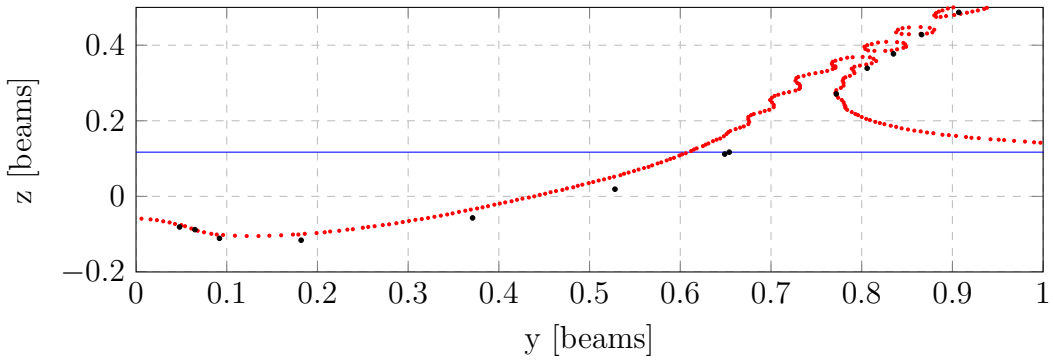

(b) Red Laser

Figure A.38: Wake Profile Comparison (Run 17)

A.4.5 Run 18 - Step A

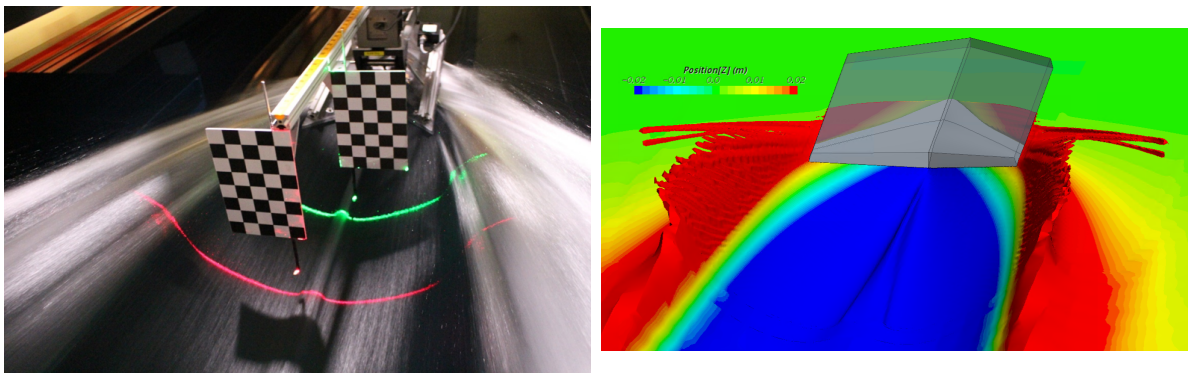

Figure A.39: Laser Wake Profile (Run 18)

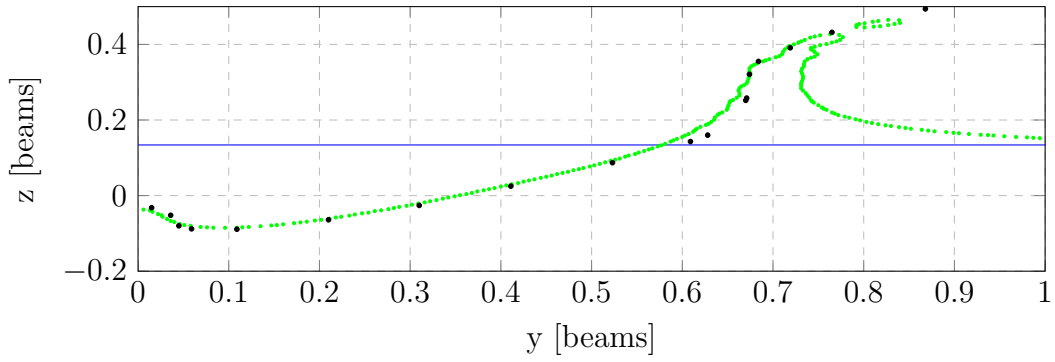

(a) Green Laser

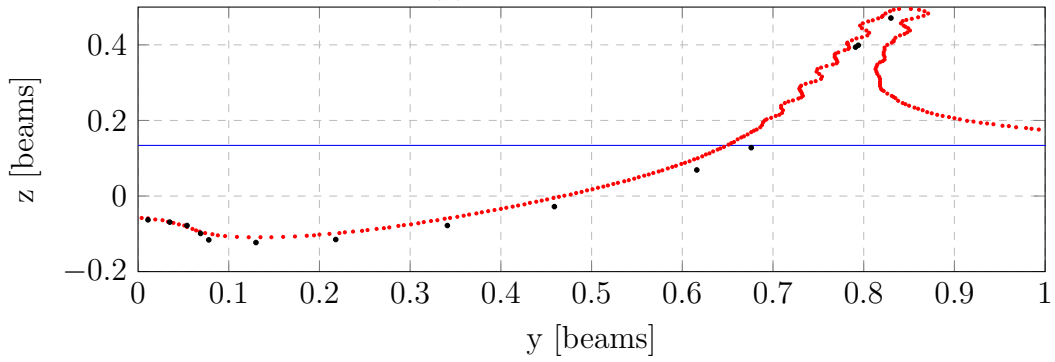

(b) Red Laser

Figure A.40: Wake Profile Comparison (Run 18)

A.4.6 Run 19 - Step A

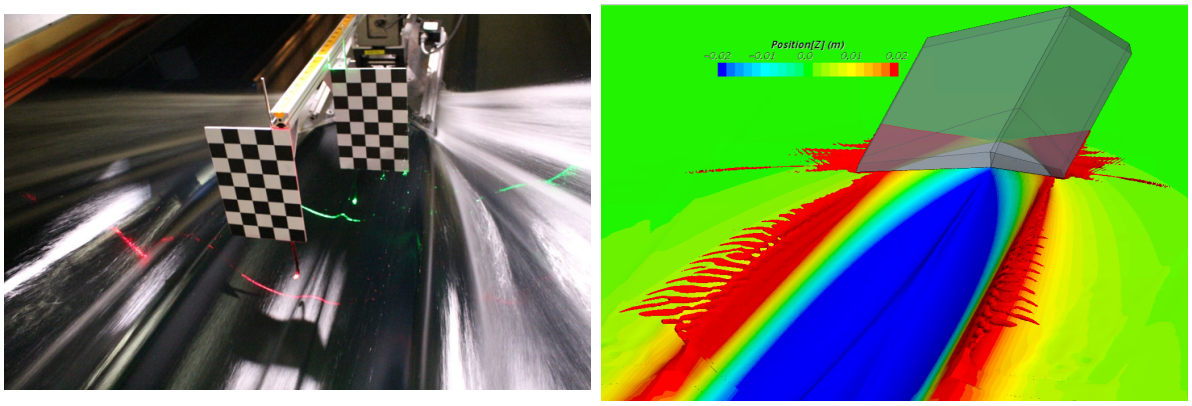

Figure A.41: Laser Wake Profile (Run 19)

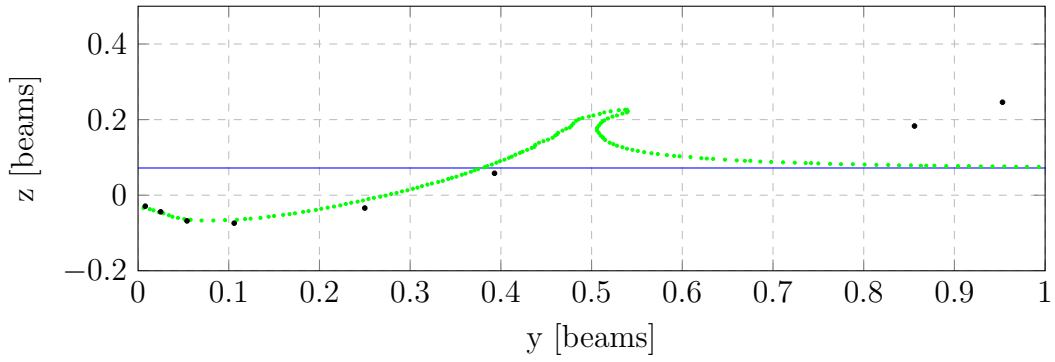

(a) Green Laser

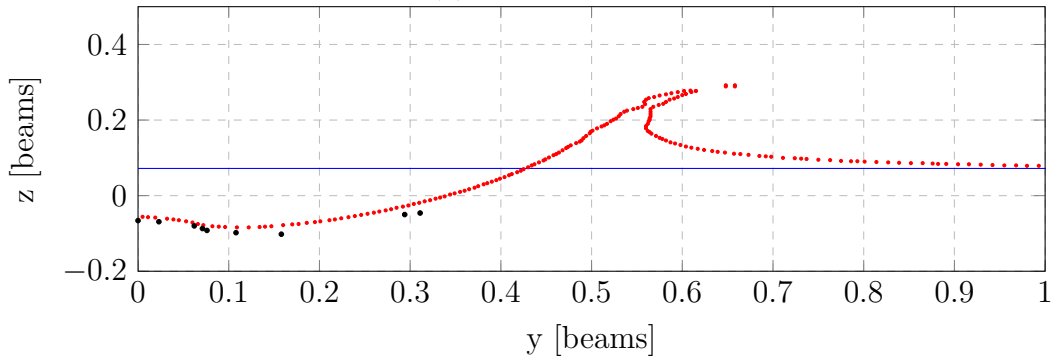

(b) Red Laser

Figure A.42: Wake Profile Comparison (Run 19)

A.4.7 Run 20 - Step A

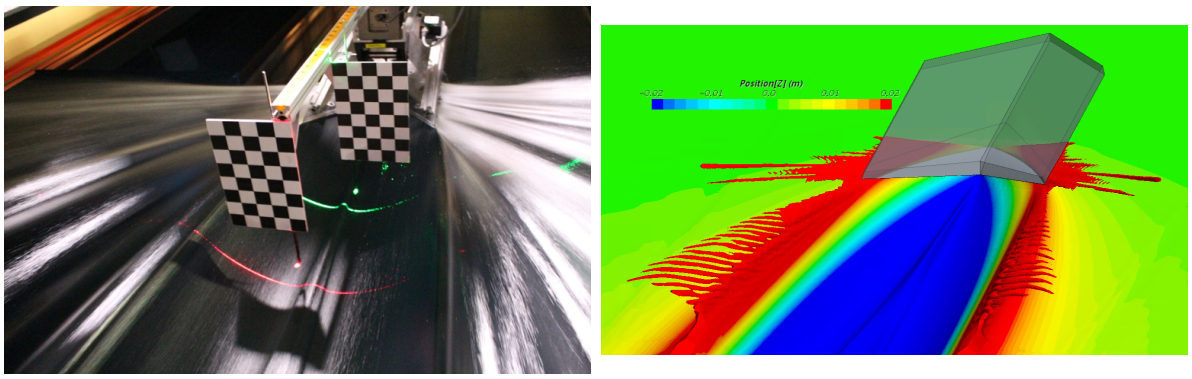

Figure A.43: Laser Wake Profile (Run 20)

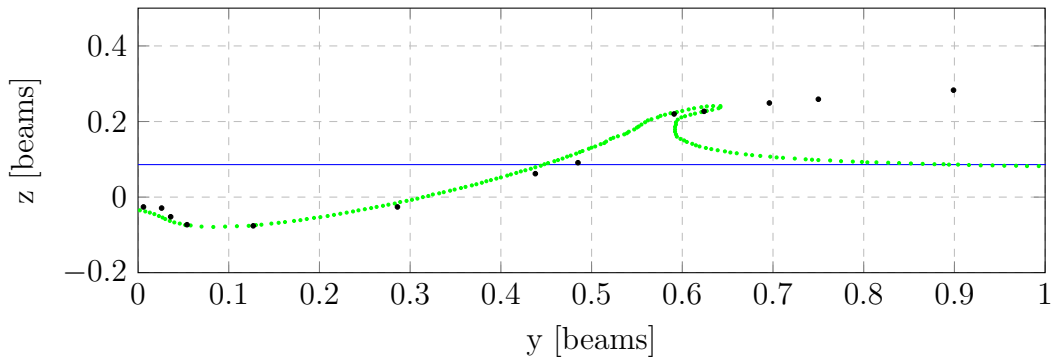

(a) Green Laser

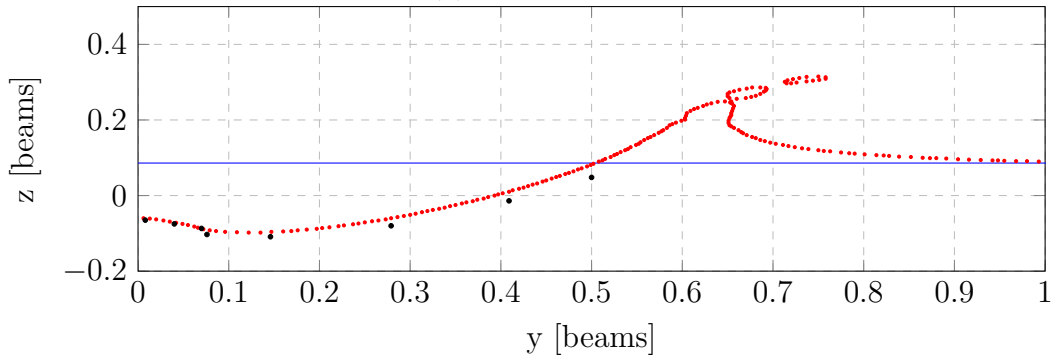

(b) Red Laser

Figure A.44: Wake Profile Comparison (Run 20)

A.4.8 Run 21 - Step A

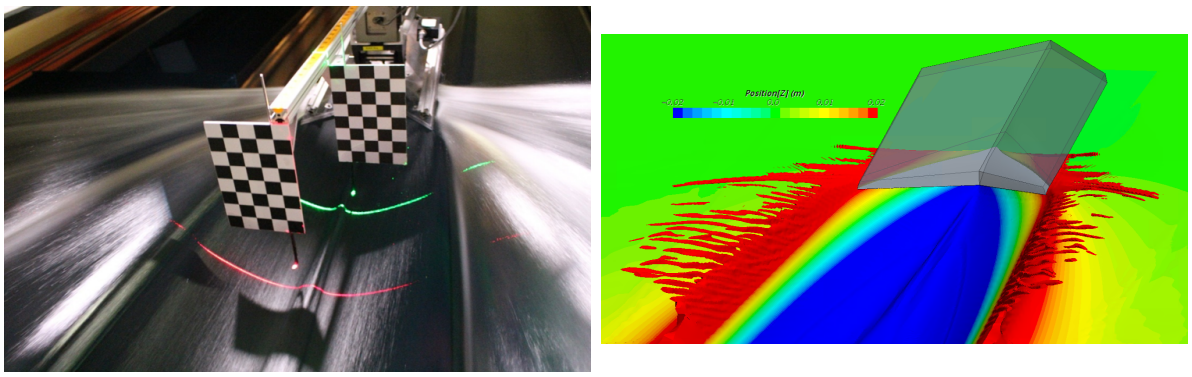

Figure A.45: Laser Wake Profile (Run 21)

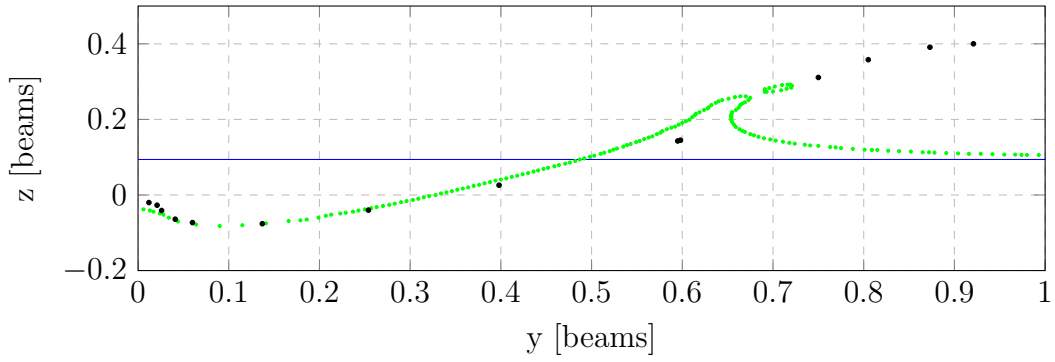

(a) Green Laser

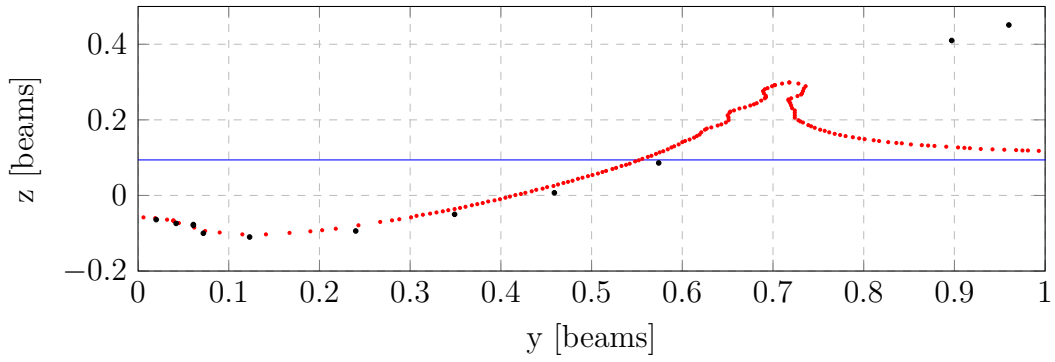

(b) Red Laser

Figure A.46: Wake Profile Comparison (Run 21)

A.4.9 Run 22 - Step A

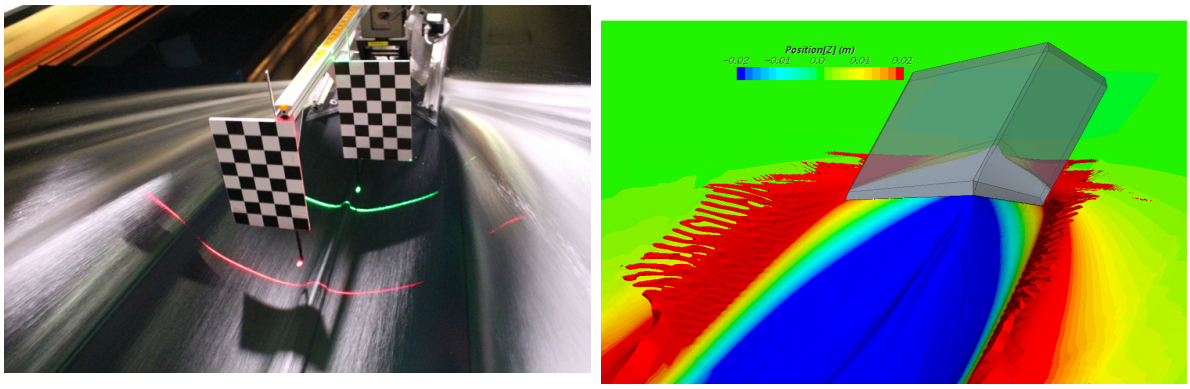

Figure A.47: Laser Wake Profile (Run 22)

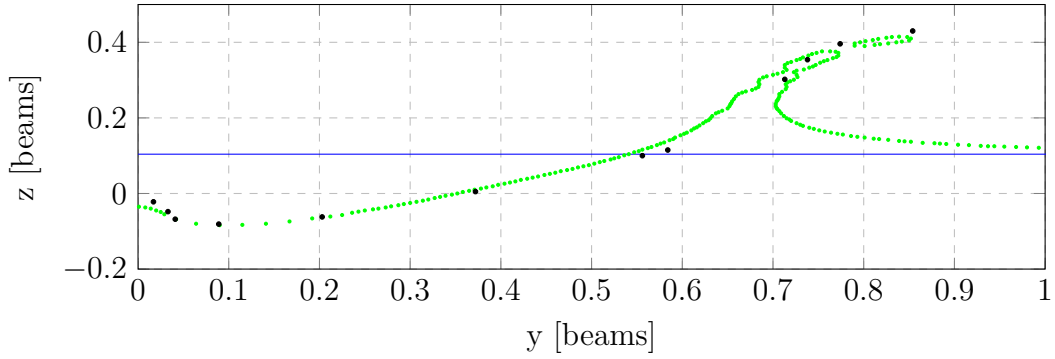

(a) Green Laser

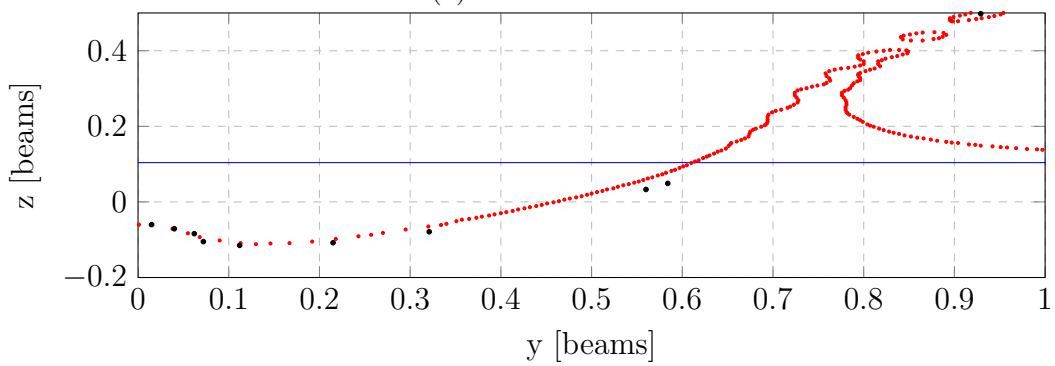

(b) Red Laser

Figure A.48: Wake Profile Comparison (Run 22)

A.4.10 Run 23 - Step A

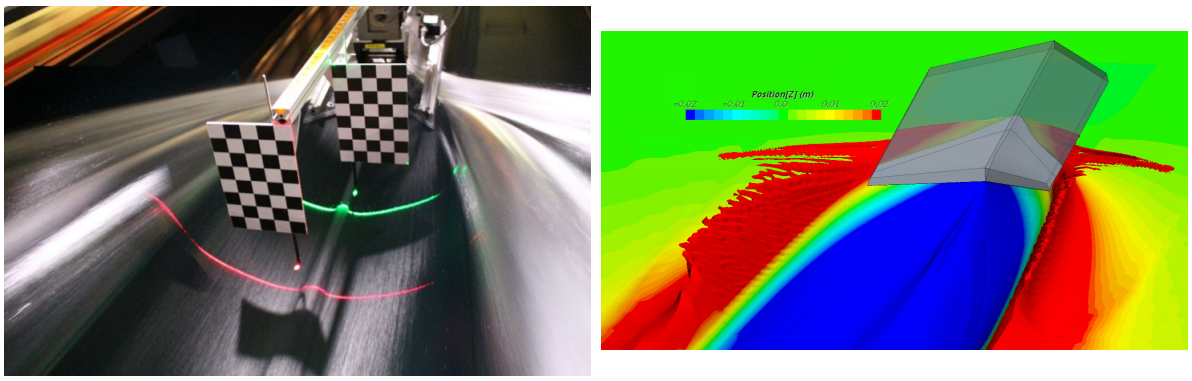

Figure A.49: Laser Wake Profile (Run 23)

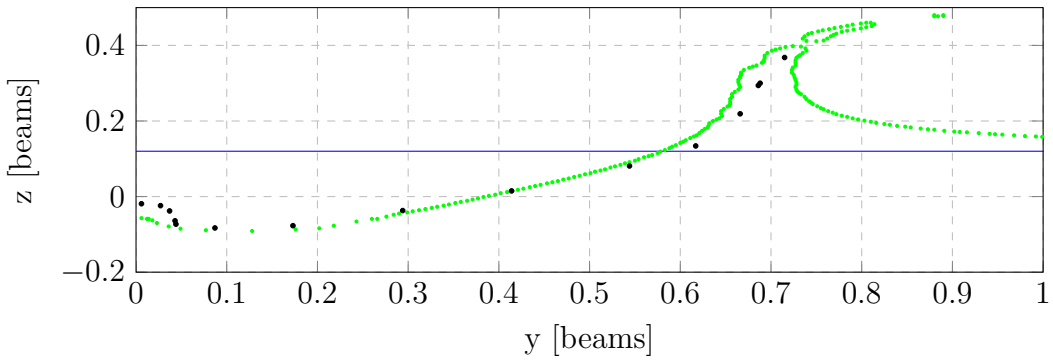

(a) Green Laser

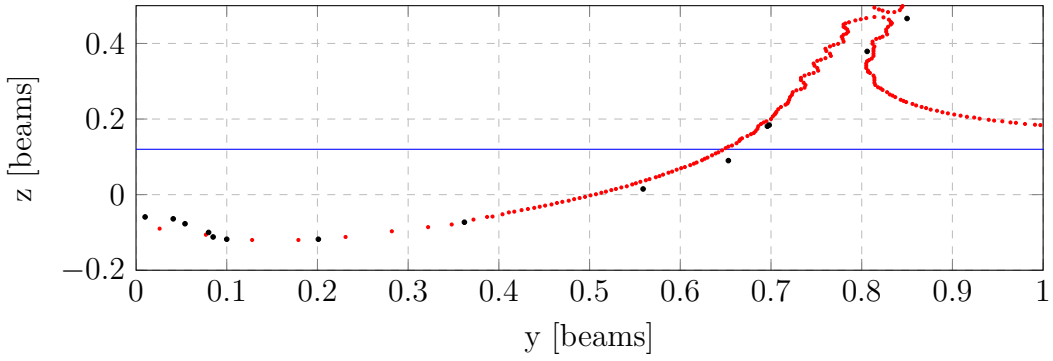

(b) Red Laser

Figure A.50: Wake Profile Comparison (Run 23)

A.4.11 Run 24 - Step A

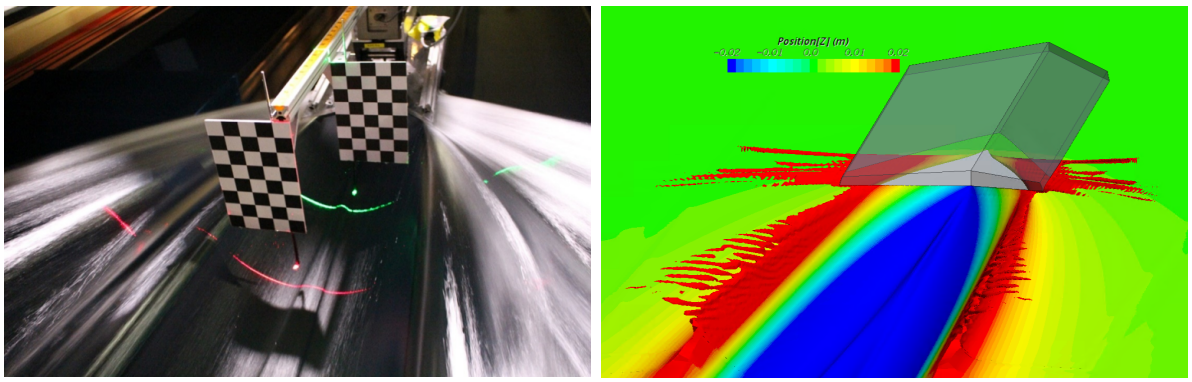

Figure A.51: Laser Wake Profile (Run 24)

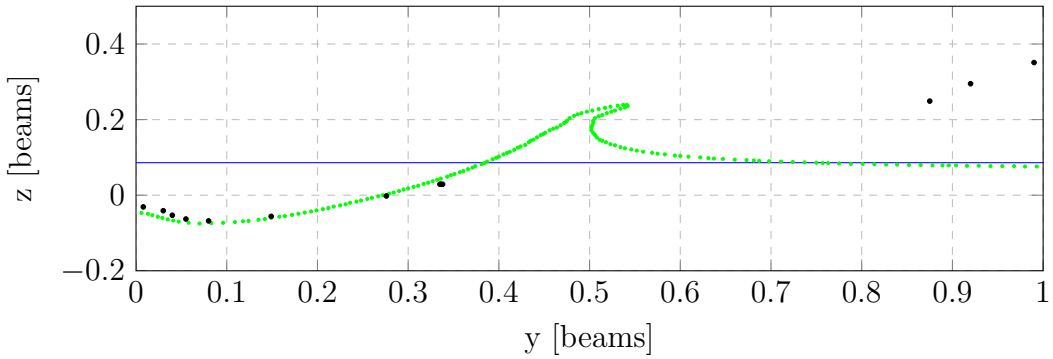

(a) Green Laser

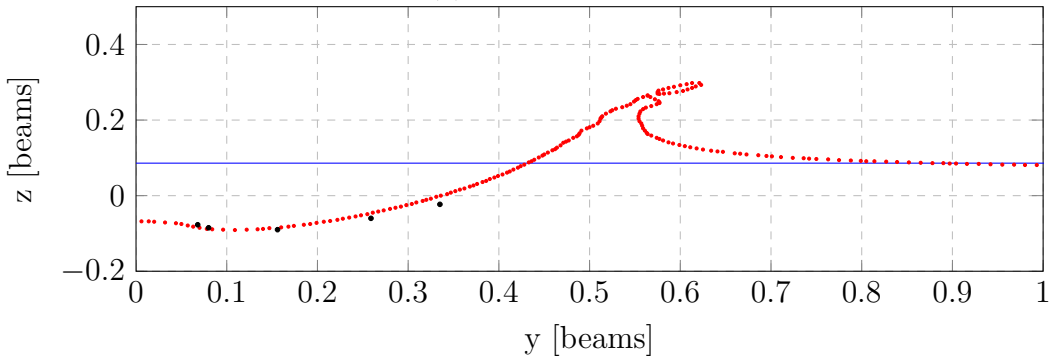

(b) Red Laser

Figure A.52: Wake Profile Comparison (Run 24)

A.4.12 Run 25 - Step A

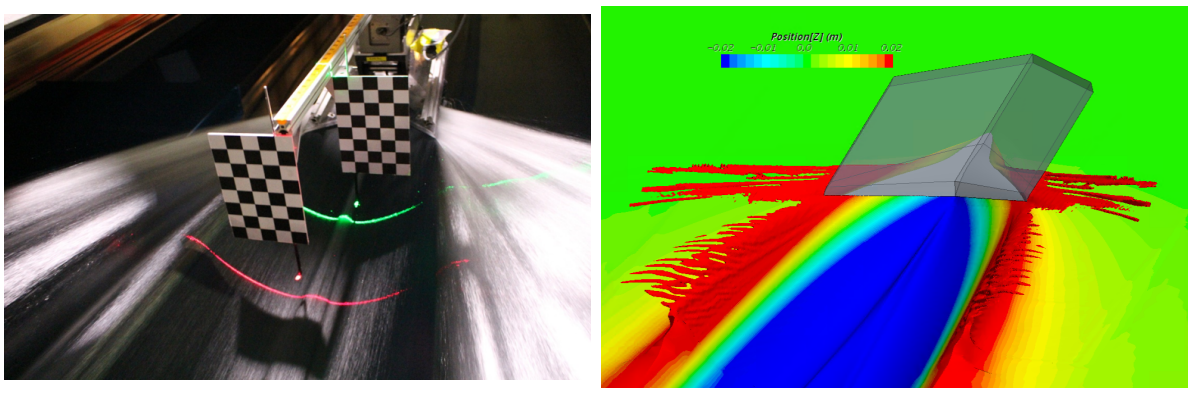

Figure A.53: Laser Wake Profile (Run 25)

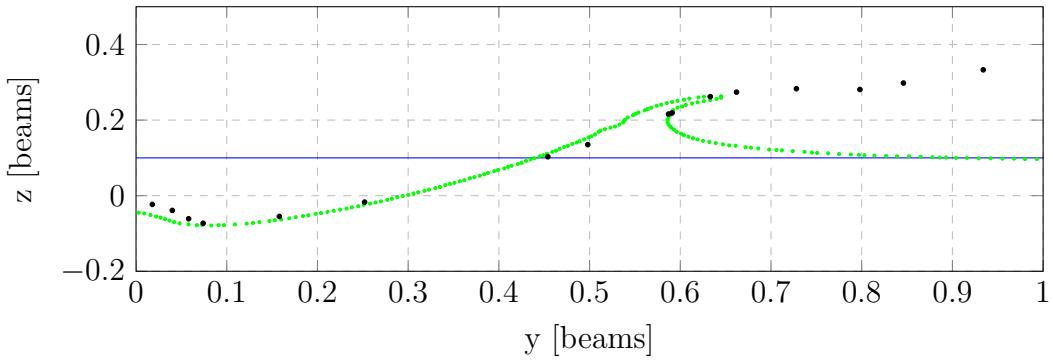

(a) Green Laser

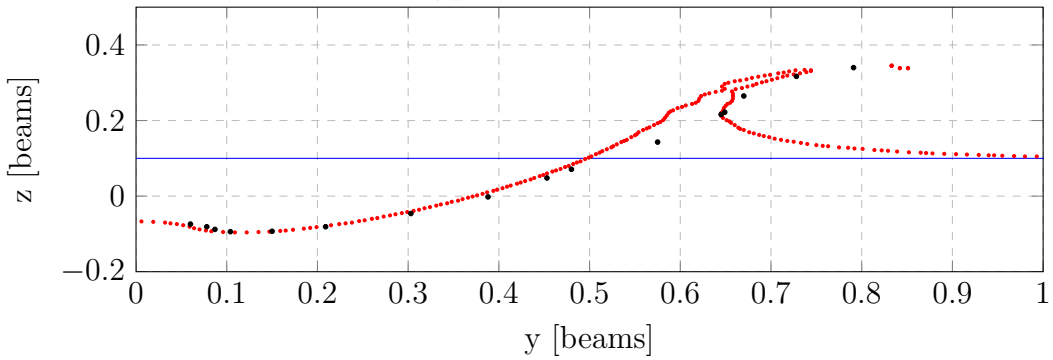

(b) Red Laser

Figure A.54: Wake Profile Comparison (Run 25)

A.4.13 Run 26 - Step A

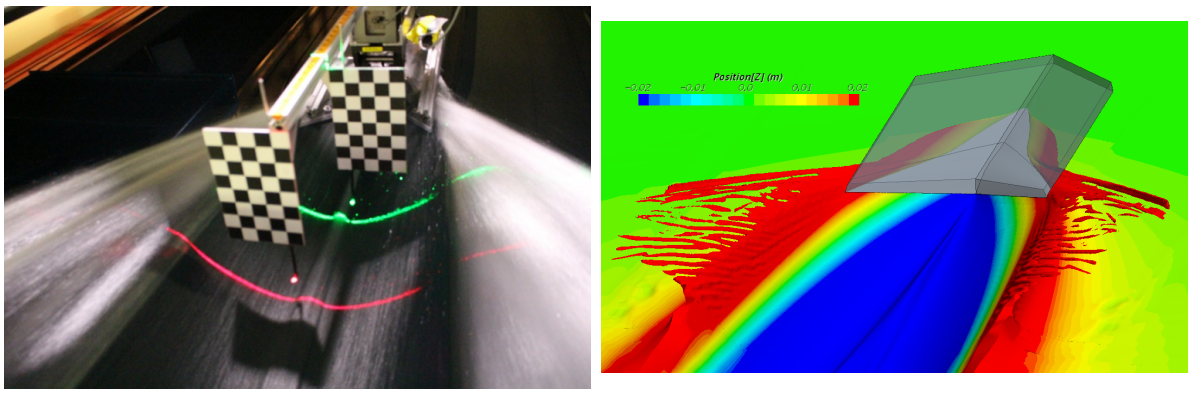

Figure A.55: Laser Wake Profile (Run 26)

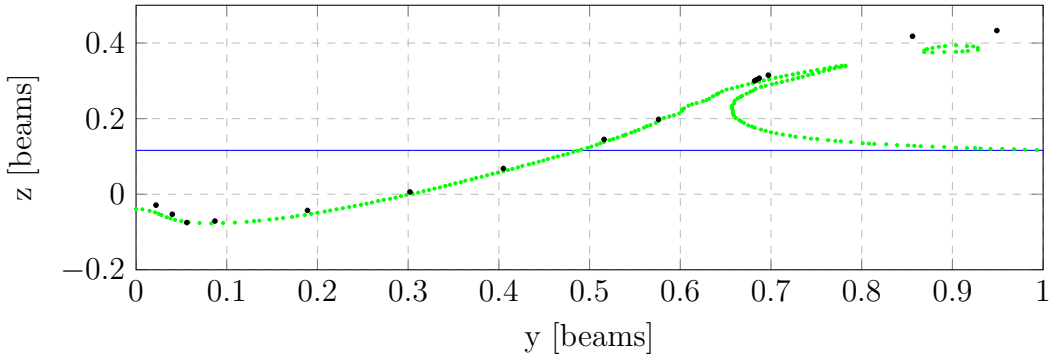

(a) Green Laser

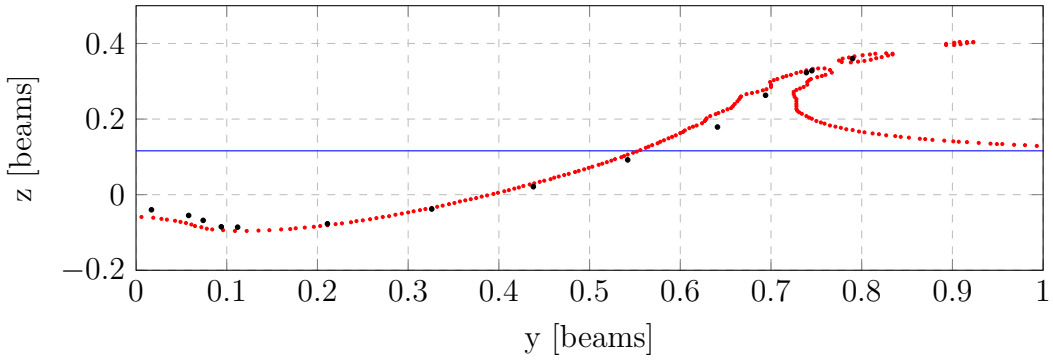

(b) Red Laser

Figure A.56: Wake Profile Comparison (Run 26)

A.4.14 Run 27 - Step A

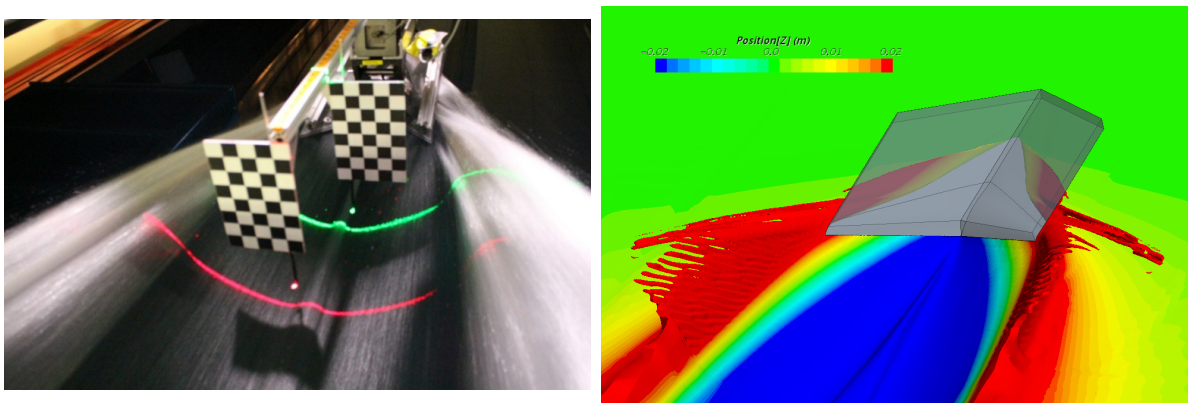

Figure A.57: Laser Wake Profile (Run 27)

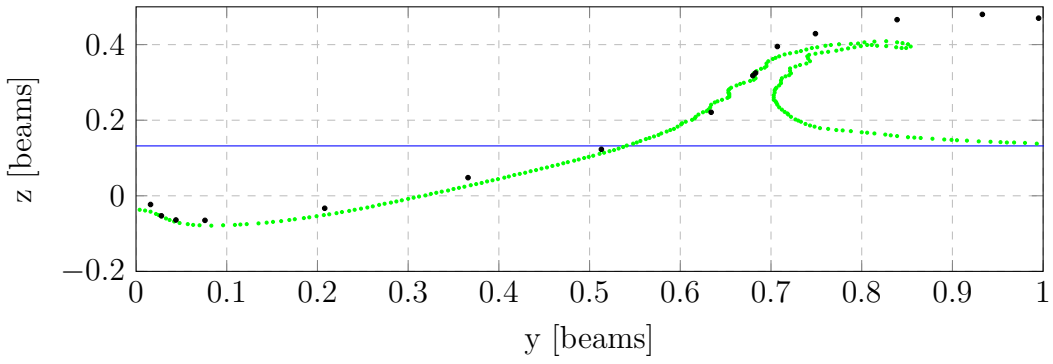

(a) Green Laser

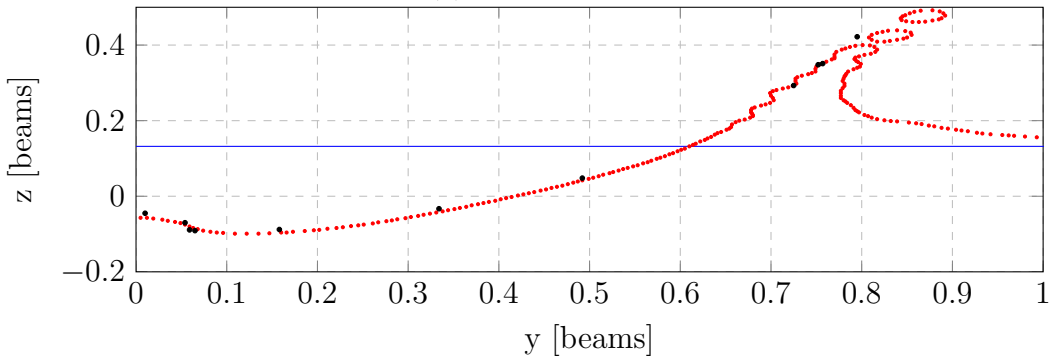

(b) Red Laser

Figure A.58: Wake Profile Comparison (Run 27)

A.4.15 Run 28 - Step A

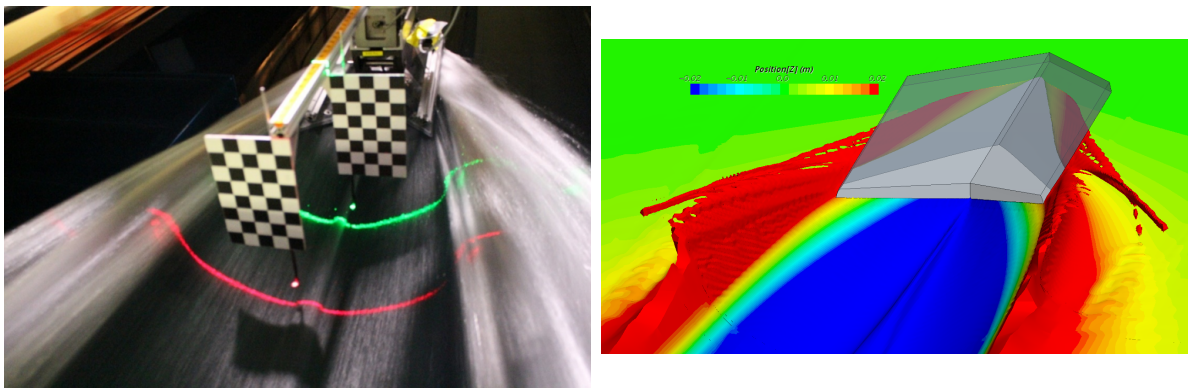

Figure A.59: Laser Wake Profile (Run 28)

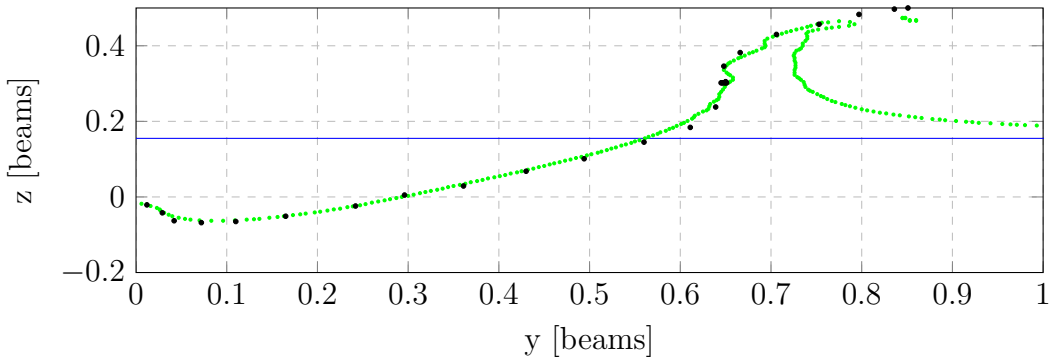

(a) Green Laser

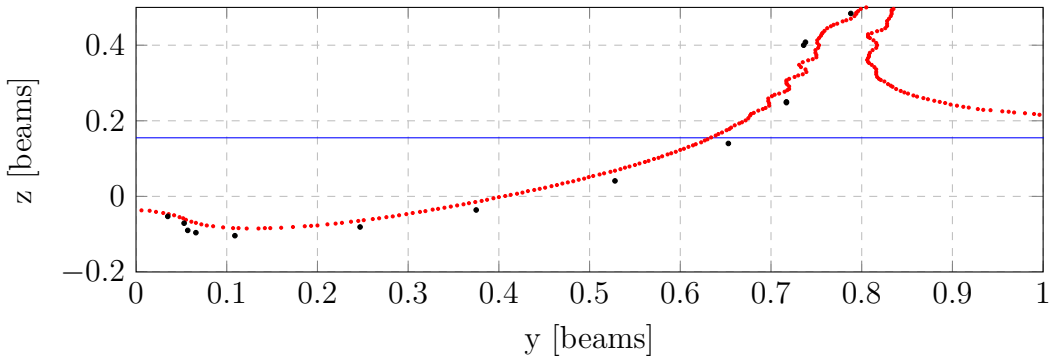

(b) Red Laser

Figure A.60: Wake Profile Comparison (Run 28)

A.4.16 Run 29 - Step B

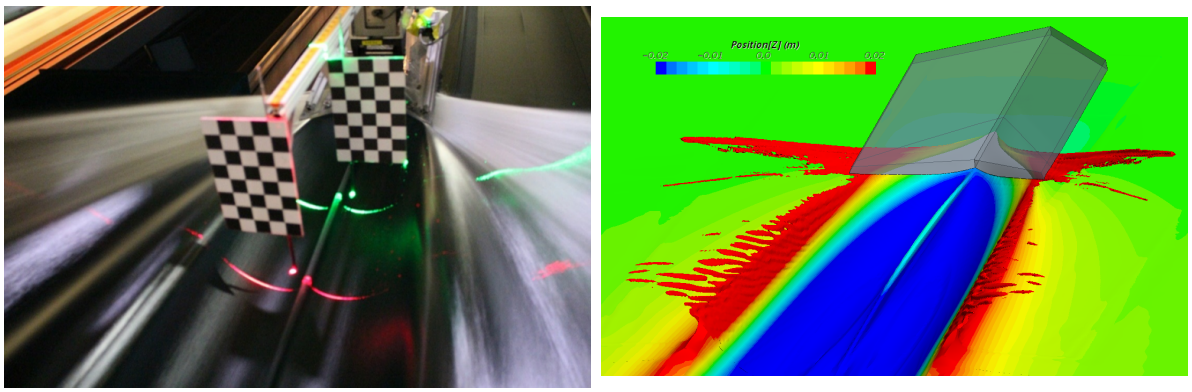

Figure A.61: Laser Wake Profile (Run 29)

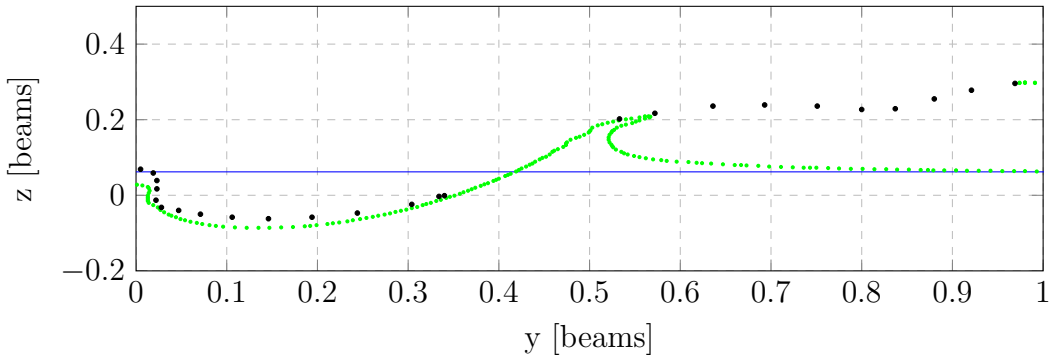

(a) Green Laser

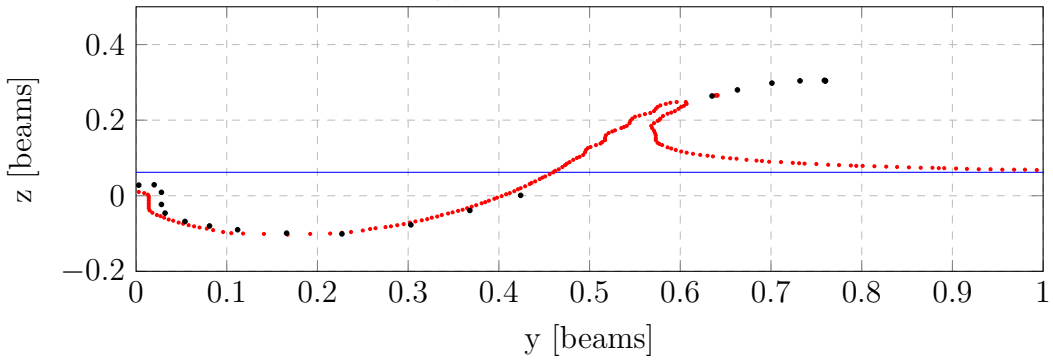

(b) Red Laser

Figure A.62: Wake Profile Comparison (Run 29)

A.4.17 Run 30 - Step B

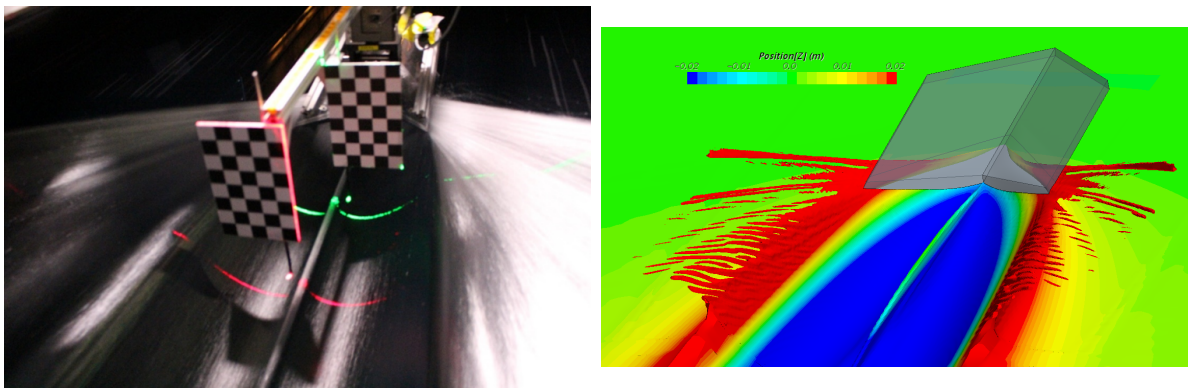

Figure A.63: Laser Wake Profile (Run 30)

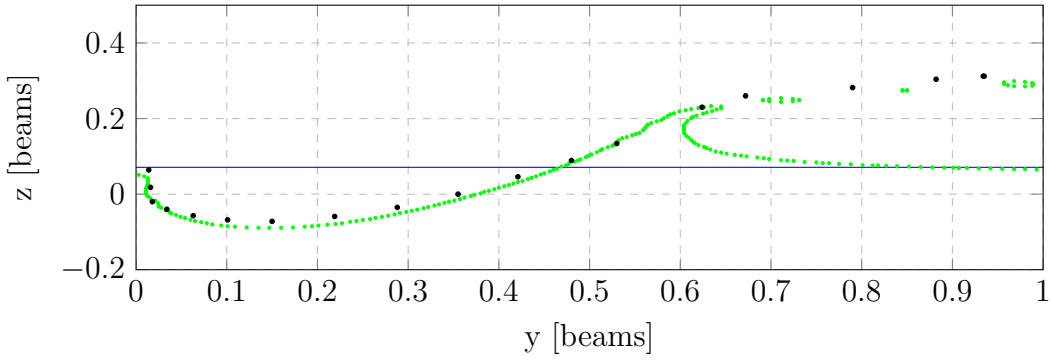

(a) Green Laser

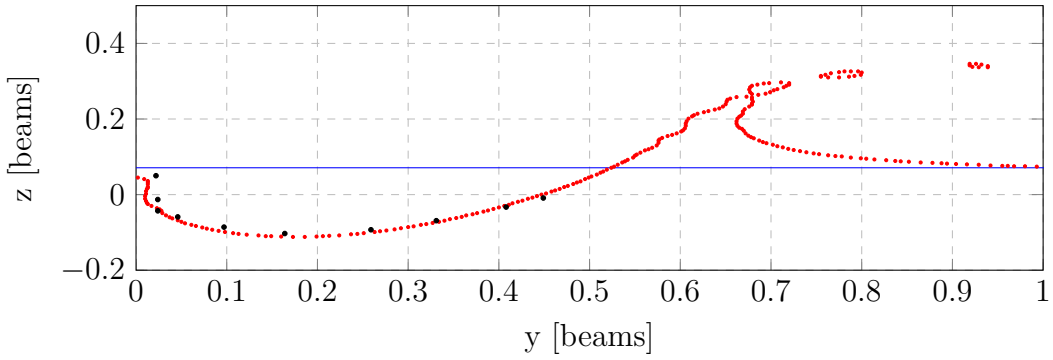

(b) Red Laser

Figure A.64: Wake Profile Comparison (Run 30)

A.4.18 Run 31 - Step B

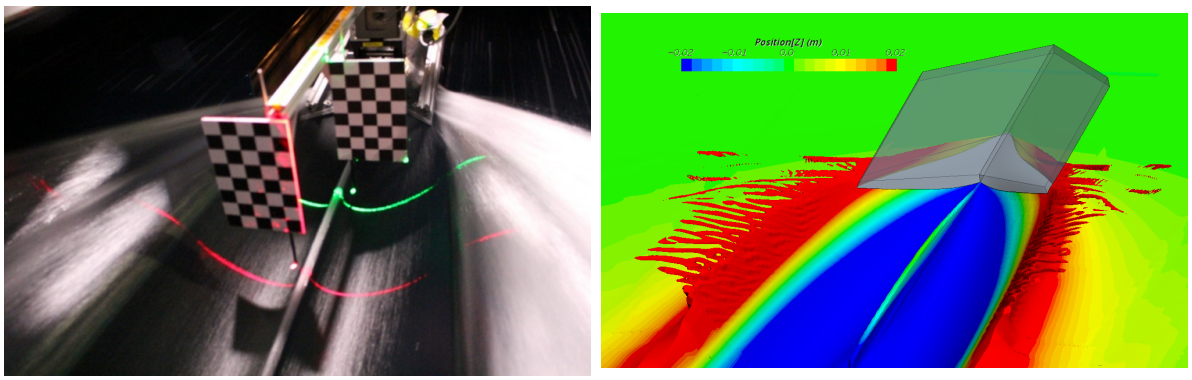

Figure A.65: Laser Wake Profile (Run 31)

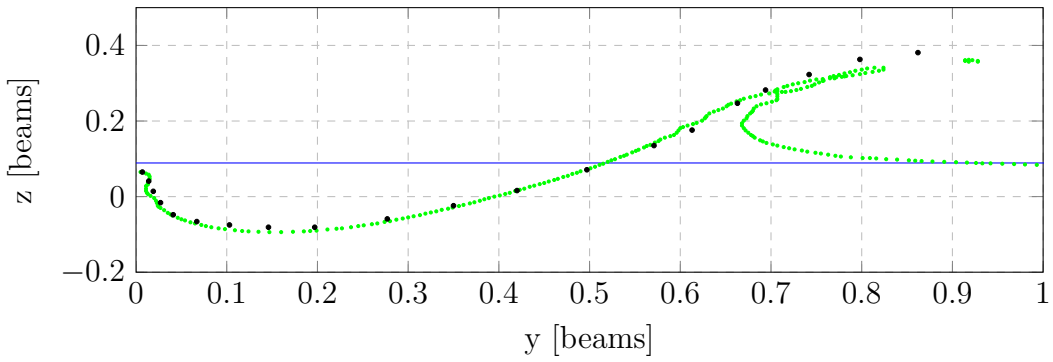

(a) Green Laser

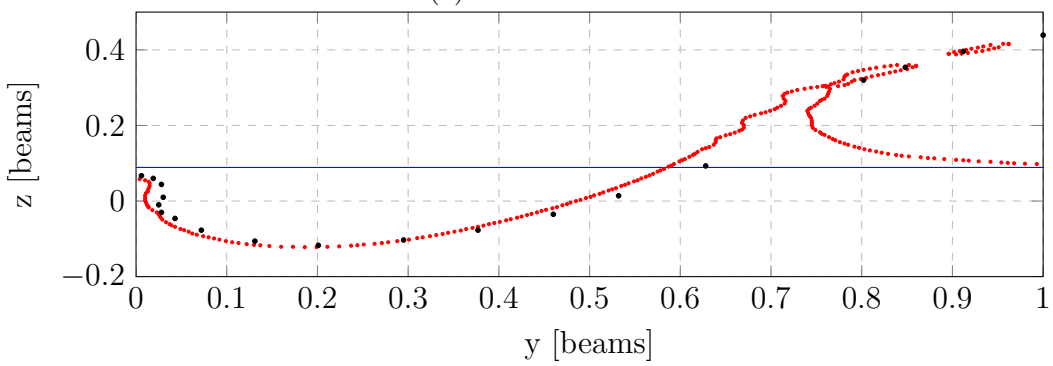

(b) Red Laser

Figure A.66: Wake Profile Comparison (Run 31)

A.4.19 Run 32 - Step B

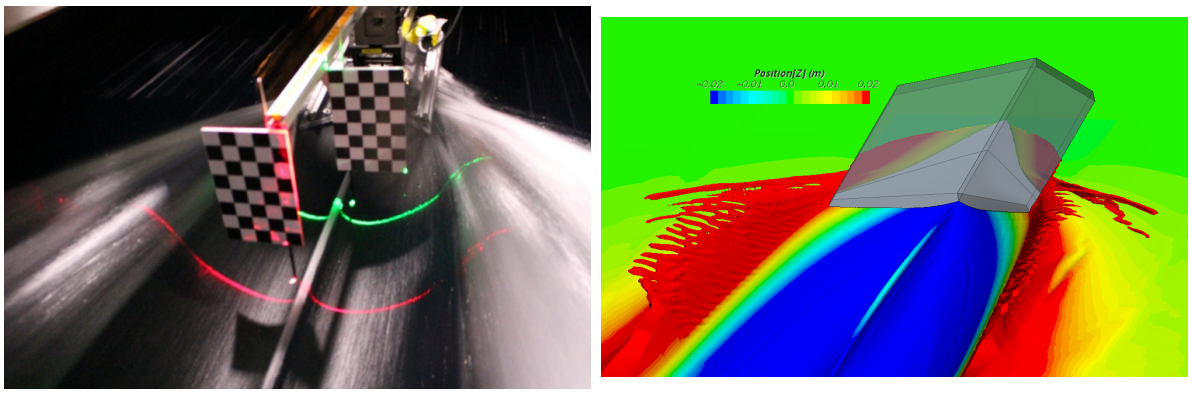

Figure A.67: Laser Wake Profile (Run 32)

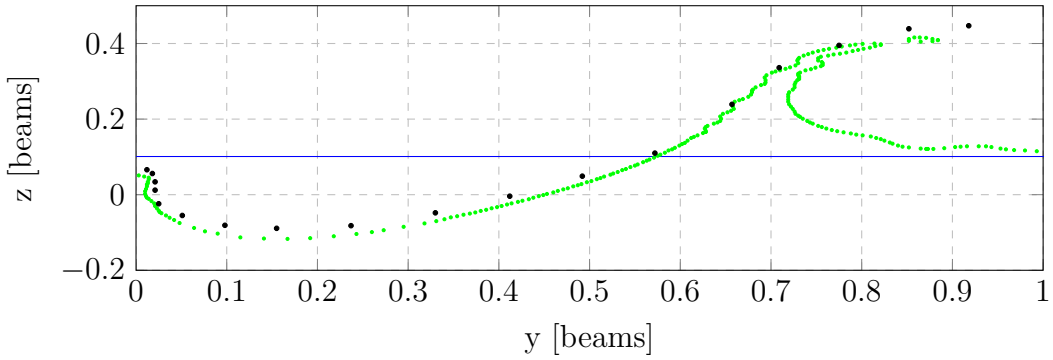

(a) Green Laser

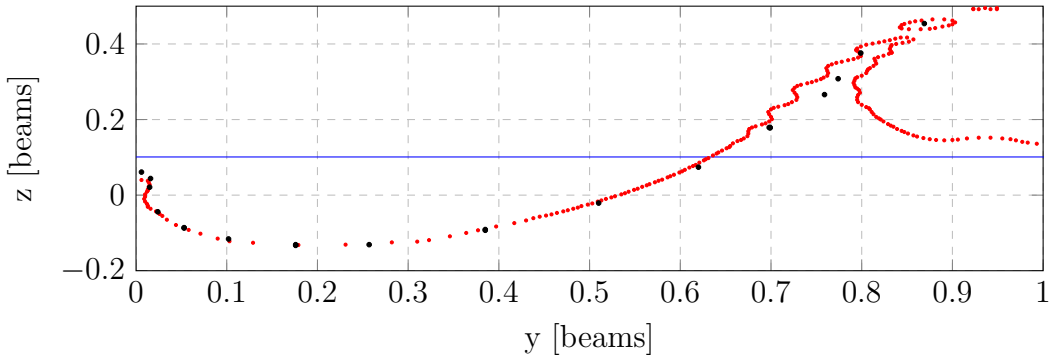

(b) Red Laser

Figure A.68: Wake Profile Comparison (Run 32)

A.4.20 Run 33 - Step B

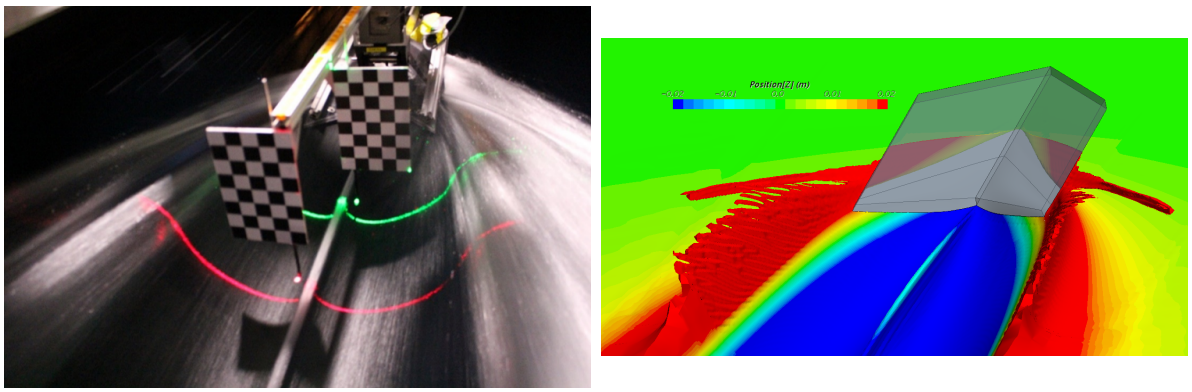

Figure A.69: Laser Wake Profile (Run 33)

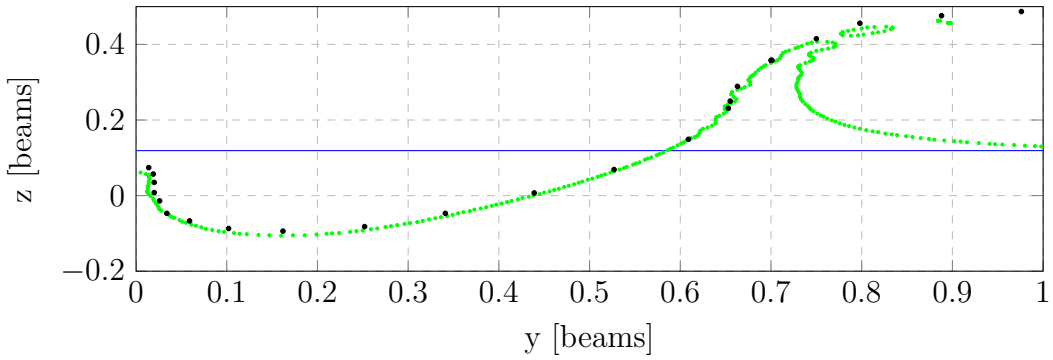

(a) Green Laser

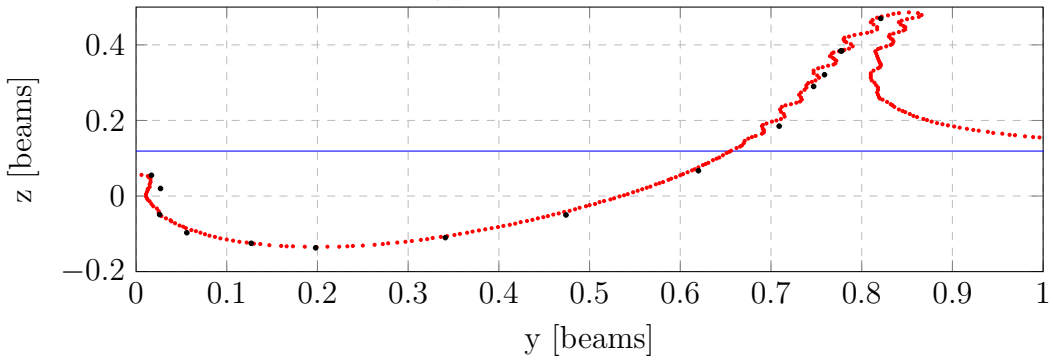

(b) Red Laser

Figure A.70: Wake Profile Comparison (Run 33)

A.4.21 Run 34 - Step B

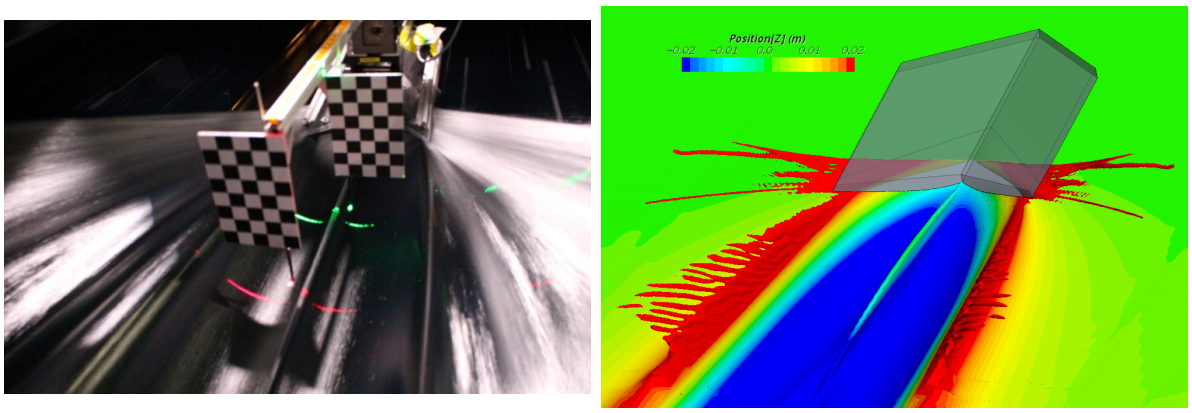

Figure A.71: Laser Wake Profile (Run 34)

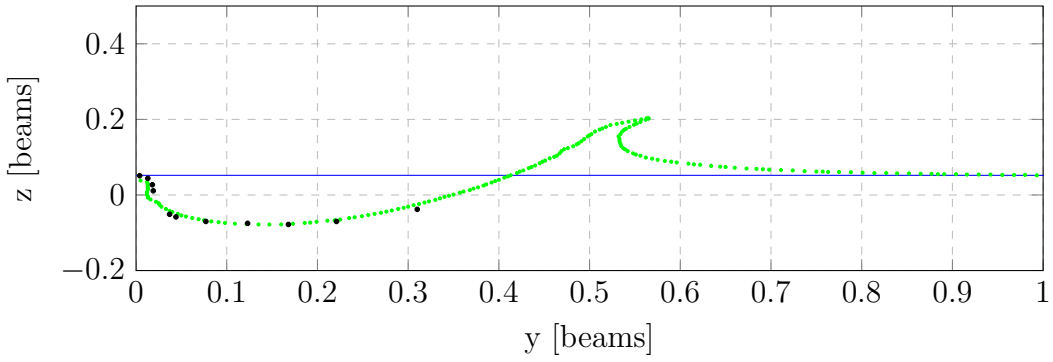

(a) Green Laser

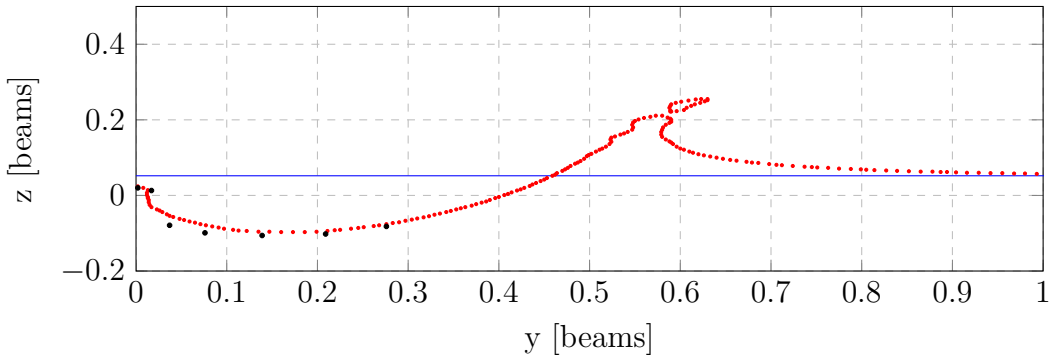

(b) Red Laser

Figure A.72: Wake Profile Comparison (Run 34)

A.4.22 Run 35 - Step B

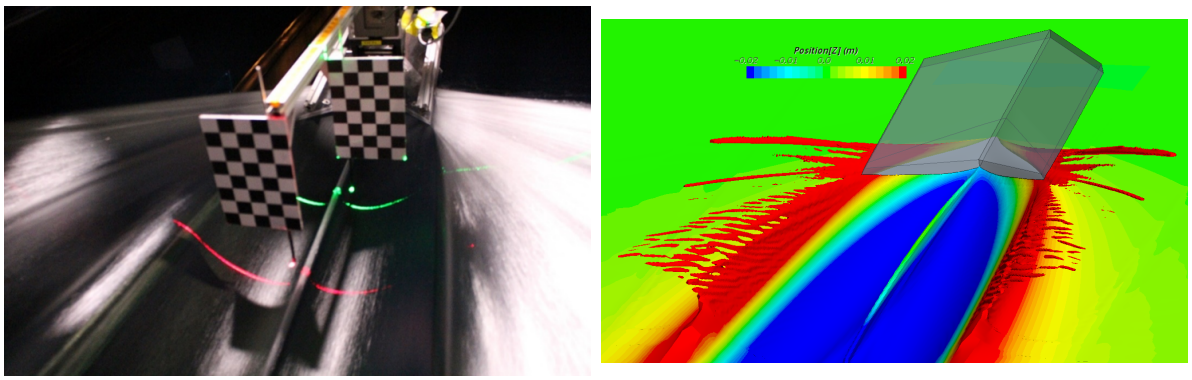

Figure A.73: Laser Wake Profile (Run 35)

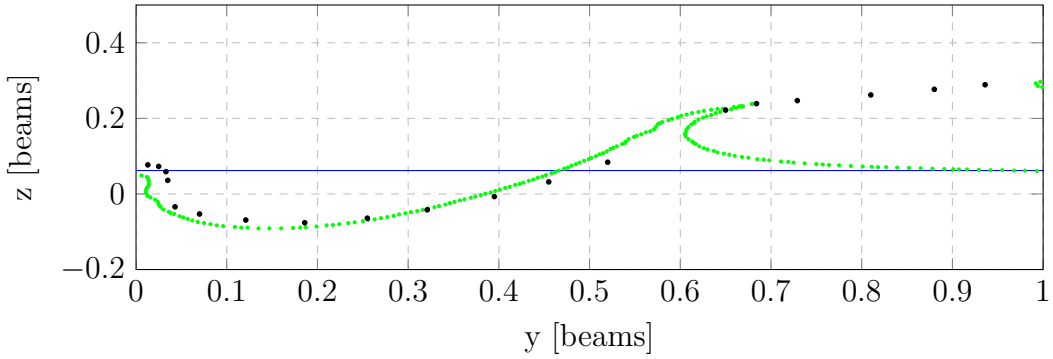

(a) Green Laser

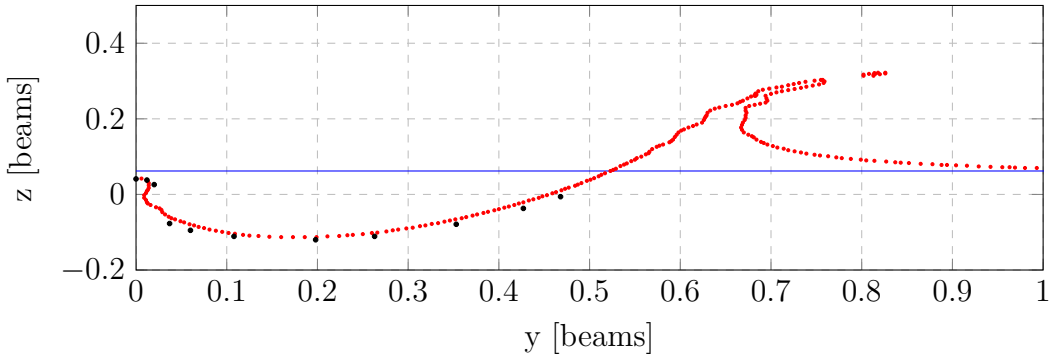

(b) Red Laser

Figure A.74: Wake Profile Comparison (Run 35)

A.4.23 Run 36 - Step B

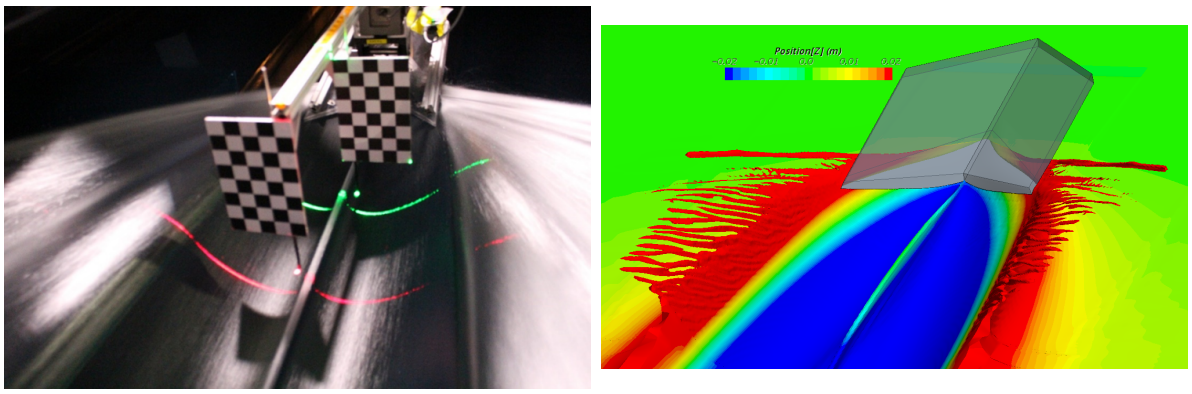

Figure A.75: Laser Wake Profile (Run 36)

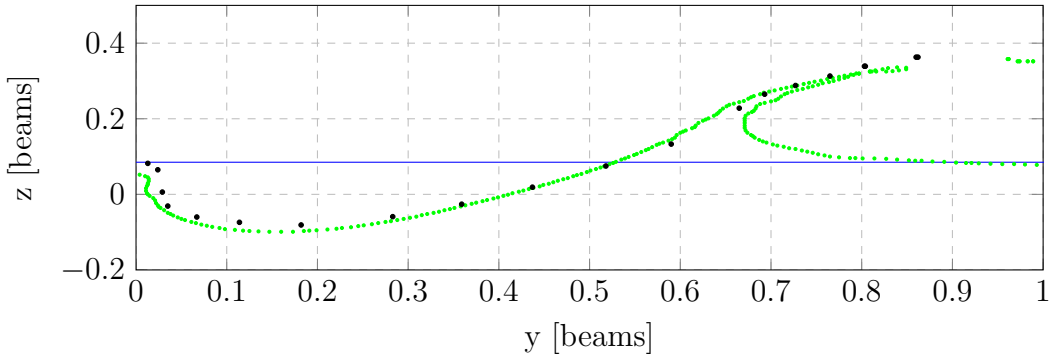

(a) Green Laser

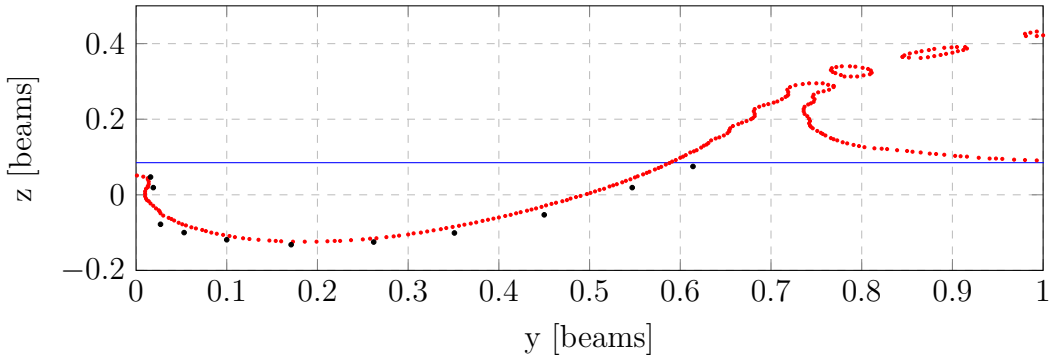

(b) Red Laser

Figure A.76: Wake Profile Comparison (Run 36)

A.4.24 Run 37 - Step B

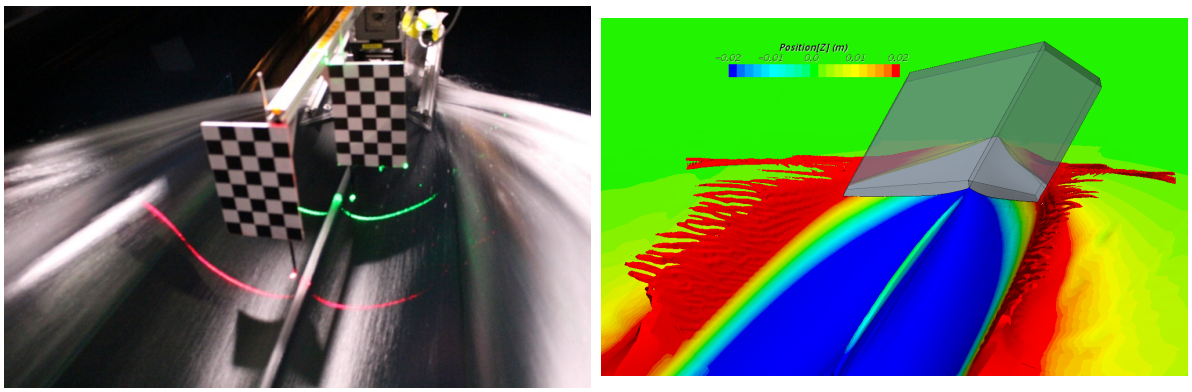

Figure A.77: Laser Wake Profile (Run 37)

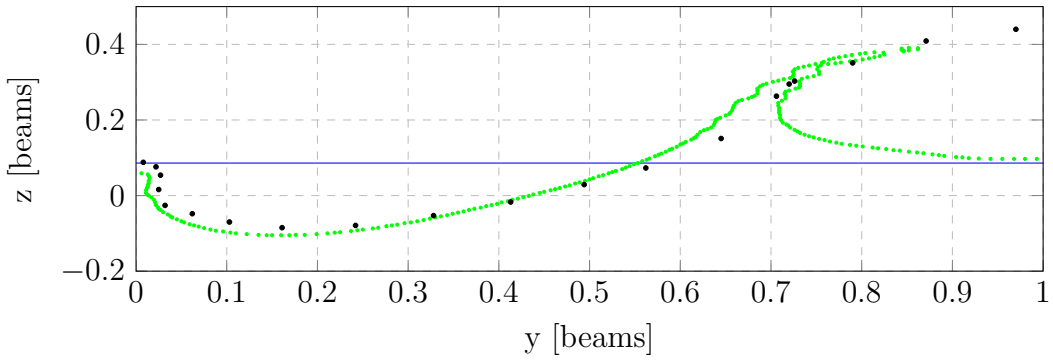

(a) Green Laser

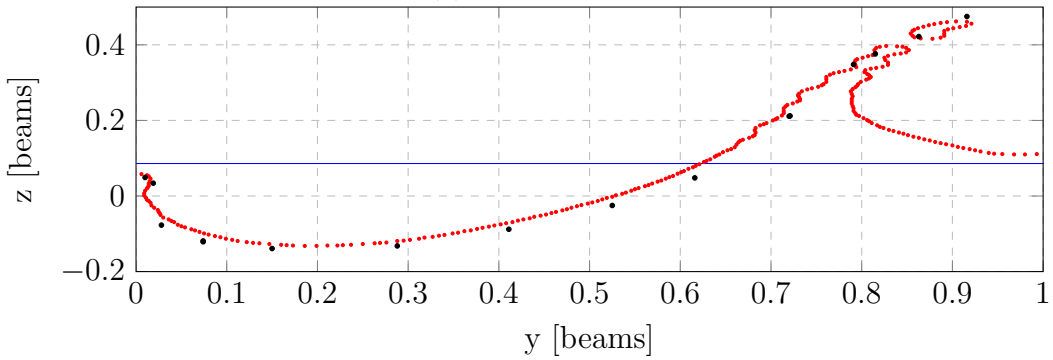

(b) Red Laser

Figure A.78: Wake Profile Comparison (Run 37)

A.4.25 Run 38 - Step B

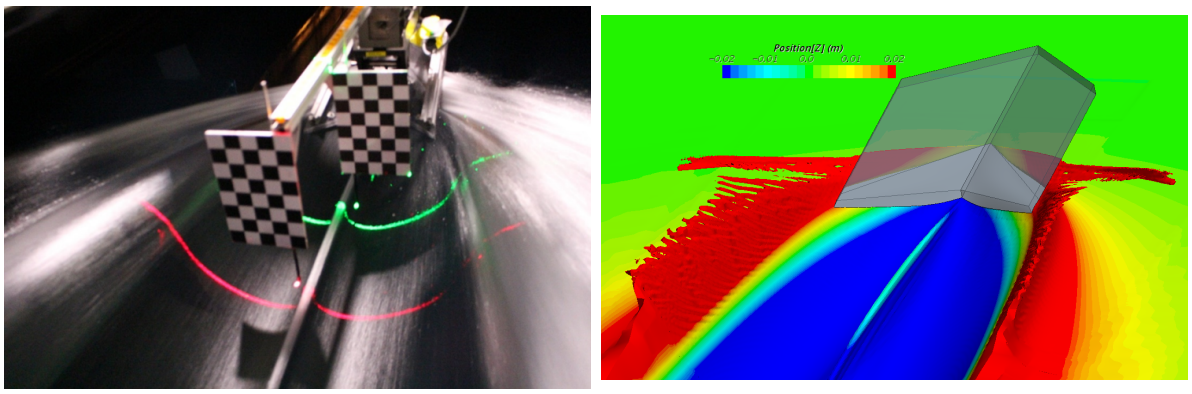

Figure A.79: Laser Wake Profile (Run 38)

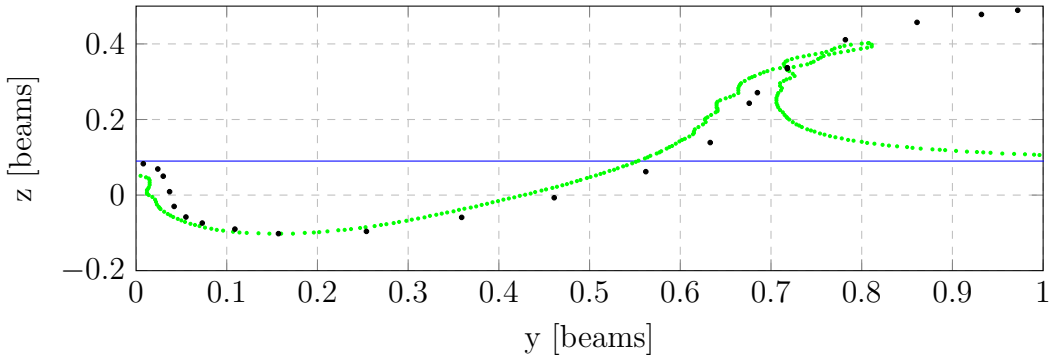

(a) Green Laser

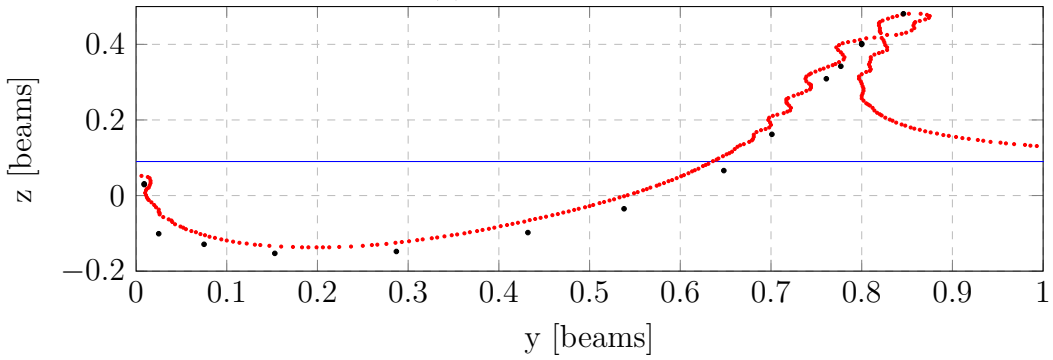

(b) Red Laser

Figure A.80: Wake Profile Comparison (Run 38)

A.4.26 Run 39 - Step B

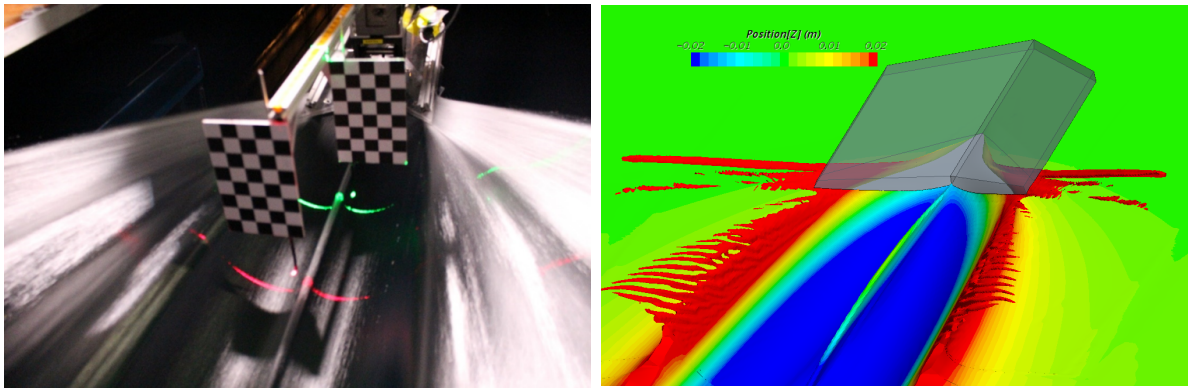

Figure A.81: Laser Wake Profile (Run 39)

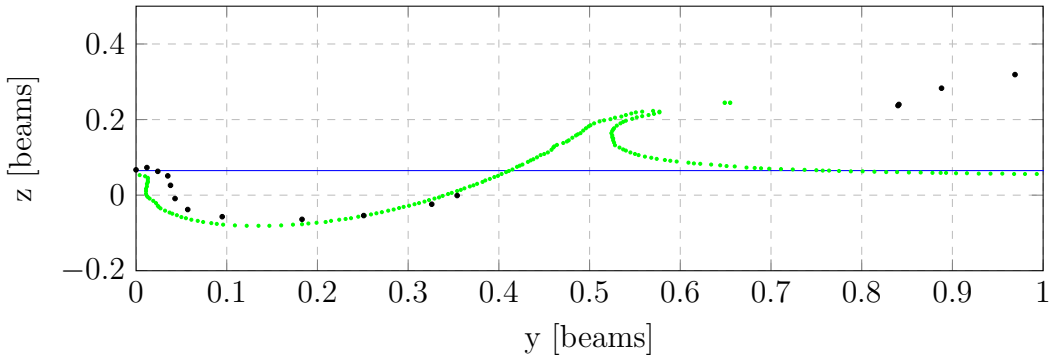

(a) Green Laser

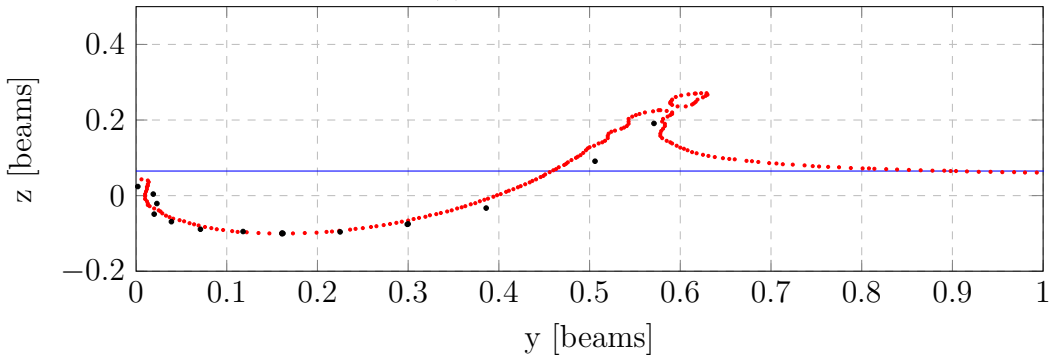

(b) Red Laser

Figure A.82: Wake Profile Comparison (Run 39)

A.4.27 Run 40 - Step B

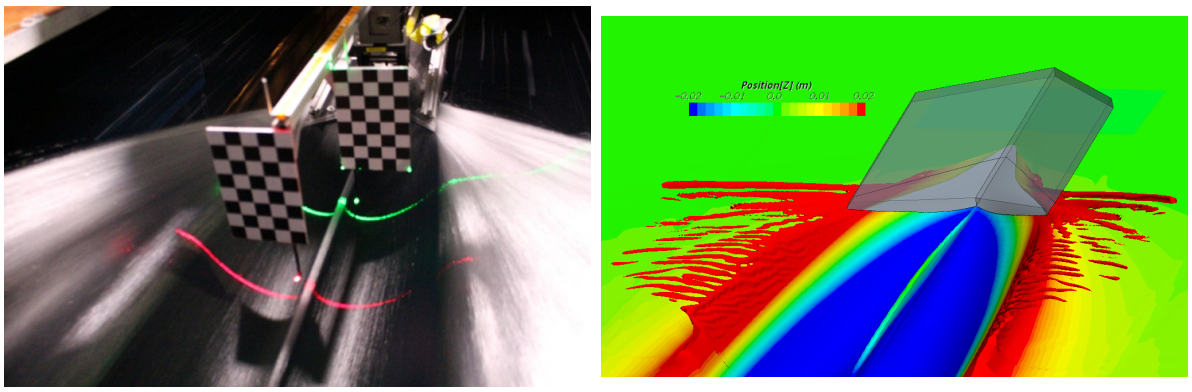

Figure A.83: Laser Wake Profile (Run 40)

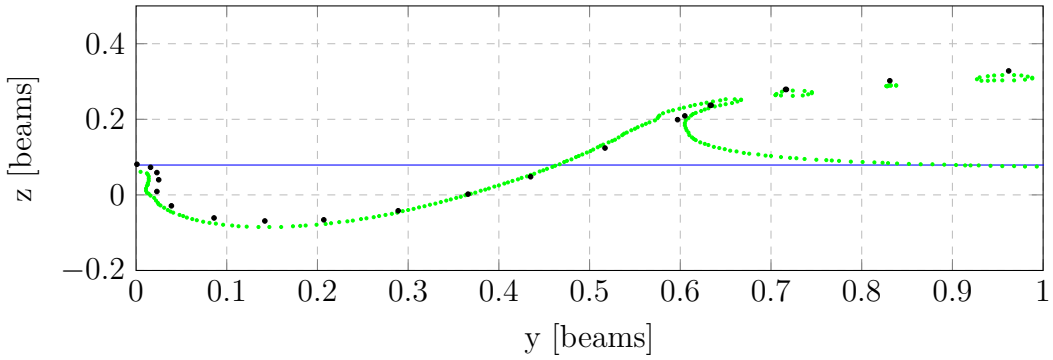

(a) Green Laser

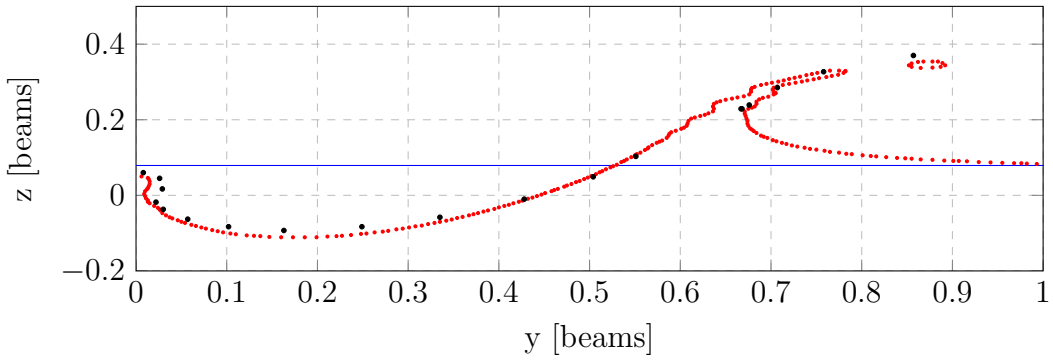

(b) Red Laser

Figure A.84: Wake Profile Comparison (Run 40)

A.4.28 Run 41 - Step B

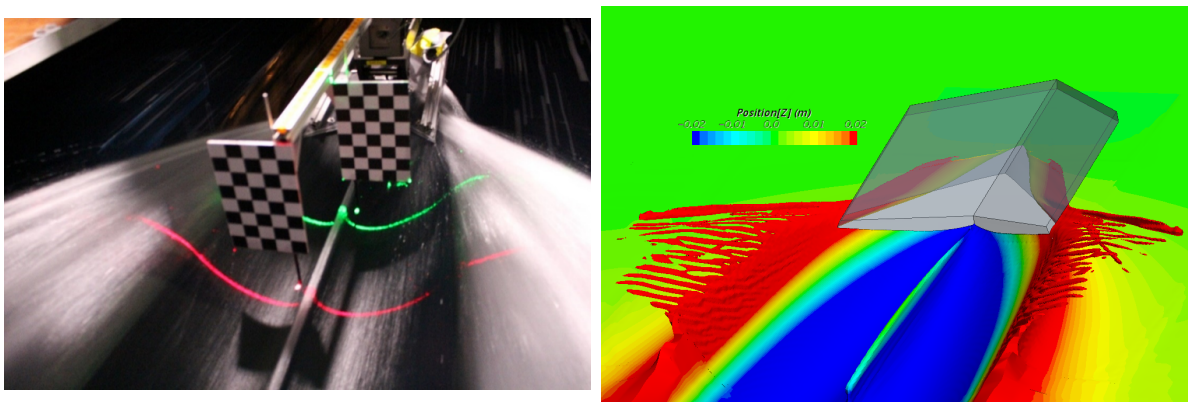

Figure A.85: Laser Wake Profile (Run 41)

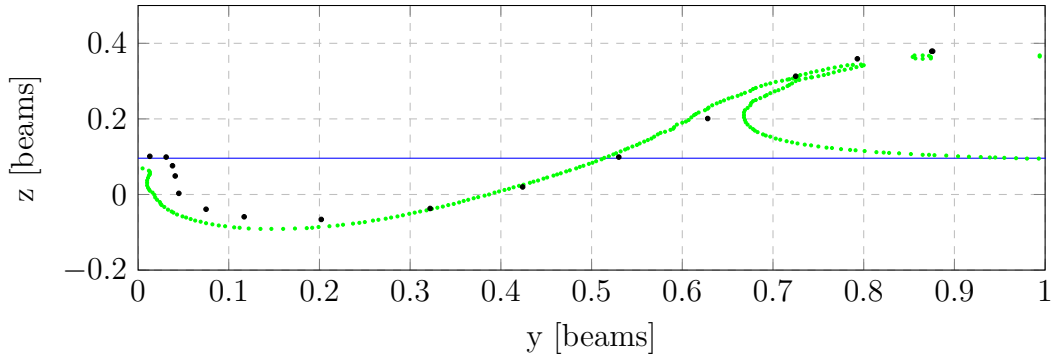

(a) Green Laser

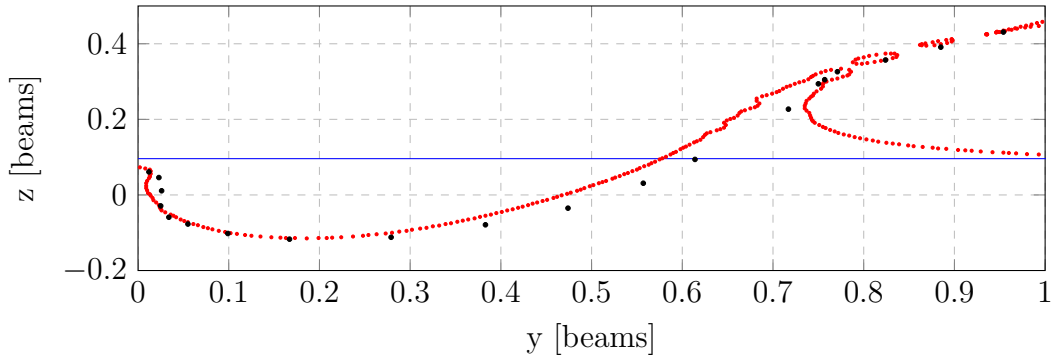

(b) Red Laser

Figure A.86: Wake Profile Comparison (Run 41)

A.4.29 Run 42 - Step B

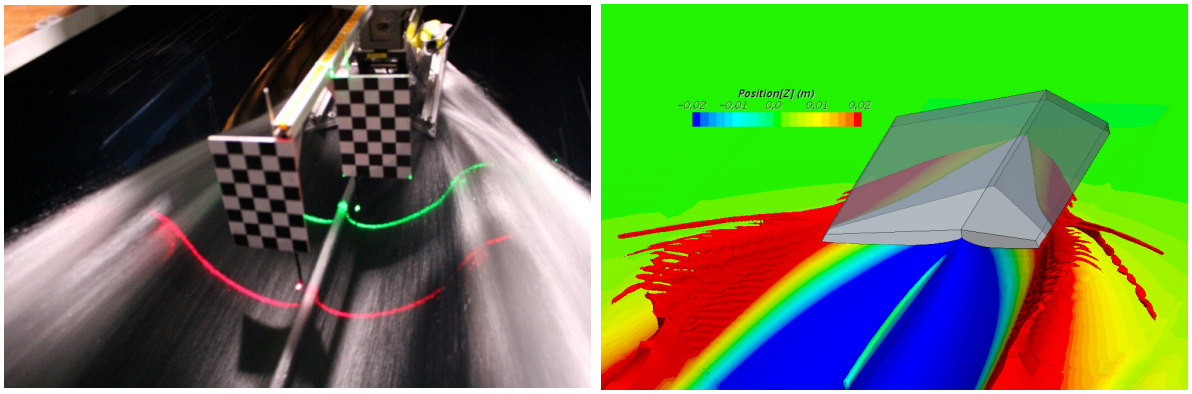

Figure A.87: Laser Wake Profile (Run 42)

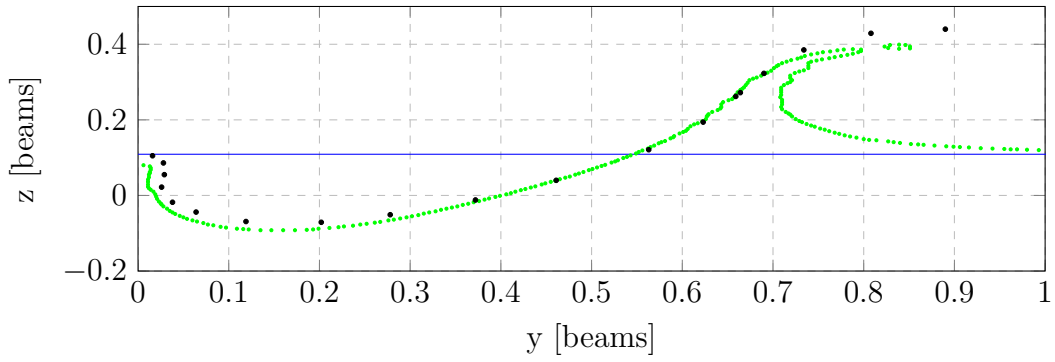

(a) Green Laser

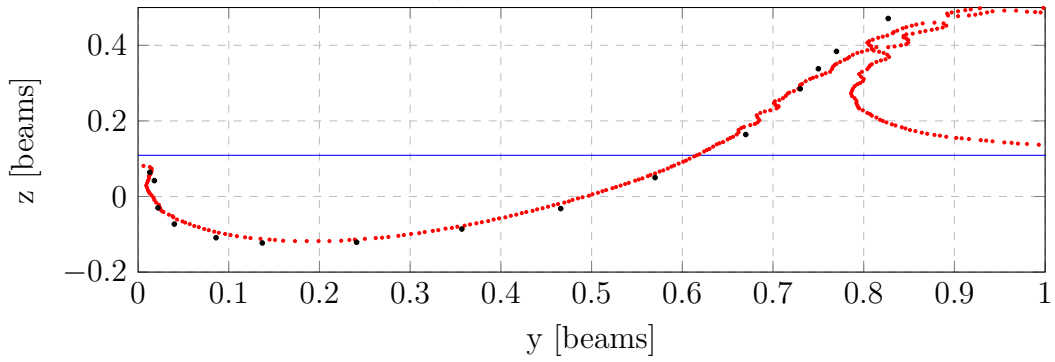

(b) Red Laser

Figure A.88: Wake Profile Comparison (Run 42)

A.4.30 Run 48 - Step B

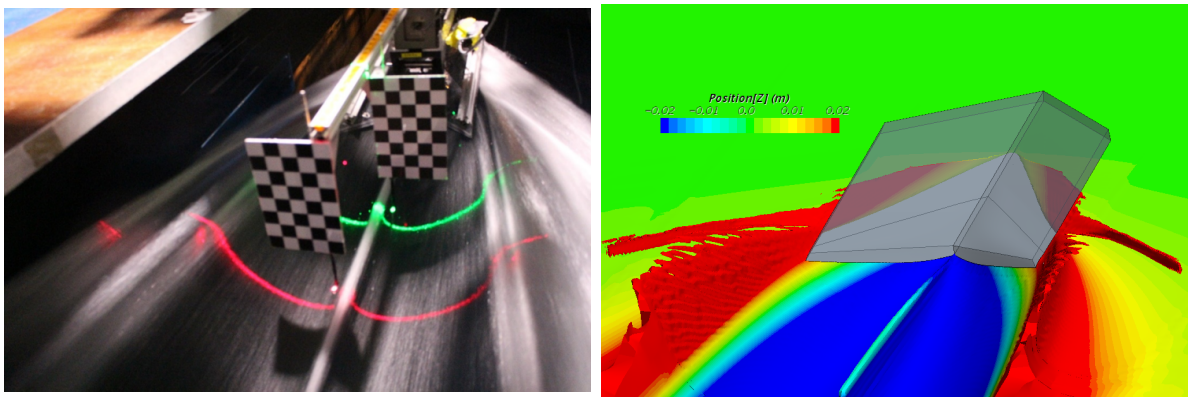

Figure A.89: Laser Wake Profile (Run 48)

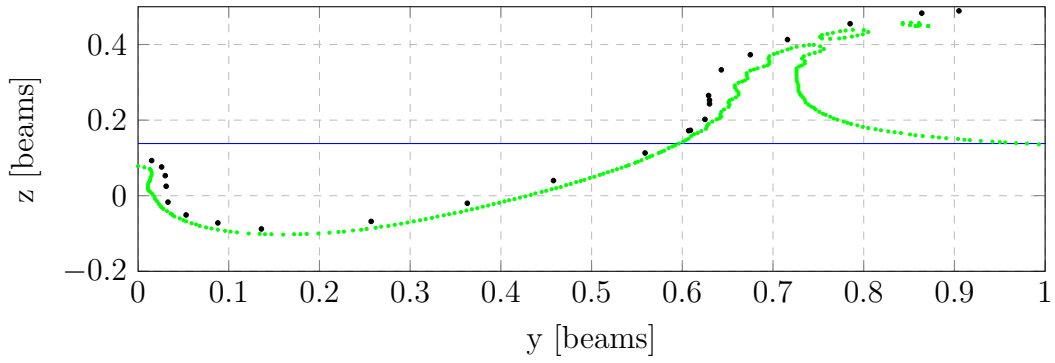

(a) Green Laser

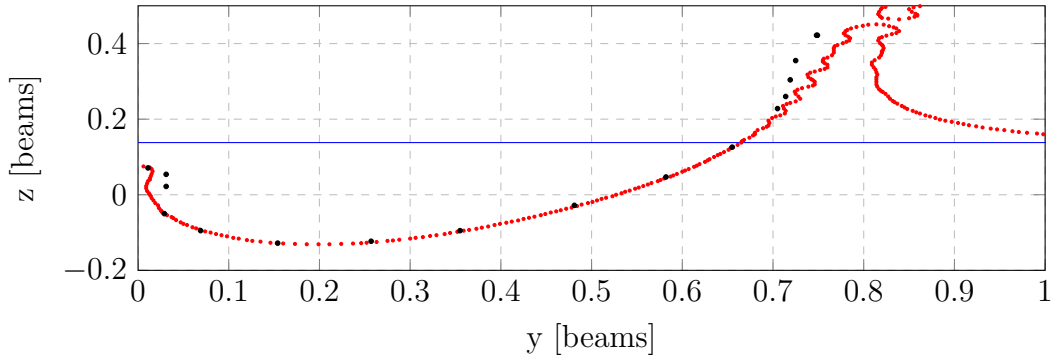

(b) Red Laser

Figure A.90: Wake Profile Comparison (Run 48)

Appendix B

Cambered Step Database

B.1 Camber Planing Surface Generator Code

```
1          clear all; close all; clc
2
3  C_L_d = 0.2159;      % 0.136 0.236 0.336
4  beta = 22;        % 15 20 25 [  ]
5  tau = 4.6489;        % 3 4 5 [  ]
6
7  b = 0.3048; % [m]
8
9  l_t = b*0.2; % [m]
10 l_r = b*0.8; % [m]
11 AR = b/((l_r+l_t)/2); % AR should equal 2
12
13 fun = @(gamma) 180/pi*atan((pi*tan(tau*pi/180))...
14     /(2*tan(beta*pi/180)))+5-gamma;
15 gamma = fzero(fun,[0 90]); % [  ]
16 phi = 180/pi*atan((1-tan(gamma*pi/180)*(l_r/b-l_t/b))...
17     /tan(gamma*pi/180)); % angle of sweep of the 50% chord line
18 theta = (180/pi)*atan(2*tan(phi*pi/180)-1/tan(gamma*pi/180)); % ...
       sweepback angle of the step
19
20 %% With Deadrise (V-Shape)
21 x_r = l_r.*[0:.01:1]; % [m]
22 z_r = l_r*C_L_d*(-20*(x_r/l_r).^1.5+80*(x_r/l_r).^2 ...
23     -64*(x_r/l_r).^2.5)*(1/(7.5*pi)); % [m]
24 y_r = [zeros(1,length([0:.01:1]))*(b/2)];
25
26 x_t = l_t.*[0:.01:1]; % [m]
27 z_t = (l_t*C_L_d*(-20*(x_t/l_t).^1.5+80*(x_t/l_t).^2-64 ...
28     *(x_t/l_t).^2.5)*(1/(7.5*pi)))+(b/2)*tand(beta); % [m]
29 y_t = [ones(1,length([0:.01:1]))*(b/2)];
30
31 figure(2)
32 subplot(2,1,1)
33 plot(x_r,z_r)
34 title('Root Cross Section','FontSize',14)
35 xlabel('x','FontSize',14)
```

```
ylabel('z','FontSize',14)
subplot(2,1,2)
plot(x_t,z_t)
title('Tip Section','FontSize',14)
xlabel('x','FontSize',14)
ylabel('z','FontSize',14)

A_r = [-x_r',y_r',z_r'].*1000; % [mm]
A_t = [-x_t'-(b/2)/tan((gamma)*pi/180),y_t',z_t'].*1000; % [mm]

figure(3)
plot(A_r(:,1),A_r(:,2),A_t(:,1),A_t(:,2))
ylim([-20,160])
title('Birds Eye View','FontSize',14)
xlabel('x','FontSize',14)
ylabel('y','FontSize',14)

filename=strcat(['DesignTest2_tip_coordinates.txt']);
fid=fopen(filename,'w+'); % open to write
for i=1:length(A_t)
    fprintf(fid, '%d %d %d \n', A_t(i,1), A_t(i,2), A_t(i,3));
end

filename=strcat(['DesignTest2_root_coordinates.txt']);
fid=fopen(filename,'w+'); % open to write
for i=1:length(A_r)
    fprintf(fid, '%d %d %d \n', A_r(i,1), A_r(i,2), A_r(i,3));
end
```

B.2 Database

Table B.1: Cambered Planing Surface for $C_{L,d} = 0.136$ and $\beta = 15°$

Design #	Trim [°]	Lift [lbf]	Shear [lbf]	Shear [%]	Pressure [lbf]	Pressure [%]	Drag [lbf]	L/D	M_Y [lbf-in]	Draft [in]	L_k [in]	A_w [in^2]
1	3	20	1.08	31%	2.39	69%	3.47	5.8	-196.3	0.525	4.67	31.86
		40	1.95	39%	3.07	61%	5.01	8.0	-375.4	1.056	10.92	84.00
		60	4.04	50%	4.03	50%	8.07	7.4	-320.1	1.278	20.69	198.24
2	4	20	0.75	19%	3.14	81%	3.89	5.14	-177.2	0.478	3.62	21.65
		40	1.16	21%	4.47	79%	5.63	7.10	-347.3	0.690	7.18	50.46
		60	2.16	28%	5.49	72%	7.64	7.85	-444.9	0.980	11.58	98.20
		80	3.90	36%	6.80	64%	10.70	7.48	-276.6	1.558	20.25	201.91
3	5	20	0.50	12%	3.69	88%	4.19	4.77	-167.0	0.480	3.17	16.12
		40	0.87	13%	5.72	87%	6.58	6.08	-321.7	0.703	5.54	37.45
		60	1.37	17%	6.78	83%	8.15	7.36	-451.3	0.868	8.11	63.21
		80	2.29	21%	8.47	79%	10.76	7.44	-464.2	1.225	12.41	112.78
		100	3.77	27%	10.16	73%	13.93	7.18	-223.9	1.859	19.66	200.40

Table B.2: Cambered Planing Surface for $C_{L,d} = 0.236$ and $\beta = 15°$

Design #	Trim [°]	Lift [lbf]	Shear [lbf]	Shear [%]	Pressure [lbf]	Pressure [%]	Drag [lbf]	L/D	M_Y [lbf-in]	Draft [in]	L_k [in]	A_w [in^2]
4	3	20	0.92	18%	4.26	82%	5.18	3.86	-202.7	0.510	2.50	25.75
		40	1.17	18%	5.39	82%	6.56	6.09	-416.8	0.685	4.38	46.79
		60	2.11	27%	5.59	73%	7.70	7.79	-552.0	0.928	11.47	100.62
		80	4.24	40%	6.46	60%	10.69	7.48	-437.7	1.520	22.14	221.99
5	4	20	0.50	9%	5.11	91%	5.62	3.56	-183.9	0.469	2.20	15.27
		40	0.77	9%	7.8	91%	8.56	4.67	-373.1	0.629	3.67	34.16
		60	1.04	11%	8.12	89%	9.15	6.55	-540.3	0.791	5.60	52.72
		80	1.94	18%	8.88	82%	10.82	7.39	-629.1	1.068	10.73	95.59
		100	3.49	26%	10.12	74%	13.62	7.34	-504.7	1.602	18.36	182.57
6	5	20	0.22	4%	5.66	96%	5.89	3.40	-171.3	0.466	2.23	12.29
		40	0.45	5%	9.21	95%	9.66	4.14	-339.0	0.639	3.61	27.51
		60	0.70	6%	11.07	94%	11.78	5.09	-495.4	0.771	4.83	40.90
		80	1.06	9%	11.05	91%	12.11	6.61	-629.5	0.942	7.24	60.05
		100	1.91	13%	12.61	87%	14.52	6.89	-665.8	1.236	10.98	99.99
		120	3.17	18%	14.30	82%	17.47	6.87	-507.9	1.775	17.01	171.66

Table B.3: Cambered Planing Surface for $C_{L,d} = 0.336$ and $\beta = 15°$

Design #	Trim [°]	Lift [lbf]	Shear [lbf]	Shear [%]	Pressure [lbf]	Pressure [%]	Drag [lbf]	L/D	M_Y [lbf-in]	Draft [in]	L_k [in]	A_w [in^2]
7	3	20	0.83	12%	6.21	88%	7.03	2.84	-209.6	0.541	1.90	19.09
		40	0.99	10%	8.56	90%	9.55	4.19	-426.7	0.703	2.89	43.01
		60	1.22	13%	8.07	87%	9.28	6.46	-615.3	0.852	4.13	58.37
		80	2.43	22%	8.48	78%	10.92	7.33	-694.3	1.167	13.16	126.00
		90		%		%						
8	4	20	0.36	5%	7.03	95%	7.39	2.71	-183.2	0.477	1.79	12.31
		40	0.51	4%	11.38	96%	11.90	3.36	-373.6	0.642	2.78	26.72
		60	0.67	5%	12.99	95%	13.66	4.39	-557.5	0.780	3.65	42.82
		80	0.96	7%	12.13	93%	13.09	6.11	-694.0	0.935	5.09	57.15
		100	1.95	13%	12.91	87%	14.86	6.73	-780.9	1.216	11.07	102.45
		120	3.44	20%	14.08	80%	17.52	6.85	-644.5	1.740	18.33	186.13
		130	4.48	23%	14.66	77%	19.13	6.79	-438.0	2.159	23.73	253.03
9	5	20	0.02	0.3%	7.67	99.7%	7.70	2.60	-172.3	0.456	1.72	8.99
		40	0.13	1%	12.95	99%	13.09	3.06	-342.6	0.645	2.62	18.65
		60	0.30	2%	16.13	98%	16.43	3.65	-505.4	0.754	3.43	28.99
		80	0.53	3%	17.04	97%	17.57	4.55	-667.1	0.877	4.57	45.63
		100	0.93	5%	16.04	95%	16.97	5.89	-792.1	1.028	6.07	58.88
		120	1.72	9%	17.61	91%	19.34	6.21	-830.0	1.322	10.51	97.78
		140	2.84	13%	19.26	87%	22.10	6.34	-706.8	1.805	15.75	159.14
		160	4.32	17%	20.68	83%	25.01	6.40	-291.8	2.574	24.30	260.83

Table B.4: Cambered Planing Surface for $C_{L,d} = 0.136$ and $\beta = 20°$

Design #	Trim [°]	Lift [lbf]	Shear [lbf]	Shear [%]	Pressure [lbf]	Pressure [%]	Drag [lbf]	L/D	M_Y [lbf-in]	Draft [in]	L_k [in]	A_w [in^2]
10	3	20	1.78	50%	1.77	50%	3.55	5.64	-207.4	0.744	10.92	67.82
		40	3.79	58%	2.74	42%	6.53	6.12	-336.5	1.204	18.70	165.93
		48	4.86	61%	3.14	39%	7.99	6.01	286.4	1.479	24.32	231.23
11	4	20	2.59	68%	1.20	32%	3.79	5.28	-188.7	0.690	6.07	36.07
		40	2.24	38%	3.72	62%	5.96	6.71	-363.3	0.998	11.49	88.19
		60	3.90	43%	5.08	57%	8.99	6.68	-365.3	1.485	19.02	178.91
12	5	20	0.93	22%	3.27	78%	4.20	4.76	-175.7	0.638	4.48	26.32
		40	1.50	24%	4.85	76%	6.35	6.29	-344.9	0.936	8.55	60.59
		60	2.48	28%	6.41	72%	8.89	6.75	-446.2	1.248	12.36	107.41
		80	3.84	32%	8.10	68%	11.93	6.70	-348.1	1.800	18.60	189.11

Table B.5: Cambered Planing Surface for $C_{L,d} = 0.236$ and $\beta = 20°$

Design #	Trim [°]	Lift [lbf]	Shear [lbf]	Shear [%]	Pressure [lbf]	Pressure [%]	Drag [lbf]	L/D	M_Y [lbf-in]	Draft [in]	L_k [in]	A_w [in^2]
13	3	20	1.47	32%	3.16	68%	4.63	4.32	-218.9	0.708	4.17	42.54
		40	2.44	40%	3.72	60%	6.16	6.49	-432.3	1.024	12.83	112.10
		60	4.69	50%	4.68	50%	9.37	6.40	-431.9	1.578	23.33	226.43
14	4	20	1.06	20%	4.32	80%	5.39	3.71	-196.4	0.658	3.03	28.28
		40	1.37	20%	5.54	80%	6.90	5.79	-401.1	0.915	7.09	57.21
		60	2.45	27%	6.50	73%	8.95	6.70	-537.4	1.222	12.31	107.82
		80	4.11	35%	7.79	65%	11.90	6.72	-490.5	1.756	20.18	198.77
15	5	20	0.73	13%	5.13	87%	5.86	3.41	-182.2	0.635	2.77	17.50
		40	1.05	12%	7.61	88%	8.67	4.62	-375.3	0.872	5.03	41.04
		60	1.46	15%	8.26	85%	9.72	6.17	-534.8	1.082	8.76	68.19
		80	2.45	20%	9.94	80%	12.39	6.46	-613.6	1.405	12.41	113.12
		100	3.76	25%	11.56	75%	15.32	6.53	-515.9	1.944	18.37	187.95
		110	4.59	27%	12.40	73%	16.99	6.47	-363.3	2.329	22.99	241.08

Table B.6: Cambered Planing Surface for $C_{L,d} = 0.336$ and $\beta = 20°$

Design #	Trim [°]	Lift [lbf]	Shear [lbf]	Shear [%]	Pressure [lbf]	Pressure [%]	Drag [lbf]	L/D	M_Y [lbf-in]	Draft [in]	L_k [in]	A_w [in^2]
16	3	20	1.44	23%	4.76	77%	6.20	3.22	-224.1	0.771	2.63	35.11
		40	1.71	25%	5.11	75%	6.82	5.87	-456.4	0.999	9.33	71.57
		60	3.22	35%	5.94	65%	9.16	6.55	-576.5	1.390	16.36	154.17
		70	4.33	40%	6.39	60%	10.72	6.53	-547.1	1.697	22.12	218.86
17	4	20	0.97	14%	6.14	86%	7.11	2.81	-199.4	0.703	2.30	22.06
		40	1.20	12%	8.43	88%	9.63	4.15	-413.2	0.927	3.63	47.52
		60	1.61	16%	8.28	84%	9.89	6.07	-591.3	1.122	9.26	76.61
		80	2.83	23%	9.64	77%	12.47	6.42	-671.9	1.486	14.33	136.90
		100	4.50	29%	10.84	71%	15.33	6.52	-549.4	2.094	22.71	233.68
18	5	20	0.61	8%	7.04	92%	7.66	2.61	-184.5	0.649	2.08	15.39
		40	0.85	7%	11.08	93%	11.93	3.35	-386.4	0.886	3.32	35.15
		60	1.06	8%	12.08	92%	13.14	4.57	-562.3	1.036	4.76	51.42
		80	1.51	11%	12.17	89%	13.68	5.85	-700.3	1.259	9.02	78.58
		100	2.57	16%	13.96	84%	16.53	6.05	-748.5	1.625	13.09	126.22
		120	3.88	20%	15.56	80%	19.44	6.17	-624.4	2.178	19.28	200.73

Table B.7: Cambered Planing Surface for $C_{L,d} = 0.136$ and $\beta = 25°$

Design #	Trim [°]	Lift [lbf]	Shear [lbf]	Shear [%]	Pressure [lbf]	Pressure [%]	Drag [lbf]	L/D	M_Y [lbf-in]	Draft [in]	L_k [in]	A_w [in^2]
19	3	20	2.94	66%	1.52	34%	4.45	4.49	-206.7	1.016	15.16	113.70
		30	4.33	68%	2.03	32%	6.36	4.72	-269.3	1.354	21.55	181.49
		40	5.99	68%	2.88	32%	8.87	4.51	-249.5	1.747	25.84	263.86
20	4	20	1.87	47%	2.10	53%	3.97	5.04	-192.5	0.923	10.01	61.95
		40	3.69	52%	3.44	48%	7.14	5.60	-332.3	1.411	17.41	151.47
		50	4.71	53%	4.14	47%	8.84	5.65	-321.8	1.751	22.11	210.27
21	5	20	1.37	32%	2.84	68%	4.20	4.76	-188.3	0.865	7.73	45.02
		40	2.50	36%	4.35	64%	6.85	5.84	-348.4	1.246	12.01	95.05
		60	3.92	39%	6.09	61%	10.01	6.00	-386.6	1.768	17.91	172.91
		70	4.78	41%	6.94	59%	11.71	5.98	-309.3	2.114	22.30	227.70

Table B.8: Cambered Planing Surface for $C_{L,d} = 0.236$ and $\beta = 25°$

Design #	Trim [°]	Lift [lbf]	Shear [lbf]	Shear [%]	Pressure [lbf]	Pressure [%]	Drag [lbf]	L/D	M_Y [lbf-in]	Draft [in]	L_k [in]	A_w [in^2]
22	3	20	2.18	50%	2.18	50%	4.36	4.59	-225.0	0.978	11.17	80.69
		30	3.05	53%	2.70	47%	5.76	5.21	-331.9	1.219	15.90	131.18
		40	4.32	57%	3.23	43%	7.55	5.30	-383.3	1.524	21.62	196.35
23	4	20	1.48	31%	3.37	69%	4.85	4.12	-206.0	0.889	5.74	45.90
		40	2.65	37%	4.43	63%	7.08	5.65	-402.0	1.262	12.92	109.40
		60	4.33	43%	5.78	57%	10.11	5.93	-454.4	1.794	20.36	198.28
		70	5.26	45%	6.46	55%	11.73	5.97	-395.9	2.158	25.84	259.60
24	5	20	1.17	21%	4.37	79%	5.54	3.61	-191.3	0.853	4.03	32.46
		40	1.70	23%	5.79	77%	7.50	5.34	-385.8	1.160	9.29	69.74
		60	2.87	28%	7.39	72%	10.26	5.85	-517.4	1.536	13.32	121.57
		80	4.27	32%	9.06	68%	13.33	6.00	-497.9	2.079	19.84	199.58

Table B.9: Cambered Planing Surface for $C_{L,d} = 0.336$ and $\beta = 25°$

Design #	Trim [°]	Lift [lbf]	Shear [lbf]	Shear [%]	Pressure [lbf]	Pressure [%]	Drag [lbf]	L/D	M_Y [lbf-in]	Draft [in]	L_k [in]	A_w [in^2]
25	3	20	1.97	37%	3.30	63%	5.27	3.80	-233.3	1.003	8.76	66.17
		40	3.39	46%	4.05	54%	7.44	5.38	-436.6	1.448	17.16	151.74
		60	6.21	52%	5.72	48%	11.93	5.03	-433.3	2.141	25.84	291.22
26	4	20	1.49	23%	4.95	77%	6.44	3.11	-211.9	0.938	3.21	44.01
		40	1.96	26%	5.67	74%	7.63	5.24	-429.4	1.235	9.96	87.12
		60	3.45	33%	7.06	67%	10.51	5.71	-557.6	1.661	16.41	157.47
		75	4.65	37%	8.03	63%	12.68	5.91	-543.4	2.094	22.25	230.37
27	5	20	1.12	15%	6.17	85%	7.29	2.74	-196.3	0.877	2.83	25.47
		40	1.38	14%	8.18	86%	9.56	4.18	-397.7	1.151	5.61	56.02
		60	2.15	19%	9.06	81%	11.22	5.35	-570.6	1.424	10.72	94.49
		80	3.28	23%	10.78	77%	14.06	5.69	-648.6	1.858	15.53	149.68